Mineralogical effects on the dense medium separation of low grade nickel sulfide ore

Keshree Pillay

a thesis submitted for the degree of

Master of Science

in the Department of Chemical Engineering

University of Cape Town

South Africa

2015

DECLARATION

I know the meaning of plagiarism and declare that all the work contained in this thesis, save for that which is properly acknowledged, is my own.

Signed by candidate

Signature Removed

Keshree Pillay

11 February 2015

ABSTRACT

Dense medium separation (DMS) is a method often used to upgrade base metal sulfide (BMS) ores before their main processing stage, with varying results achieved for different ore types. The process makes use of the density differences between the BMS minerals and the lower density silicate/carbonate gangue minerals, using a separating medium of density between the two ore components. The separation is accelerated using a dense medium cyclone (DMC) to form two products: overflow (tailings) and underflow (concentrate). The purpose of DMS is to reject large quantities of gangue upfront, resulting in reduced time, energy and costs associated with processes such as milling and flotation. Preconcentration of ores using physical methods such as DMS is becoming an important consideration as lower grade ores are mined, to increase the feasibility of mining such ores.

Two nickel sulfide deposits were chosen as case studies in order to understand differences in DMS efficiency for different ores. The first is the Main Mineralised Zone (MMZ) of the Nkomati Nickel deposit in Mpumalanga, South Africa, which is part of the Uitkomst Complex. The Phoenix deposit is also considered, and forms part of the Tati greenstone belt in eastern Botswana. Both deposits are magmatic Cu-Ni-PGE (platinum group element) deposits with similar sulfide mineralogy and pentlandite as the main nickel host. A process mineralogy approach was used to evaluate samples of both ores, describing the differences in the mineralogical properties within the overflow and underflow of each ore in order to understand the extent to which individual properties affect the separation.

A bulk sample of each ore type was subjected to DMS using a pilot plant setup, and the overflow and underflow products further classified into a series of density classes using sink-float analysis. These density classes were mineralogically characterised by petrography, quantitative X-ray diffraction, QEMSCAN and electron probe microanalysis, to provide information on differences in bulk mineralogy, mineral textures, mineral chemistry and particle properties between the samples. The nickel contents of both ores were upgraded using DMS and the Nkomati ore experienced a more efficient separation than the Phoenix ore, which is contrary to previous tests on MMZ ore of similar grade.

Both the Nkomati and Phoenix ores consisted of primary magmatic minerals such as pyroxene and plagioclase, as well as a variety of secondary silicates formed by alteration of the original mineral assemblages, e.g. amphibole, chlorite and talc. Three sulfide textures were observed: disseminated / bleb-textured, net-textured and massive. Both ores show more than one texture, with the Nkomati ore displaying all three textures and the Phoenix ore mostly consisting of disseminated sulfides with minor massive sulfides. Pentlandite in the disseminated zones dominantly occurs as fine exsolution lamellae in pyrrhotite, with granular pentlandite mostly located within massive sulfide regions. Apart from overall particle density, sulfide texture is the main controlling factor affecting the individual particle recovery by DMS, with massive and net-textured sulfides having larger grain sizes and therefore higher liberation than disseminated sulfides. In addition to the DMS concentration of sulfide minerals, primary and secondary silicate minerals are separated by their density differences,

which can affect the recovery of finely disseminated sulfides associated with them. Silicate-hosted nickel is another factor that accounts for higher nickel losses to the overflow, observed particularly in the Phoenix ore.

Particle size is also an important control on DMS, where particles near the cut-point have a more-or-less equal chance of sinking or floating, and tend to separate on size rather than density. Small particles of less than ~2 mm are also more likely to float, causing even dense, sulfide-rich particles to be lost to the overflow. An evaluation of particle shapes shows that shape separation plays a minor role for the ores studied, and shape differences are most pronounced nearer to the DMS cut-point, where a higher proportion of irregular-shaped and elongated particles have been concentrated to the underflow.

The ultimate aim of the characterisation of the DMC products would be to use the information gathered to be able to predict the behaviour of an ore being subjected to DMS, based on its mineralogy.

PUBLICATIONS AND PRESENTATIONS

Pillay, K., Becker, M., Mainza, A.N. and Chetty, D. (2014) Mineralogical factors affecting the dense medium separation of nickel sulfide ores. *21st General meeting of the International Mineralogical Association*, 1 – 5 September 2014, Johannesburg.

Pillay, K., Becker, M., Mainza, A.N. and Chetty, D. (2013) Mineralogical factors affecting the dense medium separation of nickel ores. *SAIMM Mineral Processing Conference*, 7 – 8 August 2013, Cape Town.

Pillay, K., Becker, M., Mainza, A.N. and Chetty, D. (2012) Mineralogical effects on the dense medium separation of low grade nickel ore. *Proceedings of the MEI Process Mineralogy Conference,* 7 – 9 November 2012, Cape Town.

Pillay, K., Becker, M., Mainza, A.N. and Chetty, D. (2012) Mineralogical effects on the dense medium separation of low grade nickel ore. *UCT Centre for Minerals Research Student Research Day,* 1 November 2012, Cape Town.

Pillay, K., Becker, M. and Chetty, D. (2011) The effect of gangue mineralogy on the density separation Nkomati MMZ nickel ore. *UCT Centre for Minerals Research Student Research Day,* 1 November 2011, Cape Town.

Pillay, K., Becker, M., Chetty, D. and Thiele, H. (2011) The effect of gangue mineralogy on the density separation of low grade nickel ore. *Proceedings of the SAIMM 6th Southern African Base Metals Conference,* Phalaborwa, 493 – 510.

Pillay, K., Becker, M. and Chetty, D. (2011) Mineralogical effects on the gravity concentration of low grade Selkirk nickel ore. *Colloquium of African Geology 23*, 10 – 14 January 2011, Johannesburg.

Pillay, K., Becker, M. and Chetty, D. (2010) The effect of gangue mineralogy on the pre-processing of low grade nickel ore. *UCT Centre for Minerals Research Student Research Day,* 19 October 2010, Cape Town.

ACKNOWLEDGEMENTS

Many people have contributed in various ways to the completion of this project. I would like to express my gratitude to the following:

My supervisor, Megan Becker, and co-supervisor, Desh Chetty, who have provided constant guidance, support and encouragement throughout this degree.

Mintek, for funding the project and for use of laboratory facilities for the research.

Nkomati Joint Venture and Tati Nickel Mining Company, for providing ore samples.

Density separation tests were carried out by Mintek's Minerals Processing Division, with special thanks to Heloise Thiele, Victor Mailole, Carl Bergmann, Mike Bryson, Stephan van Zyl and Senrika Govender for their valuable advice on the testwork and data interpretation.

The Analytical Services Division at Mintek conducted all chemical assays. I am grateful to the staff for their assistance and information.

The many people of the Mineralogy Division at Mintek have been a great source of help, from technical assistance to discussion of ideas and general encouragement. In particular, I would like to thank Archie Corfield for his valuable assistance throughout with EPMA, specialised sample preparation and original drawings, Wilma Clark for help with many different aspects, especially quantitative XRD, and Charles Bushell, for sharing his QEMSCAN expertise.

Aubrey Mainza, for his helpful feedback throughout on my papers and thesis. Also Narasimha Mangaddody (Indian Institute of Technology), for his useful comments.

Johan de Villiers (University of Pretoria), Sabine Verryn (XRD Analytical and Consulting) and Kirsten Corin, for their help and advice regarding XRD and Rietveld refinement.

Gaynor Yorath, Kerryn Gray and Thelma Chirwa are thanked for assistance with running QEMSCAN samples at UCT and Mintek.

The staff of the Mintek library, particularly Vivian Mdlalose and Kathleen Petersen, for their help with acquiring references.

The following people, with whom I have discussed my research and gained valuable insight from: Sandy Lambert, Tim Napier-Munn (JKMRC), Gerhard Nel (formerly Norilsk Nickel), Philip Swart (ARM) and J-P Franzidis.

My friends and family, for their patience and understanding, as well as the incredible support, encouragement and help wherever needed.

TABLE OF CONTENTS

CHAPTER 1: INTRODUCTION 1

1.1. Introduction 1
1.2. Aim and key questions 3
1.3. Scope 4
1.4. Thesis outline 5

CHAPTER 2: LITERATURE REVIEW 7

2.1. Introduction 7
2.2. Geology and mineralisation 7
2.2.1. Uitkomst Complex 7
2.2.2. Tati greenstone belt 11
2.3. Dense medium separation 13
2.3.1. Fundamentals 13
2.3.2. DMS on Nkomati and Phoenix ores 20
2.3.3. Factors affecting gravity separation processes 21
2.4. Process mineralogy 26
2.5. Critical discussion 32

CHAPTER 3: METHODS 35

3.1. Introduction 35
3.2. Bulk sample preparation 35
3.2.1. Crushing 36
3.2.2. Sub-sampling 36
3.3. Sink-float analysis 37
3.4. Dense medium separation 38
3.5. Chemical analysis 39
3.5.1. ICP-OES 39
3.5.2. Combustion ("LECO") 39
3.6. Mineralogy 40
3.6.1. X-ray diffraction (XRD) 40
3.6.2. Petrography 42
3.6.3. Electron probe microanalysis (EPMA) 42
3.6.4. QEMSCAN analysis 42

CHAPTER 4: CHARACTERISATION OF NKOMATI ORE 47

4.1. Introduction 47
4.2. Density separation testwork 47
4.3. Mineralogy and mineral chemistry 52
4.3.1. Petrography 52
4.3.2. Mineral compositions 57
4.3.3. Bulk mineralogy 59
4.3.4. Nickel deportment 66

4.3.5. Grain size, liberation and mineral associations *67*
4.3.6. Particle properties *70*
4.4. Summary 76

CHAPTER 5: CHARACTERISATION OF PHOENIX ORE 79

5.1. Introduction 79
5.2. Density separation testwork 79
5.3. Mineralogy and mineral chemistry 83
5.3.1 Petrography *83*
5.3.2 Mineral compositions *87*
5.3.3 Bulk mineralogy *89*
5.3.4 Nickel deportment *96*
5.3.5 Grain size, liberation and mineral associations *97*
5.3.6 Particle properties *99*
5.4. Summary 104

CHAPTER 6: DISCUSSION 107

6.1. Introduction 107
6.2. Comparison of efficiency 107
6.3. Alteration effects 110
6.3.1. Partitioning of gangue *111*
6.3.2. Nickel deportment *112*
6.4. Effect of texture 113
6.4.1. Textural characteristics of the Nkomati and Phoenix ores *113*
6.4.2. Sulfide grain size *114*
6.4.3. Sulfide liberation *115*
6.4.4. Mineral associations *117*
6.5. Effect of particle properties 117
6.5.1. Particle size *118*
6.5.2. Particle shape *119*
6.5.3. Size and shape separation for the Nkomati and Phoenix ores *121*

CHAPTER 7: CONCLUSIONS AND RECOMMENDATIONS 123

7.1. Conclusions 123
7.2. Recommendations 125

REFERENCES 127

APPENDIX A: QEMSCAN DATA VALIDATION 135
APPENDIX B: DENSITY SEPARATION DATA 137
APPENDIX C: CHEMICAL ASSAYS 143
APPENDIX D: MINERALOGICAL DATA 149

LIST OF FIGURES

Figure 2.1 A: Geological map showing the location of the Uitkomst Complex relative to the Bushveld Complex. **B:** Simplified map of the Uitkomst Complex. **C:** Cross section through the Uitkomst Complex showing layering (from Li *et al*., 2002). 8

Figure 2.2 IUGS classification of ultramafic rocks based on olivine (ol), orthopyroxene (opx) and clinopyroxene (cpx) content (from www.geol.lsu.edu; after Streckeisen, 1972). 11

Figure 2.3 Geological map showing **a:** the Tati greenstone belt, and **b:** the location of the Phoenix and Selkirk deposits within the central portion of the belt (from Maier *et al*., 2008) 12

Figure 2.4 Schematic drawing of a DMC, showing major components and flow directions (modified after Mainza *et al.*, 2004 and Dunglison, 1999)..... 17

Figure 2.5 Simplified DMS circuit (modified after Bergmann *et al.*, 2010) 18

Figure 2.6 Example of a partition curve, showing region of particle misplacement or error area (from Dunglison, 1999)..... 19

Figure 2.7 Mean partition curves for particles of different shapes (from Ferrara *et al*., 2000)23

Figure 2.8 Heywoods elongation ratio for gold grains within different size fractions of a gravity concentrate and tailings (from Houseley *et al*., 1994)..... 24

Figure 2.9 Heywoods flakiness ratio for sized gold grains for a gravity concentrate and tailings (from Houseley *et al*., 1994) 25

Figure 2.10 Volume shape coefficients for sized gold grains in a gravity concentrate and tailings (from Houseley *et al*., 1994) 25

Figure 2.11 Example of mapped particles from a QEMSCAN, which are categorised above according to the liberation of a particular mineral of interest (in red) and minimum particle size in microns (y-axis). Liberation classes: locked = <30% of particle area, middlings = 30 – 80% of particle area, liberated = >80 of particle area. 27

Figure 2.12 Calculated Concentration Criterion for various mixtures at different particle sizes (from Burt, 1984) 29

Figure 2.13 Comparison of the particle size distribution of a chromite feed sample using QEMSCAN analysis and a Malvern laser particle sizer (from Pascoe *et al*., 2007) 30

Figure 2.14 Textures of the geometallurgical units of a Ni-Cu-PGE deposit, as observed from QEMSCAN mapping (Lotter *et al.*, 2011)..... 31

Figure 3.1 Flow diagram showing sequence followed. *A crush top size of 12 mm was used for the Nkomati ores, and 25 mm for the Phoenix ore..... 35

Figure 3.2 Pilot-scale jaw crusher used to break down large ore particles to less than ~20 cm36

Figure 3.3 A: Blending and homogenising of the Nkomati bulk sample using a hopper on rails; **B:** Sub-sampling prior to riffle splitting. 37

Figure 3.4 Dense medium cyclone at the Mintek pilot plant 38

Figure 3.5 Refinement pattern for the NIST 660a LaB_6 standard, showing the measured and calculated patterns, as well as the difference between the two. In this instance the measured pattern is not easily seen because of the similarity between both patterns..... 41

Figure 3.6 Sample holder containing carbon-coated polished block (75x80 mm) used for the analysis 43

Figure 3.7 Example of Field Image procedure. **A**: Individually-mapped fields of view, **B**: Fields stitched into a single image, **C**: Separated ('particulated') particles. 44

Figure 4.1 Washability curve for the Nkomati bulk sample 48

Figure 4.2 Grade and recovery curves for Ni and Cu in the Nkomati bulk sample 49

Figure 4.3 Flowsheet for the testwork showing different streams 50

Figure 4.4 Partition curve showing the separation efficiency 52

Figure 4.5 A: Photomicrograph of olivine crystals with intercumulus plagioclase, transmitted cross polarised light (DMC underflow, 3.1 floats). **B:** Deformed actinolite, transmitted plane polarised light (DMC underflow, 2.9 floats) 53

Figure 4.6 Sulfide textures in the Nkomati ore (reflected light, plane polarised). **A:** Net-textured sulfides – chalcopyrite (cpy), pyrrhotite, (po), pentlandite (pn) and magnetite (mt) interstitial to serpentine (dark grey). **B:** Granular pentlandite (pn) associated with chalcopyrite (cpy), pyrrhotite (po), sphalerite (sph), and magnetite (mt), dark grey areas show silicates. **C:** Pentlandite (pn) flames in pyrrhotite (po). **D:** Chalcopyrite (cpy) and pyrrhotite (po) penetration along actinolite (act) cleavage planes. 54

Figure 4.7 Petrographic images showing the settling of the magnetic colloid (brown) on magnetic pyrrhotite, with pentlandite (pn) and non-magnetic pyrrhotite unaffected. **A:** particle in which all pyrrhotite is magnetic. **B:** particle containing both magnetic and non-magnetic pyrrhotite 55

Figure 4.8 Example of two particles: Particle **A** showing two mineral types, a grain (red) included within a matrix (green); Particle **B** is a liberated grain or a monomineralic particle 55

Figure 4.9 Particles illustrating the three classes used to describe liberation of a mineral of interest (red) from associated gangue (green): **A** = locked (<30 area % of the particle), **B** = middlings (30 – 80 area % of the particle), **C** = liberated (>80 area % of the particle). As liberation is described on a 2D surface, it is the apparent liberation of a grain. 57

Figure 4.10 Identified minerals in order of increasing SG 61

Figure 4.11 Bulk mineral composition of the DMC feed as determined by QXRD 62

Figure 4.12 Bulk mineral composition of the DMC overflow samples as determined by QXRD (F – floats, S – sinks) 63

Figure 4.13 Bulk mineral composition of the DMC underflow samples as determined by QXRD (F – floats, S – sinks) 63

Figure 4.14 QEMSCAN bulk mineralogy 66

Figure 4.15 Nickel deportment within the selected density classes of the DMC overflow and underflow. Alteration minerals = serpentine, chlorite, talc and epidote. 67

Figure 4.16 Cumulative grain size distribution for composite sulfide grains 68

Figure 4.17 Degree of sulfide mineral liberation in each of the samples (mass %) 69

Figure 4.18 False colour mineral maps of particles in the 3.0 floats of the DMC overflow and underflow 71

Figure 4.19 False colour mineral maps of particles in the 3.1 floats of the DMC overflow and underflow 72

Figure 4.20 False colour mineral maps of particles in the 3.1 sinks of the DMC overflow and 3.2 floats of the underflow 73

Figure 4.21 Particle size distributions in the density fractions of the DMC overflow and underflow 74

Figure 4.22 Examples of outlines of measured particle shapes within the different shape factor categories, from <10 (low shape factor) to >60 (very high shape factor) 75

Figure 4.23 Examples of outlines of measured particle shapes within the elongation categories, from <0.2 (low elongation) to >0.8 (very high elongation)..... 75

Figure 4.24 Shape factors of particles in the DMC overflow and underflow 75

Figure 4.25 Distribution of particle elongation in the DMC overflow and underflow 76

Figure 5.1 Washability curve for the Phoenix bulk sample 80

Figure 5.2 Grade and recovery curves for Ni and Cu in the Phoenix bulk sample..... 81

Figure 5.3 Partition curve showing the separation efficiency..... 83

Figure 5.4 Photomicrographs showing igneous textures (transmitted crossed polarised light). **A:** medium-grained rock with plagioclase (plag) laths associated with olivine. **B:** fine-grained plagioclase associated with amphibole (amph)..... 84

Figure 5.5 Photomicrographs showing alteration textures in the Phoenix rocks. **A:** altered section of rock composed of amphibole (hornblende; transmitted plane polarised light) **B:** deformed sulfides within amphibole cleavage planes (transmitted crossed polarised light). 84

Figure 5.6 Photomicrographs showing sulfide mineral textures (reflected plane polarised light); **A:** finely disseminated sulfides (bright) among silicates. **B:** angular sulfide disseminations formed by recrystallisation along silicate grain boundaries. **C:** net-textured sulfides. **D:** pyrrhotite (po) containing pentlandite flames, and granular pentlandite (pn), associated with chalcopyrite (cpy). 85

Figure 5.7 Photomicrographs showing the settling of the magnetic colloid (brown) on magnetic pyrrhotite with clean pentlandite (pn, reflected plane polarised light). 86

Figure 5.8 Identified minerals in order of increasing SG 91

Figure 5.9 Bulk mineral composition of the DMC feed, as determined by XRD 92

Figure 5.10 Bulk mineral composition of the DMC overflow samples, as determined by XRD 93

Figure 5.11 Bulk mineral composition of the DMC underflow samples, as determined by XRD 93

Figure 5.12 QEMSCAN bulk mineralogy 96

Figure 5.13 Nickel deportment within the selected density classes of the DMC overflow and underflow. Alteration minerals = serpentine, chlorite, talc and epidote. 97

Figure 5.14 Cumulative grain size distribution for composite sulfide grains 98

Figure 5.15 Degree of sulfide mineral liberation in each of the samples (mass %) 98

Figure 5.16 False colour mineral maps of particles in the 2.95 floats fractions of the DMC overflow and underflow 100

Figure 5.17 False colour mineral maps of particles in the 3.0 floats fractions of the DMC overflow and underflow 101

Figure 5.18 False colour mineral maps of particles in the 3.1 floats fractions of the DMC overflow and underflow 102

Figure 5.19 Particle size distributions in the density fractions of the DMC overflow and underflow 103

Figure 5.20 Shape factors of particles in the DMC overflow and underflow 103

Figure 5.21 Distribution of particle elongation in the DMC overflow and underflow 104

Figure 6.1 Comparison of grade and recovery curves for the Nkomati and Phoenix ores ... 108

Figure 6.2 Comparison of partition curves for the Phoenix and Nkomati ores 109

Figure 6.3 Washability curves for the feed as calculated from the DMC products 109

Figure 6.4 Proportion of near-gravity material at ± 0.05 SG units from the cut-point 110

Figure 6.5 Bulk mineralogy comparison for the Phoenix and Nkomati DMC feeds..... 111

Figure 6.6 Particles mapped by QEMSCAN, showing observed sulfide textures and corresponding changes in grain size 114

Figure 6.7 Cumulative grain size distribution at the cut-point density fractions of the Nkomati and Phoenix DMC products (O/F – overflow, U/F – underflow). 115

Figure 6.8 Cumulative sulfide liberation in the cut-point samples of the Nkomati and Phoenix DMC products (O/F – overflow, U/F – underflow)..... 116

Figure 6.9 Cumulative particle size distribution in the high density fractions of the Nkomati and Phoenix DMC products..... 119

Figure 6.10 Distribution of particle shape at the DMS cut-point..... 120

Figure 6.11 Thin sections showing Nkomati ore particles belonging to the 2.9 floats density class of the DMC overflow and underflow..... 120

Figure 6.12 Schematic drawing of a DMC showing direction of particle movement towards the overflow and underflow 121

LIST OF TABLES

Table 2.1 Lithological units of the Uitkomst Complex and their characteristics (from Li *et al*., 2002) 9

Table 3.1 Plant operating conditions for the bulk samples 39

Table 3.2 Instrument parameters for the Bruker D8 diffractometer 41

Table 4.1 Stream masses and nickel grades for the Nkomati bulk sample 47

Table 4.2 Sink-float analysis data for the Nkomati bulk sample (cut-point data highlighted) 48

Table 4.3 Summary of DMS results for the Nkomati bulk sample 49

Table 4.4 Mass-balanced mass, grade and recovery information at different points in the flowsheet 50

Table 4.5 Partition coefficients calculated for the Nkomati bulk sample 51

Table 4.6 Measured silicate mineral compositions in the Nkomati ore 58

Table 4.7 Measured sulfide mineral compositions in the Nkomati ore 58

Table 4.8 Minerals identified in the MMZ ore 60

Table 4.9 Samples subjected to QEMSCAN analysis 64

Table 4.10 Modal mineralogy of selected SG fractions of the DMC overflow and underflow (mass %) 65

Table 4.11 Nickel concentrations of sulfide and silicate minerals 67

Table 4.12 Sulfide mineral associations (mass %) 70

Table 5.1 Stream masses and nickel grades for the Phoenix bulk sample 79

Table 5.2 Sink-float analysis data for the Phoenix bulk sample (cut-point data highlighted) 80

Table 5.3 Summary of DMS testwork results for the Phoenix bulk sample 81

Table 5.4 Mass-balanced mass, grade and recovery information at different points in the flowsheet 82

Table 5.5 Partition coefficients calculated for the Phoenix bulk sample 82

Table 5.6 Measured silicate mineral compositions in the Phoenix ore 88

Table 5.7 Measured sulfide compositions in the Phoenix ore 88

Table 5.8 Minerals identified in the Phoenix ore 90

Table 5.9 Samples subjected to QEMSCAN analysis 94

Table 5.10 Modal mineralogy of selected SG fractions of the DMC overflow and underflow (mass %) 95

Table 5.11 Nickel concentrations of sulfide and silicate minerals 96

Table 5.12 Sulfide mineral associations (mass %) 99

GLOSSARY

accessory mineral	mineral present in very low quantities and not important in the classification of the rock
alteration	change in the original mineral composition of a rock
Archaean	period in geological history between ~4 600 and 2 500 million years ago
amphibolite facies	metamorphic conditions characterised by medium to high temperature and pressure
AutoSEM	automated scanning electron microscope / microscopy
BMS	base metal sulfide/s
cleavage	crystallographic planes of weakness within minerals
coarse-grained	an igneous rock with crystals larger than ~2 mm
concentration criterion	(CC) formula described by Burt (1984) to determine whether an ore is amenable to gravity concentration
cpy	chalcopyrite
cumulate texture	igneous rock texture formed by interlocking crystals that have solidified and settled out from a magma
cumulus minerals	minerals forming an interlocking cumulate texture
cut-point	density of the separating medium during DMS
D_{50} / ρ_{50}	actual separation density
deportment	distribution of an element amongst the minerals present
disseminated sulfides	fine sulfide mineral grains that are sparsely distributed throughout the rock
DMC	dense medium cyclone
DMS	dense medium separation
EDS	energy dispersive spectrometry
elongation	1 – (width/length)
E_p	Ecarte probable, probable error of separation $[(D_{75} – D_{25})/2]$

EPMA	electron probe microanalysis
equigranular	rock texture characterised by grains that are more-or-less equal in size
ESD	equivalent sphere diameter
euhedral	a mineral grain showing its true crystal shape
exsolution	the separation of one mineral phase into two distinct phases, commonly as a result of cooling
felsic	descriptive of a light-coloured igneous rock rich in high Si and Al minerals such as quartz and feldspar
FeSi	ferrosilicon powder, mixed with water and used as a separating medium for DMS
fine-grained	an igneous rock in which individual crystals cannot be seen with the naked eye
free surface	in mineral association data, the proportion of the mineral grain boundary that is exposed, i.e. not in contact with another mineral
Ga	gigaannum; one billion years ago
gabbronorite	coarse-grained igneous rock composed of plagioclase and pyroxene
gangue	economically unimportant minerals within an ore
grain	monomineralic constituent of a rock or rock particle
granitoid	coarse-grained igneous rock with a granitic composition (dominated by quartz and feldspar)
greenschist facies	metamorphic conditions characterised by low temperature and pressure
harzburgite	igneous rock composed of mainly orthopyroxene and olivine
HLS	heavy liquid separation
hydrothermal alteration	alteration of a rock produced by interaction with heated fluids, e.g. groundwater or magmatic fluids
intercumulus minerals	minerals that have crystallised interstitially to the interlocking cumulus minerals in an igneous cumulate texture

ktpm	kilo tonnes per month
lens	a convex lens-shaped layer of rock or ore
lld	lower than the limit of detection
liberated	a grain making up >80 volume percent of a particle
liberation	the degree to which a mineral grain is free of attached gangue
locked	a grain making up <30 volume percent of a particle
Ma	megaannum; one million years ago
mafic	descriptive of a dark-coloured igneous rock rich in ferromagnesian minerals such as olivine and pyroxene
massive sulfides	ore consisting of a large, dense mass of sulfide minerals
medium-grained	an igneous rock in which the individual crystals are visible with the naked eye but <2 mm in size
metamorphism	the change in mineralogy and texture in rocks associated with temperature and pressure changes in its geological environment
middlings	a grain that makes up between 30 and 80 volume percent of a particle
mineral association	degree of grain boundary-sharing between different minerals
mineralisation	occurrence or formation of the economically important component of a rock
MMZ	Main Mineralised Zone of the Uitkomst Complex
mt	magnetite
net-texture	sulfide texture formed by a network of BMS occurring interstitially to rounded silicate and oxide grains
O/F	overflow
overflow	floats fraction produced from a dense medium cyclone
particle	aggregate of rock generally consisting of more than one mineral grain
partition coefficient	proportion of the feed of a certain SG that has been recovered to the sinks or floats

partition curve	a plot of partition coefficients against density; describes the separation efficiency
pentlandite flames	small flame-like exsolution lamellae of pentlandite in pyrrhotite
petrography	microscopic description and classification of rock samples
pn	pentlandite
po	pyrrhotite
preconcentration	early-stage of mineral processing involving the rejection of large amounts of gangue by physical methods
primary mineral	mineral formed during the original crystallisation of the rock
process mineralogy	the use of mineralogical information to enhance mineral processing techniques
pseudomorph	replacement of one mineral by another, while retaining the form of the original mineral
pyroxenite	ultramafic igneous rock composed dominantly of pyroxene
QEMSCAN	Quantitative Evaluation of Minerals by Scanning Electron Microscopy
QXRD	quantitative X-ray diffraction
ROM	run-of-mine
saussurite	fine-grained mass of epidote, clays, sericite, calcite, mica and chlorite, usually formed by alteration of plagioclase
saussuritisation	process of alteration to saussurite, normally in feldspars
secondary mineral	mineral formed after formation of the host rock, usually by alteration of the primary minerals
SEM	scanning electron microscopy
sericitisation	alteration of primary mineral such as plagioclase to sericite (fine-grained mica)
serpentinisation	alteration of olivine and pyroxene to serpentine during low grade metamorphism
SG	specific gravity
shape factor	perimeter^2 / area of a grain or particle

sink-float analysis	separation of a feed using heavy liquids into a range of density classes
solid solution	substitution of one element for another within the crystal structure of a mineral
sph	sphalerite
t/hr	tonnes per hour
Tati greenstone belt	sequence of metamorphosed volcanic and sedimentary rocks in eastern Botswana containing the Phoenix and Selkirk nickel deposits
TBE	tetrabromoethane, heavy liquid used for laboratory-scale density separations
texture	relationship between minerals making up a rock or particle, in terms of grain sizes, shape, intergrowths, liberation and associations
U/F	underflow
Uitkomst Complex	Igneous intrusion containing the Nkomati nickel deposit
ultramafic	descriptive of an igneous rock containing >90% ferromagnesian minerals such as olivine and pyroxene
underflow	sinks fraction recovered through the spigot of a dense medium cyclone
undulose extinction	optical property under crossed polarised light indicating deformation of mineral grains
uralite	amphibole formed by the alteration of pyroxene whilst retaining the pyroxene crystal form
vein	mineralised body formed by precipitation within a fracture of a rock
washability curve	cumulative mass distribution of a feed throughout a series of density classes determined by sink-float analysis
XRD	X-ray diffraction

CHAPTER 1: INTRODUCTION

1.1. Introduction

Low grade ore deposits are of increasing interest in mineral processing owing to dwindling resources of high grade, easily exploited ores. For nickel ores, sulfide deposits have historically been the main source of nickel production worldwide as they are relatively simple to process, as compared with laterite-hosted nickel ores (Mudd, 2009). As high grade sulfide ores become depleted, importance is placed on the mining of low grade disseminated ores. These deposits commonly display complex mineralogy in terms of mineral composition and texture, the understanding of which is important in the processing of the ore.

Preconcentration of low grade ores, generally using physical separation methods, is also of growing importance in mineral processing, as it contributes to making the beneficiation of previously uneconomic ore deposits possible, and significantly reduces processing time and costs (Burt, 1999; Cresswell, 2001). Mining is also gradually shifting towards laterite ores as less economically viable sulfide ores are available. Low grade disseminated sulfide ores, however, are still being considered for mining as more complex processing methods are required to recover nickel from laterites (Mudd, 2010). A focus on the development and optimisation of preconcentration methods may be useful for the future exploitation of lateritic ores, owing to the high costs associated with the extraction of nickel from these ores (Mudd, 2010).

The focus of this thesis is on the mineralogy of low grade, disseminated nickel sulfide ores in southern Africa and their behaviour during preconcentration by dense medium separation (DMS). Dense medium separation is widely used in the base metals industry, and in southern Africa it is the main concentration stage for many industrial minerals, iron ore, coal and diamonds (Cresswell, 2001). This technique separates ore based on the relative density differences between minerals. A process mineralogy approach is undertaken in order to assess the mineralogical properties of nickel ores in terms of composition and texture, particularly of the gangue minerals, that may affect nickel concentration by DMS, thereby contributing to a better understanding of this technique.

Two southern African nickel deposits were selected for the study, which aims to link the mineralogical differences of each ore type with their differences in behaviour during processing. The first ore under consideration is low grade nickel ore from the Nkomati Nickel Mine in Mpumalanga, South Africa. The Nkomati deposit is part of the Uitkomst Complex, a magmatic sulfide Cu-Ni-PGE deposit, which is genetically related to the intrusion of the Bushveld Complex. The ore was sourced from the Main Mineralised Zone (MMZ) of the Uitkomst Complex, which has an average nickel grade of approximately 0.66-0.68% (Hammerbeck and Schürmann, 1998). The nickel occurs as pentlandite, with a small amount found in solid solution within pyrrhotite. Pentlandite usually occurs as small flame-like exsolution lamellae within the pyrrhotite and less commonly as larger granular aggregates (Gauert *et al*., 1995). Preconcentration of the nickel using density separation methods was shown to be generally inefficient for this ore type (G. Nel, pers. comm., 2010; Sibanyoni, 2006)

Low grade nickel ore from the Phoenix nickel deposit, which occurs south-east of Francistown in eastern Botswana, was also selected for comparative purposes. The Phoenix ore shows similar sulfide mineralogy to the Nkomati ore, and DMS is used successfully at the mine to preconcentrate the nickel. A comparative study is useful in understanding the mineralogical differences between the ore types which can be used to explain their behavioural differences during processing. The Phoenix deposit is hosted by metagabbronorite and forms part of the Tati greenstone belt. Mineralisation is in the form of massive, vein-like and disseminated sulfides (Maier *et al*., 2008).

Tati Nickel Mining Company runs the Phoenix open pit mine (www.miningtopnews.com). The high grade ore from the Phoenix mine and related Selkirk underground mine has been extracted and treated by crushing, milling and flotation on a plant based at the Phoenix mine. The Selkirk mine has since been put on care and maintenance while the Phoenix mine treats increasingly lower grade ore. The nickel content of the ore is upgraded by DMS, prior to recovery by flotation. Flotation of the concentrate produced by DMS, or the underflow, is then able to produce a high enough nickel grade for smelting.

In the low grade sections of these magmatic sulfide deposits, the properties of the gangue minerals should have a significant influence on the behaviour of particles during mineral processing. This is especially important for gravity concentration processes, such as DMS, which is being used successfully on Phoenix ore and is conducted with large particle sizes of

between 1 and 25 mm. Very little research has been done on the influence of individual mineralogical factors on density separation processes, particularly of aspects such as particle size, shape and roughness (e.g. Pascoe *et al*., 2007; Grobler and Bosman, 2009). This project therefore concentrates on the mineralogy of the sulfide and gangue minerals, and the properties of the particles subjected to DMS, as observed from the different products of the DMS process. If the reason for the nickel upgrade in the selected deposits can be understood, predictions can be made of the suitability of DMS as preconcentration method for different ore types.

The investigation involves density separation testwork and techniques commonly used in process mineralogy. A process mineralogy approach is important to understand the behaviour of different ore types during the different stages of their processing, and assists in the designing and optimising of these processes. An important function of process mineralogical characterisation is to evaluate feed samples to processes and use the observed mineralogical data to predict the outcome of a process. This project concentrates rather on the analysis of the products of DMS in order to understand functioning of the process. Automated scanning electron microscopy (AutoSEM) is widely used for two-dimensional particle analysis and forms a major part of the study. Bulk mineralogy and textural information of ores (size, shape, liberation and mineral associations) are quantified using this technique. A better understanding of these properties in each of the ore types will aid in an improved understanding of their contribution towards the DMS process.

1.2. Aim and key questions

The aim of the research is to evaluate the mineralogy of different nickel sulfide ores, particularly of the gangue component, in order to understand its effect on the recovery of nickel by DMS in low grade sulfide ores. This involves the characterisation of each of the three ore types based on the mineralogical composition, texture and particle properties of the different separation products, and the comparison of these properties between the different ores. In order to carry out the aim of the project, two key questions were addressed:

1. To what extent do mineral compositions and textural features such as size, density, shape, cleavage, degree of alteration, associations and liberation, affect the dense medium separation of low grade nickel ores?

2. How do differences in the mineralogy between the two ores affect their behavioural differences during DMS, and therefore the effectiveness of this process for each deposit?

If the reasons for the differences in processing behaviour of these ore types can be understood, mineralogical analysis can be used to aid models predicting processing performance and determine whether preconcentration is a viable option.

1.3. Scope

This project was undertaken as a process mineralogy study, combining aspects of economic geology and mineral processing. The focus was on the use of analytical techniques in mineralogy that are commonly utilised in the field of process mineralogy in industry to characterise ores and metallurgical products. X-ray diffraction, petrography and electron probe microanalysis were used to determine the bulk mineralogy, textures and mineral compositions in the samples, with QEMSCAN analysis being an essential part of the quantification of mineral and particle properties of the ores. The analyses were concentrated on the product samples rather than the feeds, in order to determine differences in mineralogy after the separation. Additional feed sample analyses were not feasible for the size of the project, given the large number of product samples from both deposits that were required to be analysed.

Mineral processing testwork was limited to pilot plant DMS and laboratory sink-float analyses by heavy liquid separation (HLS) using standard techniques, on one bulk sample of each ore. The purpose of these tests was to produce a set of results for each ore type to be evaluated, and a series of samples for the mineralogical analyses. Further information on the samples is given in Chapter 3. This thesis does not attempt to improve on the DMS process or the grades/recoveries attained for any of the ores, or to evaluate the performance of DMS in general, but aims to link the actual results achieved with the mineralogical properties of the ores. The research did not address the suitability of different density separation methods for the preconcentration of the selected ores. Flotation, the main processing stage for the selected ores, also does not form part of the study.

1.4. Thesis outline

This thesis consists of a total of seven chapters. Chapter 1 gives an introduction to the project, including the aim and scope of the study and structure of the thesis. Chapter 2 contains the literature review, which covers the geology and mineralisation of the selected ore deposits, as well as the topics of dense medium separation and process mineralogy and their applications. The limitations of the existing literature are also discussed, indicating the scope for the present study. Chapter 3 covers the experimental procedure followed, with details of the testwork procedure and analytical methods applied. Chapters 4 and 5 follow an identical format, presenting results acquired for the Nkomati and Phoenix ores, respectively. In each chapter, the results for the density separation testwork are first given, followed by mineralogical characterisation of the products of the separation. The mineralogical information is compared amongst different density classes of the products with a view to better understand the mineralogical factors responsible for the separation of the particles. Chapter 6 discusses the effect that each mineralogical aspect studied may have on DMS, and compares the differences in DMS behaviour and mineralogy of the two ores. Chapter 7 provides the conclusions of the study, with recommendations for further research. The reference list follows at the end of the thesis, with the appendix containing all original metallurgical, mineralogical and chemical data.

CHAPTER 2:LITERATURE REVIEW

2.1. Introduction

This chapter reviews the relevant literature published within the fields of this study to provide a background to the main focus areas of the thesis. The geology and mineralisation of each of the chosen ore deposits is described, together with the fundamentals of DMS, factors affecting DMS, and its application in base metal preconcentration. A description of the main field of study, process mineralogy, is included, with its application to the characterisation of Cu-Ni-PGE (platinum group element) ores and density separation products. Lastly, an assessment of the existing knowledge is presented, showing its limitations and providing the platform upon which this research is based.

2.2. Geology and mineralisation

2.2.1. Uitkomst Complex

The Uitkomst Complex is a layered mafic intrusion and a satellite body related to the intrusion of the Bushveld Igneous Complex (Li *et al*., 2002). It is found intruding quartzitic to dolomitic and pelitic sediments of the late Archaean Transvaal Supergroup close to the contact with the Archaean basement rocks (Gauert, 2001; Sarkar *et al*., 2008). Most of the Uitkomst Complex crystallised from magma similar in age and composition to the high-Mg basaltic parent magma of the 2.054 Ga Bushveld Complex but intruded approximately 10 km lower than the current base of the Bushveld Complex (Li *et al*., 2002; Sarkar, *et al*., 2008). Structurally the Uitkomst Complex is a plunging tubular body with a width and thickness of approximately 800 m and at least 8 km in length, and is made up of seven lithological units (Figure 2.1; Li *et al*., 2002). The definitions of the different rock units are given below (Table 2.1) according to Li *et al*. (2002). The rock types documented by Sarkar *et al*. (2008) differ slightly from those of Li *et al*. (2002). According to Sarkar *et al*. (2008) the oldest unit is the Basal Gabbronorite, which is overlain by the lower harzburgite, chromitiferous harzburgite, main harzburgite, pyroxenite, main gabbronorite and upper gabbronorite units.

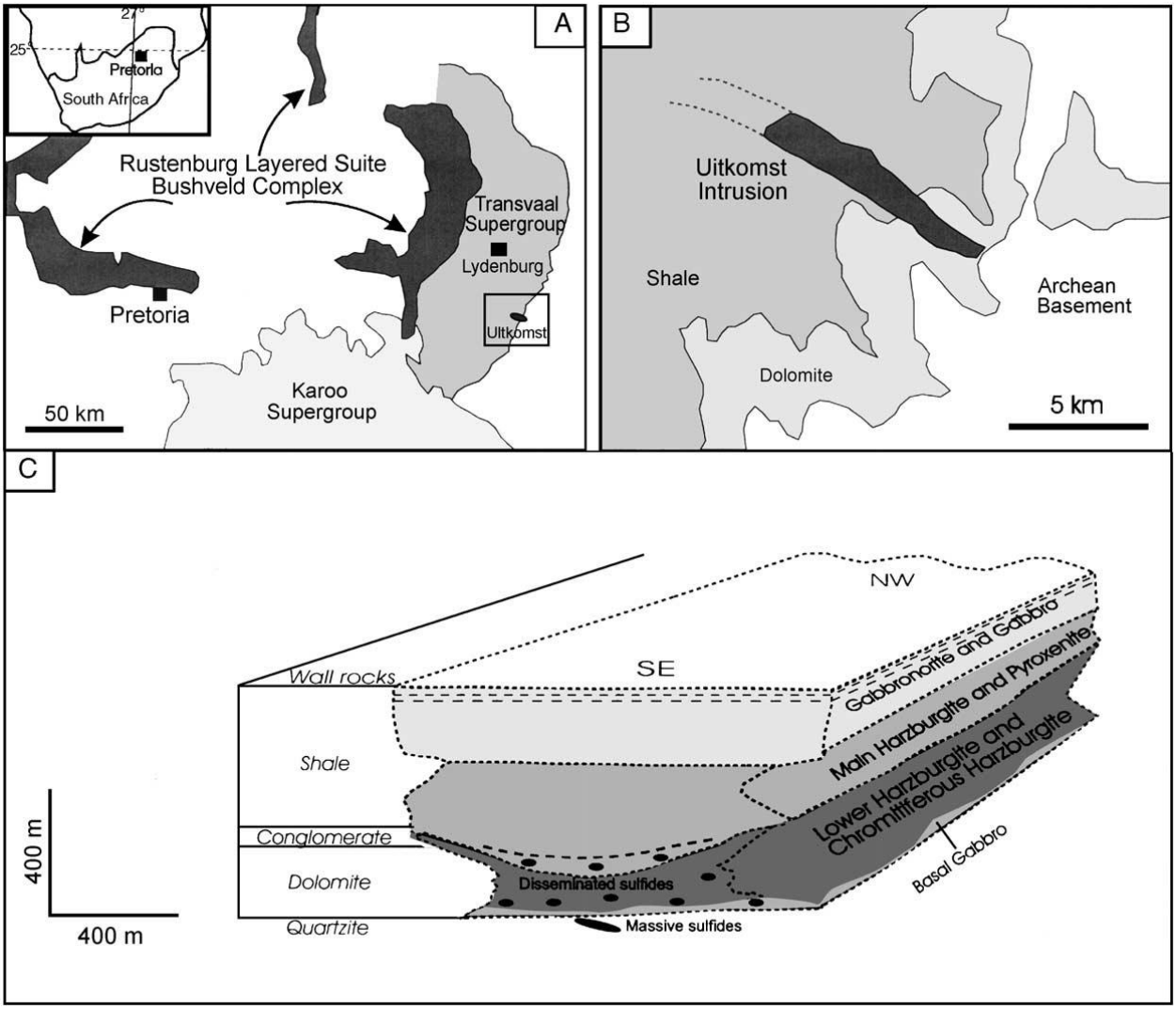

Figure 2.1 A: Geological map showing the location of the Uitkomst Complex relative to the Bushveld Complex. **B:** Simplified map of the Uitkomst Complex. **C:** Cross section through the Uitkomst Complex showing layering (from Li *et al*., 2002).

Table 2.1 Lithological units of the Uitkomst Complex and their characteristics (from Li *et al*., 2002)

Lithologic Unit	Type of Contact	Petrography	Sulfide Mineralisation	Alteration
Basal Gabbro	Transitional with Lower Harzburgite, discontinuity along strike	Phaneritic with plagioclase, augite, and rare olivine	Blotchy sulfide to massive vein	Moderate uralitisation and saussuritisation
Lower Harzburgite	Grading into Chromitiferous Harzburgite with increasing olivine and chromite	Variable between feldspathic harzburgite to olivine websterite with cumulus olivine and chromite	Disseminated to net-textured	Moderate serpentinisation, talc-carbonate alteration
Chromitiferous Harzburgite	Grading into Main Harzburgite	Olivine + chromite orthocumulate	Weakly disseminated	Extensive serpentinisation, talc-carbonate alteration
Main Harzburgite	Transitional with Pyroxenite	Olivine + minor chromite cumulate	Weakly disseminated sulfide in places	Moderate serpentinisation
Pyroxenite	Gradational with Gabbronorite	Intergranular with cumulus augite	Sulfide-barren to weakly disseminated sulfide	Weak saussuritisation
Gabbronorite	Sharp with Upper Gabbro	Massive to intergranular	Mostly sulfide-barren	Weak uralitisation and saussuritisation
Upper Gabbro	Chilled contact with hangingwall sediments	Subhorizontal modal layering	Mostly sulfide-barren	Weak uralitisation and saussuritisation

The ore minerals occurring within the Uitkomst Complex are, in decreasing abundance, pyrrhotite, pentlandite, chalcopyrite, magnetite, ilmenite, chromite, digenite and pyrite (Gauert *et al*., 1995). Minerals present in minor amounts include violarite, mackinawite, galena, sphalerite, platinum-group minerals, awaruite, native Cu, arsenopyrite, cobaltite and millerite. The pentlandite is commonly associated with pyrrhotite as exsolution lamellae but forms granular aggregates enclosed in, or interstitial to, the pyrrhotite as the nickel grade of the ore increases (Gauert *et al*., 1995).

Massive sulfide lenses of around 200 m in width, 400 m in length and up to 20 m thick, are found in the footwall sediments a few metres from the contact with the base of the complex (Li *et al*., 2002). The basal gabbronorite, lower harzburgite, chromitiferous harzburgite and the lower part of the main harzburgite contain mainly disseminated sulfides, with some small massive sulfide pods and veins occurring locally in the basal gabbronorite and lower harzburgite units (Li *et al*., 2002). The disseminated sulfide ores of the complex form discrete subhorizontal zones which are contained within specific lithological units (Theart and de Nooy, 2001). Nickel grades in wt% for the different units are 2.04, 0.54, 0.60 and 0.43 for the

footwall massive sulfides, basal gabbronorite disseminated sulfides, lower harzburgite disseminated sulfides and the chromitiferous harzburgite disseminated sulfides respectively (Li *et al*., 2002).

The areas containing economic disseminated sulfide mineralisation are referred to as the Basal Mineralised Zone (BMZ) hosted by the basal gabbronorite unit, the Main Mineralised Zone (MMZ) hosted by the lower harzburgite unit and the Chromititic Peridotite Mineralised Zone (PCMZ) located within the chromitiferous harzburgite (Bradford *et al*., 1998; Maier *et al*., 2004). The Massive Sulfide Body (MSB) is hosted by the sedimentary rocks and granite/gneiss below the intrusion (Theart and de Nooy, 2001).

The lower harzburgite unit in which the MMZ ore is hosted, is a heterogenous unit consisting of different ultramafic rocks (rocks that contain >90% ferromagnesian minerals e.g. olivine and pyroxene) including poikilitic harzburgite, feldspathic harzburgite, wehrlite, lherzolite, olivine websterite, and rare amphibolite (Sarkar *et al.*, 2008; Li *et al.*, 2002; Kearey, 2001). The IUGS (International Union of Geological Sciences) classification of ultramafic rocks is given in Figure 2.2, showing the compositional differences between these rock types, based on their olivine, orthopyroxene and clinopyroxene contents (Streckeisen, 1972).

Numerous calc-silicate xenoliths occur in the host rock; these xenoliths are also sulfide-containing, mostly close to the contact with the host rock. This leads to variable lithology, textures and metal grades throughout the MMZ (Hulley, 2005; Sibanyoni, 2006).

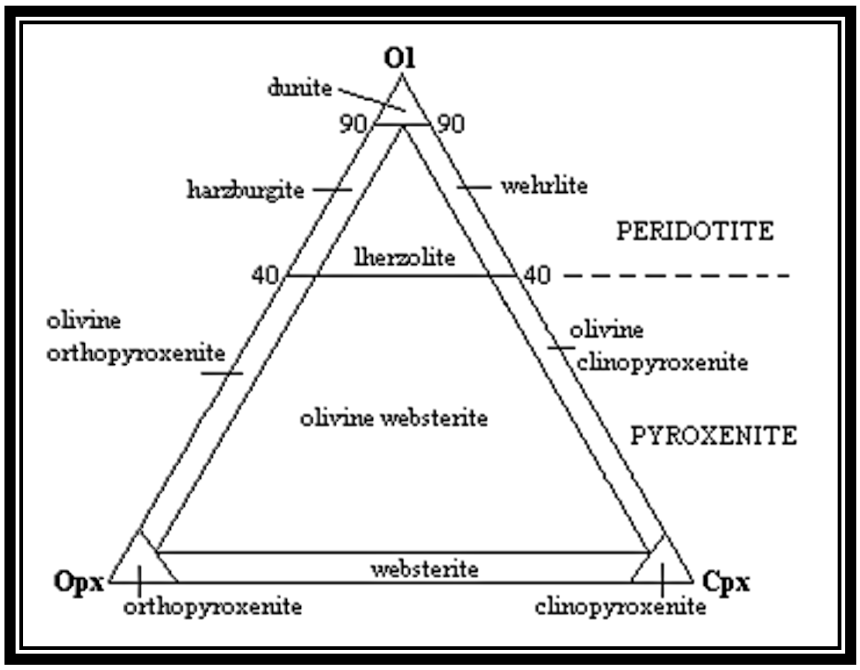

Figure 2.2 IUGS classification of ultramafic rocks based on olivine (ol), orthopyroxene (opx) and clinopyroxene (cpx) content (from www.geol.lsu.edu; after Streckeisen, 1972).

The economic nickel mineralisation is mined at the Nkomati Mine, where initial mining activity was centred on the now completely mined out MSB. More recently, the mining has been focused on the lower grade MMZ and PCMZ ores (Becker, 2009). Average nickel and copper grades for the MMZ are 0.66-0.68% and 0.22-0.24% respectively, with ~1 ppm platinum-group elements (PGE) in the disseminated ore (Hammerbeck and Schürmann, 1998; Li *et al.*, 2002).

2.2.2. Tati greenstone belt

The ~2.7 Ga Tati greenstone belt occurs on the southwestern margin of the Zimbabwe craton, and consists of a sequence of metavolcanic and metasedimentary rocks subjected to lower greenschist to lower amphibolite facies metamorphism (Maier *et al*., 2008). These rocks are largely surrounded and intruded by granitoids of ~2.73–2.65 Ga in age (Johnson, 1986; Bagai *et al*., 2002).

The Tati greenstone belt has been divided into three formations, in which the volcanic rocks become increasingly felsic towards the top of the succession (Key, 1976; Maier *et al*., 2008). The Lady Mary Formation is found at the base of the greenstone belt, and mainly includes ultramafic, mafic and metasedimentary rocks. The ultramafic and mafic rocks are altered komatiites and komatiitic basalts respectively, with the metasediments consisting of meta-

arkose, quartz-rich schists, metamorphosed limestone, banded iron formation and calcareous rocks (Johnson, 1986). The overlying Penhalonga Formation is characterised by metamorphosed basaltic, andesitic and rhyolitic lavas and volcaniclastic rocks, with the significant metasediments including calcareous phyllites, black shale, limestone and jaspilites (Johnson, 1986). The uppermost Selkirk Formation is mainly composed of dacitic and rhyolitic volcaniclastic rocks, with smaller amounts of mafic volcanics, quartzites and quartz sericite schists (Maier *et al*., 2008). These rocks were intruded by the Phoenix, Selkirk and Tekwane meta-gabbronorites and the Sikukwe meta-peridotite (Figure 2.3; Maier *et al*., 2008).

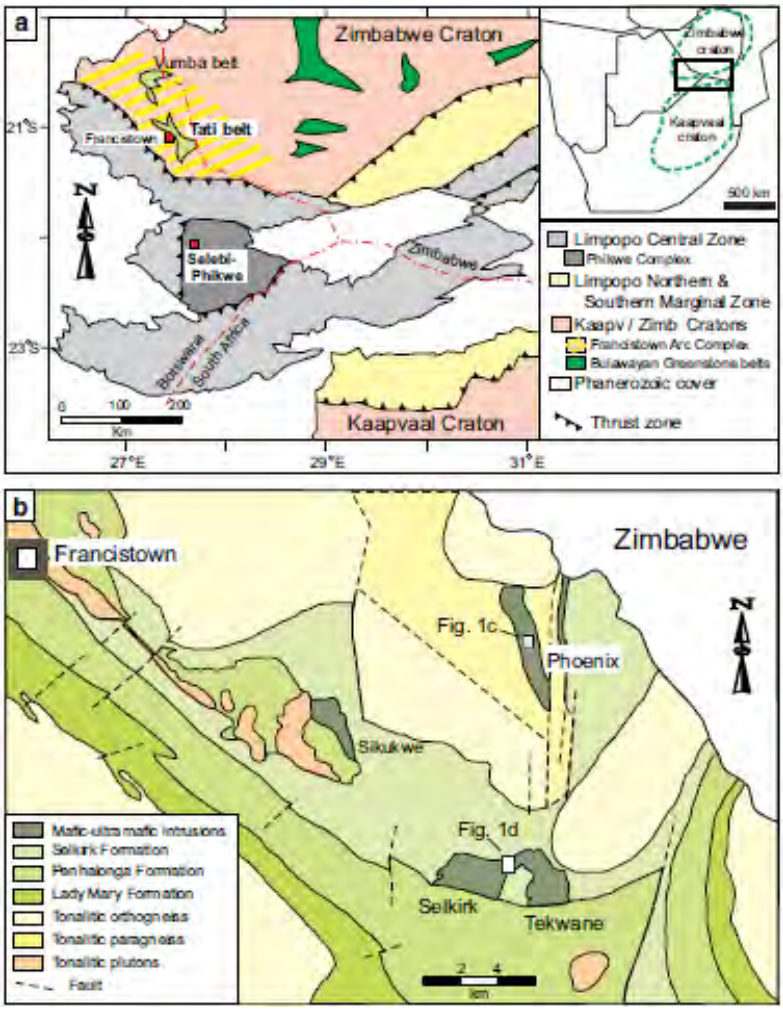

Figure 2.3 Geological map showing **a:** the Tati greenstone belt, and **b:** the location of the Phoenix and Selkirk deposits within the central portion of the belt (from Maier *et al*., 2008)

The Phoenix and Selkirk Cu-Ni-PGE deposits are contained within intrusions that occur approximately 25-30 km south-east of Francistown in eastern Botswana (Johnson, 1986;

Maier *et al*., 2008). The intrusion that contains the Phoenix deposit is an elongated, N-S-trending body approximately 5 km long and 400-1500 m wide (Maier *et al*., 2008). It is made up of weakly deformed metagabbronorites with a mineral composition of hornblende, albite, oligoclase, chlorite, epidote-sericite and quartz (Maier *et al*., 2008). The essential non-sulfide minerals of the rock are plagioclase (often altered to saussurite or sericite), amphibole, chlorite, epidote and quartz, with accessory calcite.

The Phoenix deposit can be classed within the Archaean mafic intrusive type of Ni-Cu deposits, in which disseminated sulfides were formed by igneous processes (Johnson, 1986). Metamorphic re-mobilisation of the disseminated sulfides during later-stage granitoid intrusions is possibly responsible for formation of massive sulfide lenses (Johnson, 1986; van der Wel *et al*., 1998). The dating of zircons in leucogranite intruding the Phoenix deposit gives an age of 1022 ± 16 Ma, and massive sulfide veins are found intruding the leucogranite, indicating massive sulfide mineralisation younger than 1022 ± 16 Ma (van der Wel *et al*., 1998).

The mineralisation of the Phoenix deposit is present as disseminated, massive and vein-like sulfides throughout the metagabbronorite, with the ore minerals being pyrrhotite, pentlandite and chalcopyrite (Maier *et al*., 2008). Average nickel and copper grades are 2.05% and 0.85% respectively (Maier *et al*., 2008). Pyrrhotite is the most abundant sulfide mineral in the Phoenix and Selkirk deposits, containing very small amounts of nickel in solid solution (Becker *et al*., 2010a). Pentlandite is the main source of nickel, occurring mainly as granular inclusions or small flame-like lamellae in pyrrhotite (Maier *et al*., 2008).

2.3. Dense medium separation

2.3.1. Fundamentals

Silicate and carbonate gangue minerals often form a significant proportion of base metal run-of-mine (ROM) ores. Crushing of the rock to obtain partial liberation of the ore minerals makes it possible to separate the host rock from the ore using a gravity separation process such as DMS prior to milling and flotation, with only a minor loss in the valuable metal content (Burt, 1999; Creswell, 2001). This is due to the difference in density between the host rock and the ore, and the partial liberation of the ore minerals at coarse sizes (+1 mm) by crushing. Although the lower density fractions of the host rock normally contain fewer

valuable minerals, they can make up a large mass proportion of the ROM (Creswell, 2001). A preconcentration stage can be used to reject a large mass of ROM with a similar or lower grade to the tailings that would be obtained from the main processing stage (Creswell, 2001), which is flotation in the case of the selected nickel ores. Some important benefits of preconcentration are given below, from Cresswell (2001) and Schena *et al.* (1990):

- Preconcentration increases the throughput of an existing plant without increasing the milling and flotation capacity, or of a new plant to use a smaller milling and flotation section. The improved feed rates are sometimes accompanied by higher overall efficiency.

- Previously uneconomical ores may be considered for mining if they can be upgraded before processing.

- Energy consumed by milling can be reduced by the removal of generally harder host rock silicates.

- The ore eventually subjected to flotation will have a higher grade than the discarded material, which would potentially improve the metal recovery and grade and reduce some of the reagent consumption.

- Mining processes can be simplified by allowing variable proportions of the diluting host rock to be included in the ROM, as it will be removed during DMS.

Dense medium separation is used to preconcentrate ore minerals and reject gangue before grinding for final liberation. Initially, DMS was applied only to the separation of coal from shale, with close to ideal separation conditions and low separation densities, between 1.4 and 1.6 $kg.L^{-1}$ (Burt, 1984). It is now often used on metalliferous ores that are associated with relatively light gangue minerals, where large density differences occur (Wills, 2006). With metallic ores a higher density separating medium is required as compared with coal, of more than 2.65 $kg.L^{-1}$. This is the approximate density of quartz and feldspars, which are often major gangue components of base metal sulfide ores (Burt, 1984). For laboratory separations, naturally heavy organic liquids can be used, such as tetrabromoethane (TBE) and bromoform, which have relative densities of 2.95 and 2.89, respectively. These can be diluted with various other solutions to give a range of densities (Woollacott and Eric, 1994). Due to the high toxicity and cost of natural heavy liquids, they are not used for plant operations.

Suspensions are rather created using finely-ground, high density solid particles such as ferrosilicon (SG 6.7 – 6.9) or magnetite (SG 5.1) mixed with water. The solids used are required to be hard, stable and unlikely to slime as this would affect the medium viscosity. The density of the medium is controlled by varying the solids concentration in the water (Woollacott and Eric, 1994; Wills, 2006). In order to keep operating costs to a minimum, the solid particles of the dense medium should be inexpensive and easily recoverable from the ore particle surfaces and the water, and medium losses should be minimised. Losses usually occur from adhesion to the ore particles after draining and washing, and by the medium remaining in the final effluent after the medium recovery process (Napier-Munn *et al.*, 1995). Medium reclamation circuits are therefore included as part of the DMS procedure so that the solid component can be recycled from the concentrate and waste products (Wills, 2006; Burt, 1984; Woollacott and Eric, 1994).

The most common medium in use for metalliferous ores is ferrosilicon, with magnetite mostly used for coal recovery. The magnetic susceptibility of both of these media enables their efficient recovery using magnetic separation (Wills, 2006; Woollacott, 1994). Ferrosilicon is an iron-silicon alloy, requiring a minimum of 82% Fe for DMS purposes. A higher Fe content will cause corrosion of the alloy and a lower Fe content will reduce its density and magnetic susceptibility. Ferrosilicon is produced in a range of size distributions between 30 and 95% passing 45 μm, and in milled (irregular) or atomised (rounded) shapes, which affect the sedimentation and rheological properties of the medium (Napier-Munn, 1985a; Wills, 2006; Dunglinson *et al.*, 2000).

The separation process is further accelerated by increasing the settling rate of the particles using a centrifugal force (Burt, 1999). Cyclone dense medium separators, also known as hydrocyclones, provide a high centrifugal force and low viscosity in the medium, which enables finer separations than gravitational units, in which the floats are removed by paddles or overflow (Wills, 2006). Other advantages to cyclone separations include a high capacity and sharpness of separation, even when a large mass of the ore is near the density cut-point (Suresh *et al.*, 2010; Magwai and Bosman, 2008). Dense medium separation is mostly applied when the density difference is at a coarse particle size (typically between 0.5 and 40 mm), as the efficiency of the separation decreases with size due to the slower settling rate of the particles (Wills, 2006). Feeds to the cyclones are normally deslimed at approximately 0.5 mm to avoid contamination of the medium and to minimise medium consumption (Dunglison, 1999; Wills, 2006). This is the smallest particle size generally accepted to

produce an efficient separation (Burt, 1984). Particles less than 0.5 mm are also more sensitive to changes in the medium rheology, and clay material contamination within a cyclone contributes to an increased effect of the medium; both these factors contribute to reduced separation efficiency (He and Laskowski, 1994; Davis and Napier-Munn, 1987).

The dense medium cyclone (DMC) typically consists of a cylindrical vessel with a lower conical section, the largest cyclones exceeding 1 m in diameter (Figure 2.4; Ntengwe and Witika, 2011; Wills, 2006). The suspension containing the ore particles is fed into the cyclone through a tangential feed inlet at high velocity and pressure (Gilchrist, 1989). During the separation the feed is rotated under the pressure and the ore particles move radially under centrifugal force, with a low pressure zone produced towards the centre of the cyclone (Suresh *et al.*, 2010). The material denser than the fluid medium (concentrate material in this case) is centrifuged to the wall of the cyclone and is discharged through a spigot to produce the DMC underflow (sinks fraction). The less dense gangue moves inwards to the central axis and exits via the vortex finder to be discharged to the overflow, and is referred to as the DMC overflow (floats fraction). The overflow pipe extends into the cyclone to form the vortex finder, the purpose of which is to avoid the short-circuiting of feed material out through the overflow pipe (Gilchrist, 1989; Ntengwe and Witika, 2011). The underflow and overflow are then passed onto separate vibrating drainage screens, where more than 90% of the separating medium in the products is recovered and pumped back through a sump into the separating vessel (Wills, 2006). Figure 2.5 shows a simplified DMS circuit.

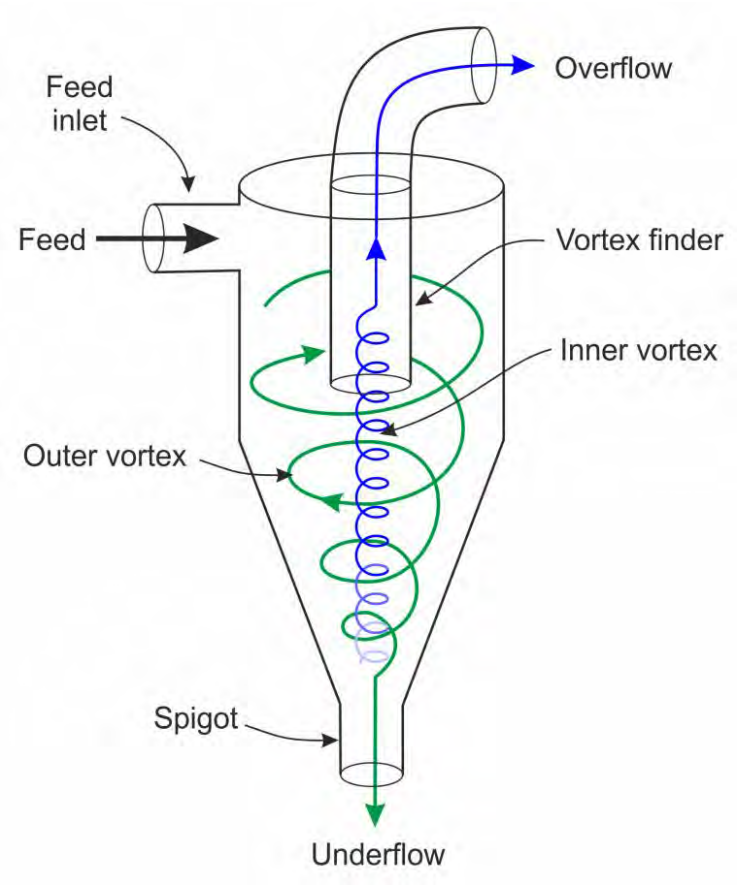

Figure 2.4 Schematic drawing of a DMC, showing major components and flow directions (modified after Mainza *et al.*, 2004 and Dunglison, 1999)

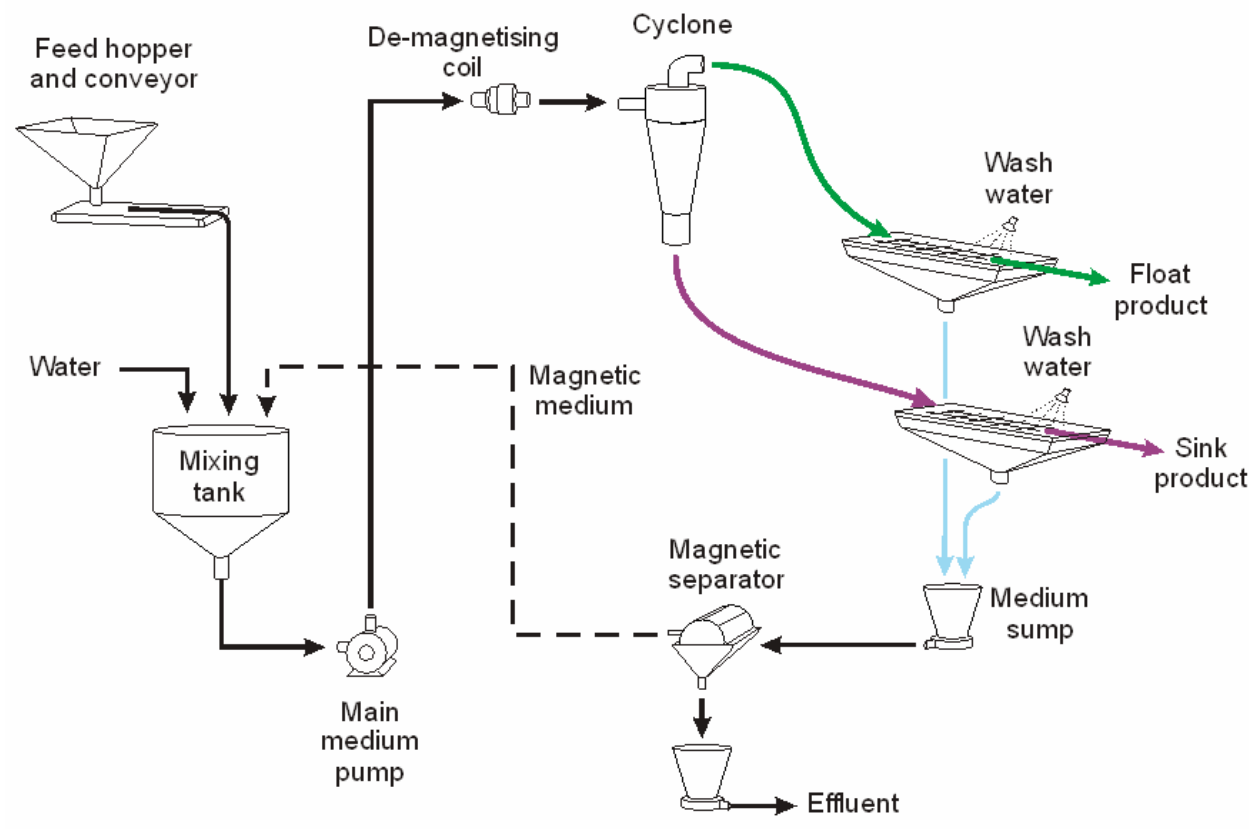

Figure 2.5 Simplified DMS circuit (modified after Bergmann *et al.*, 2010)

Dense medium separation products may be subjected to laboratory separations using heavy liquids in order to determine the separation efficiency. Heavy liquid separation (HLS) may also be performed on ores to establish whether gravity concentration is viable for that specific ore (Burt, 1984; Wills, 2006). The laboratory separation is carried out by means of a sink and float procedure, where liquids of a range of densities are prepared and used to separate the ore particles into a sequence of density classes. Each product can then be weighed and assayed to give density and elemental distributions for the sample. When the analysis is performed on a feed sample, a washability curve can be constructed to indicate the potential for upgrading of the sample, assuming a perfect separation (Bignell, 1978; Wills, 2006; Suresh *et al.*, 2010). The sink-float analyses of the DMS products are used to represent the efficiency of the DMC separation by means of a partition curve (Figure 2.6). The partition or Tromp curve is constructed by relating the partition coefficient to specific gravity. The partition coefficient is the percentage of the feed of any given specific gravity that has reported to either the sinks or floats (Napier-Munn, 1991; Wills, 2006). The sink product is usually used for high density separations (Stratford and Napier-Munn, 1987). An ideal

partition curve indicates a perfect separation, where all particles denser than the separating medium are recovered to the sinks and those lighter than the medium report to the floats, without any particles being misplaced. For actual separations, the partition curve indicates the highest separation efficiency for particles furthest from the density cut-point (Wills, 2006). The area between the theoretical and real curves is the "error area", which indicates the true floats that have reported to the sinks, and vice versa (Burt, 1984; Dunglison, 1999).

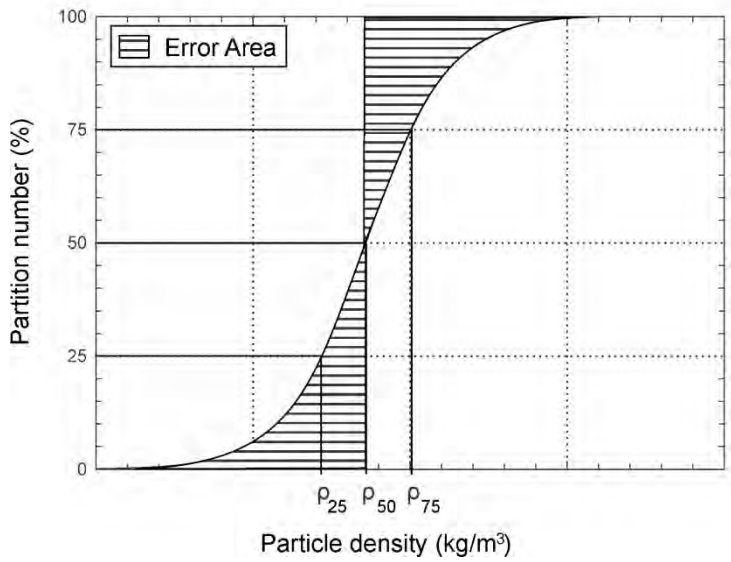

Figure 2.6 Example of a partition curve, showing region of particle misplacement or error area (from Dunglison, 1999)

From the partition curve, the Ecart Probable (Ep) and the separating density (ρ50) are derived, the Ep describing the gradient of the curve and the ρ50 describing its position (Dunglison, 1999; Burt, 1984). The Ecarte Probable, or probable error of separation, is an indication of the efficiency of the separation and is calculated as follows:

$$Ep = (\rho 75 - \rho 25)/2$$

The lower the Ep, the smaller the density difference is between the 25% and 75% partition coefficients, which signifies a smaller error. For a perfect separation the Ep = 0 (Burt, 1984). The ρ50 is the density at which the partition coefficient is 50%, thereby dividing the ore equally between the floats and the sinks (Dunglison, 1999). This is the density where particles have an equal chance of reporting to the floats or the sinks (Burt, 1984).

2.3.2. DMS on Nkomati and Phoenix ores

The Nkomati MMZ ore is processed on mine at the 375 ktpm MMZ concentrator, using fully autogenous milling and flotation (Wolmarans *et al.*, 2011). Preconcentration of the MMZ sulfide minerals has been considered in the past and studies undertaken to investigate the viability of a gravity separation stage preceding milling and flotation (S. Morgan and M. Bryson, unpubl. data; Sibanyoni, 2006). An HLS study was carried out on two disseminated sulfide MMZ samples, the first with a head grade of 0.9% Ni and the second containing 0.7% Ni, which was closer to the typical MMZ disseminated ore nickel grade mined at the time. Nickel and copper upgrades were achieved from both samples, with a waste rejection of more than 30% of the original mass. However, nickel losses to the floats were between 5 and 6%, which is higher than the specified 2 – 3% (S. Morgan and M. Bryson, unpubl. data). Further HLS testwork was conducted on MMZ material by Sibanyoni (2006). Seven samples of open pit material and drill cores were selected for the analysis, with nickel grades ranging from <0.15% to approximately 0.8%. The tests were carried out at a particle size of -25+1 mm. The results showed amenability to gravity separation only at high nickel grades, of at least 0.7%. The losses to the floats increased with a decrease in head grade; a DMS plant would therefore not be feasible owing to significant nickel losses.

The Tati Nickel processing plant is based on the Phoenix mine. Ore from the Phoenix open pit mine is treated at this plant, which additionally treated ore from the now non-operational Selkirk underground mine. Mining at Phoenix began in 1995, with a concentrator set up to process ores by crushing, milling and sulfide flotation. In 2005 an expansion project was undertaken to increase the capacity of the concentrator and the life-of-mine at Phoenix. Lowering the cut-off grade to ~0.25% Ni from between 2.0 – 1.5% was planned for increasing the life-of-mine. The decreased cut-off grade and hardness of the ore led to the consideration of a preconcentration step using a density separation method to reject gangue before milling. Subsequent DMS and flotation testwork indicated that higher nickel grades and recoveries were achieved by using a two-stage DMS process together with flotation, than by flotation only (van Wyk, 2006a). A 1 600 t/hr DMS plant was then constructed at the Phoenix concentrator, the operation of which rejects 60% of the ROM mass while increasing the capacity of the milling-flotation circuit from 470 t/hr to 650 t/hr (Morgan, 2009). A -25 mm feed, deslimed at 1 mm, is used for the DMS at the Phoenix plant. The addition of the DMS stage has contributed to increasing the life-of-mine (till 2023) and overall throughput of the concentrator, and simplified mining processes (Morgan, 2009; www.tatinickel.co.bw).

2.3.3. Factors affecting gravity separation processes

There are numerous mineralogical or particle characteristics that affect overall particle density and therefore the DMS process, such as size, shape, liberation and texture. It is therefore important to fully understand the combined effect these factors have on density separations, in order to optimise the process. To begin with, information on the composition of the minerals present is required so that predictions can be made of the quality of the concentrate that can be produced. The particle compositions and relative mineral proportions determine the minerals of interest and the gangue minerals so that they may be separated from each other. The individual mineral densities and the mineral proportions contribute to the overall particle density. The effective separation of the minerals makes use of the differences in their mineralogical properties (Burt, 1984).

Liberation or releasing of the mineral of interest from the surrounding gangue minerals by crushing is the most important mineralogical factor in a separation. For gravity separation processes, liberation is defined by the volume percent of the ore mineral within the particle. Ideal liberation would be created by breaking up the ore along grain boundaries thus producing monomineralic particles of their original grain size (Burt, 1984). However, for actual ores the rock is broken up randomly into particles containing a combination of minerals in varying proportions. The liberation size of a mineral is the size to which the rock is required to be crushed or milled to create separate particles of either ore or gangue minerals that can be removed at an acceptable efficiency (http://technology.infomine.com). This is dependent on the grain size distribution of the mineral to be liberated, as coarse grains are more easily liberated at large particle sizes, whereas small grains can be liberated only at small particle sizes (Jones, 1987). Since most mineral processing techniques operate best using a limited particle size range, the size for crushing to achieve liberation is required to be within a reasonable range for processing. For DMS, a decrease in particle size towards 1 mm is associated with a decline in efficiency because of the lower settling rate of the smaller particles, the higher viscosity produced by finer particles, and also ore contamination of the medium (Wills, 2006; Napier-Munn and Scott, 1990). Contamination of the medium by fine ore particles creates a higher medium viscosity due to both their small size and lower solids density (Napier-Munn and Scott, 1990). The composition and degree of alteration of the rock contribute towards the production of fines during crushing, as soft alteration minerals such as clays and talc are generally easily broken down into smaller particles. These soft minerals can also break down during separation, contaminating the medium and changing its viscosity.

The breakage and liberation properties of the ore are also governed by the rock texture, which includes grain size, crystallinity, inclusions, associations between ore and gangue minerals and grain boundary relationships (Petruk, 2000, Preti *et al*., 1989). Preti *et al.* (1989) and Ferrara *et al.* (1989) also developed models to predict liberation based on ore textures, including grain shape. Different rock textures were modelled into simplified forms and general equations were developed to relate each type of texture to a particular degree of liberation. Wightman *et al.*, (2014) used mineral mapping to predict ore breakage characteristics and liberation based on meso-scale textures in drill cores.

Cyclones are known to separate on both particle density and size (Burt, 1984; Wills, 2006). Smaller particles are generally associated with a decrease in separation efficiency, as they are more susceptible to medium instabilities (He and Laskowski, 1994). He and Laskowski (1994) reported much higher Ep values for 0.5x0.355 mm feed particles than for 4x2 mm particles. The lower settling rate of smaller particles can also cause them to be pulled into the overflow, creating misplacement of small dense particles (Burt, 1984). Other size effects have also been observed in gravity separation, such as documented by Napier-Munn and Alford (1991), where coarse particles are lost by spirals concentration, which favours finer particle sizes.

Particle shape has been identified as a property that influences the behaviour of particles in a fluid medium as it has an effect on the specific surface area between a solid particle and the surrounding liquid (Jones, 1987). Rounded particles, or those with smooth surfaces, are known to contribute to a lower medium viscosity than rough, angular particles (Napier-Munn and Scott, 1990). For example, the shape of fine FeSi particles within the dense medium suspension (atomised *vs*. milled) produce different medium viscosities within a cyclone, altering the efficiency of the separation (Jones, 1987; Scott *et al.*, 1987). The terminal velocity of particles of different shape was also shown to differ while settling through a fluid medium, with a lower terminal velocity evident for flatter or elongated particles as compared with spherical particles of the same volume. This is due to the higher drag coefficient experienced by the non-spherical particles, with the experiment carried out using glass beads (Furuuchi and Gotoh, 1992). The residence time of particles in a cyclone has also been shown to be longer for cubes than for flatter particles (Napier-Munn, 1985b). Jig separation tests on coal by Brożek and Surowiak (2007) further indicate that the range in settling velocity for a set of particles is strongly influenced by the distribution of their particle shape coefficients.

This results in flatter, high density particles reporting to the light product. The study reported, on average, a 70% higher process inefficiency with irregular-shaped particles.

A study by Napier-Munn and Alford (1991) using wet gravity concentration methods on heavy mineral sands showed that the concentrator tailings contained more elongated rutile grains than the concentrate streams. Wright trays and spiral sluices were used, and statistical chi-square tests showed that, usually with 95% confidence, particle shape is a function of the product (concentrate or tailings) and elongated grains preferentially report to the tailings of both the trays and spirals. Approximately 20% of the heavy mineral losses were attributed to the tendency of the wet gravity concentrators to lose elongated grains (Napier-Munn and Alford, 1991). According to Ferrara *et al*. (2000), after a study on the DMS behaviour of plastics, differences in shape can hinder the density separation process as a result of the complex flow patterns within a cyclone and the high centripetal flow, which selectively drags flat and elongated particles to the overflow, regardless of their density. They also showed that finer particles may be preferentially dragged to the overflow, and that more compact particles such as cubes may have sharper separations than elongated or flattened/platy particles (Ferrara *et al*., 2000). Figure 2.7 shows partition curves for cubes, plates and elongated prisms, assuming an equal size distribution for each sample. A fourth partition curve was also calculated by mixing all the particles of different shapes and sizes (Ferrara *et al*., 2000).

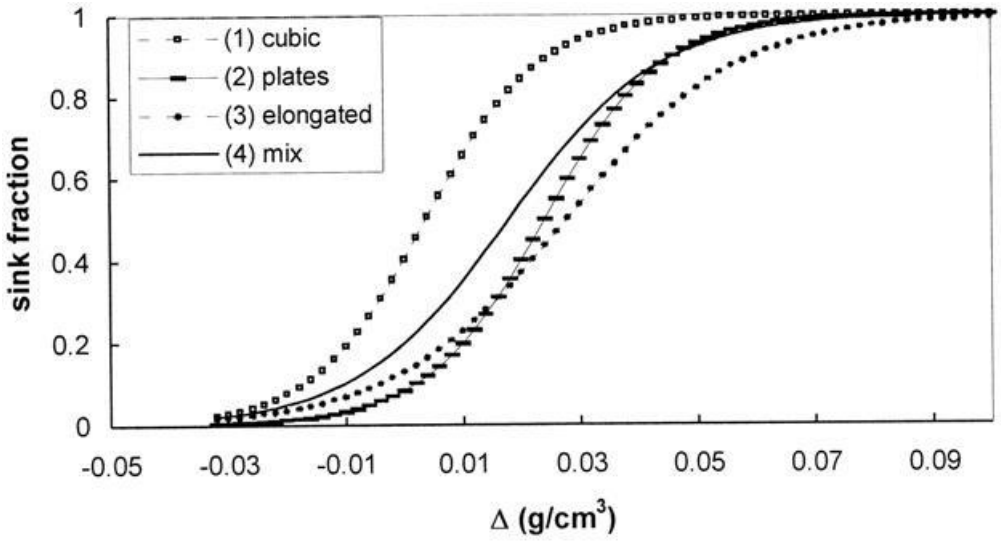

Figure 2.7 Mean partition curves for particles of different shapes (from Ferrara *et al*., 2000)

Houseley *et al*. (1994) studied the behaviour of gold grains during comminution and gravity concentration. The project involved the characterisation of gold grains within the different

products of a gravity separation process. The geometry of the particles was quantified using mathematically-derived shape factors based on work by Heywood and calculated in terms of length (L), breadth (B) and thickness (T). In this instance, grains reporting to the concentrate and tailings did not show any difference in length and breadth, and therefore no variation in Heywoods elongation ratio (n = L/B) (Figure 2.8). There was, however, a significant difference in thickness between the particles of the concentrate and tailings, especially in the larger size fractions of the samples. Variations of up to 90% were observed, with much lower particle thicknesses occurring in the tailings. This was quantified using the Heywoods flakiness ratio (m = B/T) and volume shape coefficients. Both these shape factors indicate that tailings particles have a higher degree of flakiness than particles of the same size within the concentrate (Figures 2.9 and 2.10; Houseley *et al*., 1994).

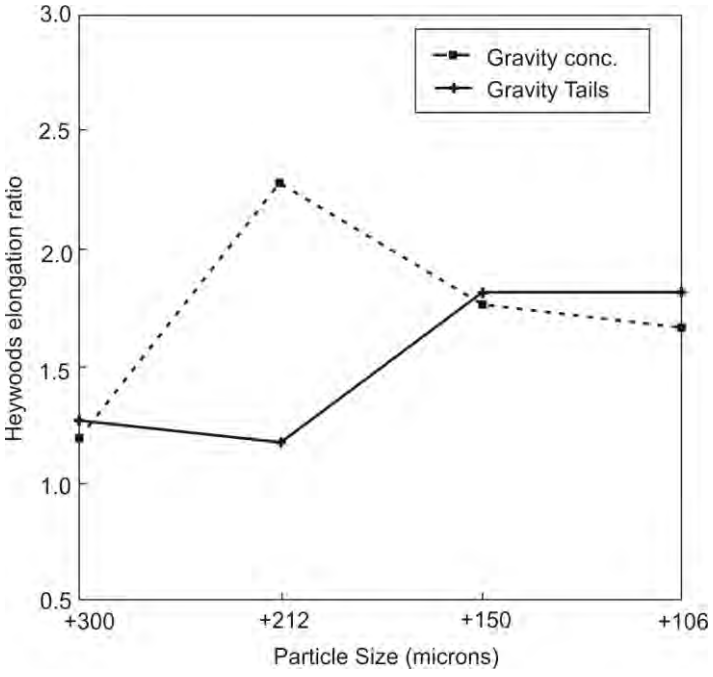

Figure 2.8 Heywoods elongation ratio for gold grains within different size fractions of a gravity concentrate and tailings (from Houseley *et al*., 1994)

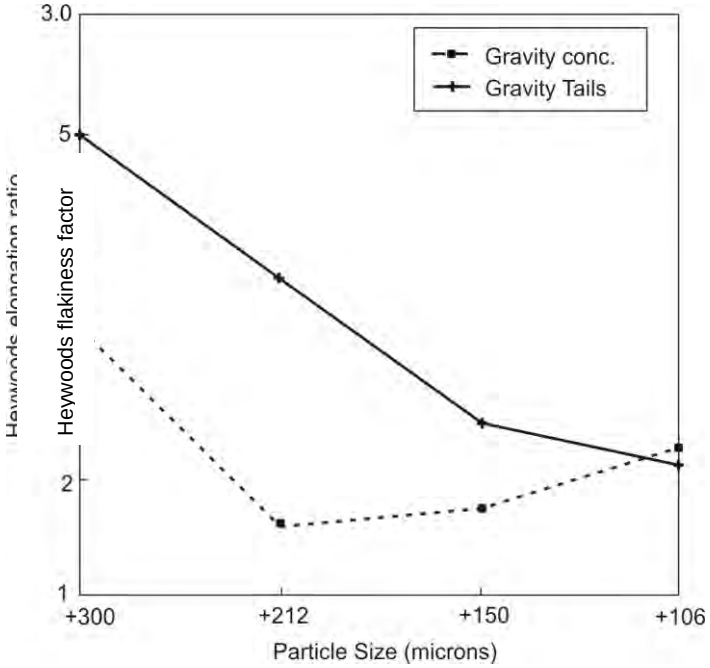

Figure 2.9 Heywoods flakiness ratio for sized gold grains for a gravity concentrate and tailings (from Houseley *et al*., 1994)

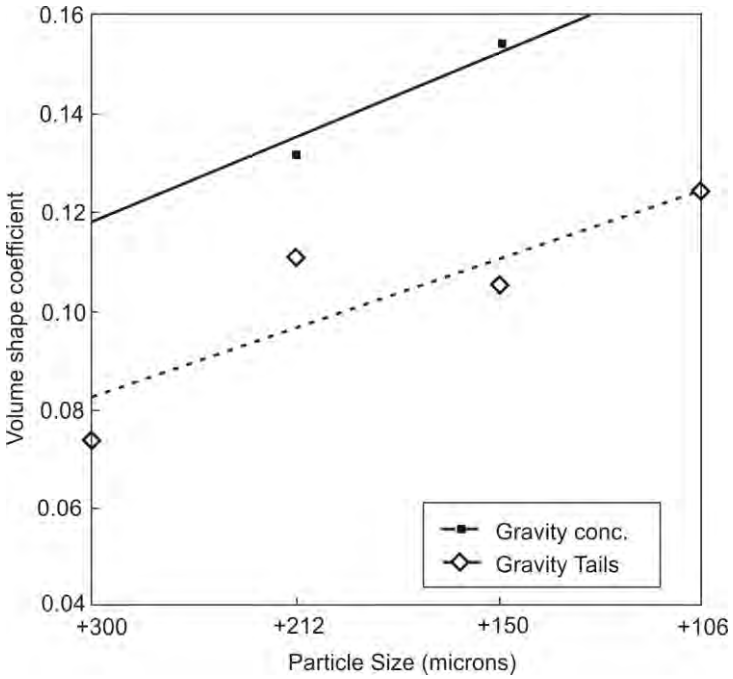

Figure 2.10 Volume shape coefficients for sized gold grains in a gravity concentrate and tailings (from Houseley *et al*., 1994)

2.4. Process mineralogy

From the scoping stage of a resource to the processing of ores, mineralogy can be a useful tool in ore process design and optimisation. This has given rise to modern process mineralogy, which is defined by Lotter *et al.* (2011) as an integrated discipline incorporating aspects of quantitative mineralogy, metallurgical testing, representative sampling and geometallurgy. Process mineralogy is widely used in various metallurgical processes, from preconcentration to flotation, bioleaching and smelting (e.g. Goodall *et al.*, 2005; Grobler and Bosman, 2009; Lee *et al.,* 2011; Lotter *et al.*, 2011; Mkhize and Andrews, 2011; Bushell, 2012).

Owing to the complexity of many orebodies, mineralogical characteristics and microtextures cannot always be properly quantified using manual optical microscopy methods (Gottlieb *et al*., 2000). Quantitative automated scanning electron microscopy (SEM) techniques such as QEMSCAN (Quantitative Evaluation of Minerals using Scanning Electron Microscopy), MLA (Mineral Liberation Analyser), TIMA (TESCAN Integrated Mineral Analyser) and Mineralogic have therefore become important in ore characterisation for mineral processing. These methods work using automated image analysis fitted to SEM systems, which identifies minerals and textures with the aid of energy-dispersive spectrometry (EDS) and backscattered electron (BSE) imaging (Hagni, 2008, Fandrich *et al.*, 2007, Gu, 2003; Gottlieb *et al.*, 2000). Such automated SEM analyses provide fully-quantified modal mineralogy and textural information including grain or particle sizes, degree of liberation, mineral association, elemental deportment and shape factors. The accurate description of these properties is important for metallurgical processing, and with automated SEM technology, they can be measured for large particle populations at fast rates with high accuracy using automated measurements (Fandrich *et al.*, 2007). Gu *et al.* (2014) have recently attempted to quantify the value of the information provided by automated mineralogy in optimising processing plant performance. Their methodology showed a higher return on investment for projects where automated mineralogy is an early step in ore characterisation. The importance of mineralogical input into processing operations is expected to give rise to more plant-based automated mineralogy systems providing quick, routine analysis (Baum, 2014).

The importance of liberation analysis in particular has been noted by Burt (1984), Jones (1987), Petruk (2000) and Lastra (2007) as the aim from the primary stages of processing is to liberate the ore minerals from the gangue minerals, and the assessment of the mineral

liberation is key to improving plant operations. Figure 2.11 shows mapped particles from a QEMSCAN measurement and how they can be classified according to different mineral or particle properties, in this case liberation and particle size classes.

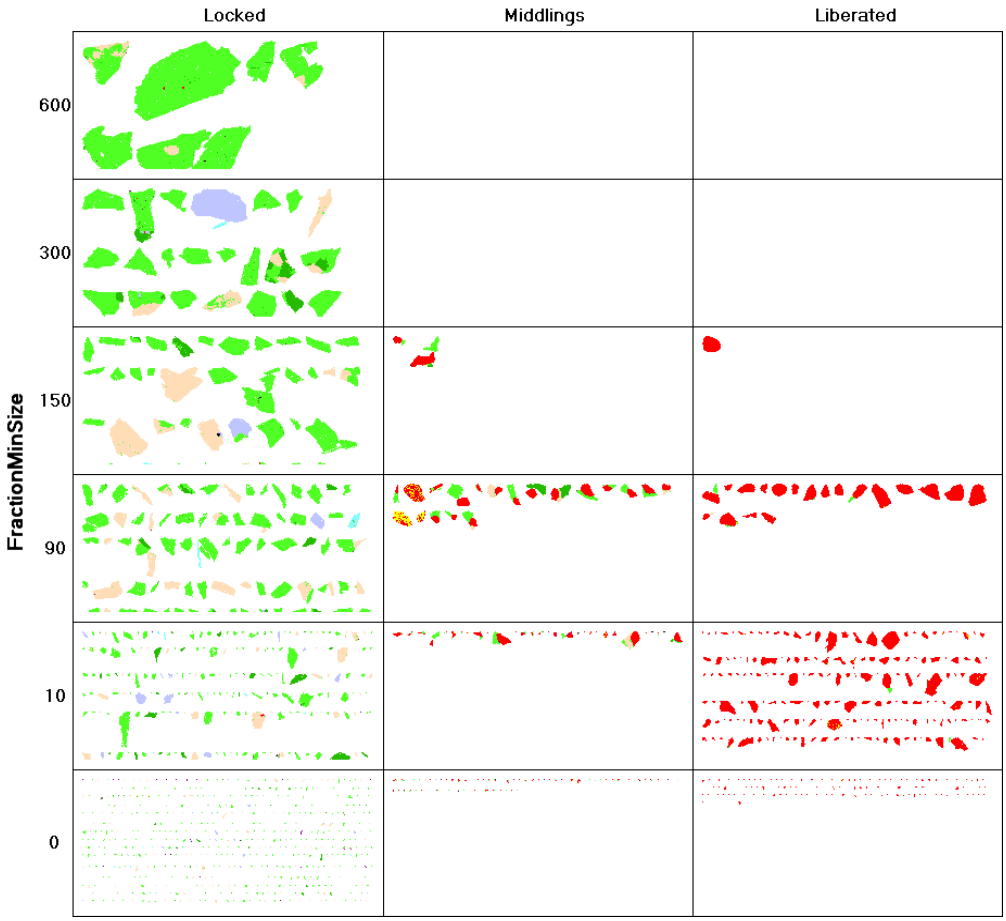

Figure 2.11 Example of mapped particles from a QEMSCAN, which are categorised above according to the liberation of a particular mineral of interest (in red) and minimum particle size in microns (y-axis). Liberation classes: locked = <30% of particle area, middlings = 30 – 80% of particle area, liberated = >80 of particle area.

Although automated SEM methods dominate the field of process mineralogy, traditional mineralogical techniques such as X-ray diffraction (XRD), optical microscopy and electron probe microanalysis (EPMA) are still widely used in the characterisation of ores and metallurgical products for mineral processing applications (Dold and Fontboté, 2001; de Villiers and Verryn, 2007; Chetty, 2008). Chemical analyses using methods such as X-ray fluorescence (XRF) spectrometry and Inductively Coupled Plasma Optical Emission Spectrometry (ICP-OES) are important complementary techniques to mineralogical analysis, to determine elemental distribution and metal grades, and for quality assurance of

mineralogical data. These mineralogical and chemical techniques are often used in conjunction with automated SEM analysis (Lotter *et al.*, 2011; Becker, 2009). Quantitative XRD using the Rietveld refinement procedure (Rietveld, 1969; Young, 1995) is one of the techniques commonly in use for quantitative phase analysis in the metallurgical industry. Knorr and Yang (2011) and Chetty (2008) have demonstrated the use of Rietveld quantification in the characterisation of iron and manganese ores respectively, in order to provide a means of quality control for feed material into furnaces. The method is especially useful for the classification and cluster analysis of large numbers of samples, and for ferrous metal ores, as shown by Knorr and Yang (2011) and Chetty (2008), where metal oxide minerals of similar composition cannot be easily distinguished using automated SEMs. Recent developments in 3D X-ray computed tomography have contributed to the three-dimensional evaluation of ores for process mineralogy studies (Miller *et al.*, 2009; Ghorbani *et al.*, 2013).

The importance of mineralogy in gravity concentration processes was highlighted by Burt (1984), stating that the thorough understanding of the mineralogy of the ore being treated was essential to effective gravity separation. The essential mineralogical information required in order to produce a detailed characterisation prior to gravity separation was listed as: identification, composition, proportions, grain size, mineral properties, texture and liberation. In addition, Burt (1984) described the concept of Concentration Criterion (CC), which is an expression used to determine whether an ore is amenable to gravity concentration. This can be shown by the equation:

$$CC = (\sigma_h - \sigma_f) / (\sigma_l - \sigma_f)$$

where:

σ_h = specific gravity of the heavy mineral in $kg.m^{-3} \times 10^{-3}$
σ_l = specific gravity of the light mineral in $kg.m^{-3} \times 10^{-3}$
σ_f = density of suspending fluid in $kg.L^{-1}$

The Concentration Criterion is highest when particles are composed of liberated minerals. It must, however, allow for particle shape differences, which affect the settling rates of the particles. This is done by multiplying the Concentration Criterion by a shape ratio factor. The calculated Concentration Criterion is usually compared with a standard curve, at the correct

particle size (Figure 2.12). The curve represents the point at which gravity separation is not possible (Burt, 1984).

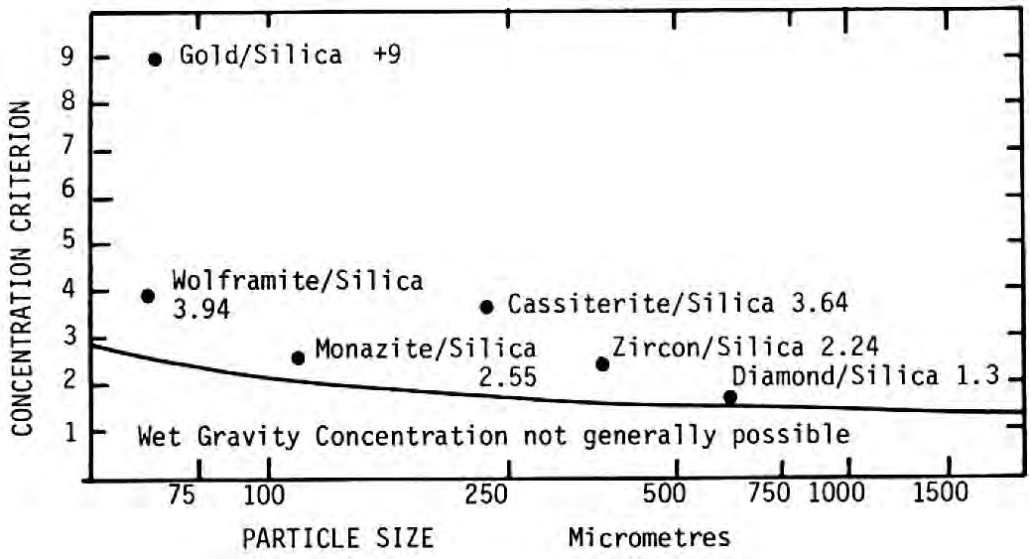

Figure 2.12 Calculated Concentration Criterion for various mixtures at different particle sizes (from Burt, 1984)

Grobler and Bosman (2009) showed, using heavy mineral sands, that it is possible to use QEMSCAN analysis for the characterisation of particles being fed through gravity separators. The particle mineral analysis (PMA) measurement mode was used to map individual particles of a sample and derive textural as well as mineralogical data from these particles. The PMA data can then be used to plot particle size, shape and density distributions, which are all gained from a single measurement (Grobler and Bosman, 2009). The use of the iExplorer software package on a QEMSCAN also makes it possible to group particles on the basis of a variety of mineralogical and particle properties such as mineral association, degree of liberation, grain or particle size and density, and obtain the data associated with each category (Pascoe *et al*., 2007). This information is useful in the modelling of gravity separator performance (Grobler and Bosman, 2009).

QEMSCAN analysis was also used by Pascoe *et al*. (2007) on a chromite feed sample to show that QEMSCAN data can be used as a semi-quantitative measure for the modelling of gravity separation equipment. Particle and grain sizes measured on a QEMSCAN tend to be, on average, underestimated as these are measured across a two-dimensional surface, but these

errors can be significantly reduced if sufficient particles are analysed (Pascoe *et al*., 2007; Figure 2.13).

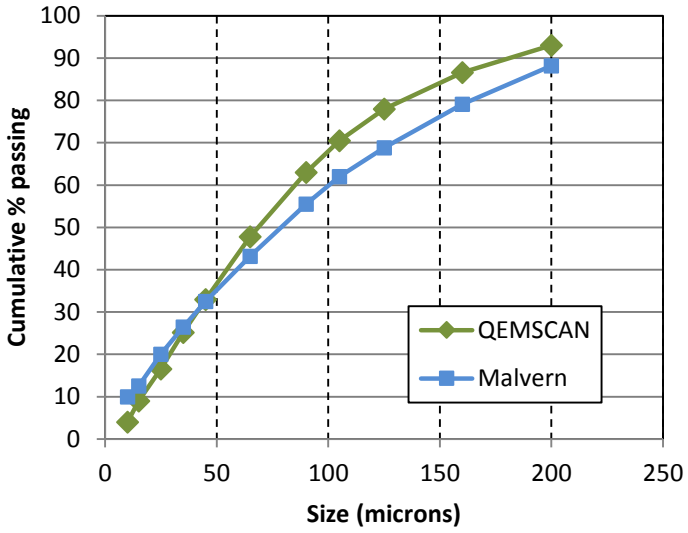

Figure 2.13 Comparison of the particle size distribution of a chromite feed sample using QEMSCAN analysis and a Malvern laser particle sizer (from Pascoe *et al*., 2007)

Recent process mineralogy studies on nickel ore were conducted by Lotter (2011) and Lotter *et al.* (2011) using QEMSCAN analysis on ore from selected Canadian high grade Ni-Cu-PGE deposits (>1% Ni). In-situ QEMSCAN mapping of defined geometallurgical units of each deposit produced information on host rock textures and the sulfide mineral distribution within the units, with EPMA used to accurately calculate elemental deportment (Figure 2.14). The mineralogical data acquired, including grain sizes, liberation, metal deportment and mineral associations, were then integrated into testwork programmes and were used to optimise milling and flotation conditions at their concentrators for each unit.

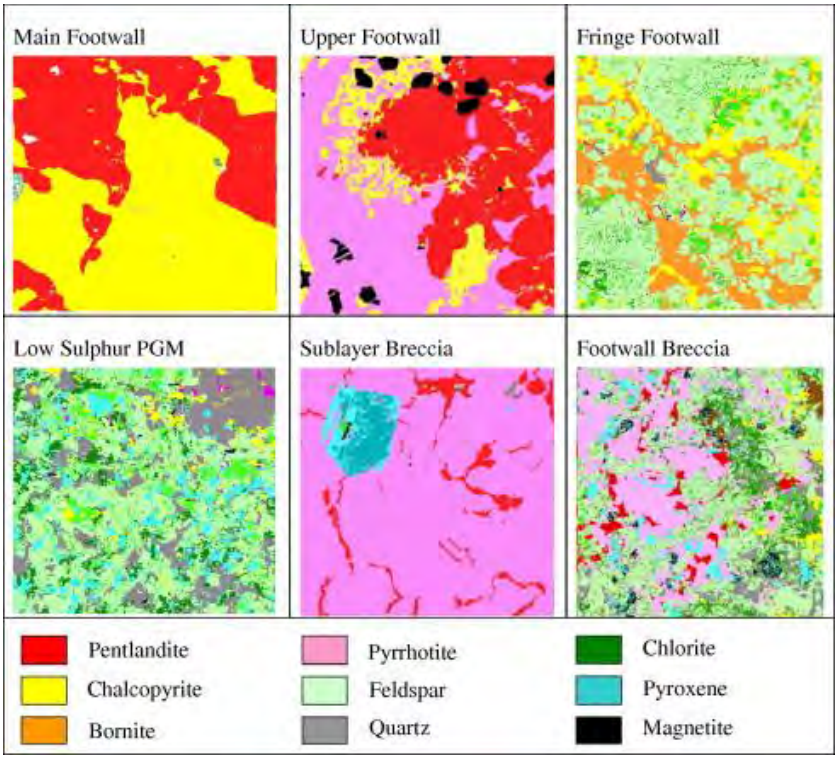

Figure 2.14 Textures of the geometallurgical units of a Ni-Cu-PGE deposit, as observed from QEMSCAN mapping (Lotter *et al.*, 2011)

Evans *et al.* (2011) carried out quantitative mineralogy on a Ni-Cu sulfide ore from the Timmins area in Canada. The MLA was utilised to perform modal analysis and sulfide mineral liberation analysis on concentrator samples as part of the development of a "Mill to Melt" methodology. This method is used to model and optimise energy consumption throughout the processing stages from milling and flotation to smelting. Pentlandite liberation characteristics were used upfront to optimise the primary grind size of the ore in terms of energy consumption. The gangue minerals present were also an important consideration in terms of their natural flotation behaviour, and their properties were important in predicting the entrainment of gangue to the concentrate. The mineral compositions of the final nickel and copper concentrates and the chemical composition of the samples as calculated from the mineralogy were incorporated into smelter models in order to calculate the energy required to produce blister copper and nickel matte from the concentrates. The final results indicate a significant reduction in energy requirements throughout the processing chain if a small amount of energy is used to regrind the rougher concentrate.

Other studies on nickel-bearing ores incorporating process mineralogy include Marape and Vermaak (2012), Becker (2009), Becker *et al.* (2010b), Ekmekçi *et al.* (2010), Mphela

(2010), Mulaba-Bafubiandi and Medupe (2007) and Mishra *et al.* (2013). Becker (2009) in particular, combined a variety of mineralogical tools to characterise pyrrhotite in a variety of deposits worldwide, including the Nkomati and Phoenix ores. Pyrrhotite was focused on owing to its importance in the sulfide mineral assemblages of these ores, and in nickel flotation. The mineralogical, crystallographic and electrochemical properties of the different pyrrhotite types were used to assess their flotation behaviour. For laterite ores, a major study was carried out by Whittington *et al.* (2003), tracking the occurrence of the nickel from a leach feed, to the leach liquor and residue. The mineralogical properties of an ore were shown to govern the composition of the leach liquor and residue, affecting further extraction of the nickel.

2.5. Critical discussion

Dense medium separation has been tested previously on various samples of Tati and Nkomati ore (Sibanyoni, 2006; van Wyk, 2006b; King *et al.*, 2007; van Zyl *et al.*, 2009; Morgan, 2009; S. Morgan and M. Bryson, unpubl. data). The results have demonstrated the highest upgrade potential for the Tati ores, particularly from the Phoenix deposit, with the Nkomati samples showing that for most of the regions sampled at the mine, DMS was not viable. There is, however, no understanding of the reason for the differences in the separation of these ores. This is due to the lack of mineralogical data available on the majority of samples that were tested, from which differences in the ores could be observed. The few mineralogical analyses carried out did not include any quantitative characterisation of the mineral properties (e.g. van Wyk, 2006a).

Process mineralogy is well-established in minerals processing, playing an essential role in most metallurgical operations. The characterisation of the particles that are meant to undergo separation is very important in assessing the mineral processing potential of ores at all processing stages (Evans *et al.*, 2011). During processing, mineralogical information is also a valuable problem solving tool and can provide vital information regarding process inefficiencies. Automated SEM analysis is commonly used for the particle measurements as high quality, quantitative data can be produced. Theoretical grade-recovery curves can be calculated for a process from automated SEM data, and are determined by the mineralogy and texture of a particular feed sample (Cropp *et al.*, 2013). Cropp *et al.* (2013) also showed the importance of gangue mineralogy as an influence on mineral recoveries. Although generally an expensive undertaking, upfront process mineralogy has been shown to provide a

high return on investment and generate cost savings by predicting potential plant problems (Gu *et al.*, 2014).

Regarding DMS, very little has been published on mineralogical controls on the process, with some literature available on process mineralogy of samples derived from other gravity concentration methods (e.g. Grobler and Bosman, 2009). Historically, laboratory heavy liquid separation tests were considered sufficient assessment of the ore characteristics prior to DMS. Laboratory separations are, however, considered perfect separations, with a number of particle properties present that would additionally affect separation in a dynamic cyclone environment. It is therefore important to study the combined mineralogical properties using quantitative minerals in order to understand their effect on cyclone DMS. There are difficulties in analysing large particles by automated SEM, which may have contributed to the technique seldom being applied to gravity separation. These are related to the instrument magnification and the number of particles required to be analysed to collect a statistically valid dataset.

There have been various studies undertaken on the geology and ore mineralogy of nickel sulfide deposits including Phoenix and Nkomati, with the sulfide mineral assemblages, mineral chemistry and textural relationships well-documented (Li *et al.*, 2002; Maier *et al.*, 2008; Mishra *et al.*, 2013). Much has also been published on the process mineralogy of nickel sulfide ores, relating the sulfide mineral characteristics to their processing behaviour in order to improve their recovery (Mulaba-Bfubiandi and Medupe, 2007; Becker, 2010b; Evans *et al.*, 2011; Lotter *et al.*, 2011; Mishra, 2013). Little focus has been placed on the gangue mineralogy in the past; this is of growing interest due to the need for the processing of low grade ores. Even with respect to DMS, gangue minerals have always been evaluated together and their combined properties used to predict particle behaviour. This approach may be inadequate for assessing the gravity separation amenability of an ore sample, as there can be significant differences in density and other properties of gangue minerals alone. The characteristics of individual gangue minerals of an ore therefore need to be accounted for in order to fully understand the separation characteristics of the ore.

Based on the limitations of the existing literature, this thesis aims to focus on the detailed characterisation of the gangue mineralogy of the selected ore deposits, using modern quantitative process mineralogy techniques. The information produced is used to better understand the differences in DMS recovery for each of the ores, and the mineralogical factors influencing the process.

CHAPTER 3: METHODS

3.1. Introduction

The methods of approach followed for addressing the objectives of the study include bulk sampling, sink-float analysis, dense medium separation, bulk chemical assaying and mineralogical analyses. These are illustrated schematically in Figure 3.1 with details given in the subsections following. Bulk chemical assays were performed on all samples, and mineralogical analyses on samples highlighted in blue (Figure 3.1).

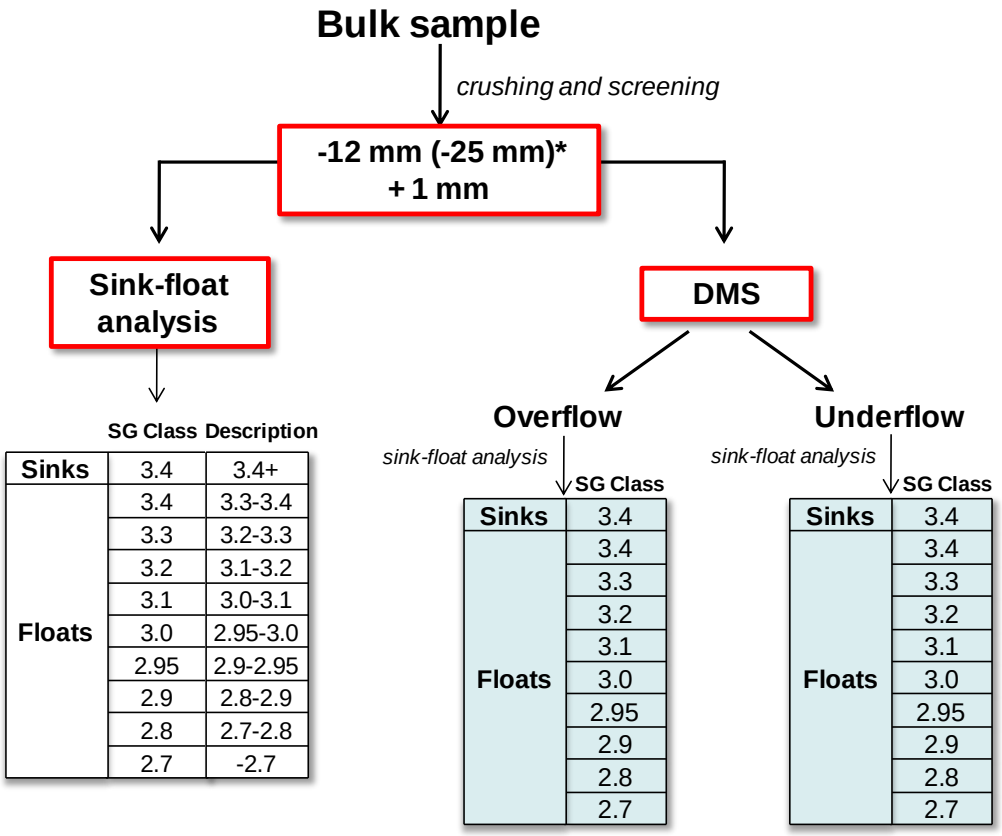

Figure 3.1 Flow diagram showing sequence followed. *A crush top size of 12 mm was used for the Nkomati ores, and 25 mm for the Phoenix ore.

3.2. Bulk sample preparation

The MMZ ore that was sampled originates from Pit 2 of the Nkomati Mine. The ore is sent to a primary crusher, and then passed onto a conveyor belt to the secondary crusher. This conveyor belt was stopped, and ore within a 3 m length was sampled to make up

approximately one tonne of material. For the Phoenix ore a 1 023 kg portion of DMC feed from the Phoenix plant was supplied for this study, crushed to -25 mm.

3.2.1. Crushing

A DMC feed size of -12 mm was chosen for the testwork on the Nkomati MMZ ore. A pilot-scale jaw crusher was used for the first stage of crushing (Figure 3.2). This breaks down particles to less than ~20 cm in size. Particles smaller than 12 mm were screened out and the +12 mm material then subjected to crushing using a laboratory jaw crusher. This crusher breaks down the particles to sizes less than ~20 mm. After each stage of crushing, the -12 mm material was screened out and only the +12 mm was put through the crusher until all particles passed through a 12 mm screen. The repeated screening out of the -12 mm particles during stage crushing results in the generation of a lower overall amount of fines in the sample.

Figure 3.2 Pilot-scale jaw crusher used to break down large ore particles to less than ~20 cm

3.2.2. Sub-sampling

The mass of the bulk sample was recorded before any further sampling was done. The bulk sample was then blended over a concrete pad using a hopper on rails, to homogenise the material for sub-sampling (Figure 3.3). A sub-sample of approximately 20 kg was removed and halved using a riffle splitter to produce a ~10 kg representative head sample for assaying.

The remaining sample was then de-slimed by screening out material of less than 1 mm particle size, as the fines cause contamination of the medium during DMS, and the efficiency of the process is reduced with a decrease in particle size. The resulting two fractions (+1 mm and -1 mm) were then sub-sampled into portions of ~10 kg each, and an additional 50 kg of the +1 mm material was removed for the laboratory sink-float analysis. The three 10 kg samples were split using a spinning riffler, to provide representative samples for chemical analyses. The remaining +1 mm bulk samples of each ore were put through the DMS pilot plant. These sub-sampling processes are important for ensuring that the samples subjected to density testwork, chemical analysis and mineralogical analysis are all equally representative of the original bulk sample and the results from these tests are comparable.

Figure 3.3 A: Blending and homogenising of the Nkomati bulk sample using a hopper on rails; **B:** Sub-sampling prior to riffle splitting.

3.3. Sink-float analysis

Sink-float analyses using laboratory heavy liquid separation (HLS) at Mintek were carried out on a representative head sample of each ore to separate the sample into particles within different density classes. This was performed on each dense medium cyclone (DMC) feed prior to the pilot plant testwork, to establish whether a nickel upgrade could be achieved by DMS and to choose a suitable density cut-point at which to run the DMS plant, and also on the DMC overflow and underflow to evaluate the efficiency of the separation.

The chemical used for the sink-float analysis is tetrabromoethane (TBE), which has a specific gravity (SG) of 2.96. To obtain a SG of less than 2.96, the TBE is diluted using acetone in varying concentrations depending on the required liquid density. Tetrabromoethane is highly toxic and various safety precautions were taken, according to standard operating procedures at Mintek, when working with the substance to avoid any exposure. For SGs greater than 2.96, -25 μm atomised ferrosilicon (FeSi) powder, with an approximate SG of 7, is mixed with the TBE to produce the required cut-points. The quality and size of the FeSi creates a stable suspension with a very low FeSi settling rate. The medium is therefore stable for the duration of the test, and the test is considered a perfect separation. The SG cut-points used for the HLS were 2.7, 2.8, 2.9, 2.95, 3.0, 3.1, 3.2, 3.3 and 3.4. The material less dense than each liquid density is referred to as the "floats" for that specific cut-point, and the material denser than the medium is referred to as the "sinks".

3.4. Dense medium separation

The bulk of each ore sample was put through a DMS pilot plant at Mintek, which consists of a Multotec cyclone model CL350-20-1/BB-A, with a 360 mm diameter and 100 mm spigot (Figure 3.4).

Figure 3.4 Dense medium cyclone at the Mintek pilot plant

Cyclone 150D FeSi (approximately 80% passing 45 μm) was mixed with water to create the dense medium. The FeSi is continuously recycled during the running of the plant. The

operating conditions given in Table 3.1 were used for both the Nkomati and Phoenix ores and monitored throughout the separations to ensure consistency.

Table 3.1 Plant operating conditions for the bulk samples

Condition	
Feed density (SG)	2.60
Underflow density (SG)	3.10
Overflow density (SG)	2.43
Pressure (kPa)	100

The aim of the DMS testwork was to achieve a meaningful nickel upgrade to the DMC underflow in order to compare the mineralogical properties of the separation products.

3.5. Chemical analysis

Major element chemical analyses were conducted on pulverised sub-samples of all samples to measure the metal grades of the various feeds and products and for validation of the mineralogical data. The analyses were carried out by Mintek's Analytical Services Division.

3.5.1. ICP-OES

The major element composition of each sample was determined by ICP-OES (Inductively Coupled Plasma Optical Emission Spectrometry). The samples were analysed in solution using a Varian Vista-PRO spectrometer with scandium added as an internal standard. The instrument was calibrated with synthetic solutions containing the elements that were analysed. Certified reference standards were run together with the samples as check standards for quality control.

3.5.2. Combustion ("LECO")

The samples were analysed for total sulfur content using LECO CS-200 and Eltra CS-2000 carbon/sulfur analysers. The instruments were calibrated using certified reference standards, and check standards were analysed together with the samples for quality control purposes.

3.6. Mineralogy

3.6.1. X-ray diffraction (XRD)

A representative sub-sample of each sample was pulverised using a swing mill. Two grams of material were then removed from each sample and micronised in ethanol for 10 minutes using a McCrone micronising mill. X-ray diffraction analysis was performed on the powdered material to determine the differences in the bulk mineralogy of each sample. A Bruker D8 Advance diffractometer with a LynxEye detector was used, with Fe-filtered CoKα radiation. Samples were measured over a range of 5 – 80° 2θ, with a step size of 0.02° 2θ and a counting time of 8 seconds per step. The instrument was operated at 35 kV and 40 mA.

The data produced were quantified using Rietveld refinement together with the fundamental parameters approach (FPA). The FPA is based on an accurate description of the physical characteristics and configuration of the diffractometer in which the sample is measured (Pecharsky and Zavalij, 2005; Chetty, 2008). The Rietveld method is possible if all minerals have been identified prior to the refinement, all phases are crystalline, and if their crystal structures are known (Knorr and Yang, 2011). The refinement compares a calculated profile with the measured diffraction profile, and aims to minimise the difference between the two by means of refining specific parameters so that multiple phases may be quantified together (Taylor and Hinczak, 2003). The Inorganic Crystal Structure Database (ICSD) was the source of the crystal structure information that was used to calculate the diffraction pattern (FIZ-Karlsruhe, 2003; Smith, 1989). The Bruker TOPAS (Total Pattern Analysis Solutions) software package was employed for the quantification.

The NIST standard reference material (SRM) 660a, lanthanum hexaboride (LaB_6), was prepared and run on the instrument to be refined using TOPAS. A LaB_6 crystal structure file was used to fit the pattern acquired in order to verify the instrument parameters. The refined instrument parameters were then saved and used for the refinement of subsequent samples (Table 3.2). The LaB_6 pattern is given in Figure 3.5, showing the measured diffraction profile (in blue), the profile calculated using the known crystal structures (in red), and the difference between the measured and fitted patterns (grey residual pattern). Two criteria are generally used to assess the fit achieved. The weighted pattern residual, R_{wp}, shows the progress of the refinement and indicates the fit of the calculated profile to the measured profile. The goodness-of-fit (GOF) is also an assessment of the data quality, showing how well the fitted profile accounts for the data observed. Theoretically, the R_{wp} of a perfect fit is 0, and an ideal

GOF is 1 (Chetty, 2008; Young, 1993). The R_{wp} is generally used to track the progress of the refinement with the number being lowered as the refinement is improved on. For GOF, values <2 are generally accepted. The R_{wp} calculated for the LaB_6 standard is 5.43 and the GOF is 1.85, which are acceptable values. The residual pattern also shows that a reasonably good fit was achieved between the measured and calculated patterns. Given this result, the instrument parameters were considered accurate, and fixed prior to refinement of diffractograms, such that only sample effects were refined.

Table 3.2 Instrument parameters for the Bruker D8 diffractometer

Parameter	Range
Primary radius (mm)	280
Secondary radius (mm)	280
Linear PSD 2Th angular range (°)	4
FDS angle (°)	0.3
Beam spill, sample length (mm)	20
Filament length (mm)	12
Sample length (mm)	15
Receiving Slit length (mm)	12
Primary Sollers (°)	2.5
Secondary Sollers (°)	2.5

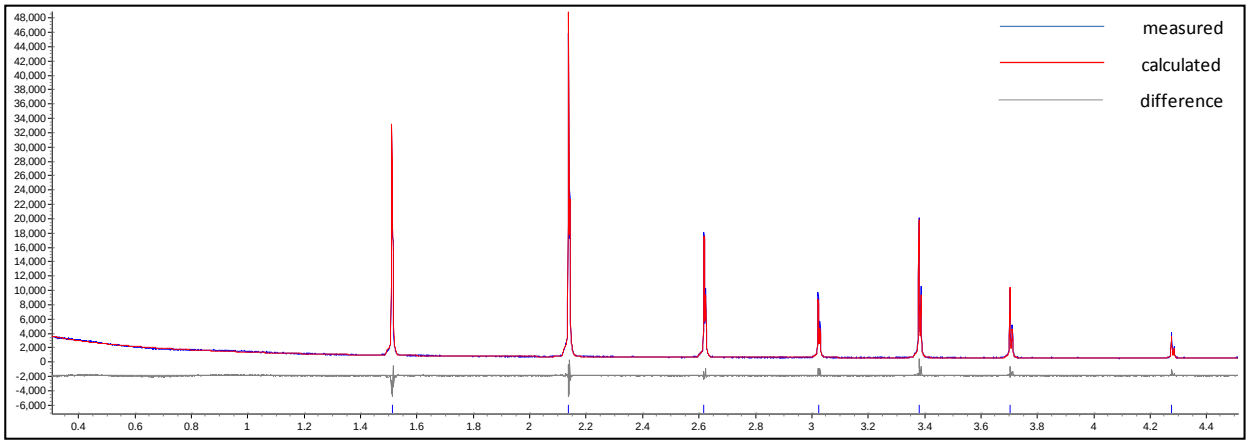

Figure 3.5 Refinement pattern for the NIST 660a LaB_6 standard, showing the measured and calculated patterns, as well as the difference between the two. In this instance the measured pattern is not easily seen because of the similarity between both patterns.

3.6.2. Petrography

Polished thin sections were prepared for observation under a petrographic microscope using transmitted and reflected light, in order to describe the textures and associations between the ore and gangue minerals. The particles were mounted vertically in epoxy resin before being cut longitudinally and mounted onto glass slides to make the thin sections, to increase the representativeness of particles of different sizes and densities. The microscopic observations were also used to confirm the presence of minerals detected by XRD, and identify accessory minerals occurring below the XRD detection limit. Pyrrhotite types (i.e. magnetic versus non-magnetic) were distinguished by the use of a magnetic colloid, to aid the selection of suitable crystal structure files for XRD quantification. The colloid is made up of a mixture of $FeCl_2$ and $FeCl_3$ particles, which create an insoluble magnetite precipitate that is stored in a sodium oleate solution (Becker, 2009). The solution was applied onto the surfaces of the polished thin sections, while being viewed under the microscope. The colloid settled on magnetic pyrrhotite, with non-magnetic pyrrhotite being free from colloid particles. Photomicrographs were taken of the pyrrhotite to show the distribution of the colloid.

3.6.3. Electron probe microanalysis (EPMA)

Selected polished thin sections were analysed using a Cameca SX50 electron probe microanalyser to classify minerals by their chemical composition. Since many minerals are non-conductive, the samples were carbon-coated for the analysis to prevent a charge build-up that can otherwise interfere with imaging and analysis. The analysis was conducted using wavelength-dispersive spectrometry (WDS). The system was calibrated and checked with sulfide reference standards for analysis of the sulfide minerals and oxide standards for the silicate analyses. Analysis was performed at an accelerating voltage of 20kV with a beam current of 30nA. Counting times of 20 seconds on peak and 5 seconds on each of the two background positions were used. Matrix correction was automatically done by the ZAF procedure in the SAMx Analysis software, which corrects for atomic number (Z), absorption (A) and fluorescence (F) effects. The minerals were identified by comparison with EPMA mineral compositions given by Deer *et al.* (1978), Deer *et al.* (1992) and Deer *et al.* (1997).

3.6.4. QEMSCAN analysis

Six samples of each ore type were analysed by QEMSCAN (Quantitative Evaluation of Minerals by Scanning Electron Microscopy). These samples are products of the sink-float analyses on the DMC overflow and underflow of each ore, with corresponding density

classes selected from each product. The density fractions nearest to the DMS cut-point of each ore were chosen as these classes generally contain the largest mass proportions, and particles within these classes are most likely to be misplaced in a DMC. Samples were also selected from a higher density class and a lower density class of each product to compare the differences in the mineralogy between particles of the same density in the underflow and the overflow.

Each sample was screened into two size fractions, +5.6 mm and -5.6 mm, and mounted with epoxy resin into polished blocks of approximately 75 x 80 mm in size, as a standard 30 mm polished section will not accommodate more than a few particles of this size. A custom made sample holder, previously designed at Mintek, was used to fit the samples into the QEMSCAN sample chamber (Figure 3.6). A total of five blocks were carbon-coated and analysed per sample (three from the +5.6 mm fraction and two from the -5.6 mm fraction) in order to increase the representativeness of the sub-samples analysed.

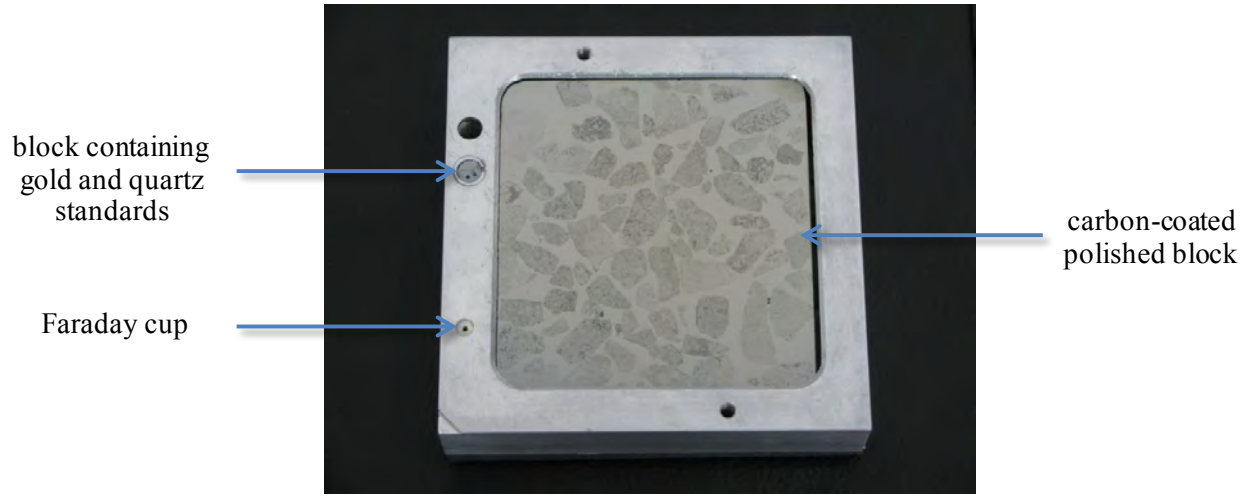

Figure 3.6 Sample holder containing carbon-coated polished block (75x80 mm) used for the analysis

Owing to sample top sizes of 12 mm and 25 mm, particles are still not able to be mapped as a whole using the lowest magnification of the QEMSCAN. The Field Image measurement mode therefore was used to map individual fields of view, which were then stitched together to produce a single image of each polished block. These mapped images were then 'particulated' using the iExplorer software to separate individual particles from each other so that mineral liberation, size and shape may be described (Figure 3.7). The polished blocks were analysed at a magnification of 20X (2 mm field size), at a pixel size of 25 µm, which results in an analysis time of approximately 20 hours per block. From the particle maps, the minerals identified and their relative proportions, mineral liberation, association, grain and

particle sizes, and particle shapes, were derived. The QEMSCAN results were validated by comparing the chemistry of the samples calculated from the modal analysis with measured major element chemistry (Figures A.1 and A.2, Appendix A and Tables C.1 – C.6, Appendix C).

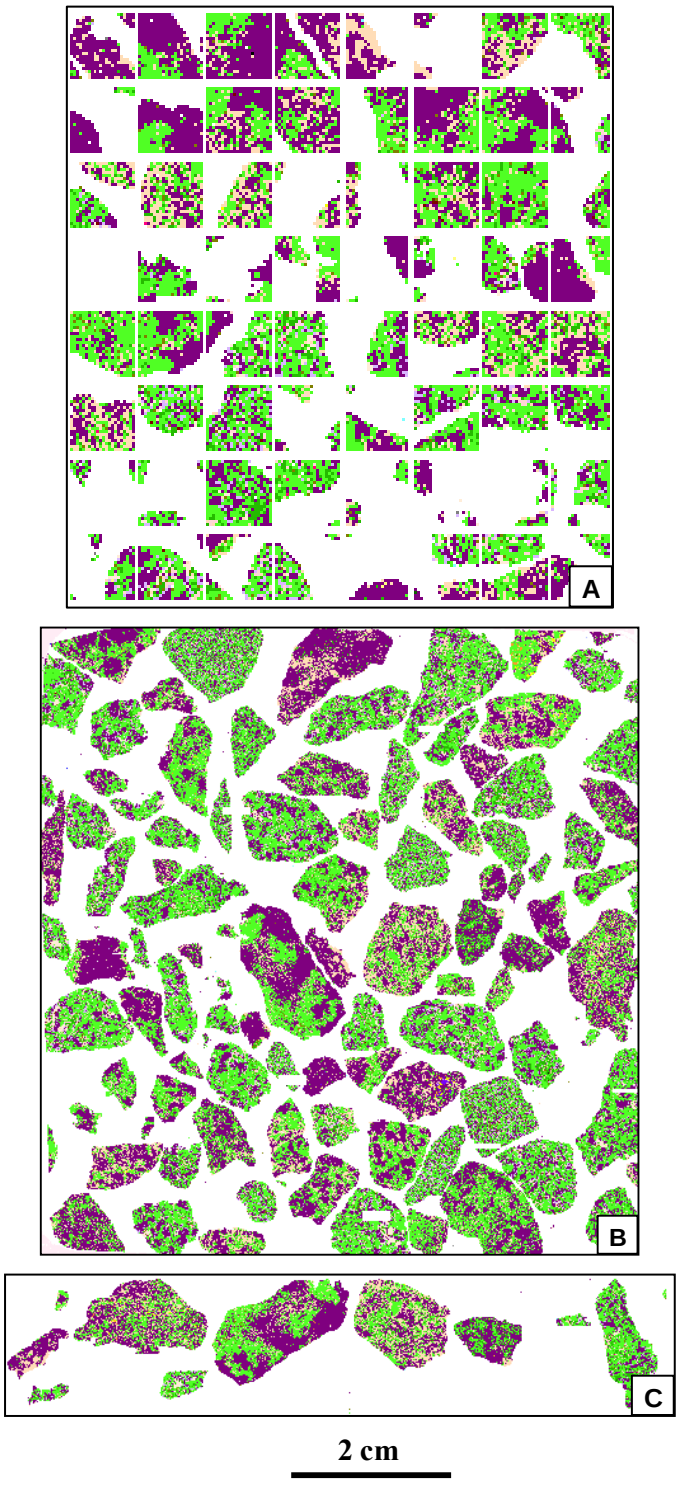

Figure 3.7 Example of Field Image procedure. **A**: Individually-mapped fields of view, **B**: Fields stitched into a single image, **C**: Separated ('particulated') particles.

An average of 3 400 particles was measured in total per sample from the Field Image measurements. Using pentlandite as the mineral of interest, a statistical error formula given by Jones (1987) was applied to determine if the number of particles would be sufficient to achieve representative data. The formula is represented as:

$$N = \frac{4pq}{e^2}$$

where:

e = absolute error
N = number of particles needed for *e* at 95% confidence
p = proportion of selected mineral
q = 1 – p

According to this calculation, a statistically representative number of particles was measured for all samples except the 3.0 floats of the Phoenix overflow and underflow.

CHAPTER 4: CHARACTERISATION OF NKOMATI ORE

Density Separation and Mineralogy

4.1. Introduction

All results obtained from characterisation of the Nkomati MMZ bulk ore sample are provided in this chapter. The results of the laboratory sink-float analyses and pilot DMS testwork are presented first. The aim of the tests was to collect a basic set of data from which the DMS amenability could be assessed, and to produce a series of samples for mineralogical evaluation and comparison. Only cumulative sink-float analysis data are presented in this chapter; discrete results are contained in Appendix B. The mineralogy results for the DMC products follow, providing information on changes in mineralogical composition and texture of the samples with density, as well as contrasting particles of the DMC overflow and underflow. The full mineralogical data are presented in Appendix D. The detailed mineralogical characterisation of the products aims to contribute to a better understanding of the way in which the particles separate during DMS. The most important features gathered from all tests conducted on the Nkomati MMZ bulk sample are summarised at the end of the chapter.

4.2. Density separation testwork

The masses of the DMC feed, fines and run-of-mine (ROM) and their nickel grades are given in Table 4.1.

Table 4.1 Stream masses and nickel grades for the Nkomati bulk sample

Stream	Mass (kg)	Ni Grade (wt%)
DMC feed	642	0.40
Fines (<1 mm)	123	0.63
ROM	765	0.44

The preliminary sink-float analysis was performed on a representative sample of the -12+1 mm DMC feed. The sample mass, nickel, copper and sulfur grades were measured for each density class produced from the sink-float analysis, and were used to calculate recoveries

(Table 4.2). The results for the head sample indicate upgrades in nickel and copper towards the higher density classes and therefore amenability to DMS. The cumulative mass distribution in the different density classes is plotted as a washability curve (Figure 4.1).The results show that, at a density cut-point of 3.0, 48 mass % of the ore reported to the sinks and 52% to the floats. The nickel head grade was measured at 0.40% (calculated at 0.43%) and the grade in the highest density class, the 3.4 sinks fraction, is 2.52%. At a cut-point density of 3.0 the cumulative nickel grade attained is 0.74% at a recovery of 83% (Figure 4.2). This would give a 76% copper recovery at a grade of 0.25%. This density cut-point was chosen and targeted for the DMS plant in order to maximise the waste rejection while obtaining a low nickel grade in the overflow.

Table 4.2 Sink-float analysis data for the Nkomati bulk sample (cut-point data highlighted)

SG Fraction	Relative SG to Sinks	Cumulative Mass %	Cumulative Grade to Sinks [%]			Cumulative Recovery to Sinks [%]		
			S	Cu	Ni	S	Cu	Ni
+ 3.4	3.4	3.9	19.08	0.55	2.52	24.0	13.1	22.5
- 3.4 + 3.3	3.3	6.1	15.95	0.48	2.10	32.0	18.2	29.9
- 3.3 + 3.2	3.2	12.9	10.92	0.37	1.45	46.2	29.4	43.5
- 3.2 + 3.1	3.1	29.3	7.34	0.27	0.99	70.3	48.6	67.4
- 3.1 + 3.0	3.0	48.4	5.48	0.25	0.74	86.8	75.8	83.4
- 3.0 + 2.95	2.95	63.4	4.42	0.20	0.60	91.7	80.5	89.0
-2.95 + 2.9	2.9	74.4	3.90	0.19	0.54	95.0	88.0	92.8
-2.9 + 2.8	2.8	92.7	3.27	0.16	0.46	99.2	93.7	99.2
- 2.8	2.7	100.0	3.06	0.16	0.43	100.0	100.0	100.0

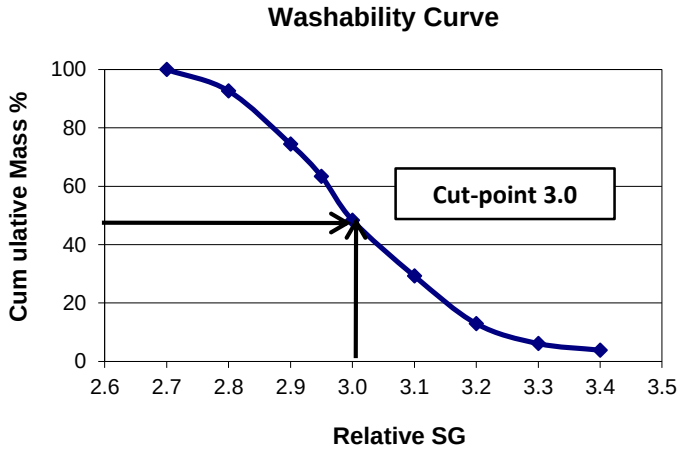

Figure 4.1 Washability curve for the Nkomati bulk sample

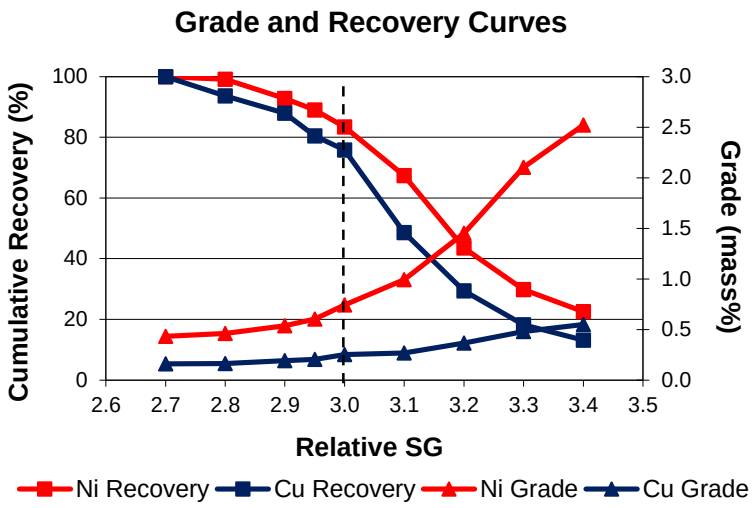

Figure 4.2 Grade and recovery curves for Ni and Cu in the Nkomati bulk sample

The results of the DMS pilot plant run are given in Table 4.3, with calculated head grades from the underflow and overflow grades. The mass recovery to the underflow is 48% at a density cut-point of 3.0, which is in agreement with preliminary sink-float analysis conducted on the feed sample. The nickel was upgraded from 0.39% to 0.67% at a recovery of 83%. No significant copper upgrade was achieved.

Table 4.3 Summary of DMS results for the Nkomati bulk sample

Fraction	Mass	Grade [%]			Recovery [%]		
	[%]	S	Cu	Ni	S	Cu	Ni
Underflow	48	5.63	0.23	0.67	85	68	83
Overflow	52	0.95	0.10	0.13	15	32	17
Total (head)	100	3.2	0.16	0.39	100	100	100

Figure 4.3 gives the flowsheet for the DMS testwork showing the different streams, which ends with the production of a flotation feed composed of the DMC underflow and fines. The nickel grades and recoveries, as well as mass distribution for the MMZ ore sample, were calculated for different streams of the flowsheet. This includes mass-balanced data from the ROM material to the calculated flotation feed, which is made up of the DMC underflow and the -1 mm fines that were initially removed (Table 4.4). The bulk ore sample showed a 54% upgrade from 0.43% in the ROM to 0.66% in the flotation feed, with an 87% Ni recovery to

the flotation plant. Approximately 44% of the ROM mass was rejected in the DMC overflow, with the Ni grade of the overflow at 0.13%.

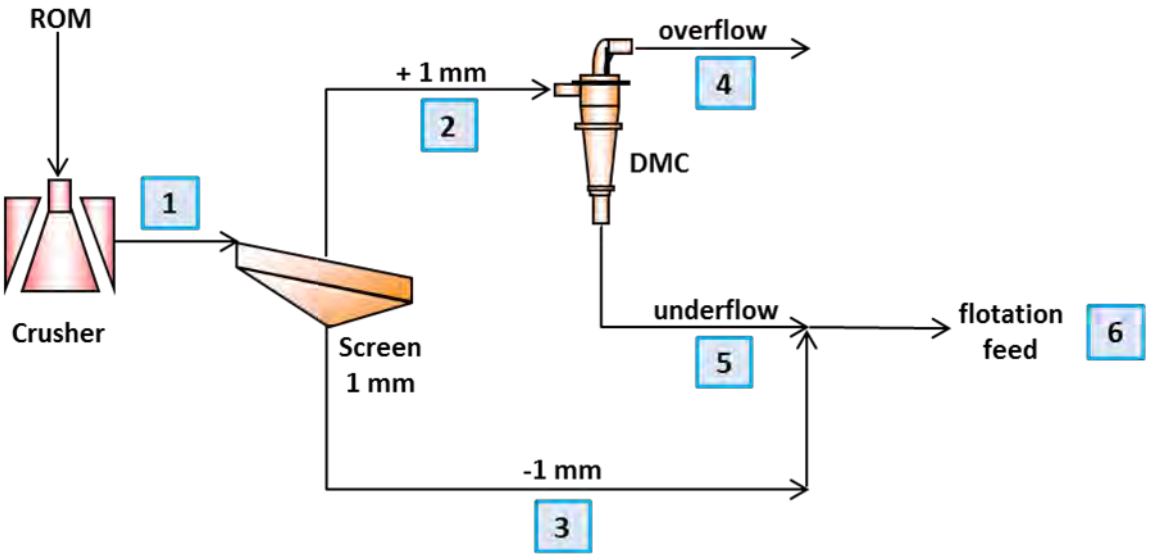

Figure 4.3 Flowsheet for the testwork showing different streams

Table 4.4 Mass-balanced mass, grade and recovery information at different points in the flowsheet

Stream No.	Stream Name	Mass	Ni Grade	Ni Recovery
		[%]	[%]	[%]
1	ROM	100	0.43	100
2	-12+1mm	84	0.39	76
3	-1mm	16	0.62	24
4	DMC overflow	44	0.13	13
5	DMC underflow	40	0.67	63
6	Flotation feed	56	0.66	87

Sink-float analyses were performed on representative sub-samples of the DMC underflow and overflow in order to evaluate the separation efficiency. Partition coefficients were calculated from these results in order to plot a partition curve, which describes the efficiency of the separation (Table 4.5, Figure 4.4). The partition coefficient is the percentage of the feed of a specific density that reports either to the sinks or floats; in a partition curve this is plotted against density. In an ideal separation, all particles with a density higher than the separating density report to the sinks, and the lighter material to the floats, without any

particles being misplaced. In an actual separation particles far from the separation density are effectively separated and near density material are less efficiently separated (Wills, 2006).

From the partition curve, the probable error of separation or the Ecart probable (Ep) is calculated. This is half the difference between the densities where 75% and 25% is recovered to the sinks (Wills, 2006). The lower the Ep, the more efficient the separation is. The Ep calculated from the Nkomati sink-float analysis results is 0.04, which indicates a low error in the separation, with little misplacement of particles. The planned density cut-point of 3.0 was achieved in the separation, with the actual separation density, the D_{50} (or $\rho 50$), calculated at 3.01. This created a more-or-less equal actual split between the overflow and underflow.

Table 4.5 Partition coefficients calculated for the Nkomati bulk sample

SG Fraction	Nominal SG	Mass (%)		Reconstituted Feed	Partition Coefficient
		Underflow	Overflow		
+ 3.4	3.45	3.2	0.0	3.2	100.0
- 3.4 + 3.3	3.35	2.5	0.0	2.5	100.0
- 3.3 + 3.2	3.25	8.4	0.0	8.4	100.0
- 3.2 + 3.1	3.15	9.6	0.2	9.8	97.8
- 3.1 + 3.0	3.05	19.3	6.9	26.2	73.7
- 3.0 + 2.95	2.98	3.7	9.4	13.1	28.0
-2.95 + 2.9	2.93	0.9	16.1	17.0	5.5
-2.9 + 2.8	2.85	0.3	11.6	12.0	2.9
- 2.8	2.75	0.1	7.7	7.8	1.3
Actual Split		**48.0**	**52.0**		
Ep					**0.04**

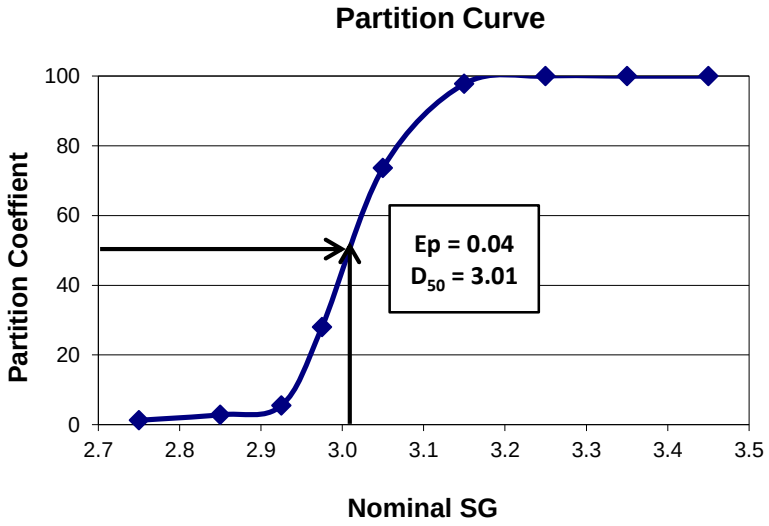

Figure 4.4 Partition curve showing the separation efficiency

4.3. Mineralogy and mineral chemistry

The mineralogical characterisation of the DMC overflow and underflow begins with a petrographic evaluation of the sink-float analysis products. This provides a basic description of the minerals present and their textural relationships in the rock. The identified minerals were then classified using their mineral chemistry, with bulk mineralogy determined by quantitative XRD (QXRD) and QEMSCAN. Further quantitative data from the QEMSCAN analysis were derived to give information on the deportment of nickel, sulfide grain size distribution, liberation and mineral associations. The size and shape distribution of the particles were also calculated and compared between the products to determine the extent of particle separation based on size and shape.

4.3.1. Petrography

The samples analysed are medium-grained and a variety of textures was observed petrographically. A medium grain size indicates that the individual crystals making up the rock are visible in hand specimen but less than 2 mm in size. Cumulate textures are common and indicated by rounded or euhedral olivine and pyroxene crystals as the cumulus minerals, usually with plagioclase as the intercumulus phase (Figure 4.5 A). In many of the samples studied, the original mafic igneous minerals are altered to metamorphic minerals, mostly serpentine (chrysotile), talc, chlorite and actinolite (calcic amphibole, Figure 4.5 B).

Amphibole of actinolite composition is also commonly found in the form of uralite, a fine-grained alteration product of clinopyroxene, which maintains the form of the pyroxene crystal. Alteration rims of serpentine can sometimes be seen surrounding olivine crystals in thin section. Plagioclase is commonly altered to saussurite (fine-grained mass that may include clays, epidotes, chlorite, mica and calcite). In these cases the cumulate texture is preserved by the alteration minerals.

In the sink-float analysis density fractions, fresh olivine, pyroxene and plagioclase are generally found in the higher density fractions, with highly altered sections of the rock usually reporting to the lower density fractions. In some high density fractions, particles free of sulfides are found due to their high density. These particles are normally dominated by unaltered pyroxene with some containing chromite.

Deformation textures due to metamorphism are also visible in the samples. Zones showing metamorphic textures are generally fine-grained, with elongate or platy minerals such as chlorite and actinolite showing preferred orientation. Kinked and fractured biotite and actinolite were also observed (Figure 4.5 B), as well as grains with curved cleavage planes and deformation twins in plagioclase. Straining of quartz is evident from undulose extinction and sutured grain boundaries.

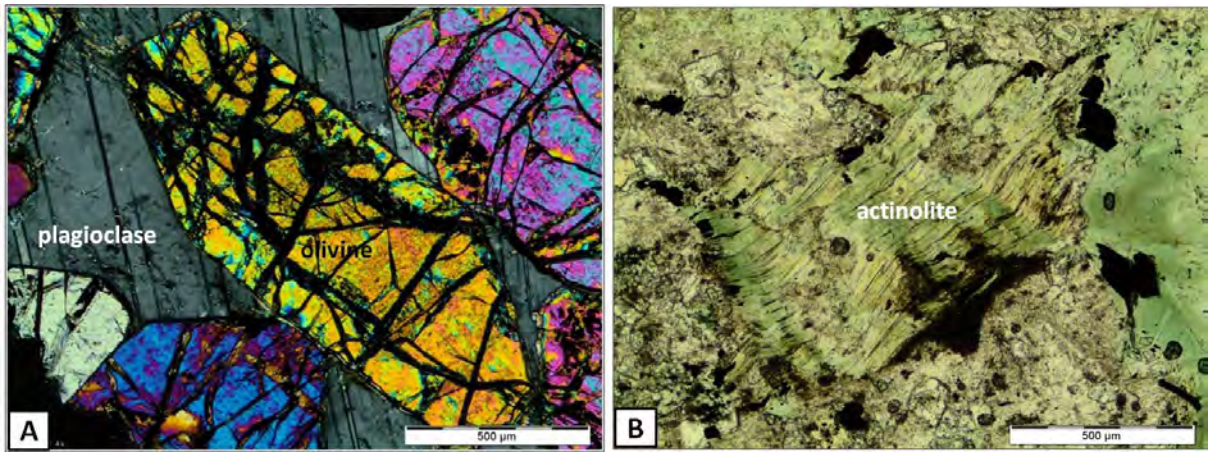

Figure 4.5 A: Photomicrograph of olivine crystals with intercumulus plagioclase, transmitted cross polarised light (DMC underflow, 3.1 floats). **B:** Deformed actinolite, transmitted plane polarised light (DMC underflow, 2.9 floats)

Massive sulfides are not common in the MMZ; the sulfides usually occur in disseminated form as blebs, or net-textured. Microscopically, net-textured sulfides are generally seen to have formed interstitial to the cumulus minerals (Figure 4.6 A). These are commonly

associated with magnetite rims surrounding rounded serpentine grains, both formed by the alteration of olivine.

Pentlandite is the nickel ore mineral and occurs in two major forms throughout the samples, most commonly as granular aggregates and also as flame-like exsolution lamellae in pyrrhotite (Figure 4.6 B and C). Chalcopyrite is the primary copper ore mineral. Pyrrhotite is the most abundant sulfide mineral, followed by chalcopyrite, with smaller amounts of sphalerite, pyrite and arsenopyrite. As with the silicate minerals, deformation is also evident from the sulfide mineral textures. It is usually observed where generally softer sulfide minerals such as pyrrhotite, pentlandite and chalcopyrite are found to penetrate silicate mineral cleavage planes (Figure 4.6 D). Both magnetic and non-magnetic pyrrhotite were observed from the magnetic colloid tests (Figure 4.7).

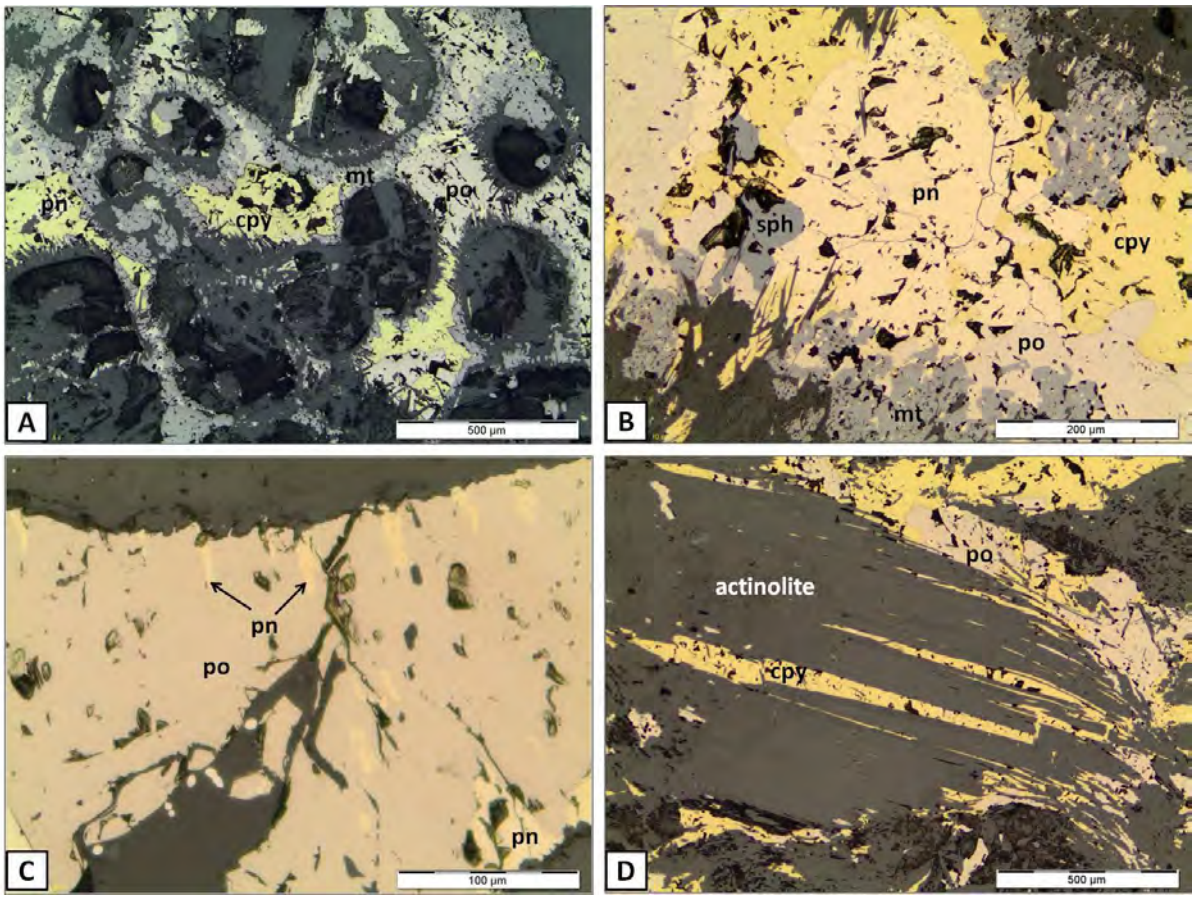

Figure 4.6 Sulfide textures in the Nkomati ore (reflected light, plane polarised). **A:** Net-textured sulfides – chalcopyrite (cpy), pyrrhotite, (po), pentlandite (pn) and magnetite (mt) interstitial to serpentine (dark grey). **B:** Granular pentlandite (pn) associated with chalcopyrite (cpy), pyrrhotite (po), sphalerite (sph), and magnetite (mt), dark grey areas show silicates. **C:** Pentlandite (pn) flames in pyrrhotite (po). **D:** Chalcopyrite (cpy) and pyrrhotite (po) penetration along actinolite (act) cleavage planes.

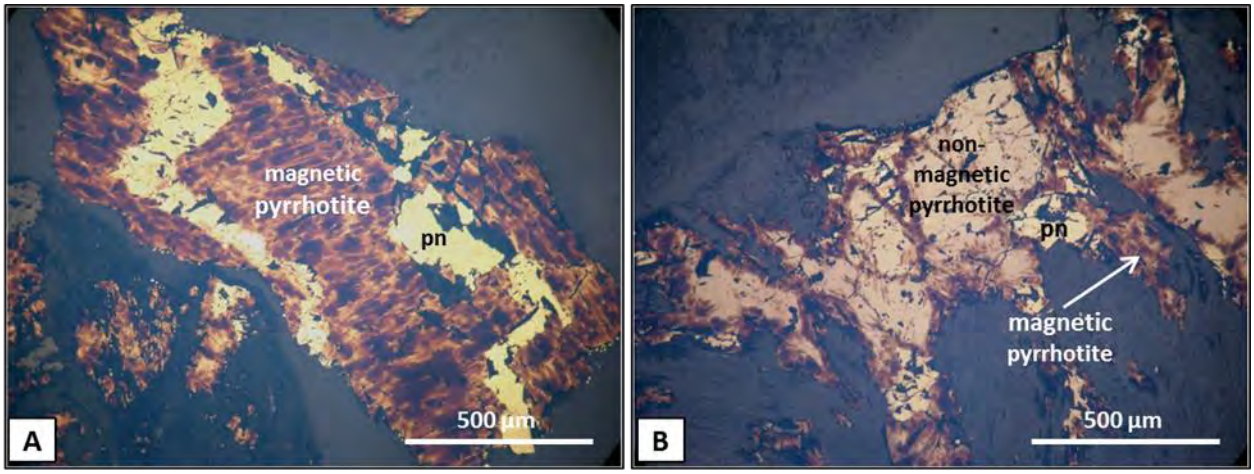

Figure 4.7 Petrographic images showing the settling of the magnetic colloid (brown) on magnetic pyrrhotite, with pentlandite (pn) and non-magnetic pyrrhotite unaffected. **A:** particle in which all pyrrhotite is magnetic. **B:** particle containing both magnetic and non-magnetic pyrrhotite

For the purposes of grain size and liberation descriptions, a 'grain' is defined as a feature composed of only one mineral, whether liberated or intergrown with other minerals. This is different from a 'particle', which is a rock fragment that can consist of many different mineral grains (Figure 4.8; Jones, 1987).

Figure 4.8 Example of two particles: Particle **A** showing two mineral types, a grain (red) included within a matrix (green); Particle **B** is a liberated grain or a monomineralic particle.

The grain size of pyrrhotite increases steadily from the lower to the higher density classes in each of the DMC underflow and overflow products. In the DMC overflow the average pyrrhotite grain size increases from approximately 70 µm in the 2.7 floats to ~580 µm in the 3.1 sinks. The largest pyrrhotite grain found in the DMC overflow is ~1.6 mm and reported to the subsequent 3.1 sinks fraction. In the DMC underflow pyrrhotite is generally larger than in the DMC overflow per size class, reaching up to 4.6 mm in the 3.4 sinks.

Pentlandite grain sizes also increase with higher density fractions but show a slightly erratic distribution compared to pyrrhotite. The grain size distribution generally depends on the occurrence of the pentlandite in the sample. Flames are the more dominant occurrence in the lighter density classes, where most of the sulfide is disseminated and the average size measured for pentlandite flames in the samples is 3 µm x 30 µm. Granular pentlandite reaches up to approximately 2 mm in size in the 3.4 sinks of the DMC underflow. Pentlandite is always associated with pyrrhotite in these samples. Similar grain size trends are observed with chalcopyrite, pyrite and sphalerite.

In general, an increase in sulfide grain sizes corresponds to a change in texture from disseminated to net-textured, which leads to increased apparent liberation. Because pyrrhotite is the most abundant sulfide, it is also the biggest control on sulfide liberation and therefore nickel recovery. Pentlandite is the main host of nickel in the ore and its successful preconcentration depends on the recovery of pyrrhotite, as it would be very difficult to liberate pentlandite from pyrrhotite in this case owing to its fine grain size, particularly for density separation methods. Pentlandite liberation from pyrrhotite is more likely to form part of a cleaner stage in flotation. Liberation is therefore described here as the area percent of total sulfides in a particle, as seen in thin section. Chalcopyrite and sphalerite are also included as they are closely associated with pentlandite and pyrrhotite.

The DMC overflow shows poor sulfide liberation in most density fractions except for the densest (3.1 sinks). The sulfides are mostly locked in silicates, generally making up <10 area % of the particle (Figure 4.9). The 3.1 sinks fraction contains particles with varying degrees of liberation from locked (<30 area %) to completely liberated (100 area %). These particles have not been recovered to the DMC underflow possibly because of their size, which nears the fines cut-off size of 1 mm. Most of the particles in this sample are <2 mm in size, with the largest particle measured at ~6 mm.

The total sulfide liberation in the DMC underflow is much better than in the overflow, except at the lowest density classes where all the sulfides are completely locked in gangue. Most of the particles found in the lighter fractions of the DMS underflow are elongate in shape. The sulfide minerals are most commonly associated with the original minerals of the ultramafic rock – pyroxene and olivine – and with their alteration products (usually serpentine and amphibole). In the higher density classes, where sulfide liberation is generally in the middlings (30-80 %) or liberated (80-100 %), sulfide-free particles have still been recovered to the underflow owing to their inherent high densities or through association with sulfides.

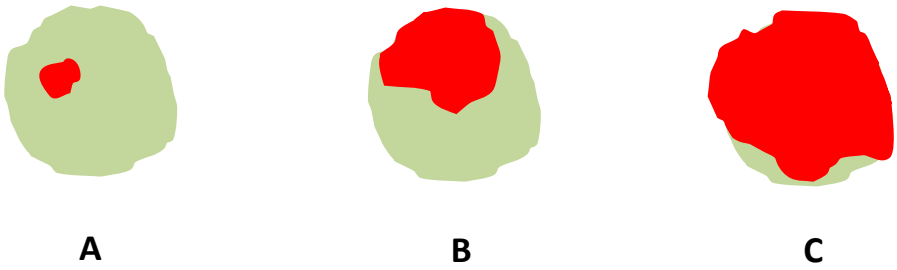

Figure 4.9 Particles illustrating the three classes used to describe liberation of a mineral of interest (red) from associated gangue (green): **A** = locked (<30 area % of the particle), **B** = middlings (30 – 80 area % of the particle), **C** = liberated (>80 area % of the particle). As liberation is described on a 2D surface, it is the apparent liberation of a grain.

4.3.2. Mineral compositions

Electron probe microanalysis was carried out on minerals that show solid solution substitution, so that the chemical composition could be determined. Solid solution affects the crystal structure of the mineral and consequently its XRD pattern, therefore the mineral chemistry is important for selecting suitable crystal structure information for Rietveld refinement. Additionally, elemental substitution creates variation in the overall mineral density. Nickel was also measured by EPMA within sulfide and silicate minerals, in order to identify solid solution nickel in gangue minerals. These data are used in combination with the bulk mineralogy to calculate nickel deportment in selected samples. Of the silicate minerals, amphibole, plagioclase, chlorite, pyroxene, talc, serpentine and biotite were analysed by EPMA, with pyrrhotite and pentlandite from the sulfides.

Chlorite was identified as the Mg-Fe-Al variety, clinochlore (Table 4.6). Most of the plagioclase in the samples is of albite (Na-plagioclase) composition. Two calcic amphiboles are identified – tremolite (Mg-rich) and actinolite (containing significant amounts of both Fe and Mg), of which actinolite is dominant. The clinopyroxene phase is identified as augite. All the mafic silicate minerals contain solid solution nickel, with average NiO contents varying from 0.05 wt% in actinolite to 0.11 wt% in serpentine. Pyrrhotite hosts an average of 0.51 wt% nickel and pentlandite contains approximately 1.93 wt% Co in solid solution (Table 4.7). Analyses for individual mineral grains are given in Appendix D.

Table 4.6 Measured silicate mineral compositions in the Nkomati ore

Mineral	No. of Analyses		Mineral Composition (Weight %)										
			Na_2O	MgO	Al_2O_3	SiO_2	K_2O	CaO	TiO_2	Cr_2O_3	FeO	NiO	Total
chlorite	10	Average	0.04	28.55	19.96	30.53	0.05	0.35	0.50	0.08	7.43	0.09	87.58*
		Std dev.	*0.02*	*3.94*	*3.05*	*1.16*	*0.03*	*0.37*	*0.43*	*0.06*	*5.35*	*0.06*	*1.99*
biotite	11	Average	0.20	20.64	14.26	38.81	7.78	0.48	1.86	0.31	10.66	0.09	95.08*
		Std dev.	*0.20*	*5.96*	*1.80*	*1.72*	*1.87*	*1.08*	*2.13*	*0.17*	*5.30*	*0.05*	*2.36*
serpentine	6	Average	0.02	40.33	0.70	43.26	0.04	0.25	0.23	lld	3.39	0.11	88.33*
		Std dev.	*0.01*	*2.89*	*1.01*	*1.69*	*0.02*	*0.41*	*0.24*	*-*	*1.55*	*0.07*	*2.19*
talc	11	Average	0.08	29.46	0.25	62.71	0.04	0.15	lld	0.05	4.06	0.10	96.89*
		Std dev.	*0.07*	*1.67*	*0.23*	*0.79*	*0.02*	*0.24*	*-*	*0.02*	*2.01*	*0.06*	*1.11*
augite	8	Average	0.39	16.66	2.90	52.23	0.15	20.36	0.37	0.30	6.58	0.07	100.01
		Std dev.	*0.45*	*3.61*	*2.34*	*2.80*	*0.15*	*6.67*	*0.31*	*0.25*	*6.29*	*0.03*	*2.08*
actinolite	22	Average	0.31	17.01	2.02	55.55	0.15	12.52	0.29	0.14	11.34	0.05	99.37
		Std dev.	*0.36*	*3.25*	*1.81*	*2.30*	*0.20*	*0.71*	*0.47*	*0.11*	*4.41*	*0.01*	*1.07*
albite	22	Average	11.78	lld	19.74	68.00	0.06	0.11	lld	lld	0.11	lld	99.81
		Std dev.	*0.11*	*-*	*0.20*	*0.28*	*0.01*	*0.05*	*-*	*-*	*0.10*	*-*	*0.40*

**low totals are due to the presence of structural water, which cannot be measured by EPMA. lld = lower than limit of detection*

Table 4.7 Measured sulfide mineral compositions in the Nkomati ore

Mineral	No. Of Analyses		Mineral Composition (Weight %)				
			S	Fe	Co	Ni	Total
pyrrhotite	13	Average	38.94	60.18	lld	0.51	99.63
		Std dev.	*0.48*	*0.45*	*-*	*0.11*	*0.30*
pentlandite	48	Average	33.38	30.75	1.93	34.28	100.32
		Std dev.	*0.18*	*0.31*	*0.07*	*0.19*	*0.27*

lld = lower than limit of detection

4.3.3. Bulk mineralogy

The bulk mineral composition of the DMC feed, and each SG class of the DMC overflow and underflow, was determined using quantitative XRD. For the overflow, particles were not separated into different classes above a SG of 3.1 due to mass constraints. The detection limits of XRD do not allow for minerals in very low quantities, of less than approximately 1 mass %, to be identified. For the selected ores, it is therefore mostly suitable for the comparison of gangue mineral proportions among the different samples.

A list of the minerals identified by a combination of petrography and XRD is given in Table 4.8, together with their ideal chemical formulae and average SG, as derived from the Webmineral Mineralogy Database (http://webmineral.com). The actual SG is variable within a range, depending on the mineral composition, particularly for minerals with extensive solid solution substitution. Figure 4.10 shows the identified minerals arranged according to their SG. The general trend is for alteration and secondary silicate minerals to be of lower SG than the primary silicates. The higher SG minerals consist of sulfide and oxide minerals.

Table 4.8 Minerals identified in the MMZ ore

Mineral	Ideal Chemical Formula	SG
serpentine	$Mg_3Si_2O_5(OH)_4$	2.53
plagioclase	$(Na,Ca)Al(Si,Al)_3O_8$	2.62
quartz	SiO_2	2.62
chlorite	$(Mg,Fe)_3(Si,Al)_4O_{10}(OH)_2$	2.65
calcite	$CaCO_3$	2.71
talc	$Mg_3Si_4O_{10}(OH)_2$	2.75
dolomite	$CaMg(CO_3)_2$	2.84
biotite	$K(Mg,Fe)_3AlSi_3O_{10}(OH,F)_2$	3.00
amphibole	$Ca_2(Mg,Fe)_4Al(Si_7Al)O_{22}(OH,F)_2$	3.04
olivine	$(Mg,Fe)_2SiO_4$	3.27
clinopyroxene	$(Ca,Na)(Mg,Fe,Al,Ti)(Si,Al)_2O_6$	3.40
epidote	$Ca_2(Fe,Al)Al_2(SiO_4)(Si_2O_7)O(OH)$	3.45
orthopyroxene	$(Mg,Fe)_2Si_2O_6$	3.55
sphalerite	ZnS	4.08
chalcopyrite	$CuFeS_2$	4.10
rutile	TiO_2	4.25
pyrrhotite	$Fe_{1-x}S$	4.61
ilmenite	$FeTiO_3$	4.72
chromite	$FeCr_2O_4$	4.79
pentlandite	$(Fe,Ni)_9S_8$	4.80
pyrite	FeS_2	5.01
magnetite	Fe_3O_4	5.20
arsenopyrite	$FeAsS$	6.07

primary silicate secondary silicate sulfide oxide / carbonate

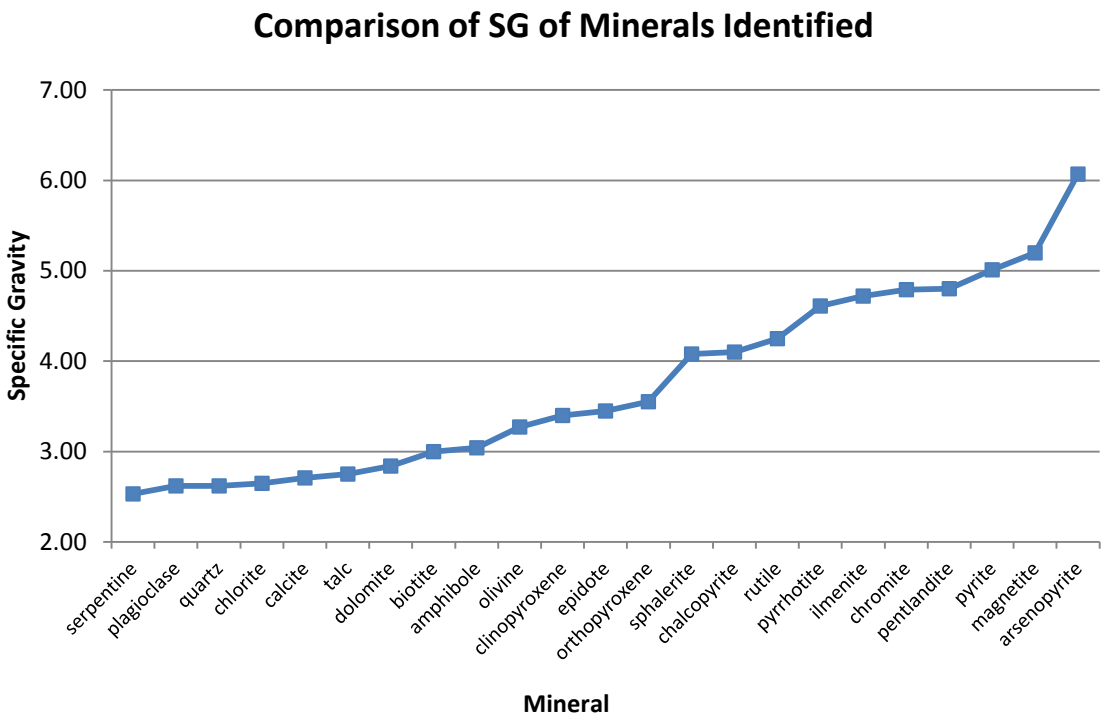

Figure 4.10 Identified minerals in order of increasing SG

The DMC feed sample is mostly composed of amphibole, pyroxene, chlorite, talc, carbonate minerals (calcite, dolomite and siderite) and pyrrhotite (Figure 4.11). Differences can be seen in the mineralogy of corresponding SG classes of the overflow and underflow. In general, the DMC underflow samples contain a larger proportion of denser minerals than the overflow, most notably pyrrhotite and pyroxene (Figures 4.12 and 4.13). High levels of quartz and calcite are found in the low density overflow samples; these minerals, together with feldspar, and chlorite, talc and serpentine (less dense alteration minerals) decrease in abundance with an increase in SG in both the overflow and underflow. Amphibole levels peak around the cut-point SG of 3.0 in both the overflow and underflow and decrease away from the cut-point.

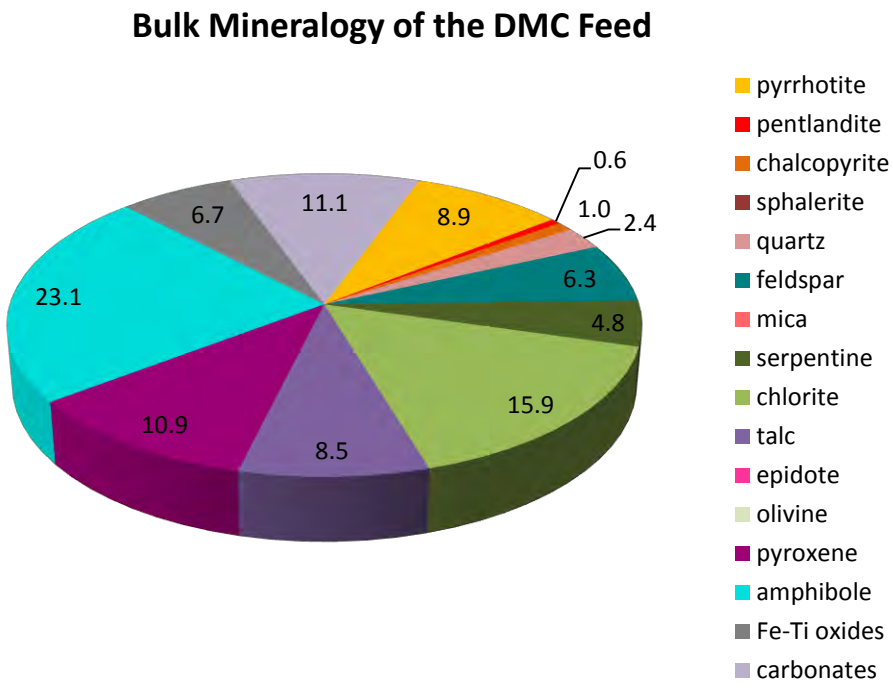

Figure 4.11 Bulk mineral composition of the DMC feed as determined by QXRD

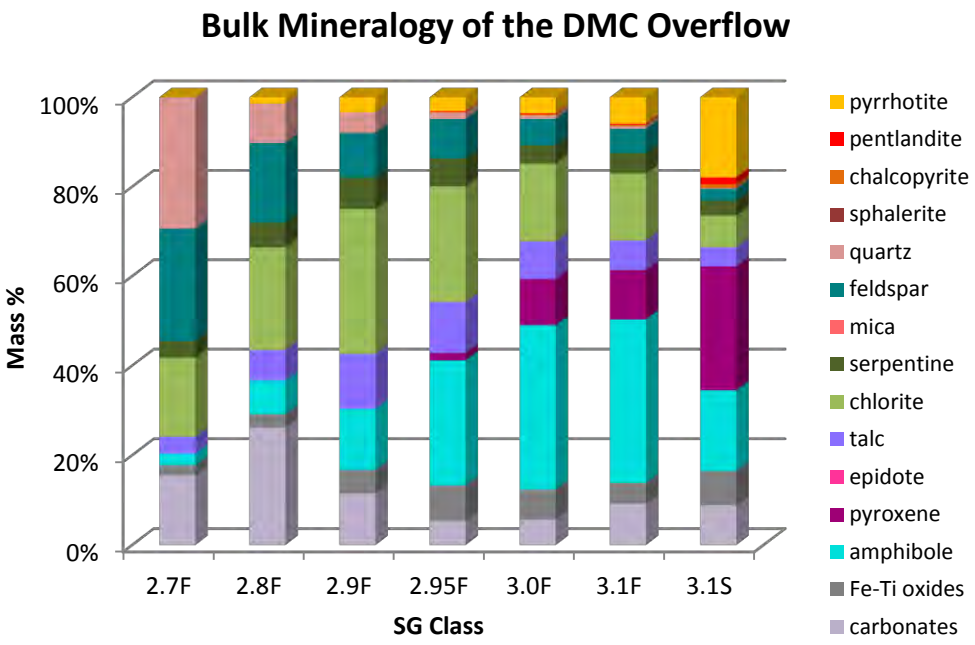

Figure 4.12 Bulk mineral composition of the DMC overflow samples as determined by QXRD (F – floats, S – sinks)

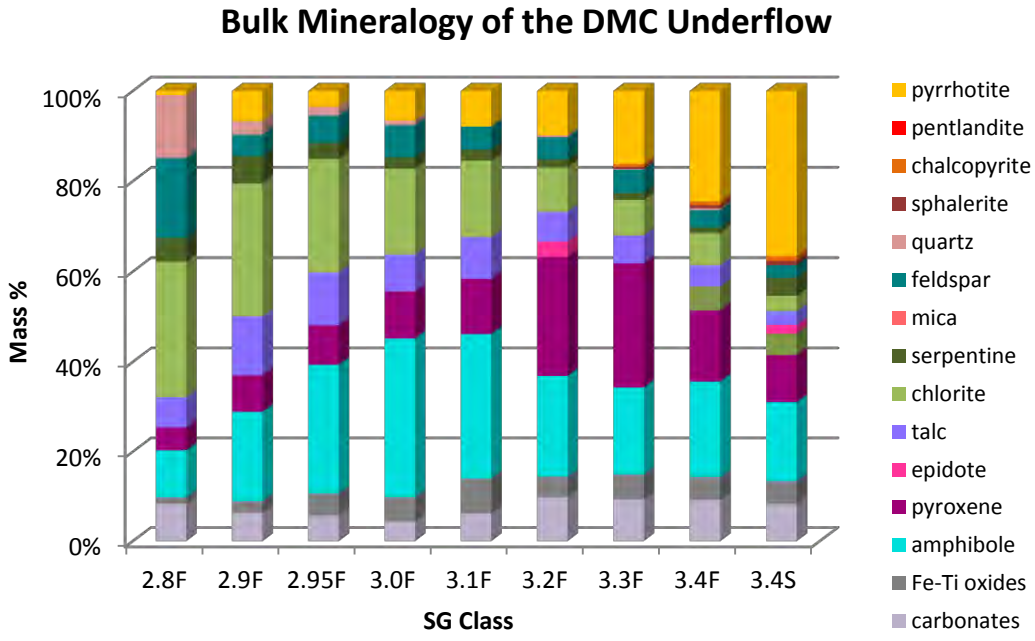

Figure 4.13 Bulk mineral composition of the DMC underflow samples as determined by QXRD (F – floats, S – sinks)

Three corresponding density fractions were chosen from each DMC product (underflow and overflow) for comparison of their mineralogical properties using QEMSCAN analysis (Table 4.9). The analysis of these samples provides information relating to the separation of the ore

at the DMS cut-point (SG 3.0), and further away from the cut-point, which will help understand any mineralogical controls acting on the particles at the different densities. The mass proportion of each fraction as a total of the whole DMC product is given, as well as the number of particles measured by QEMSCAN. A lower number of particles were measured in the 3.1 floats of the DMC overflow compared with other samples due to sample losses.

Table 4.9 Samples subjected to QEMSCAN analysis

DMC Overflow		
SG Class	**Mass %**	**No. of Particles**
3.0 floats (SG 2.95 – 3.0)	18.13	4 321
3.1 floats (SG 3.0 – 3.1)	13.26	890
3.1 sinks (SG 3.1+)	0.42	5 854
DMC Underflow		
SG Class	**Mass %**	**No. of Particles**
3.0 floats (SG 2.95 – 3.0)	7.66	3 223
3.1 floats (SG 3.0 – 3.1)	40.19	2 606
3.2 floats (SG 3.1 – 3.2)	20.02	3 616

From the QEMSCAN modal analysis, the major gangue minerals identified are amphibole, pyroxene, chlorite and talc (Table 4.10, Figure 4.14). Quartz, feldspar, mica and olivine are less abundant silicate gangue minerals in these samples. Accessory oxide/carbonate minerals include magnetite, chromite, ilmenite, calcite and dolomite. The DMC underflow generally contains more BMS than the overflow, although the highest BMS proportion is observed from the 3.1 sinks of the overflow (19.6%). Apart from the expected increase in sulfide mineral content from the lower to the higher density classes in each product, pyroxene has been concentrated owing to its high density, from approximately 19% in the 3.0 floats of the overflow to ~36% in the 3.2 floats of the underflow. The lower density silicate alteration minerals are more abundant in the lower density fractions, decreasing to <20% in the 3.1 sinks of the overflow and 3.2 floats of the underflow.

Table 4.10 Modal mineralogy of selected SG fractions of the DMC overflow and underflow (mass %)

Mineral	Ideal Chemical Formula	Overflow			Underflow		
		3.0 floats	**3.1 floats**	**3.1 sinks**	**3.0 floats**	**3.1 floats**	**3.2 floats**
pyrrhotite	$Fe_{1-x}S$	2.7	4.0	15.2	6.7	6.3	9.1
pentlandite	$(Fe,Ni)_9S_8$	0.5	0.7	2.5	1.1	1.1	1.5
chalcopyrite	$CuFeS_2$	0.4	0.5	1.1	0.6	0.6	0.8
pyrite	FeS_2	0.1	0.2	0.8	0.5	0.4	0.6
quartz	SiO_2	1.1	1.3	0.3	0.7	1.3	0.4
feldspar	$(K,Na,Ca)Al(Si,Al)_3O_8$	4.3	5.1	0.9	3.6	2.9	2.3
mica	$K(Mg,Fe)_3AlSi_3O_{10}(OH,F)_2$	6.6	4.6	2.2	5.1	3.6	2.8
serpentine	$Mg_3Si_2O_5(OH)_4$	4.3	3.6	3.7	4.0	4.5	3.1
chlorite	$(Mg,Fe)_5Al(Si_3Al)O_{10}(OH)_8$	11.3	8.3	3.2	8.4	6.9	4.3
talc	$Mg_3Si_4O_{10}(OH)_2$	13.7	15.5	8.3	11.0	15.1	7.6
epidote	$Ca_2(Fe,Al)Al_2(SiO_4)(Si_2O_7)O(OH)$	1.7	1.2	1.6	2.1	1.3	2.8
olivine	$(Mg,Fe)_2SiO_4$	2.6	1.5	2.7	2.6	2.5	2.5
pyroxene	$(Ca,Na)(Mg,Fe,Al,Ti)(Si,Al)_2O_6$	18.9	19.5	32.8	24.5	23.8	36.4
amphibole	$Ca_2(Mg,Fe)_4Al(Si_7Al)O_{22}(OH,F)_2$	26.3	27.8	13.8	23.9	23.6	19.7
Fe-Ti oxides	-	2.3	2.4	6.7	2.6	2.0	2.0
carbonates	$CaCO_3/CaMg(CO_3)_2$	2.9	3.6	4.0	2.2	3.5	3.2
others*	-	0.3	0.1	0.5	0.5	0.8	1.0
Total BMS		**3.7**	**5.5**	**19.6**	**8.9**	**8.4**	**12.0**
Total		**100**	**100**	**100**	**100**	**100**	**100**

**accessory minerals present in amounts of <0.1%, e.g. zircon and apatite*

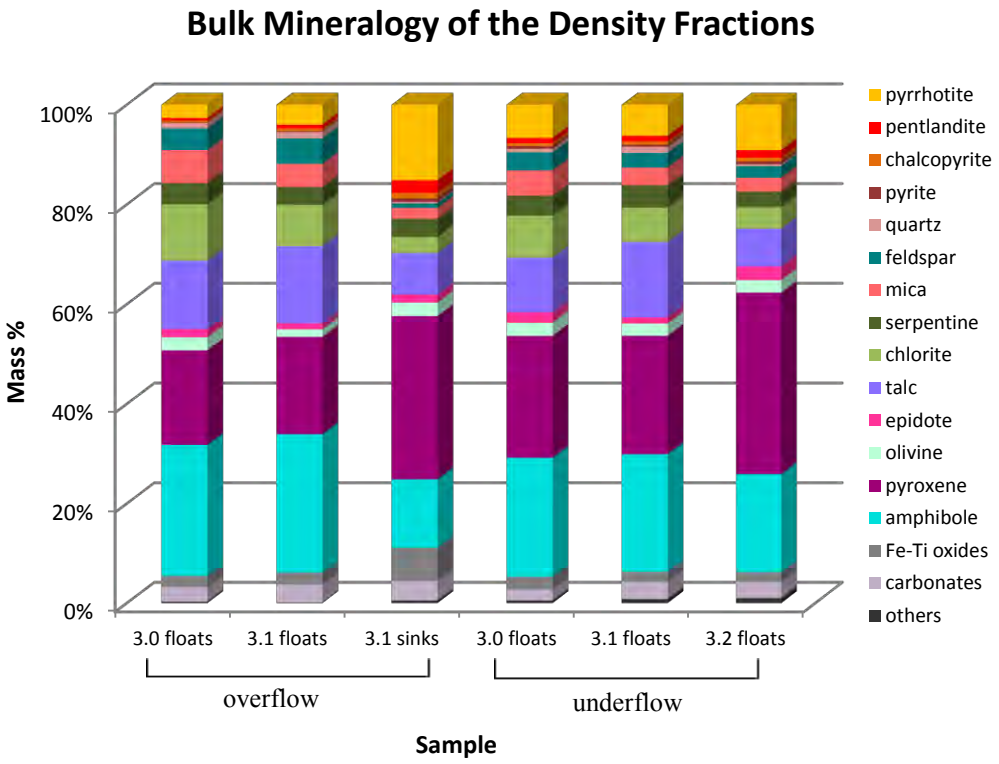

Figure 4.14 QEMSCAN bulk mineralogy

4.3.4. Nickel deportment

Nickel deportment gives the distribution of nickel within its host minerals throughout the samples. This is calculated using the nickel contents of the individual minerals as measured by EPMA as well as the modal abundances of the nickel-bearing minerals. Secondary silicates have been grouped together as 'alteration minerals' for the deportment calculations; however amphibole is presented separately owing to its high abundance in the samples.

Pentlandite is the only nickel ore mineral present, with a 34.28% nickel concentration. Nickel was also detected in minor quantities in solid solution within pyrrhotite and silicate minerals. The nickel concentrations of the various minerals are given in Table 4.11. Pentlandite hosts the bulk of the nickel in all the samples, ranging from 76% in the 3.0 floats of the overflow to 89% in the 3.1 sinks of the overflow, with pyrrhotite containing an average of 7.6% of the total nickel content (Figure 4.15). All the underflow samples show similar amounts of nickel contained in silicate minerals, of approximately 8%. The overflow samples, however, indicate an increase in silicate-hosted nickel with a decrease in density, with approximately 17% of the total nickel occurring in silicates in the 3.0 floats.

Table 4.11 Nickel concentrations of sulfide and silicate minerals

Mineral	Nickel Content (wt%)
pentlandite	34.28
pyrrhotite	0.51
chlorite	0.07
biotite	0.07
serpentine	0.09
talc	0.08
clinopyroxene	0.06
amphibole	0.04

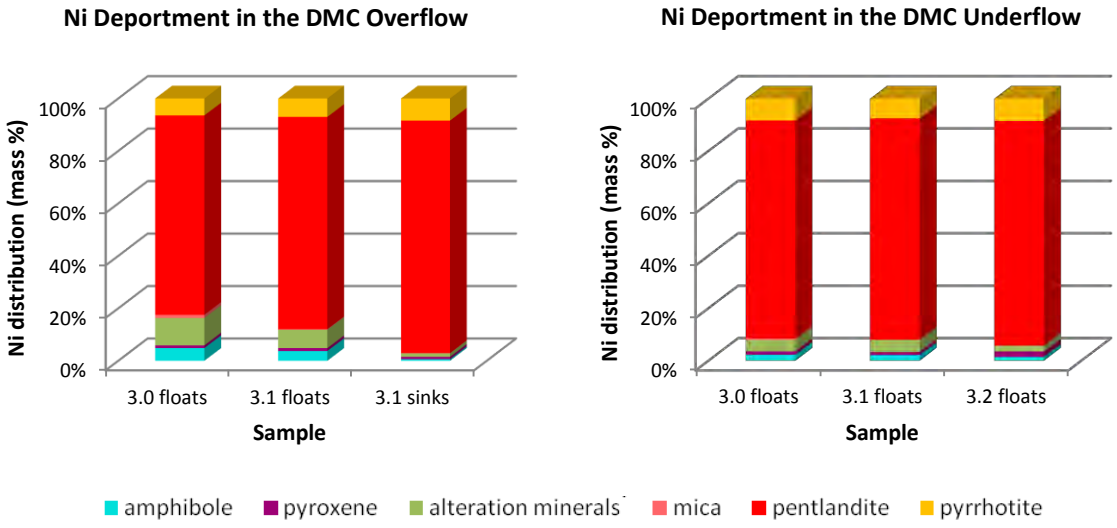

Figure 4.15 Nickel deportment within the selected density classes of the DMC overflow and underflow. Alteration minerals = serpentine, chlorite, talc and epidote.

4.3.5. Grain size, liberation and mineral associations

Grain sizes are presented for composite grains of sulfide minerals within particles, as they cannot be separated from each other by DMS and rely on their combined density contribution towards a particle in order to report to the underflow. The sizes are reported in terms of equivalent sphere diameter (ESD), which represents the diameter of a sphere of equal volume to the grain/particle measured (Haider and Levenspiel, 1989). This calculation assumes that the measurements are random cross-sections through the particle. In general, the composite sulfides show smaller grain sizes in the overflow than in the underflow, with ~90 mass % of sulfide grains in the overflow smaller than 400 µm (Figure 4.16). The largest size difference

between grains of the same density was noted between the 3.0 floats in the overflow and underflow.

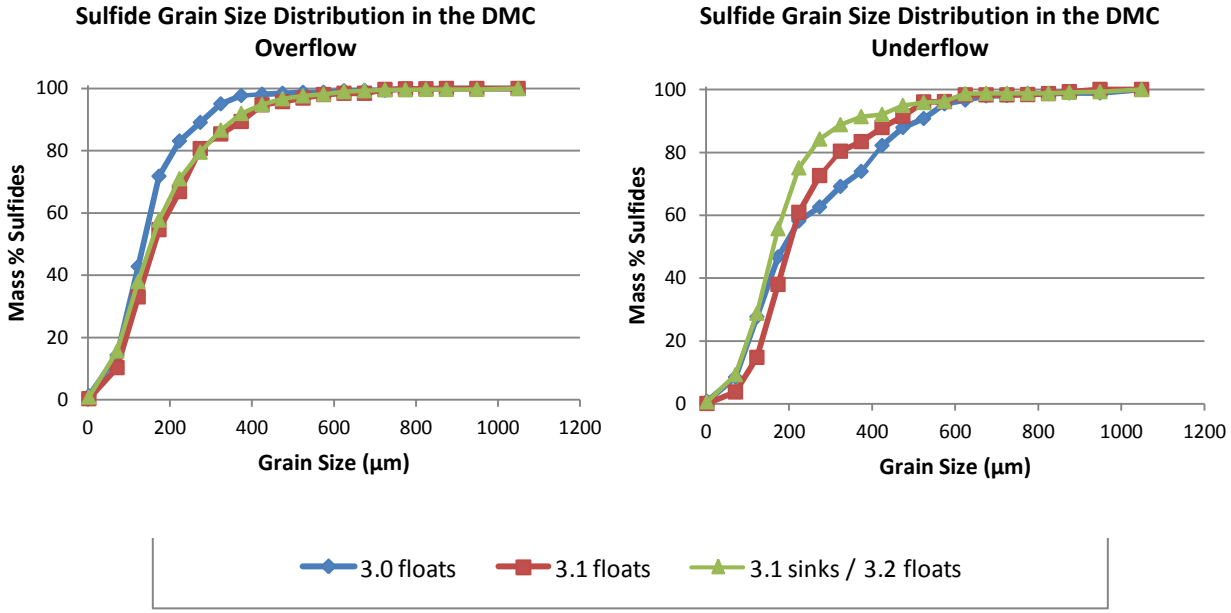

Figure 4.16 Cumulative grain size distribution for composite sulfide grains

Sulfide minerals were grouped together as composite grains in order to derive information on their combined liberation. Mineral liberation data given below are quantitative, as compared with the qualitative petrographic estimates obtained, and are calculated based on the area percent of a particle that the sulfide minerals constitute. Owing to the large particle sizes, overall sulfide liberation is very poor with few liberated grains present (Figure 4.17). The 3.1 floats of both DMS products show the lowest degree of liberation, with >99% of sulfide grains locked in gangue. The 3.1 sinks of the underflow contains the least number of locked grains, with approximately 43% by mass falling into the middlings category.

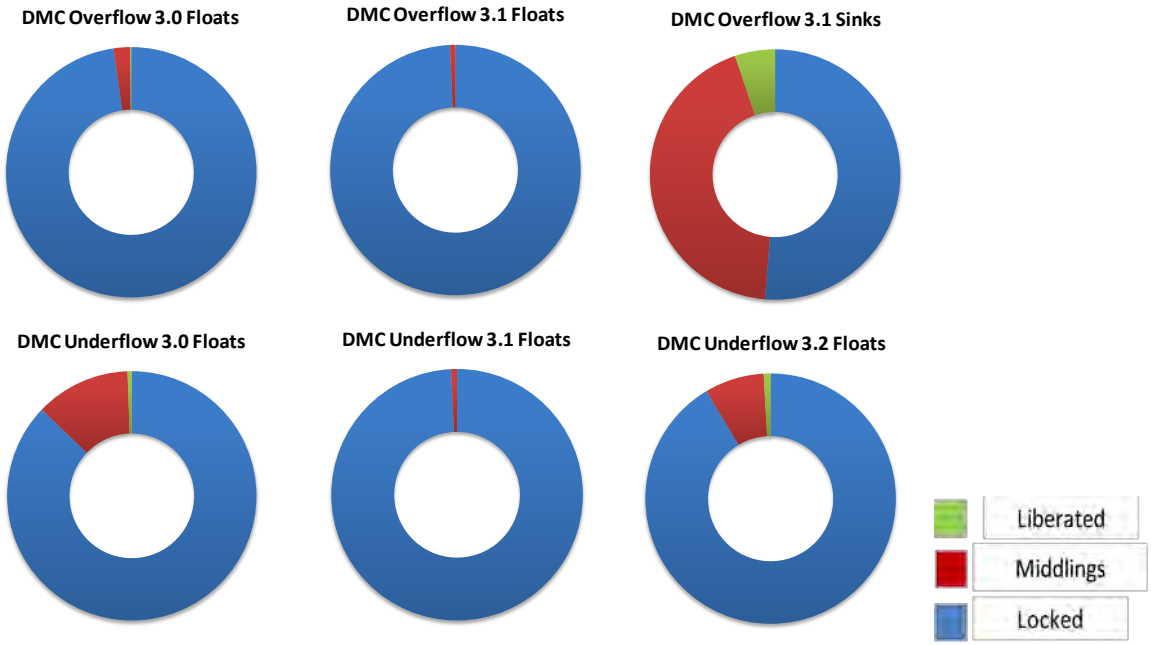

Figure 4.17 Degree of sulfide mineral liberation in each of the samples (mass %)

Mineral associations are derived from the number of shared grain boundaries between different minerals. Higher mineral associations are a product of a greater degree of grain boundary-sharing between specific minerals. Associations with 'free surface' indicate areas where a mineral grain is exposed, i.e. in contact with the mounting resin of the polished block.

The sulfide minerals are most strongly associated with the alteration minerals, amphibole and pyroxene, and in smaller amounts with oxide and carbonate minerals (Table 4.12). The 3.1 floats fractions of both the DMC overflow and underflow show the least pyroxene associations, with more alteration mineral and amphibole associations evident. In general, higher associations occur with gangue minerals present in higher proportions in the sample.

Table 4.12 Sulfide mineral associations (mass %)

Mineral	Overflow			Underflow		
	3.0 floats	**3.1 floats**	**3.1 sinks**	**3.0 floats**	**3.1 floats**	**3.2 floats**
free surface	6.4	9.9	22.2	8.6	8.0	11.3
quartz	1.0	1.2	0.4	0.4	1.4	0.3
feldspar	3.0	3.6	0.8	1.8	3.7	2.0
mica	3.0	2.5	2.1	3.0	2.5	2.6
alteration minerals	28.7	29.5	13.4	21.9	29.6	20.7
olivine	5.9	5.6	4.2	5.3	6.4	4.4
pyroxene	17.5	10.9	18.5	20.3	11.9	17.5
amphibole	13.5	20.3	15.0	17.1	20.1	20.5
oxides	11.5	4.9	13.8	13.7	5.2	10.9
carbonates	9.1	10.2	7.9	6.9	9.8	8.9
others	0.5	1.6	1.5	1.1	1.4	0.9

4.3.6. Particle properties

The measured particles in each sample are described in terms of their size and shape distributions. Particle sizes are given in mm ESD, with shape factor and elongation used to characterise the particle shapes. Figures 4.18 – 4.20 contain comparisons of the particles within the different samples.

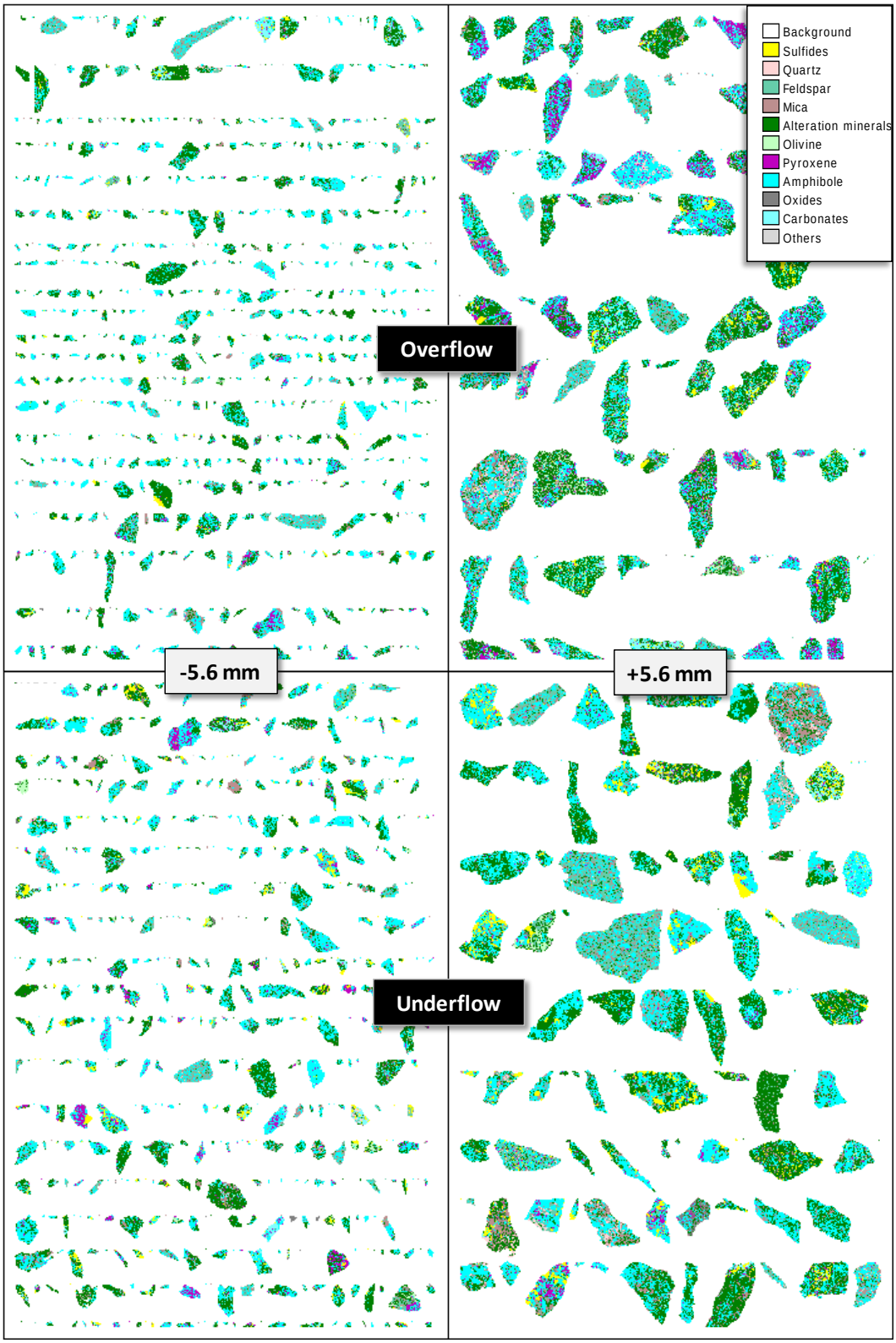

Figure 4.18 False colour mineral maps of particles in the 3.0 floats of the DMC overflow and underflow

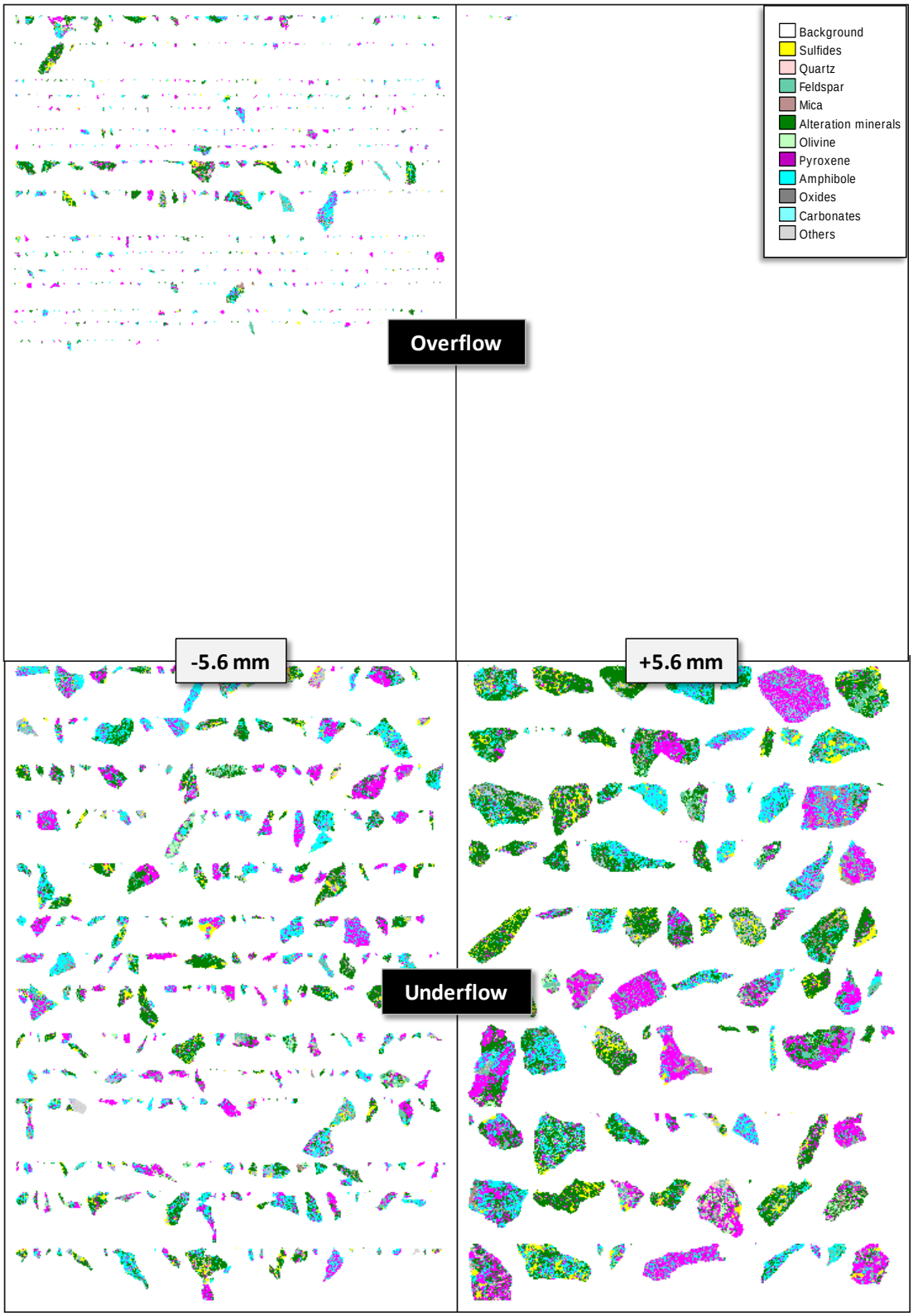

Figure 4.19 False colour mineral maps of particles in the 3.1 floats of the DMC overflow and underflow

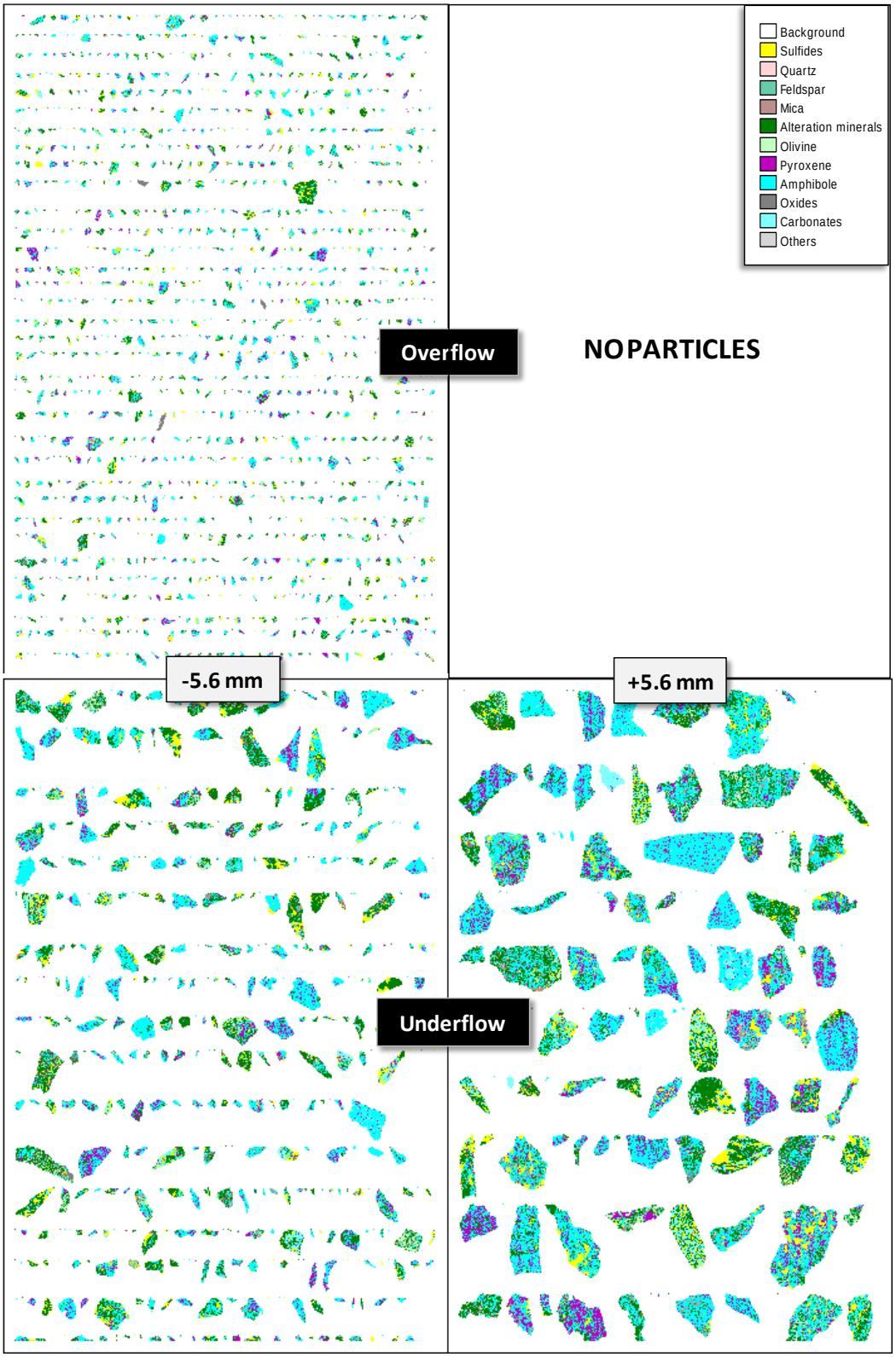

Figure 4.20 False colour mineral maps of particles in the 3.1 sinks of the DMC overflow and 3.2 floats of the underflow

The cumulative particle size distribution for each sample in ESD is given in Figure 4.21. The 3.0 floats of the overflow and underflow show similar particle size distribution. The 3.1 sinks of the overflow contains much finer particles than the rest of the samples, with most particles being smaller than 3 mm in size. A difference in particle sizes is also observed in the 3.1 floats of the DMC overflow and underflow; the overflow sample contains a larger amount of fine particles, with approximately 25% of particles less than 2 mm in size.

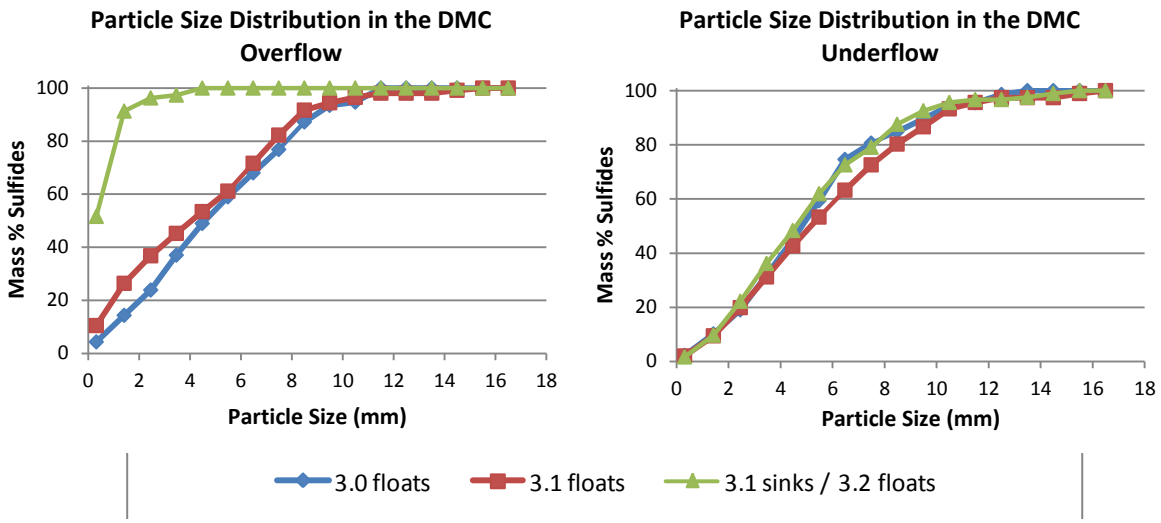

Figure 4.21 Particle size distributions in the density fractions of the DMC overflow and underflow

The distribution of particle shapes was calculated using shape factor (perimeter^2/area) and elongation (1 – width/length). These descriptors were selected to assess the effect of shape on DMS, as rounded and spherical particles are known to be easier to concentrate than elongated, angular or irregular-shaped particles (Furuuchi and Gotoh, 1992; Ferrara *et al.*, 2000). A shape factor of 12.6 corresponds to a circle, with a value of 400 calculated for a needle-shaped particle. A square has a shape factor of approximately 16, with a triangle at ~23 (Grobler and Bosman, 2009). Examples of shapes measured within the different shape factor categories for the samples are given in Figure 4.22. For elongation, values nearing 0 signify more or less equidimensional particles, whereas values closer to 1 correspond to very elongate or oblong particles. Outlines of measured particles within the different categories of elongation are also provided in Figure 4.23.

Figure 4.22 Examples of outlines of measured particle shapes within the different shape factor categories, from <10 (low shape factor) to >60 (very high shape factor)

Figure 4.23 Examples of outlines of measured particle shapes within the elongation categories, from <0.2 (low elongation) to >0.8 (very high elongation)

Little difference in shape was noted from the shape factor and elongation distributions of the samples. The shape factor calculations show that the underflow contains slightly more irregular-shaped particles than the overflow samples (Figure 4.24). The 3.1 sinks of the overflow shows more spherical particles than the other density fractions. Overall, the particles have moderate to low elongation, with slightly higher general elongation in the DMC underflow and >10 mass % of particles in all samples showing close to equidimensional shape (Figure 4.25). The 3.1 floats of the overflow and the 3.0 floats of the underflow are the density fractions with the lowest and highest particle elongation, respectively.

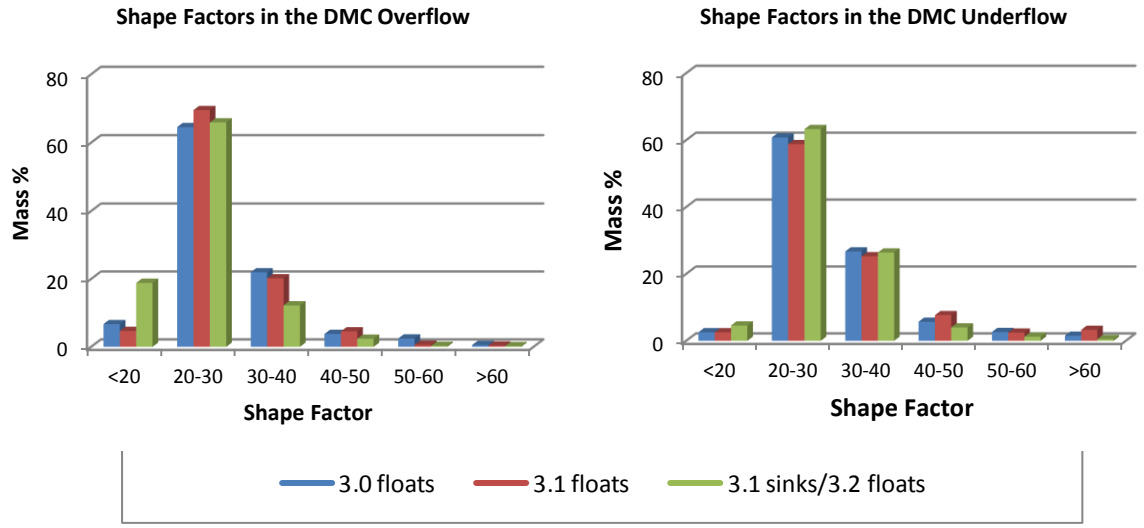

Figure 4.24 Shape factors of particles in the DMC overflow and underflow

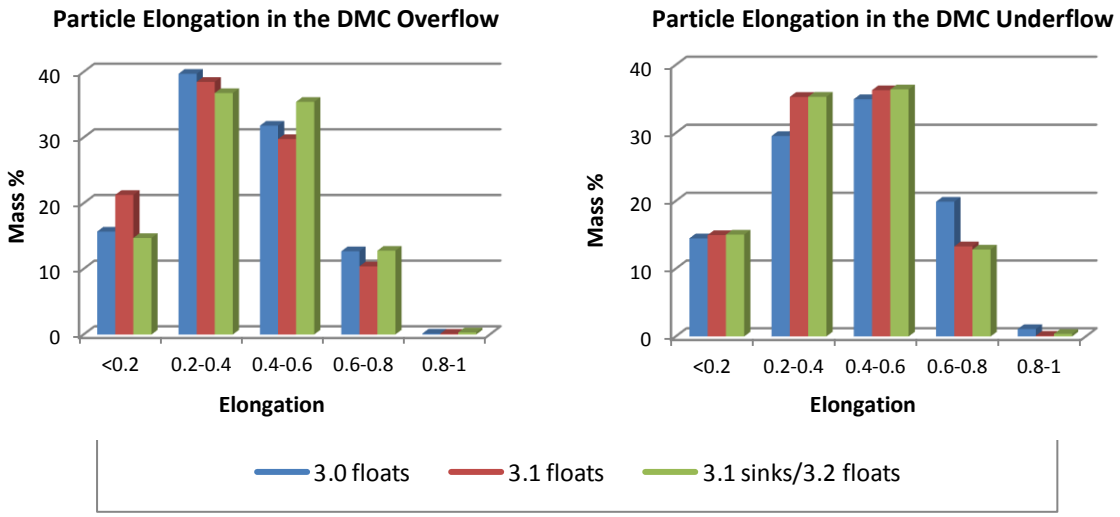

Figure 4.25 Distribution of particle elongation in the DMC overflow and underflow

4.4. Summary

The Nkomati MMZ bulk ore was sampled with a measured ROM grade of 0.40% nickel. The -12+1 mm fraction of crushed sample was preconcentrated using DMS to achieve a nickel upgrade to 0.67% at 83% recovery. Fifty two percent of the feed mass was rejected to the underflow. This correlated well with the results predicted from the preliminary sink-float analysis on the feed, which guided the selection of 3.0 as a suitable cut-point density. An Ep of 0.04 was calculated for the separation, indicating a low error and minimal misplacement of particles.

When observed petrographically, the rocks have a cumulate texture, with an original igneous mineral assemblage of pyroxene and olivine crystals with interstitial plagioclase. Alteration has occurred, producing secondary silicates such as amphibole, chlorite, talc and serpentine. The dominant sulfide minerals are pyrrhotite, chalcopyrite and pentlandite, which is the primary nickel-bearing mineral. When comparing the DMC overflow with the underflow, the underflow contains a higher proportion of sulfide minerals than the overflow, with sulfides also increasing in abundance from the lower to the higher density classes within each DMC product. Apart from an increase in sulfides, there is also separation of gangue minerals based on density. Lower density gangue minerals such as feldspar, quartz and chlorite decrease in abundance, whereas higher density silicates such as pyroxene and epidote increase in abundance in the high density fractions.

The nickel content of the Nkomati MMZ pentlandite was measured at 34.28%, with pyrrhotite containing 0.51% nickel in solid solution. Nickel also occurs in mafic silicate minerals such as pyroxene, serpentine and chlorite in amounts of between 0.05% and 0.11%. Pentlandite is the dominant nickel host, with pyrrhotite containing an average of 7.6% of the nickel within a sample. The DMC overflow contains more silicate-hosted nickel than the underflow, particularly at lower density.

The sulfide minerals commonly occur as disseminations throughout the rock, with net-textures becoming more common in the DMC underflow. The net-textured sulfides are associated with an increase in sulfide grain size and nickel grade. Pentlandite usually occurs as flame-like lamellae in pyrrhotite, particularly in the disseminated regions of the ore. Granular pentlandite is observed where the sulfides are more net-textured or massive. Sulfide grain sizes are, on average, smaller in the DMC overflow than the underflow for any given density class, with liberation being low throughout due to the large particle sizes. The highest liberation is observed from the 3.1 sinks of the overflow, as particles within this class are much smaller than those within the other density fractions. Particles within the DMC overflow are also generally smaller than those of the underflow. Subtle differences in particle shape were seen, with the underflow particles showing slightly greater elongation and high shape factor (more irregular-shaped particles) than those of the overflow.

CHAPTER 5: CHARACTERISATION OF PHOENIX ORE

Density Separation and Mineralogy

5.1. Introduction

This chapter follows the same format as Chapter 4, focusing on the Phoenix ore. The results of the density separation tests on the bulk sample are first given, followed by the mineralogical characterisation of the DMC products, with a summary of the key points of the results given at the end.

5.2. Density separation testwork

The mass and nickel grade of the DMC feed, the fines that were screened out at 1 mm and the ROM are given in Table 5.1.

Table 5.1 Stream masses and nickel grades for the Phoenix bulk sample

Stream	Mass (kg)	Ni Grade (wt%)
DMC feed	659	0.28
Fines (<1 mm)	143	0.34
ROM	802	0.29

According to the sink-float analysis on the Phoenix -25+1 mm feed sample, nickel and copper are upgradeable by separation based on density. The nickel grade in the highest density fraction is 6.92%. A density cut-point of between 2.9 and 3.1 is required if approximately half the feed is to be rejected. At a cut-point of 3.0, it is expected that around 29% of the feed mass will be concentrated, thus rejecting 71% of the mass to the overflow (Table 5.2, Figure 5.1). At this cut-point the predicted nickel grade in the underflow would be 0.59% at a recovery of 76%, with a 0.48% copper grade at 72% recovery (Figure 5.2).

Table 5.2 Sink-float analysis data for the Phoenix bulk sample (cut-point data highlighted)

SG Fraction	Relative SG to Sinks	Cumulative Mass %	Cumulative Grade to Sinks [%]			Cumulative Recovery to Sinks [%]		
			S	Cu	Ni	S	Cu	Ni
+ 3.4	3.4	1.3	23.10	2.45	6.92	39.6	17.1	41.4
- 3.4 + 3.3	3.3	1.6	21.59	2.39	5.80	44.2	19.9	41.4
- 3.3 + 3.2	3.2	1.9	19.81	2.39	5.26	46.8	22.9	43.3
- 3.2 + 3.1	3.1	6.5	7.53	1.27	1.95	62.3	42.6	56.0
- 3.1 + 3.0	3.0	28.6	2.22	0.48	0.59	81.2	71.9	75.7
- 3.0 + 2.95	2.95	42.7	1.55	0.35	0.42	84.8	77.1	79.8
-2.95 + 2.9	2.9	68.1	1.07	0.25	0.30	93.6	89.9	91.1
-2.9 + 2.8	2.8	85.7	0.89	0.22	0.25	97.7	96.3	96.8
-2.8 + 2.7	2.7	93.0	0.83	0.20	0.24	99.0	98.2	98.4
- 2.7	2.6	100.0	0.78	0.19	0.22	100.0	100.0	100.0

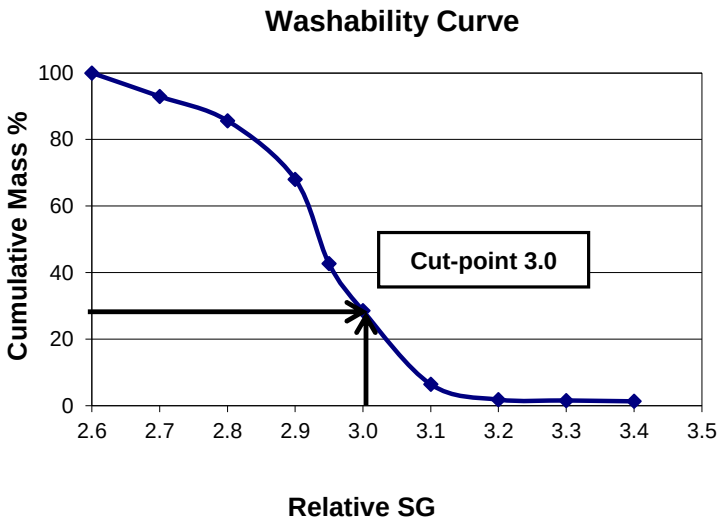

Figure 5.1 Washability curve for the Phoenix bulk sample

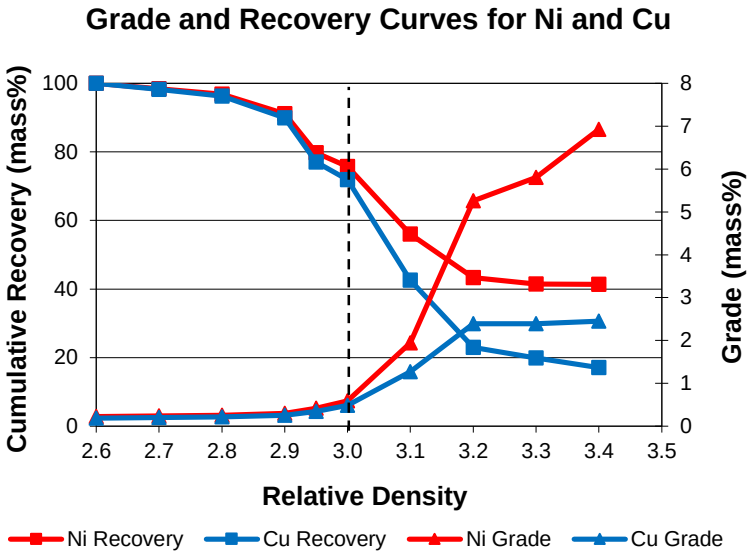

Figure 5.2 Grade and recovery curves for Ni and Cu in the Phoenix bulk sample

A summary of the DMS results is given in Table 5.3. The mass recovery to the underflow was 44.5% at a density cut-point of 3.0. The nickel was upgraded from 0.28% to 0.35% at a recovery of 85% and copper was upgraded from 0.19% to 0.33% with a 75% recovery.

Table 5.3 Summary of DMS testwork results for the Phoenix bulk sample

Fraction	Mass	Grade [%]			Recovery [%]		
	[%]	S	Cu	Ni	S	Cu	Ni
Underflow	44.5	1.29	0.33	0.35	87	75	85
Overflow	55.5	0.15	0.09	0.05	13	25	15
Total (head)	100.0	0.66	0.19	0.28	100	100	100

Table 5.4 shows the mass-balanced grade and recovery information for the Phoenix bulk sample at different points in the flowsheet represented in Figure 4.3, Chapter 4. The nickel in the Phoenix bulk sample was upgraded by 52%, from 0.28% in the ROM to 0.42% in the flotation feed. Ninety-three percent of the ROM nickel was recovered to the flotation plant. Approximately 39% of the ROM mass was rejected in the DMC overflow, with the average nickel grade of the rejected material at 0.05%.

Table 5.4 Mass-balanced mass, grade and recovery information at different points in the flowsheet

Stream No.	Stream Name	Mass	Ni Grade	Ni Recovery
		[%]	[%]	[%]
1	ROM	100	0.28	100
2	-12+1mm	82	0.22	65
3	-1mm	18	0.56	35
4	DMS overflow	39	0.05	7
5	DMS underflow	43	0.37	58
6	Float feed	61	0.42	93

Sink-float analysis was performed on the overflow and underflow obtained from the DMC in order to calculate partition coefficients for the separation (Table 5.5) and construct a partition curve (Figure 5.3). The Ep determined from the partition curve is 0.05, which shows an efficient separation. The actual separation density in the DMC was calculated as 2.98, slightly lower than the 3.0 that was aimed for. This may explain the lower nickel and copper grades and higher recoveries achieved.

Table 5.5 Partition coefficients calculated for the Phoenix bulk sample

SG Fraction	Nominal SG	Mass (%)		Reconstituted Feed	Partition Coefficient
		Underflow	Overflow		
+ 3.4	3.45	1.1	0.0	1.1	100.0
- 3.4 + 3.3	3.35	0.5	0.0	0.5	100.0
- 3.3 + 3.2	3.25	1.2	0.0	1.2	97.6
- 3.2 + 3.1	3.15	6.3	0.1	6.4	98.3
- 3.1 + 3.0	3.05	19.2	1.5	20.7	92.9
- 3.0 + 2.95	2.98	8.4	8.2	16.6	50.6
-2.95 + 2.9	2.93	5.4	13.2	18.6	29.0
-2.9 + 2.8	2.85	2.2	18.6	20.8	10.6
- 2.8	2.75	0.2	14.0	14.2	1.6
Actual Split		**44.5**	**55.5**		
Ep					**0.05**

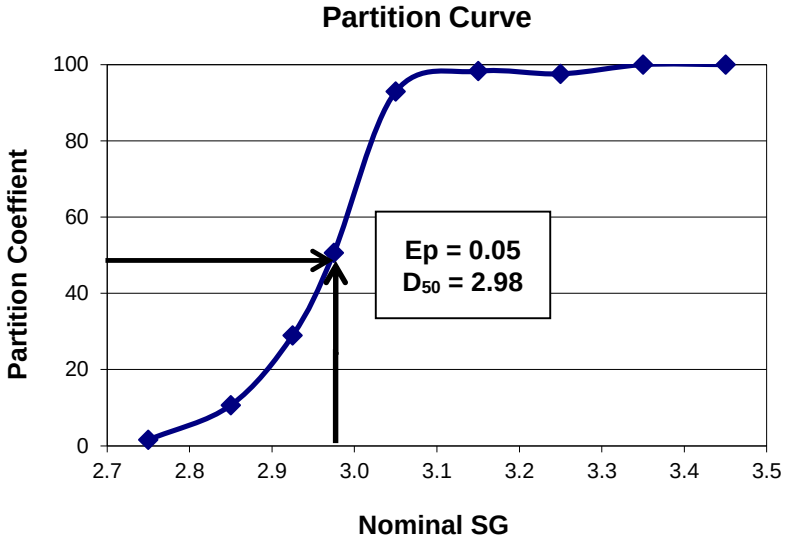

Figure 5.3 Partition curve showing the separation efficiency

5.3. Mineralogy and mineral chemistry

As in Chapter 4, this section begins with petrographic descriptions of the DMC products, followed by bulk mineralogy, mineral chemistry, nickel deportment, grain size, liberation, mineral associations and particle properties.

5.3.1 Petrography

The Phoenix ore body consists of a medium- to coarse-grained metagabbronorite, with clinopyroxene, orthopyroxene and plagioclase as primary silicate minerals. Metamorphism of the original gabbronorite parent rock has resulted in different types of alteration visible in the samples, with various mineral assemblages and textures observed. The common alteration in these rocks is for the plagioclase to alter to saussurite. Sericite (fine-grained muscovite) and carbonate minerals are frequently associated with this type of alteration process.

A significant proportion of plagioclase present in these samples has been saussuritised, forming a mixture of sericite, clays, epidote-group minerals and calcite. The mafic minerals of the original assemblage have been altered to amphibole, chlorite, serpentine and talc. Mineral grains in these samples vary from being fresh to completely altered.

The original textures have still been preserved in many of the particles observed, owing to the metamorphism of the rock being non-pervasive. The original igneous texture is shown by randomly-orientated plagioclase crystals, either fresh or saussuritised, with interstitial olivine

and pyroxene, which has often altered to amphibole or chlorite (Figure 5.4). The igneous-textured rock is generally medium- to coarse-grained. Zones with a high degree of alteration are usually fine-grained and dominated by granular masses of amphibole, chlorite and epidote (Figure 5.5). Some particles are abundant in highly-deformed quartz.

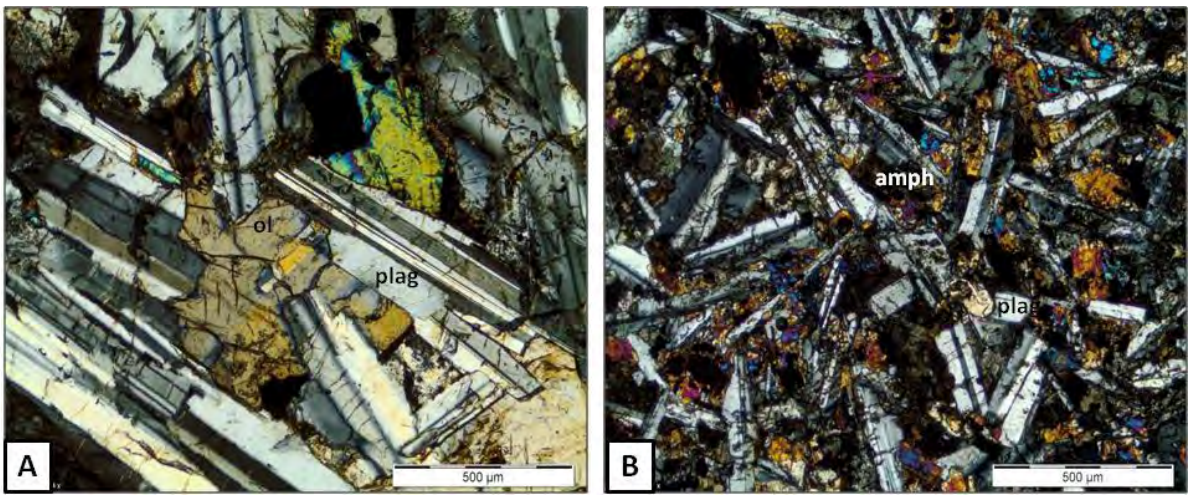

Figure 5.4 Photomicrographs showing igneous textures (transmitted crossed polarised light). **A:** medium-grained rock with plagioclase (plag) laths associated with olivine. **B:** fine-grained plagioclase associated with amphibole (amph).

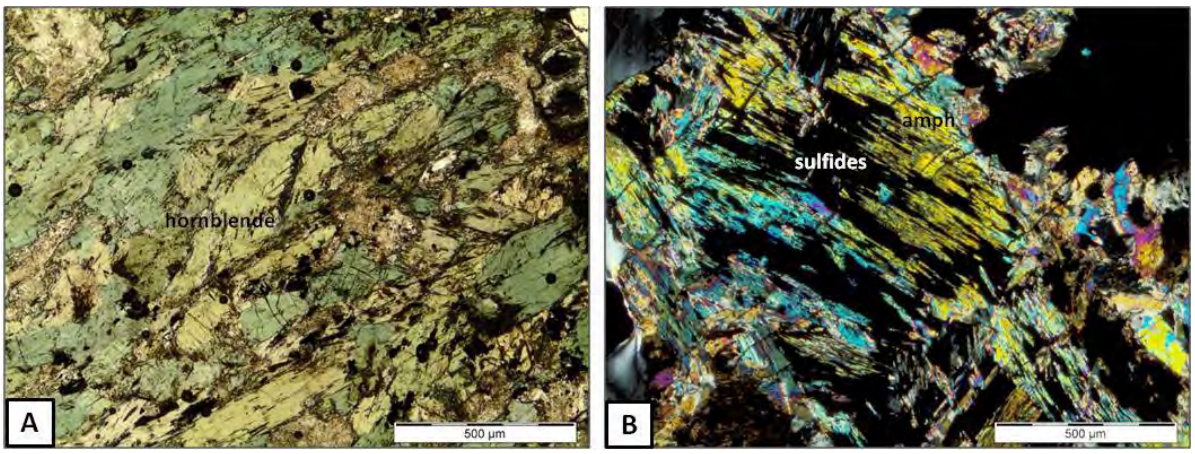

Figure 5.5 Photomicrographs showing alteration textures in the Phoenix rocks. **A:** altered section of rock composed of amphibole (hornblende; transmitted plane polarised light) **B:** deformed sulfides within amphibole cleavage planes (transmitted crossed polarised light).

The BMS are mostly disseminated in texture and finely dispersed among the silicate minerals. (Figure 5.6 A). Disseminated sulfides have also been brought about by deformation of the rock, causing the destruction of larger sulfide grains; hence the resulting sulfide grains tend to be more angular than grains that have not been deformed, or elongated when

recrystallised within amphibole cleavage planes (Figure 5.6 B). Net-textured sulfides also occur, which form interstitially to silicate crystals, but these are not common (Figure 5.6 C). The BMS may also be slightly massive in texture (Figure 5.6 D). Particles containing semi-massive sulfides have been recovered to the densest fraction of the DMC underflow.

Pentlandite is the primary nickel ore mineral and small amounts of nickel (approximately 2%) occur in solid solution in pyrrhotite. Pentlandite is almost always associated with pyrrhotite and the most common form of pentlandite in this ore is as flame-like exsolution lamellae in pyrrhotite. Pentlandite also occurs as discrete grains where the ore becomes more massive in texture, and also occasionally as veins in pyrrhotite. Application of a magnetic colloid to the surface of the polished thin sections indicates the presence of magnetic pyrrhotite only, in the Phoenix ore (Figure 5.7).

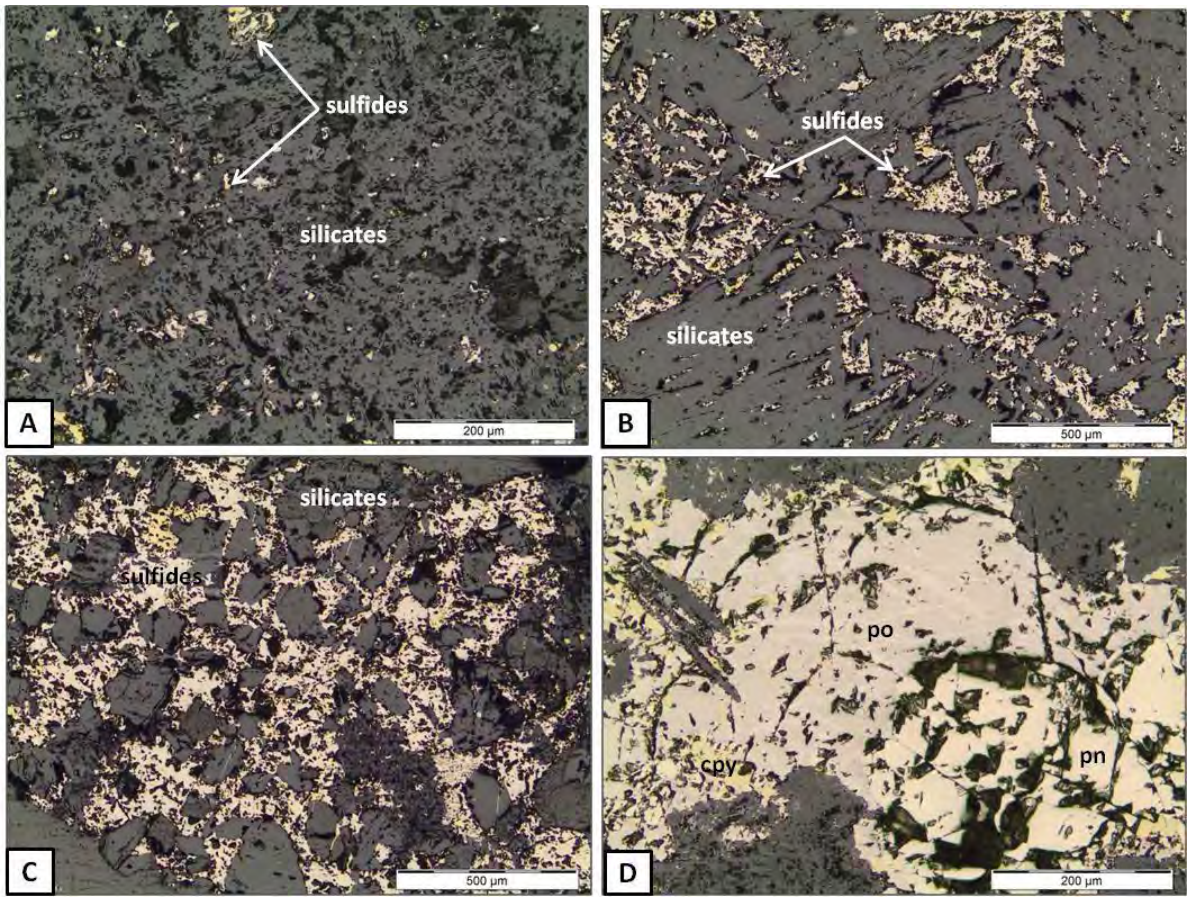

Figure 5.6 Photomicrographs showing sulfide mineral textures (reflected plane polarised light); **A:** finely disseminated sulfides (bright) among silicates. **B:** angular sulfide disseminations formed by recrystallisation along silicate grain boundaries. **C:** net-textured sulfides. **D:** pyrrhotite (po) containing pentlandite flames, and granular pentlandite (pn), associated with chalcopyrite (cpy).

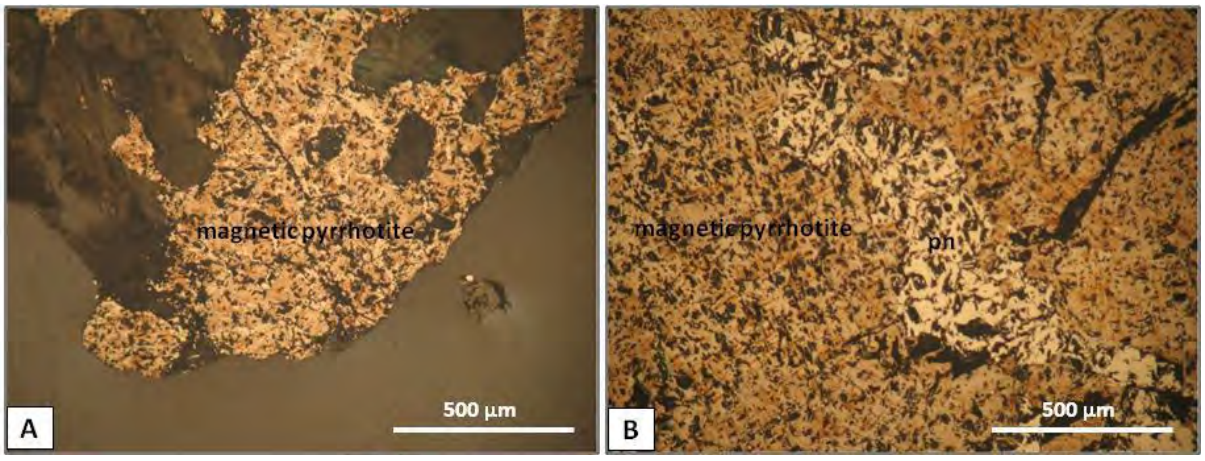

Figure 5.7 Photomicrographs showing the settling of the magnetic colloid (brown) on magnetic pyrrhotite with clean pentlandite (pn, reflected plane polarised light).

Grain sizes and liberation were estimated visually under the petrographic microscope. In general, pyrrhotite and pentlandite grains are smaller in size in the DMC overflow than in the underflow. In the overflow most of the sulfides are very finely disseminated; pyrrhotite averages from <20 to 100 µm, with the largest grain of 1.4 mm in size found in the 2.75 floats. Most of the pentlandite in the overflow occurs as minute flame-like lamellae in pyrrhotite, with few discrete grains present; granular pentlandite reaches up to approximately 480 µm. The average pyrrhotite grain size increases steadily from the lightest to the densest fractions of the underflow, from approximately 15 µm to 2.2 mm, with the largest grain found in the 3.4 sinks (~8 mm). The average pentlandite sizes are erratic but the maximum grain sizes are found in the three densest fractions of the underflow. The largest pentlandite grain was measured at approximately 1 mm.

In the overflow, the sulfides are mostly locked (<30% of the particle area) in gangue, with most making up less than 5% of the particle area. Most of the sulfides of the underflow are also locked but their liberation increases towards the higher density fractions, with a few particles in the densest fractions falling into the middlings (30-80 area %) or liberated (>80 area %) classes. There were no preferred mineral associations observed between the sulfides and any specific gangue minerals.

Some particles that do not contain sulfides were also recovered to the underflow. These were mainly highly altered particles, containing large proportions of epidote.

5.3.2 Mineral compositions

Amphibole, plagioclase, chlorite, epidote and pyroxene were the silicate minerals analysed by EPMA, with pyrrhotite and pentlandite from the sulfides. Most of the plagioclase in the ore is Ca-rich, nearing an anorthite composition, with the majority of the pyroxene having the composition of augite (Table 5.6). Two epidote-group minerals were identified, zoisite and clinozoisite, with zoisite being the more common of the two. Chlorite was identified as the Mg-Fe-Al variety clinochlore. The dominant amphibole is actinolite, with ferroactinolite and hornblende also identified. Minor nickel occurs in solid solution in pyrrhotite and mafic minerals such as chlorite and pyroxene, as detected from microprobe analyses. Pentlandite contains an average of 0.54 wt% Co in solid solution (Table 5.7). The analyses for individual mineral grains are given in Appendix D.

Table 5.6 Measured silicate mineral compositions in the Phoenix ore

Mineral	No. of Analyses		Mineral Composition (Weight %)										
			Na_2O	MgO	Al_2O_3	SiO_2	K_2O	CaO	TiO_2	FeO	Cr_2O_3	NiO	Total
hornblende	30	Average	0.44	18.55	4.56	53.31	0.05	12.43	0.14	9.10	lld	0.08	98.64*
		Std dev.	*0.20*	*1.37*	*1.84*	*1.96*	*0.05*	*0.85*	*0.10*	*1.37*	-	*0.03*	*1.27*
ferroactinolite	7	Average	0.16	14.40	1.29	50.14	0.04	7.89	0.57	24.76	lld	0.05	99.26*
		Std dev.	*0.10*	*4.61*	*0.64*	*1.66*	*0.08*	*3.53*	*0.10*	*5.60*	-	*0.01*	*0.69*
actinolite	20	Average	1.28	16.05	9.81	48.82	0.16	11.99	0.40	10.21	lld	0.07	98.74*
		Std dev.	*0.25*	*0.91*	*1.34*	*1.40*	*0.08*	*0.38*	*0.14*	*0.66*	-	*0.02*	*1.34*
augite	15	Average	0.22	15.88	2.23	51.69	lld	17.49	0.93	10.69	0.14	0.03	99.29
		Std dev.	*0.02*	*0.82*	*0.40*	*0.51*	*lld*	*0.71*	*0.14*	*1.19*	*0.10*	*0.02*	*0.24*
zoisite	10	Average	0.26	0.05	33.36	39.58	0.01	24.09	0.01	1.45	lld	0.08	98.82*
		Std dev.	*0.21*	*0.09*	*1.37*	*0.83*	*0.01*	*0.50*	*0.02*	*1.25*	-	*0.03*	*1.01*
plagioclase	26	Average	4.66	0.11	29.58	52.42	0.36	12.26	0.05	0.52	lld	0.08	99.98
		Std dev.	*1.76*	*0.24*	*2.76*	*3.67*	*0.37*	*3.08*	*0.05*	*0.33*	-	*0.04*	*0.59*
chlorite	16	Average	0.04	22.43	19.62	29.02	0.12	0.34	0.08	12.94	lld	0.13	84.71*
		Std dev.	*0.04*	*1.98*	*3.44*	*4.69*	*0.27*	*0.53*	*0.07*	*2.16*	-	*0.07*	*2.16*

**low totals are due to the presence of structural water, which cannot be measured by EPMA. lld = lower than limit of detection.*

Table 5.7 Measured sulfide compositions in the Phoenix ore

Mineral	No. of Analyses		Mineral Composition (Weight %)				
			S	Fe	Ni	Co	Total
pentlandite	24	Average	32.76	29.17	37.52	0.54	99.99
		Std dev.	*0.21*	*0.22*	*0.22*	*0.07*	*0.32*
pyrrhotite	50	Average	39.41	58.02	2.03	lld	99.46
		Std dev.	*0.16*	*0.92*	*1.02*	*lld*	*0.27*

lld = lower than limit of detection.

5.3.3 Bulk mineralogy

Table 5.8 contains all the minerals that were identified from the Phoenix ore characterisation, using a combination of XRD and petrography. Their ideal chemical formulae and average SGs are also given. Figure 5.8 compares the SGs of the identified minerals. Apart from the feldspar, the primary silicates are generally denser than most of the secondary silicates and carbonates, with oxide and sulfide minerals being the densest.

Table 5.8 Minerals identified in the Phoenix ore

Mineral	Ideal Chemical Formula	SG
zeolite	$(Ca.Na)_{2\text{-}3}Al_3(Al,Si)_2Si_{13}O_{36}\cdot 12(H_2O)$	2.20
serpentine	$Mg_3Si_2O_5(OH)_4$	2.53
K-feldspar	$KAlSi_3O_8$	2.56
plagioclase	$(Na,Ca)Al(Si,Al)_3O_8$	2.62
quartz	SiO_2	2.62
chlorite	$(Mg,Fe)_3(Si,Al)_4O_{10}(OH)_2$	2.65
calcite	$CaCO_3$	2.71
talc	$Mg_3Si_4O_{10}(OH)_2$	2.75
muscovite	$KAl_2(Si_3Al)O_{10}(OH,F)_2$	2.82
dolomite	$CaMg(CO_3)_2$	2.84
biotite	$K(Mg,Fe)_3AlSi_3O_{10}(OH,F)_2$	3.00
amphibole	$Ca_2(Mg,Fe)_4Al(Si_7Al)O_{22}(OH,F)_2$	3.04
olivine	$(Mg,Fe)_2SiO_4$	3.27
clinopyroxene	$(Ca,Na)(Mg,Fe,Al,Ti)(Si,Al)_2O_6$	3.40
epidote	$Ca_2(Fe,Al)Al_2(SiO_4)(Si_2O_7)O(OH)$	3.45
orthopyroxene	$(Mg,Fe)_2Si_2O_6$	3.55
sphalerite	ZnS	4.08
chalcopyrite	$CuFeS_2$	4.10
pyrrhotite	$Fe_{1\text{-}x}S$	4.61
zircon	$ZrSiO_4$	4.65
ilmenite	$FeTiO_3$	4.72
pentlandite	$(Fe,Ni)_9S_8$	4.80
pyrite	FeS_2	5.01
bornite	Cu_5FeS_4	5.09
magnetite	Fe_3O_4	5.20
hematite	Fe_2O_3	5.30
digenite	Cu_9S_5	5.60
arsenopyrite	$FeAsS$	6.07

primary silicate secondary silicate sulfide oxide / carbonate

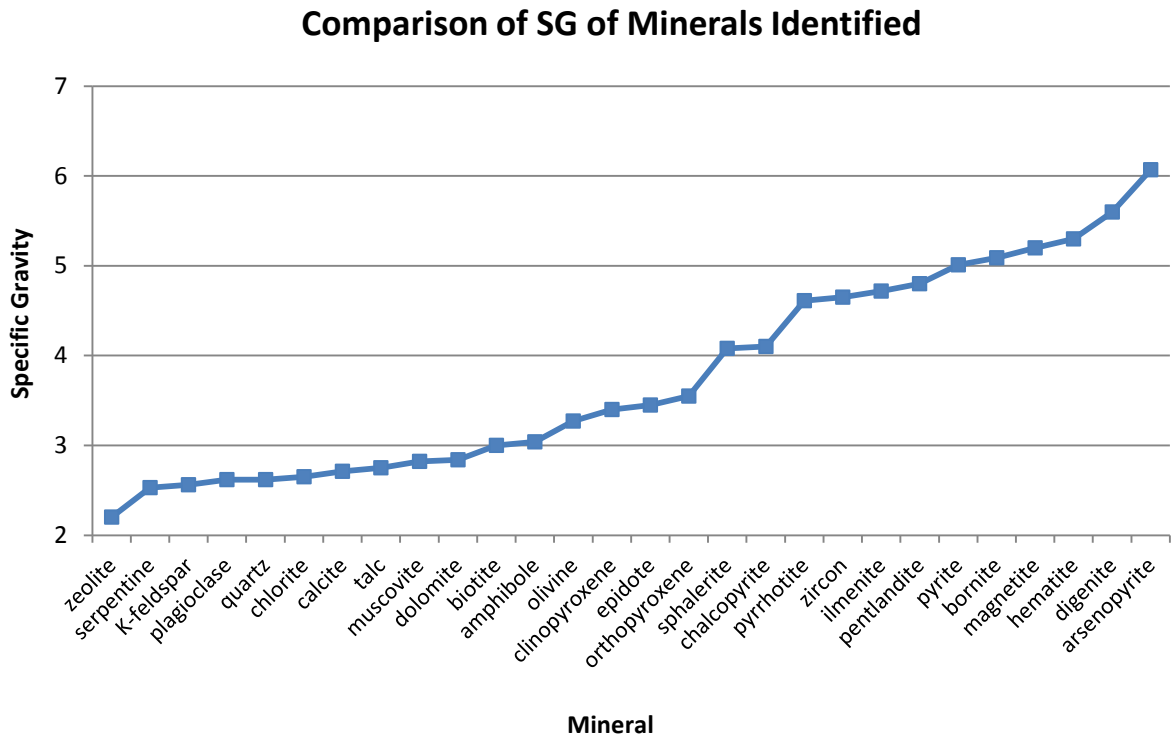

Figure 5.8 Identified minerals in order of increasing SG

The mineral proportions in the DMC feed, and each SG class of the overflow and underflow were determined using quantitative XRD. Feldspar (plagioclase and K-feldspar), amphibole, chlorite, epidote and pyroxene make up the bulk of the ore, with quartz, mica, carbonates and Fe-Ti oxides present in smaller amounts (Figure 5.9). Pyrrhotite was the only sulfide mineral present in detectable amounts in the feed with pentlandite and chalcopyrite occurring in quantities not detectable by XRD. The grouping 'others' contains gangue minerals in low quantities such as kaolinite and zeolite.

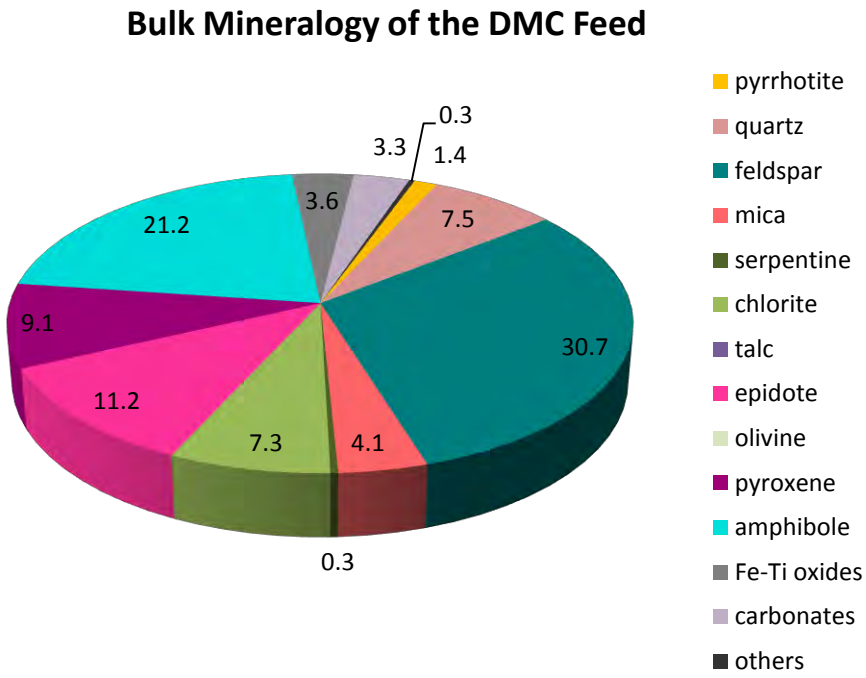

Figure 5.9 Bulk mineral composition of the DMC feed, as determined by XRD

The DMC underflow shows a higher sulfide mineral content than the overflow, with pyrrhotite detected in most of the SG classes of the underflow (Figures 5.10 and 5.11). The sulfide proportions are also higher within the underflow SG fractions, when compared with their corresponding fractions in the overflow. Pentlandite was only detectable in the high density fractions of the underflow. Gangue minerals also vary in abundance according to their SGs. Quartz and feldspar dominate the lower SG fractions and their proportions decrease steadily with an increase in SG. Mica, which has a higher content in the underflow, is also shown to decrease with an increase in SG. Fe-Ti oxides are present in higher levels in the overflow and increase with increasing SG. Amphibole increases in abundance towards the separation cut-point of approximately 3.0 in the overflow and underflow, which is also around the SG of amphibole.

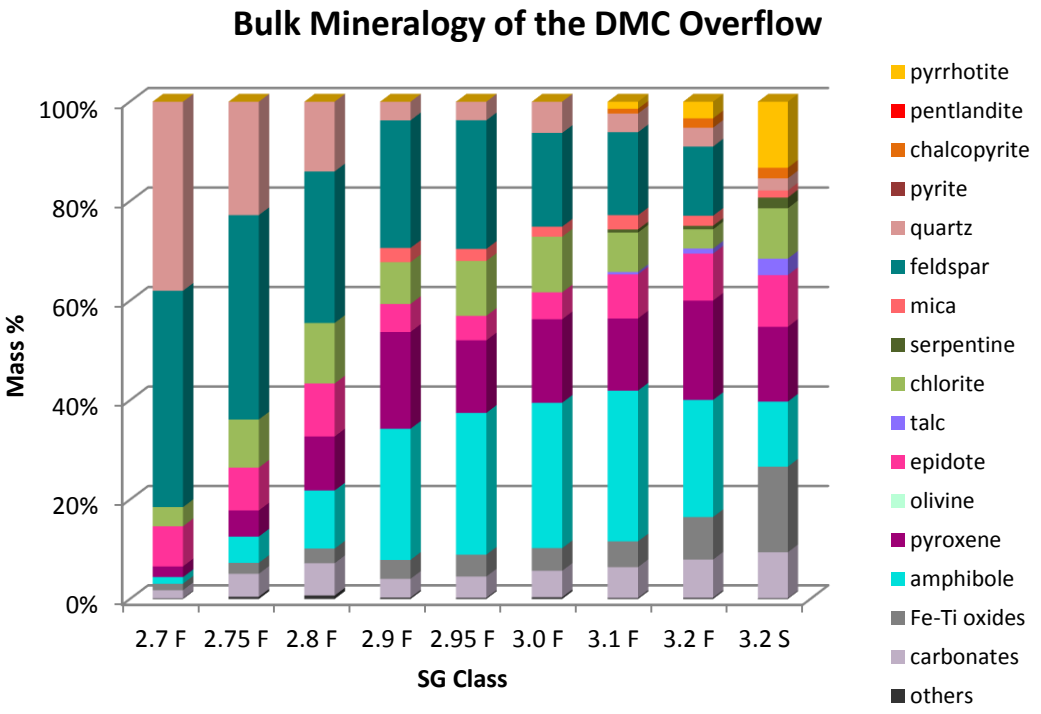

Figure 5.10 Bulk mineral composition of the DMC overflow samples, as determined by XRD

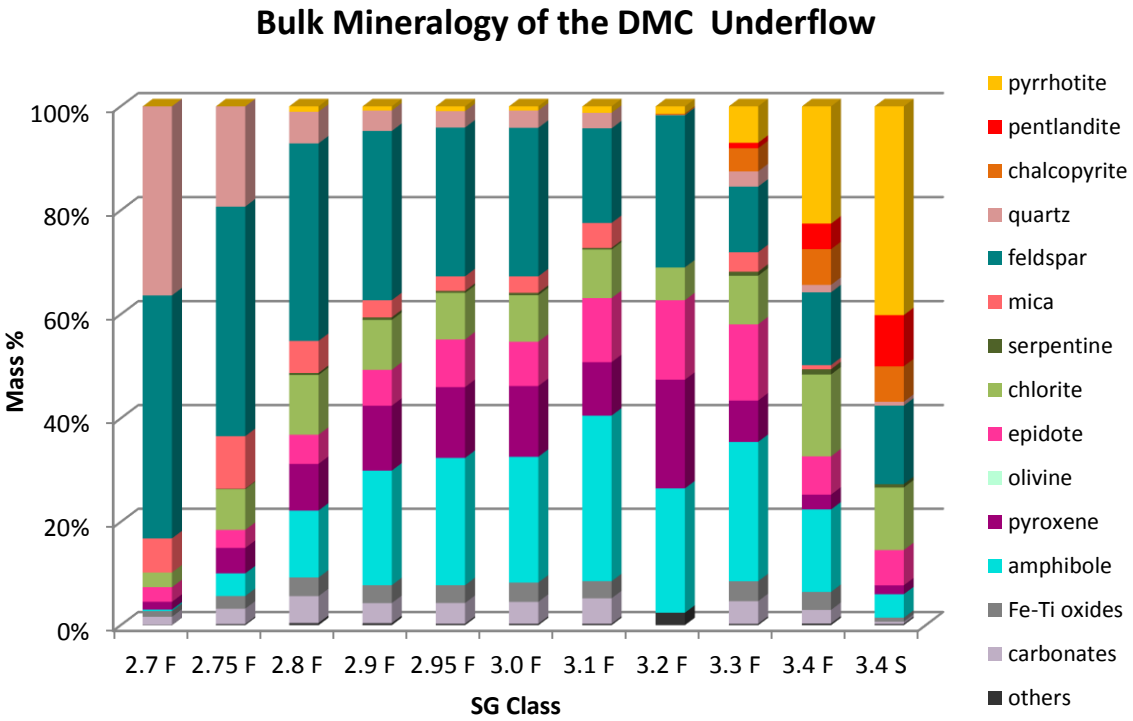

Figure 5.11 Bulk mineral composition of the DMC underflow samples, as determined by XRD

The density fractions selected from each of the DMC products (underflow and overflow) for QEMSCAN analysis are shown in Table 5.9. The DMS cut-point used was 3.0; samples were therefore chosen around this density and slightly further away from the cut-point to compare changes in their mineralogy. The mass % that each density class constitutes of the whole product is also provided, together with the number of particles measured on the QEMSCAN for each sample.

Table 5.9 Samples subjected to QEMSCAN analysis

DMC Overflow		
SG Class	**Mass %**	**No. of Particles**
2.95 floats (SG 2.9 – 2.95)	23.8	4 060
3.0 floats (SG 2.95 – 3.0)	14.7	2 755
3.1 floats (SG 3.0 – 3.1)	2.6	5 752
DMC Underflow		
SG Class	**Mass %**	**No. of Particles**
2.95 floats (SG 2.9 – 2.95)	12.1	3 058
3.0 floats (SG 2.95 – 3.0)	18.9	2 442
3.1 floats (SG 3.0 – 3.1)	43.2	2 215

The modal mineralogy results from the QEMSCAN show similar mineral proportions within the same density class of the DMC overflow and underflow (Table 5.10, Figure 5.12). The major minerals are feldspar, amphibole, alteration minerals and pyroxene. The highest BMS content is found in the 3.1 floats of the underflow.

Table 5.10 Modal mineralogy of selected SG fractions of the DMC overflow and underflow (mass %)

Mineral	Ideal Chemical Formula	Overflow			Underflow		
		2.95 floats	**3.0 floats**	**3.1 floats**	**2.95 floats**	**3.0 floats**	**3.1 floats**
pyrrhotite	$Fe_{1-x}S$	0.2	0.1	0.8	0.3	0.1	1.0
pentlandite	$(Fe,Ni)_9S_8$	0.2	0.1	0.4	0.1	0.1	0.6
chalcopyrite	$CuFeS_2$	0.2	0.2	0.4	0.4	0.1	0.7
pyrite	FeS_2	0.1	0.1	0.1	0.1	0.0	0.1
quartz	SiO_2	2.1	1.6	2.0	2.2	1.6	2.1
feldspar	$(K,Na,Ca)Al(Si,Al)_3O_8$	18.9	24.3	13.3	18.7	24.3	12.3
mica	$K(Mg,Fe)_3AlSi_3O_{10}(OH,F)_2$	4.1	2.9	4.2	4.3	3.0	4.2
serpentine	$Mg_3Si_2O_5(OH)_4$	0.0	0.0	0.0	0.0	0.0	0.0
chlorite	$(Mg,Fe)_5Al(Si_3Al)O_{10}(OH)_8$	11.4	7.5	7.5	10.2	7.5	8.9
talc	$Mg_3Si_4O_{10}(OH)_2$	1.0	0.0	1.1	0.7	0.0	0.9
epidote	$Ca_2(Fe,Al)Al_2(SiO_4)(Si_2O_7)O(OH)$	14.6	11.5	14.1	14.0	14.1	16.3
olivine	$(Mg,Fe)_2SiO_4$	0.1	0.0	0.1	0.1	0.0	0.1
pyroxene	$(Ca,Na)(Mg,Fe,Al,Ti)(Si,Al)_2O_6$	15.3	8.8	16.8	17.6	7.0	17.6
amphibole	$Ca_2(Mg,Fe)_4Al(Si_7Al)O_{22}(OH,F)_2$	28.5	38.2	33.8	27.5	38.1	32.4
kaolinite	$Al_2Si_2O_5(OH)_4$	0.0	1.3	0.0	0.0	1.4	0.0
Fe-Ti oxides	-	2.8	2.9	4.4	3.2	2.3	2.2
carbonates	$CaCO_3/CaMg(CO_3)_2$	0.0	0.1	0.1	0.1	0.0	0.1
others*	-	0.6	0.6	0.8	0.6	0.4	0.5
Total BMS		**0.7**	**0.5**	**1.7**	**0.9**	**0.3**	**2.4**
Total		**100**	**100**	**100**	**100**	**100**	**100**

**accessory minerals present in amounts of <0.1%, e.g. zircon and apatite*

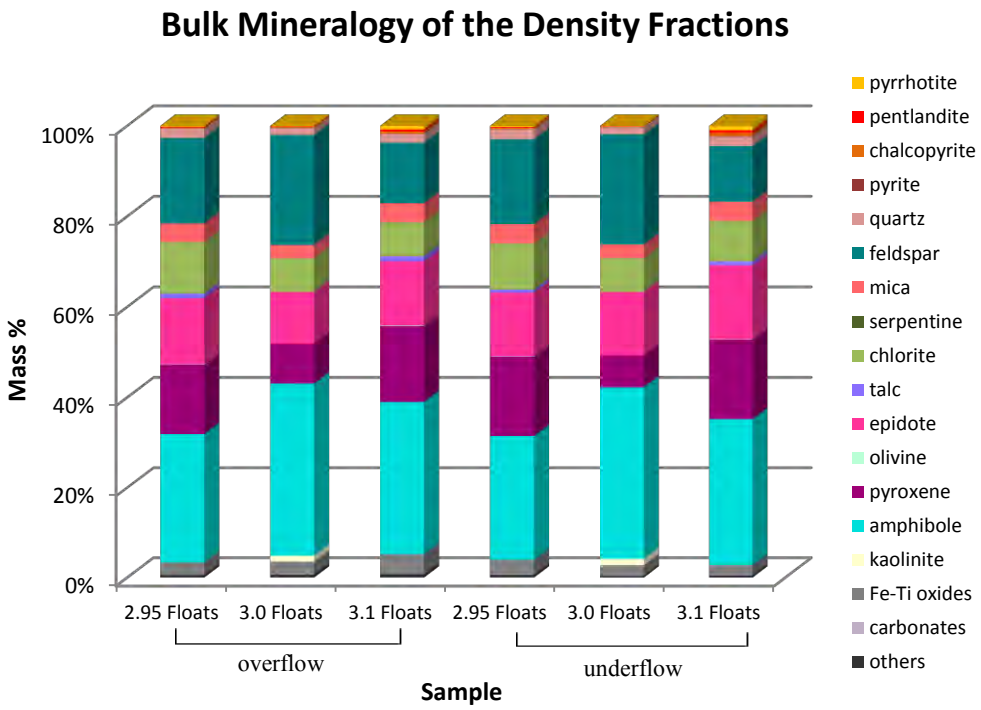

Figure 5.12 QEMSCAN bulk mineralogy

5.3.4 Nickel deportment

The nickel concentrations of all identified Ni-bearing minerals, as measured by EPMA (Tables 5.6 and 5.7), were converted from oxide to elemental form and used to calculate the deportment of nickel in each sample. Pentlandite is the only discrete nickel mineral present, with pyrrhotite containing an average of 2.03% Ni in solid solution (Table 5.11). Nickel-containing silicate minerals are chlorite, epidote, clinopyroxene and amphibole. Nickel is also likely to be found in other mafic minerals such as olivine and serpentine, but these were too low in abundance and usually very fine-grained to be able to locate grains suitable for EPMA.

Table 5.11 Nickel concentrations of sulfide and silicate minerals

Mineral	Nickel Content (wt%)
pentlandite	37.52
pyrrhotite	2.03
chlorite	0.10
epidote	0.06
clinopyroxene	0.02
amphibole	0.05

The DMC overflow density fractions show similar nickel deportment to the corresponding density fractions of the underflow (Figure 5.13). Apart from the 3.1 floats samples, a large portion of nickel is contained in silicates. This is highest in the 3.0 floats fractions, with the silicate nickel content at 53% in the 3.0 floats of the DMC underflow. The 3.1 floats contains 75.7% and 77.7% pentlandite-hosted nickel in the overflow and underflow, respectively. Pyrrhotite hosts between 2 – 8% of the total nickel in each sample.

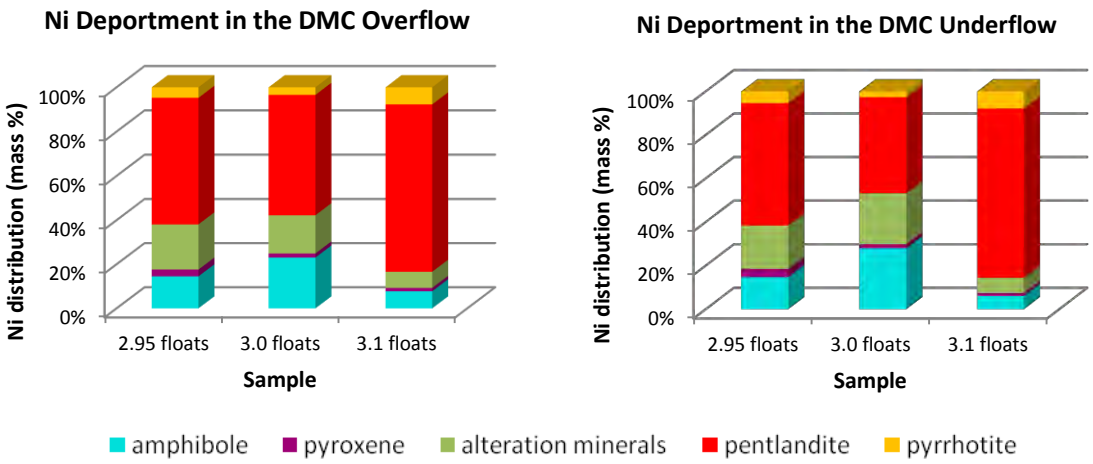

Figure 5.13 Nickel deportment within the selected density classes of the DMC overflow and underflow. Alteration minerals = serpentine, chlorite, talc and epidote.

5.3.5 Grain size, liberation and mineral associations

In the DMC overflow, composite sulfide grains in all of the density classes have similar sizes, with >95% of grains smaller than 200 µm (Figure 5.14). The 2.95 floats contains slightly larger grains than the other two density classes. The DMC underflow fractions show coarser sulfides than the overflow in the 3.0 floats and 3.1 floats, with average sizes increasing with density. The 3.1 floats of the underflow has the coarsest grains of all the samples, with grains up to ~900 µm measured. The 2.95 floats of the underflow has the smallest sulfide grains of all samples, with 94% of grains less than 100 µm in size.

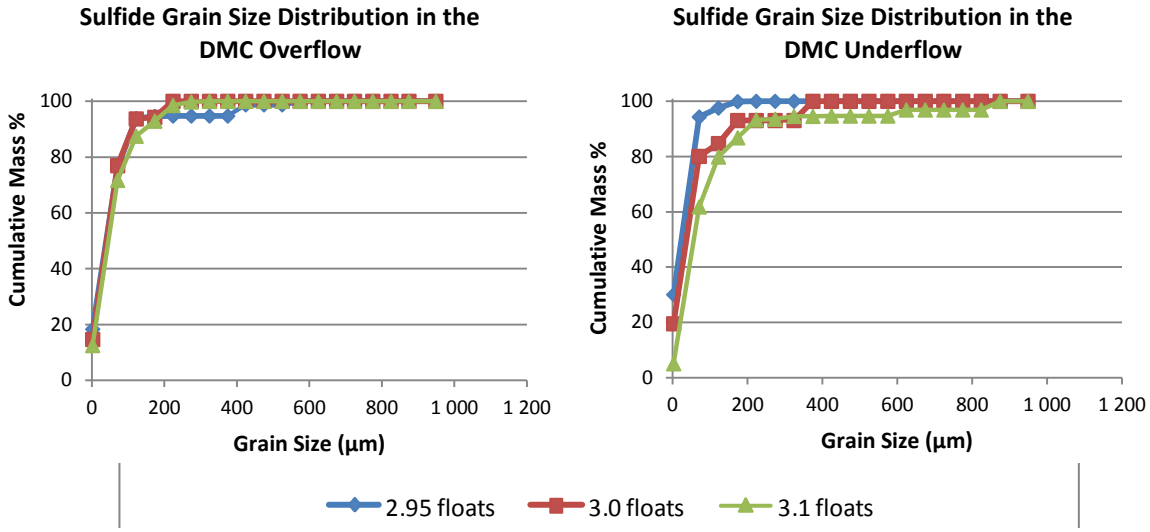

Figure 5.14 Cumulative grain size distribution for composite sulfide grains

Total sulfide liberation is poor throughout the samples, with most grains being locked in gangue (Figure 5.15). The 3.1 floats of the DMC overflow and underflow show 6% and 11% middlings grains, respectively, representing the samples with the highest sulfide liberation.

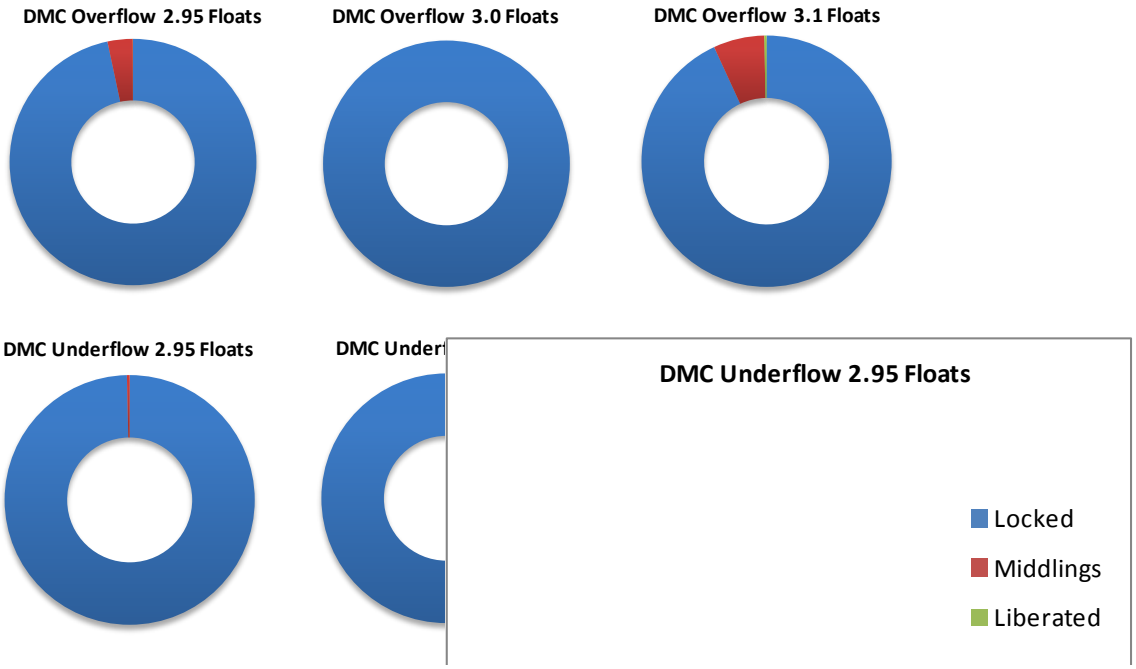

Figure 5.15 Degree of sulfide mineral liberation in each of the samples (mass %)

The BMS in all samples are most commonly associated with alteration minerals, pyroxene and amphibole (Table 5.12). The mineral associations are generally related to the abundance of the gangue minerals present in each sample.

Table 5.12 Sulfide mineral associations (mass %)

Mineral	Overflow			Underflow		
	2.95 floats	**3.0 floats**	**3.1 floats**	**2.95 floats**	**3.0 floats**	**3.1 floats**
free surface	5.2	2.8	7.0	4.4	2.5	4.9
quartz	5.2	3.0	3.9	4.8	2.5	3.9
feldspar	13.1	10.2	8.7	13.9	11.7	9.6
mica	2.6	1.3	1.8	3.7	1.9	2.5
alteration minerals	33.4	35.3	31.7	29.6	33.9	36.4
olivine	0.5	0.0	1.0	0.6	0.0	0.7
pyroxene	15.8	12.9	19.9	18.3	12.7	18.8
amphibole	15.6	27.4	16.6	16.3	26.3	15.3
Fe-Ti oxides	5.2	1.4	5.0	4.8	1.2	4.0
carbonates	0.2	0.1	0.3	0.2	0.1	0.1
others	3.2	5.6	4.1	3.6	7.2	3.7

5.3.6 Particle properties

Particle size (in ESD) and shape distributions, in terms of shape factor and elongation, were calculated from the QEMSCAN particle images. The false colour mineral maps are shown in Figures 5.16 – 5.18, comparing the particles of the DMC overflow and underflow within each density class.

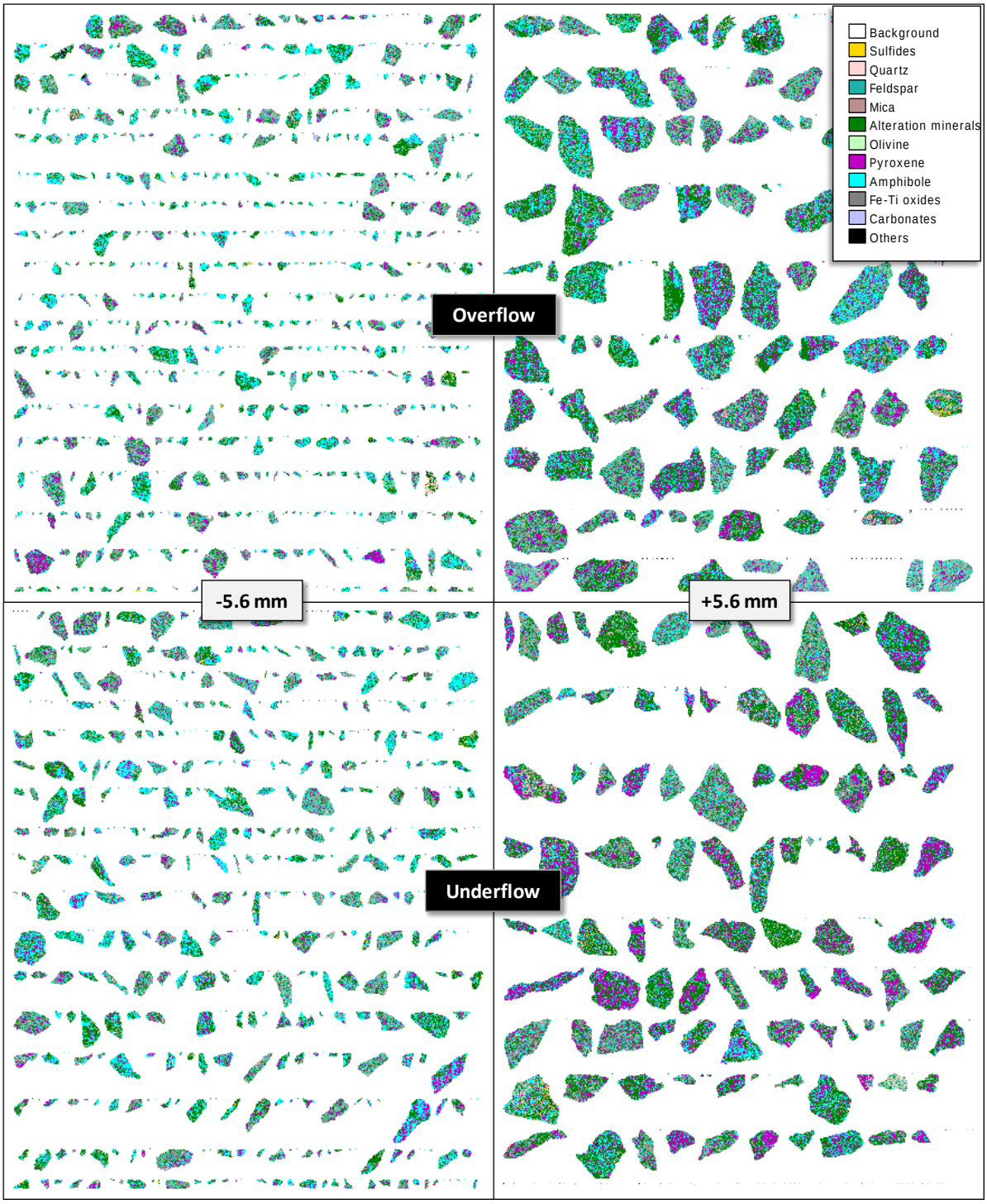

Figure 5.16 False colour mineral maps of particles in the 2.95 floats fractions of the DMC overflow and underflow

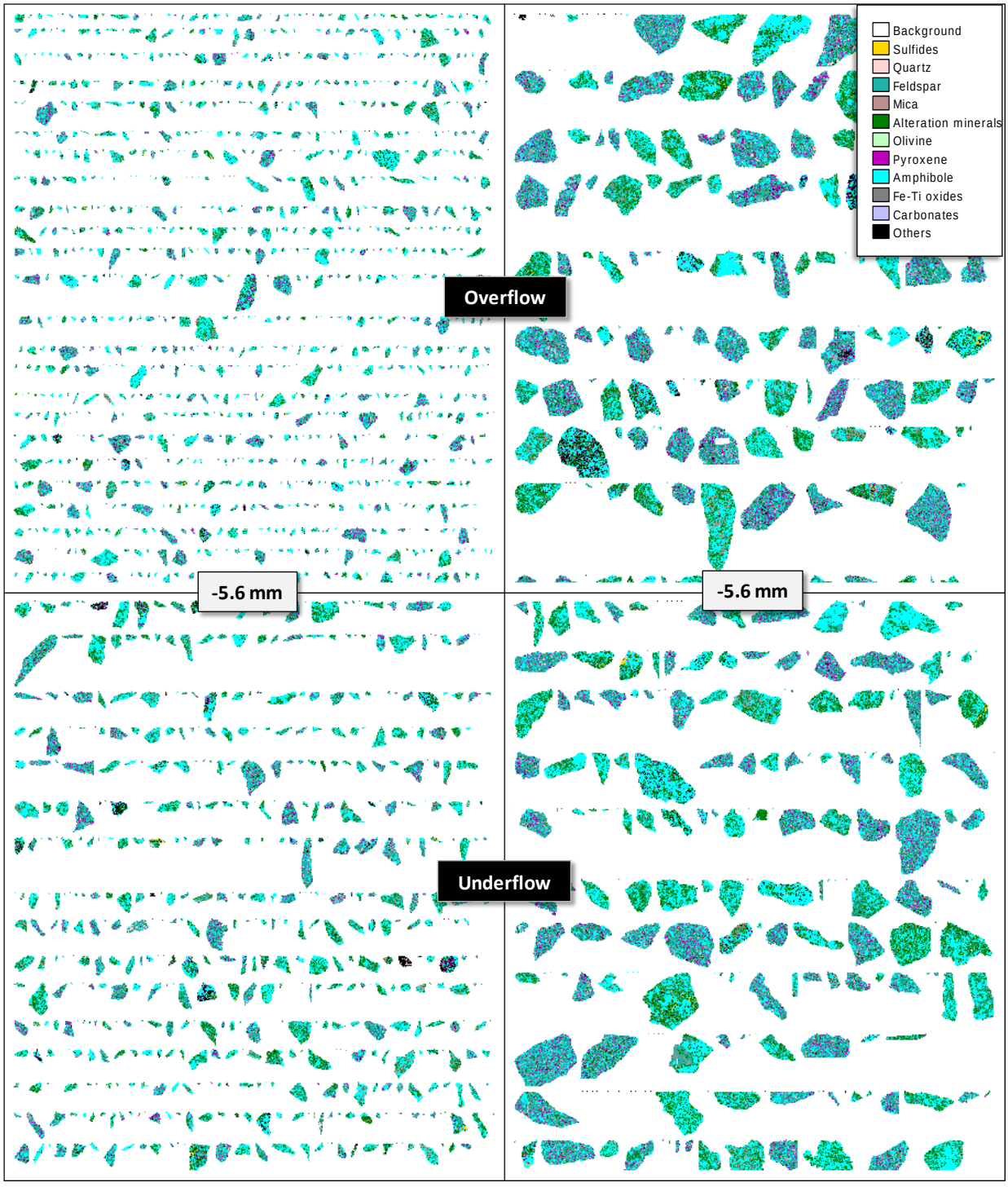

Figure 5.17 False colour mineral maps of particles in the 3.0 floats fractions of the DMC overflow and underflow

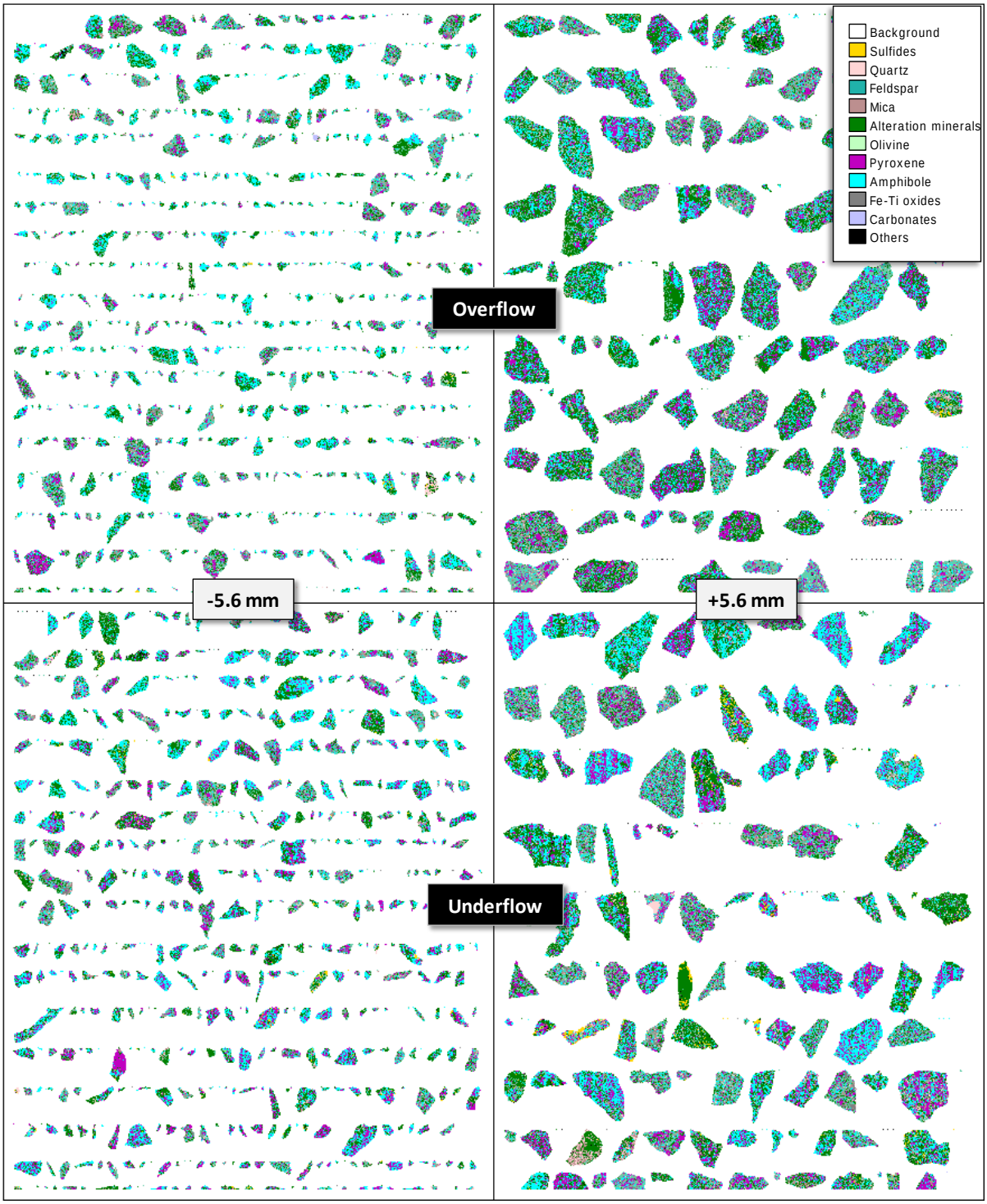

Figure 5.18 False colour mineral maps of particles in the 3.1 floats fractions of the DMC overflow and underflow

The cumulative particle size distributions for the different density classes are similar, apart from the 3.1 floats of the DMC overflow, which shows smaller particles than the other samples (Figure 5.19). Eighty percent of particles for most density classes are generally less

than 7 – 8 mm, with 80% of the particles in the 3.1 floats of the overflow being less than 5 mm.

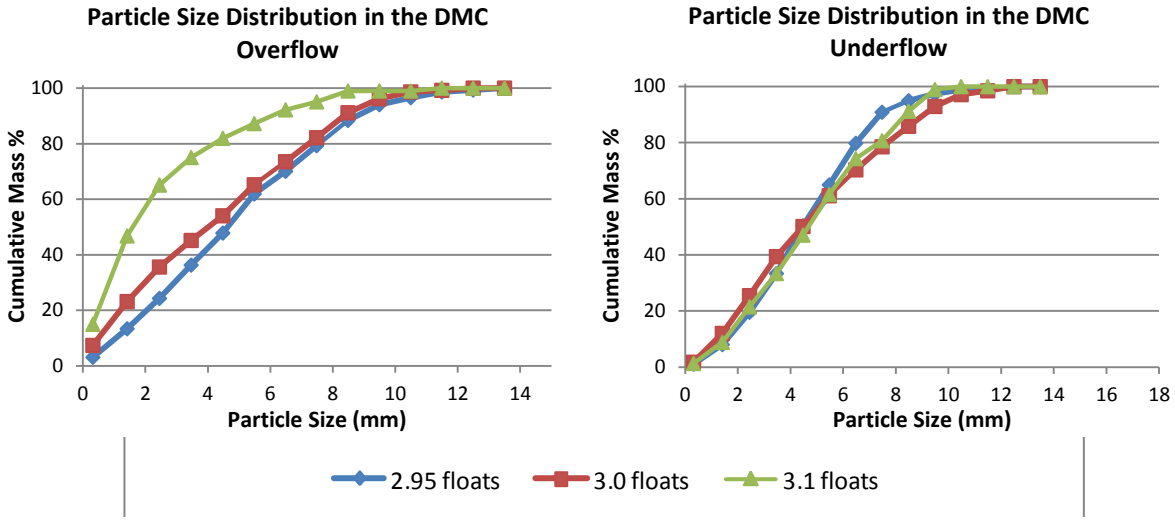

Figure 5.19 Particle size distributions in the density fractions of the DMC overflow and underflow

Shape factors of the particles in the DMC overflow and underflow show similar distributions, with the majority of particles having shape factor values of between 20 and 30, indicating irregular shapes (Figure 5.20). The samples of the underflow show a slightly higher percentage of particles with shape factors of 30 and above, of up to ~28% in the 2.95 floats.

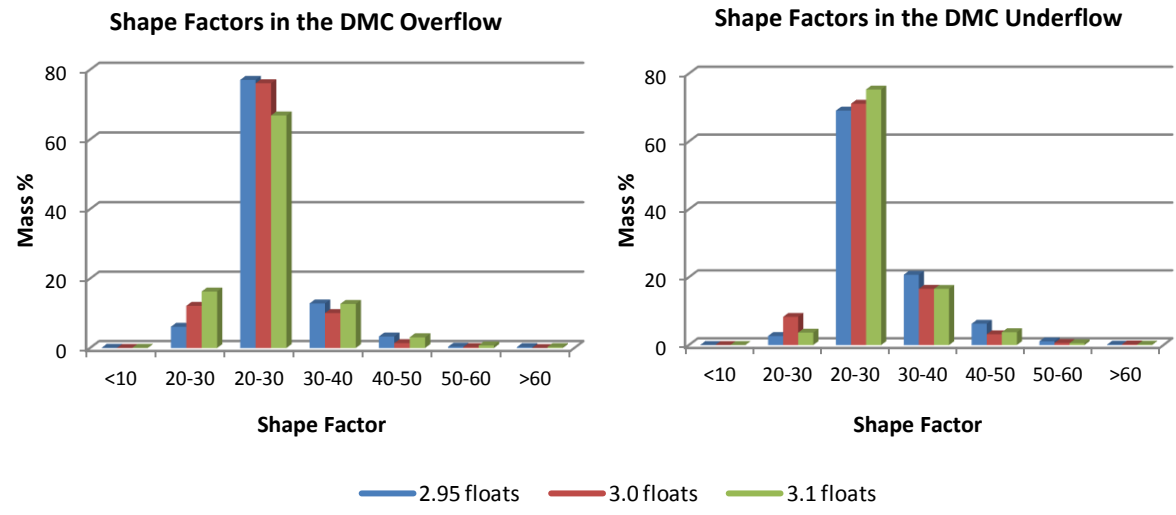

Figure 5.20 Shape factors of particles in the DMC overflow and underflow

Particle elongation also shows similar trends among the different samples (Figure 5.21). Most particles have an elongation of between 0.2 and 0.6, with not many highly elongated particles occurring. The underflow contains slightly more elongated particles than the overflow, with more than 10% of the 2.95 floats and 3.0 floats showing an elongation of >0.6 in the underflow.

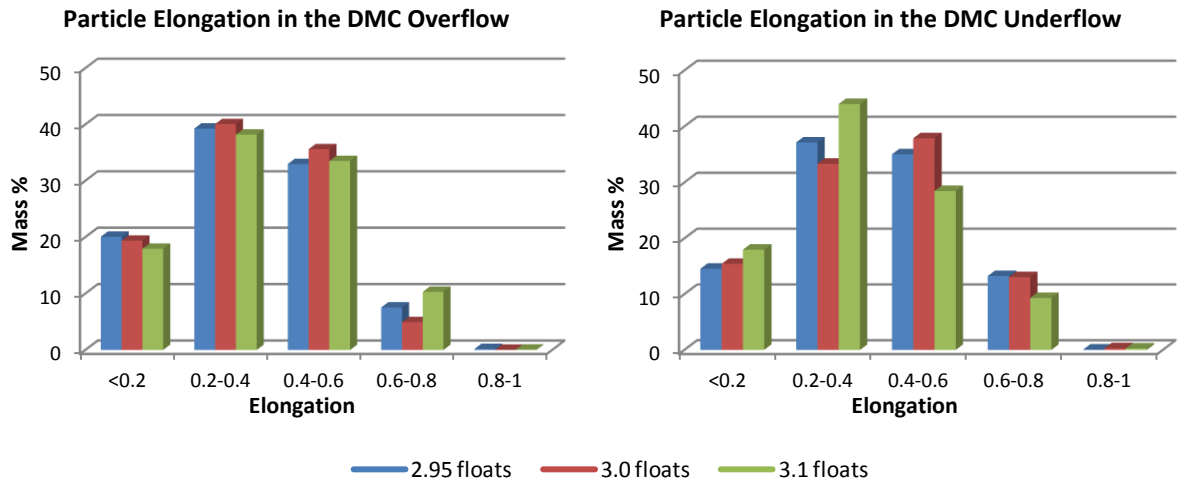

Figure 5.21 Distribution of particle elongation in the DMC overflow and underflow

5.4. Summary

The Phoenix ore sample was subjected to DMS with a feed grade of 0.18% nickel. Washability and grade-recovery curves calculated from the preliminary sink-float analysis indicated a potential nickel upgrade to 0.59% at 76% recovery, if a cut-point of 3.0 is used. This would yield a mass recovery of 29%. The actual DMS testwork produced a 0.35% nickel grade at 85% recovery, concentrating 44.5% of the feed mass. The difference in the predicted and actual data may be due to a slightly lower D_{50} of 2.98 attained during the separation. The Ep of the separation was calculated as 0.05, which shows an overall efficient separation with minimal particle misplacement in the DMC.

Mineralogical evaluation confirms the ore to be a metamorphosed gabbronorite, mainly composed of plagioclase, amphibole, chlorite and pyroxene and quartz. Different alteration styles are evident including saussuritisation of plagioclase to form epidote, calcite and clays, and sericitisation. The main sulfide minerals present are pyrrhotite, chalcopyrite and pentlandite, the primary nickel ore mineral. The underflow is more sulfide-rich than the overflow, with pentlandite only detectable by XRD in the high density fractions of the

underflow. The sulfides and denser gangue minerals also increase with density within each DMC product. The lower density classes are dominated by quartz and feldspar, with amphibole, pyroxene and alteration minerals such as chlorite and epidote more common in the higher density fractions.

Pentlandite in the Phoenix ore contains an average of 37.52% nickel, with pyrrhotite containing an average of 2.03% nickel in solid solution. Mafic silicate minerals are also hosts of solid solution nickel in small amounts, of up to 0.1% in chlorite. In the highest density class analysed by QEMSCAN, the 3.1 floats of the DMC overflow and underflow, nickel occurs mostly in pentlandite, however, a large portion of the nickel in the other density fractions is silicate-hosted, up to 53% in the 3.0 floats of the underflow.

In terms of texture, the BMS are mostly disseminated, with massive or net-textured occurrences less common. The pentlandite is mostly present as small flame-like lamellae in pyrrhotite, and more rarely as larger discrete grains, where the BMS are more massive in nature. Grain sizes of composite sulfide grains are mostly less than 200 μm in size and are generally larger in the underflow. The exception is the 2.95 floats, in which the sulfide grains are smaller than those of the overflow. Sulfide liberation is poor throughout the density classes due to small sulfide grains occurring within particles of up to 25 mm size. The 3.1 floats fractions, however, contain slightly less locked sulfides than the lower density fractions.

Particle size distributions for the density fractions are similar, apart from the 3.1 floats of the overflow, which is finer than the rest, containing mostly particles <5 mm. No particles larger than 13 mm were measured on the QEMSCAN, even though the samples are of <25 mm size, because measurements are done on a two-dimensional cross section of a particle and size information is therefore generally underestimated. No major differences in particle shape were observed between the different samples; the underflow samples show only slightly more irregular-shaped or elongated particles than those of the overflow.

CHAPTER 6: DISCUSSION

6.1. Introduction

This chapter discusses individual mineralogical factors contributing to the overall DMS behaviour of the Nkomati and Phoenix ores. The differences in DMS efficiency of the bulk ore samples that were evaluated are also discussed and compared with their mineralogy. These comparisons will serve to address the two key questions of the project, as proposed in Chapter 1:

1. To what extent do mineral compositions and textural features such as size, density, shape, cleavage, degree of alteration, associations and liberation, affect the dense medium separation of low grade nickel ores?

2. How do differences in the mineralogy between the two ores affect their behavioural differences during DMS, and therefore the effectiveness of this process for each deposit?

Discussion of these aspects will lead to a better understanding of the differences in DMS behaviour of different nickel ores, and variation in separation efficiency for different samples from the same deposit.

6.2. Comparison of efficiency

The nickel grade of the Phoenix ore was measured at 0.28%. The Nkomati MMZ ore had a higher grade of approximately 0.4% nickel. Both ores showed upgradeability from the preliminary sink-float analysis, however the Nkomati ore predicted a slightly higher grade and recovery than the Phoenix ore (Figure 6.1). This is possibly due to the higher feed grade of the Nkomati ore, which may be associated with coarser sulfide grains that are easier to concentrate.

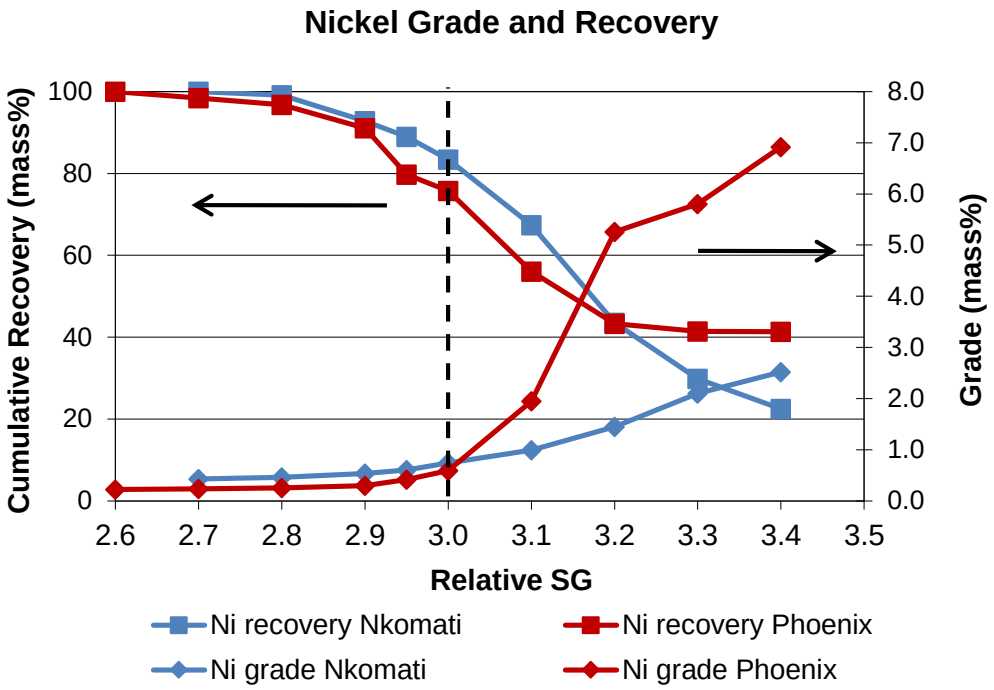

Figure 6.1 Comparison of grade and recovery curves for the Nkomati and Phoenix ores

The partition curves for the separations indicate that the Nkomati ore experienced a more efficient separation than the Phoenix ore (Figure 6.2). This is shown by the steeper slope of the Nkomati partition curve, indicating a smaller region of error. The D_{50} of 3.01 for Nkomati was the closest to the planned SG cut-point of 3.0, which was used for both ores, and the Nkomati separation had the lower Ep at 0.04, indicating a lower degree of particle misplacement. These results are contrary to previous tests on Nkomati MMZ ore, which showed inefficient recoveries for similar grades, resulting in the rejection of DMS as a viable preconcentration option (Sibanyoni, 2006). However, results from the present study are not representative of the entire MMZ ore as only one bulk sample was obtained from the region being mined at the time of sampling. The Ep shown by the Phoenix sample was acceptable but slightly higher than the Nkomati sample, at 0.05. For a DMS, efficient separations are generally found to have Ep values of 0.3 – 0.4 (Cresswell, 2001). The D_{50} for the Phoenix ore at 2.98 is still close to the estimated cut-point. Apart from the variation in ore grades, textural variation may also account for the differences in DMS behaviour of the various samples subjected to DMS testwork.

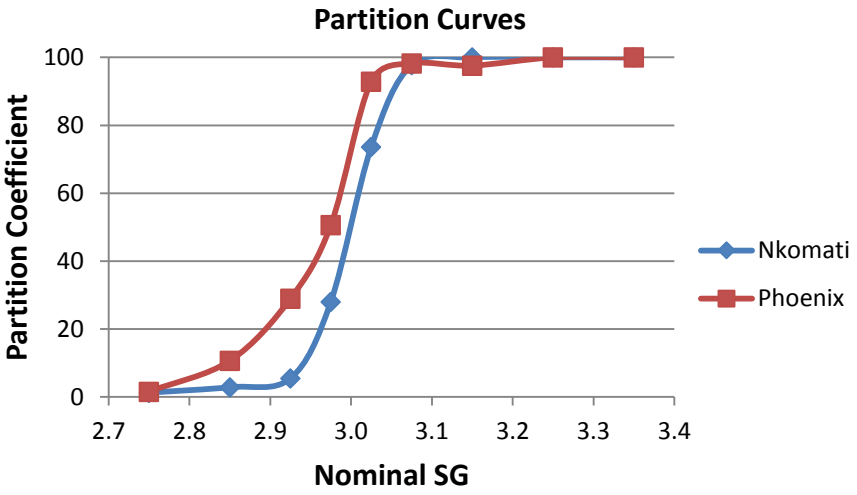

Figure 6.2 Comparison of partition curves for the Phoenix and Nkomati ores

The amount of near-gravity material may also affect the process efficiency as a high amount of material at the cut-point SG can lead to increased particle misplacement (Fuerstenau and Han, 2003). The washability curves calculated from the reconstituted feeds of the DMC overflow and underflow products are given in Figure 6.3. From these curves, near-gravity curves were plotted showing the amount of material within 0.05 SG units of the cut-point (Figure 6.4). The value of 0.05 was chosen as it is close to the Ep values of both ores, within which the error in the separation is experienced.

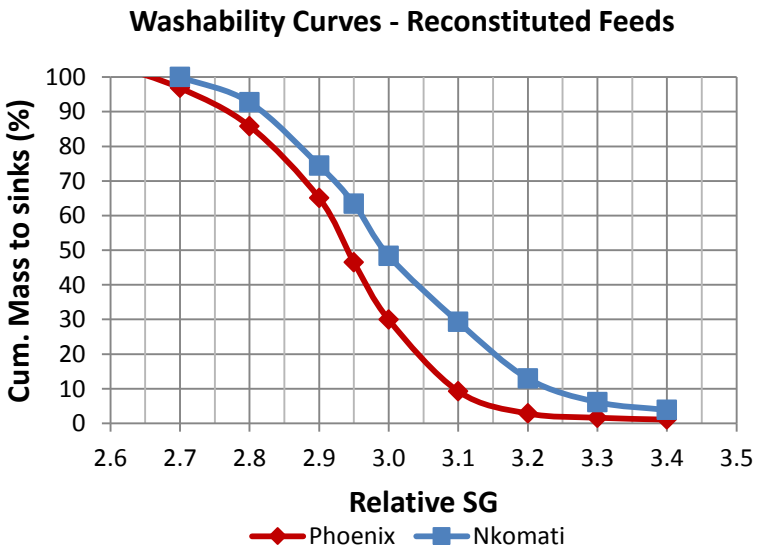

Figure 6.3 Washability curves for the feed as calculated from the DMC products

Both ores show a similar amount of near-gravity material at a cut-point of 3.0, of approximately 26%. If the D_{50} of Phoenix is lowered to 2.98 this would produce ~30% near-gravity material. According to Fuerstenau and Han (2003), amounts of near-gravity material >25% present great difficulty for separation, with particles highly likely to be misplaced. Exceptionally efficient operation of the DMS process is required for a successful separation.

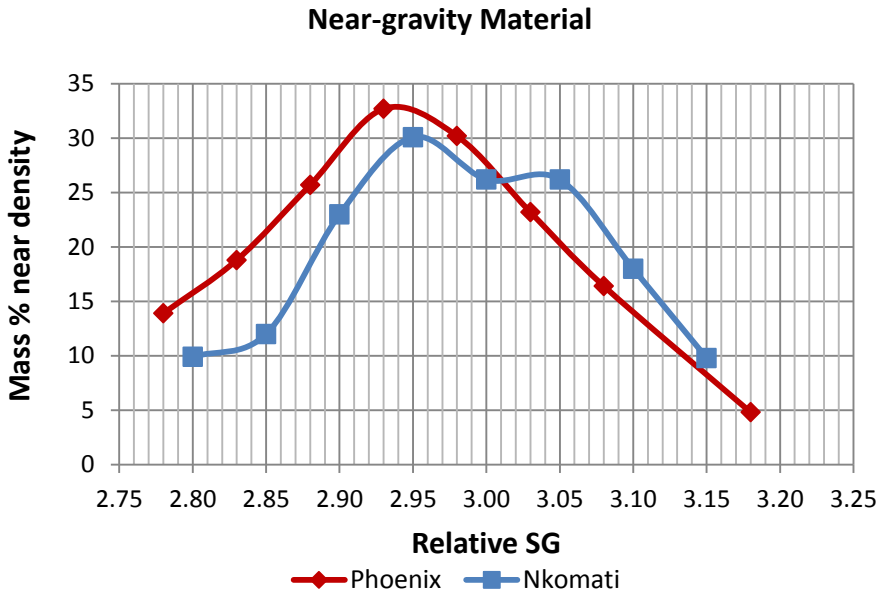

Figure 6.4 Proportion of near-gravity material at ± 0.05 SG units from the cut-point

6.3. Alteration effects

Both the Nkomati MMZ and Phoenix ores formed as magmatic sulfide deposits of mafic-ultramafic composition. They have been subjected to metamorphism at a later stage, in which the primary mineral assemblages have altered to form new secondary minerals, mainly hydrous silicates (Figure 6.5). Late stage fluid movement through the rock also created quartz and carbonate veins, which were not part of the original rock.

Alteration of the MMZ is not pervasive, with original igneous textures and minerals preserved in parts of the deposit. The original unaltered rock is an olivine-dominated harzburgite (classification shown in Figure 2.2) composed of coarse olivine and pyroxene crystals surrounded by interstitial plagioclase. Late stage magmatic hydrothermal alteration resulted in mainly serpentinisation of the rounded olivine crystals associated with magnetite rimming, and talc-carbonate alteration (Gauert, 2001; Li *et al.*, 2002; Steenkamp, 2012). In altered parts of the deposit, uralitisation has occurred, whereby pyroxene crystals have been

pseudomorphed by tremolite-actinolite. Saussuritisation is also a feature of plagioclase in altered zones.

The original gabbronorite host rock of the Phoenix deposit is more pervasively altered than the MMZ, with very little unaltered rock observed. The primary silicate minerals are pyroxene and plagioclase, with the pyroxenes mostly replaced by amphibole and chlorite due to hydrothermal activity, and some of the plagioclase saussuritised and altered to epidote.

The sulfide content of the Nkomati ore is higher than the Phoenix ore due to its higher grade, with pentlandite being detectable in the DMC feed using QXRD.

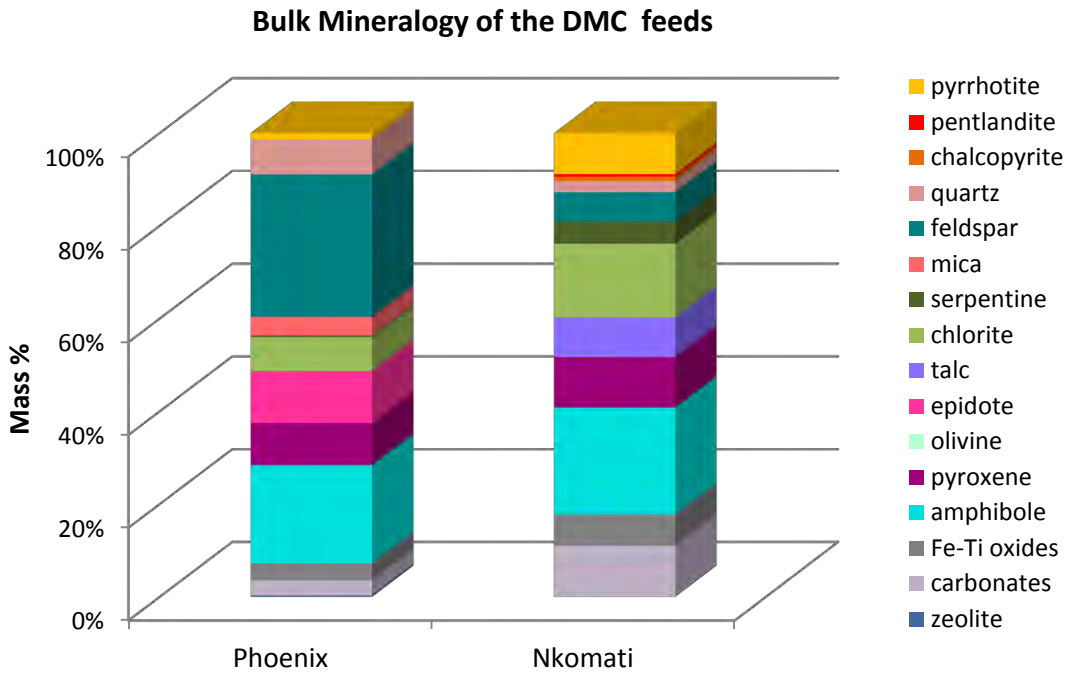

Figure 6.5 Bulk mineralogy comparison for the Phoenix and Nkomati DMC feeds

6.3.1. Partitioning of gangue

If DMS separated based on particle density only, no differences would be expected in the bulk mineralogy of material in the same density class of the overflow and underflow. However, the bulk mineralogy results presented in sections 4.3.3 and 5.3.3 show that for both the Nkomati and Phoenix ores, separation of minerals by DMS not only differentiates between the dense sulfides / oxides and less dense silicates / carbonates. Separation of silicate minerals can also be observed based on their density differences. This is more prominent in the Nkomati ore, where significant differences occur between corresponding SG classes of

the overflow and underflow. In the Nkomati ore, apart from sulfide concentration, pyroxene has also increased in proportion in the DMC underflow due to its SG of 3.4 – 3.55, which is much higher than the separation cut-point of 3.0. The gangue minerals more abundant in the DMC overflow are talc, amphibole, plagioclase, biotite, calcite, chlorite and quartz, of which chlorite is dominant.

The general trend is for primary mafic silicate minerals (pyroxene and olivine) in the rock to be of higher density than the products of their alteration, which are most commonly chlorite, amphibole, serpentine and talc. Mafic minerals, rich in Fe and Mg, are normally higher in density than felsic minerals. Plagioclase is the felsic mineral generally found in mafic-ultramafic rocks, which often alters to epidote. In this case the alteration product is of higher density than the primary silicate and reports preferentially to the underflow, particularly in the Phoenix ore, where it is more abundant.

The Phoenix ore shows similar results to Nkomati in terms of gangue mineral separation, with the major difference being a higher abundance of amphibole in the DMC underflow than in the overflow. This might be due to the actual cut-point of the separation being slightly below target at 2.98, and the SG of actinolite, the dominant amphibole in both ores, at approximately 3.04. Since the SG of amphibole is near the cut-point density, amphibole can easily report to either product, and sink-float analyses show that its abundance is highest nearest to the cut-point density. The composition of the amphibole present can also greatly influence its density, particularly with regard to the solid solution between Fe and Mg. The higher the Fe content, the higher the density of the amphibole, with ferroactinolite being denser than actinolite, and hornblende being able to have an SG of up to 3.47. This may also be able to explain the difference in amphibole separation between the Nkomati and Phoenix ores. Actinolite is the dominant amphibole in the Nkomati ore, with minor tremolite, as noted from petrographic observation and EPMA results. In addition to actinolite, the Phoenix ore contains ferroactinolite and hornblende. Since the variation in DMS cut-point is relatively minor, the higher density amphiboles present in the Phoenix ore are likely to be more responsible for the higher amphibole content in the underflow.

6.3.2. Nickel deportment

One of the most notable differences between the Nkomati and Phoenix ores is in their nickel deportment characteristics. Although many silicate minerals host nickel in the Nkomati ore, together they account for less than 20% of the total nickel contribution for the ore. This is due

to the low proportion (generally less than 0.1%) of solid solution nickel in each mafic silicate mineral. In the Phoenix ore, up to 53% of nickel is hosted in silicate minerals, in the 3.0 floats of the DMC underflow. Higher levels of silicate nickel are most likely a result of magmatic fractionation processes; however they may be also related to the degree of alteration of a deposit, as hydrothermal alteration processes may cause remobilisation of the nickel during the formation of the secondary silicates (Robb, 2009).

6.4. Effect of texture

6.4.1. Textural characteristics of the Nkomati and Phoenix ores

Mineral textures play an important role in the processing of ores, mainly because of their influence on mineral liberation (Evans, 1993; Petruk, 2000; Lastra, 2007; Mishra, 2014). Different types of textures can occur within a deposit, depending on the processes of ore genesis and later stage alteration. Massive, net-textured and disseminated sulfides often occur within a single deposit, with both the Nkomati and Phoenix deposits displaying more than one type of sulfide texture. This can be explained by the 'billiard ball' model proposed by Naldrett (1973), which gives an explanation of the formation of different sulfide textures in zones within the same deposit, and by Chung and Mungall (2009), who describe the ways in which an immiscible sulfide melt migrates through a crystal mush. This produces a massive sulfide layer at the base of the deposit, overlain by net-textured sulfides formed through upward migration of the sulfide liquid through settling cumulate crystals. Disseminated sulfide droplets would then be found at the uppermost levels of the deposit (Naldrett, 1973).

The Lower Harzburgite unit in which the Nkomati MMZ occurs is a coarse-grained cumulate rock with large euhedral to rounded crystals of olivine and pyroxene included within intercumulus plagioclase. Sulfide mineralisation is generally disseminated or net-textured. Disseminations occur either through original sulfide segregation during crystallisation, or through subsequent deformation of the rock, which destroys the original sulfide textures. Net-textured sulfides form when the immiscible sulfide liquid crystallises interstitial to the rounded silicate crystals by travelling along grain boundaries of solid or semi-solid silicate and oxide crystals (Mungall and Su, 2005; Chung and Mungall, 2009). The bases of these types of magmatic sulfide deposits usually contain a layer of massive sulfides accumulating

from the downward flow of the dense sulfide fluid (Naldrett, 1973; Evans, 1993; Chung and Mungall, 2009).

The metagabbronorite hosting the Phoenix ore is medium- to coarse-grained and equigranular, with the bulk sample studied originating from the disseminated zone of the deposit. Massive sulfides in the Phoenix deposit occur as veins and lenses up to 1.5 m thick and form a sharp contact with the disseminated ore. The zones of massive sulfide lenses and veins were formed by remobilisation of the disseminated sulfides during heating of the host rock during associated granitoid intrusions events. The remobilised sulfides then accumulated in fractures in the host rock to create veins (Johnson, 1986; van der Wel *et al.*, 1998).

6.4.2. Sulfide grain size

In both the Nkomati and Phoenix ores, composite sulfide mineral grain sizes increase steadily from the low to the high density classes of each DMC product. This has been shown to correspond to a change in texture from disseminated to net-textured or massive, with sulfide grains being larger as the texture becomes more massive (Figure 6.6). The size of composite sulfide grains is controlled mostly by pyrrhotite grain size, as the dominant sulfide mineral. Pentlandite occurrence is also observed to change as the overall sulfide texture changes. In disseminated zones, pentlandite mainly occurs as flames in pyrrhotite, with granular pentlandite only noted in association with pyrrhotite in areas containing coarse net-textured or massive sulfides.

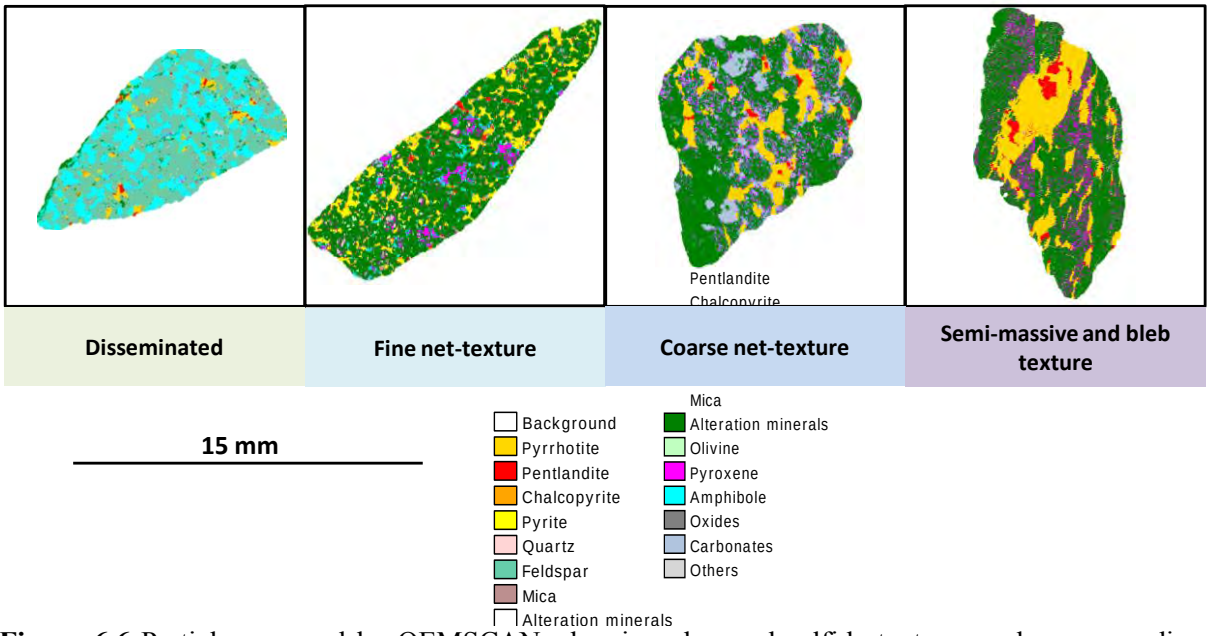

Figure 6.6 Particles mapped by QEMSCAN, showing observed sulfide textures and corresponding changes in grain size

Apart from the increase in sulfide grain size with increasing density, grains are also larger, on average, in the DMC underflow than in the overflow for a given density class. This can be attributed to the concentration of a higher proportion of net-textured sulfides to the underflow, whereas finer disseminated sulfides would be more likely to be rejected to the overflow. In general, sulfides in the Nkomati ore are larger than those of the Phoenix ore within a given density class (Figure 6.7). The smaller Phoenix sulfides are a result of the mostly disseminated texture of the ore compared with Nkomati, in which net-texture commonly occurs. The larger grains and more massive texture occurring in higher density fractions of the ores are also associated with higher nickel and copper grades than the finely disseminated sulfides.

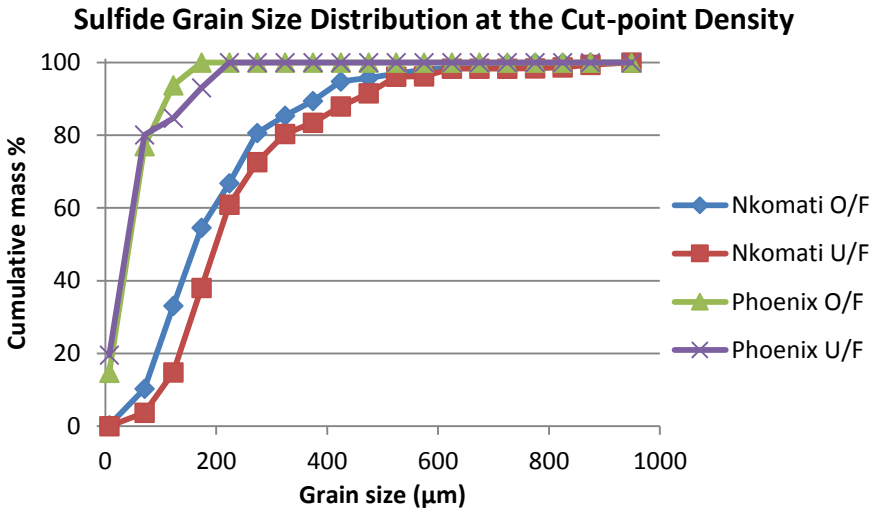

Figure 6.7 Cumulative grain size distribution at the cut-point density fractions of the Nkomati and Phoenix DMC products (O/F – overflow, U/F – underflow).

6.4.3. Sulfide liberation

Sulfide mineral liberation is also considered for composite grains, as it would be difficult to liberate the closely intergrown sulfides from each other, particularly for pentlandite where flame-like lamellae are the dominant occurrence (Becker, 2009). Pentlandite liberation in this case would be near impossible, with the average flame being approximately 3 µm x 30 µm in size. For DMS especially, the aim would be rather to liberate sulfides as a whole from silicates and other gangue minerals than to try to separate individual sulfide minerals. Even if liberation of pentlandite were feasible, it would not be achievable at the larger particle sizes required for physical separation methods.

Liberation is influenced by grain size, as larger sulfide grains make up a higher proportion of a particle at a specific size, and therefore contribute more to the overall particle density. In both the ores studied, generally >80% of sulfide grains are smaller than 300 µm. With particle sizes of -12+1 mm in Nkomati and -25+1 mm in Phoenix, it is unlikely that many sulfide grains would be liberated. This is shown from the liberation data, with most composite sulfide grains in both ores are locked in the density classes analysed by QEMSCAN, and only minor amounts reporting to the middlings class in some samples. The Phoenix sulfides, however, show slightly higher locking than the Nkomati sulfides, with most sulfides making up less than 20% of the particle volume (Figure 6.8). At the DMS cut-point the Nkomati sulfides are better liberated in the overflow than the underflow. This is possibly due to the smaller particle sizes in the overflow, which would increase the relative sulfide area in a particle. The Phoenix sulfides are also slightly smaller in size, with more than 80% of grains less than 200 µm, as compared with the Nkomati sulfides, where ~40 – 60% of grains are less than 200 µm. With smaller grain sizes and larger particles for the Phoenix bulk sample, it is possible that these size differences may have contributed to the slightly higher degree of locking. This may be a possible factor in the lower nickel recovery attained from the Phoenix bulk sample compared with the Nkomati sample, although a reduction to a top size smaller than 25 mm is unlikely to liberate <200 µm sulfide grains. Tests by van Wyk (2006b) and van Zyl *et al.* (2009) on Tati ores have shown no observable improvement in nickel grades and recoveries achieved by DMS with a decrease in crush size.

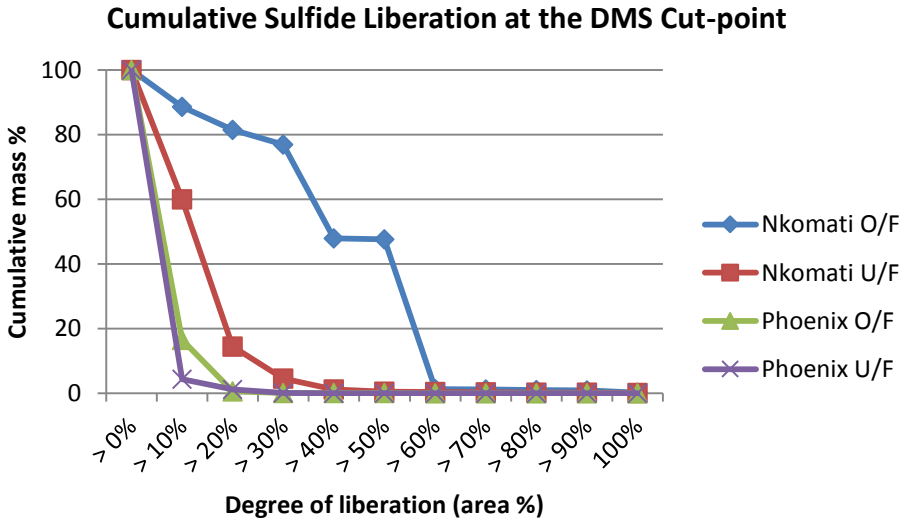

Figure 6.8 Cumulative sulfide liberation in the cut-point samples of the Nkomati and Phoenix DMC products (O/F – overflow, U/F – underflow)

6.4.4. Mineral associations

Sulfide mineral associations with gangue are linked to the relative abundance of the gangue minerals within each sample. Higher density samples contain sulfides that are more closely associated with denser minerals such as pyroxene and epidote. Near the cut-point density, amphibole associations are higher, and at low densities associations with feldspar increase. No preferred association of sulfides with any gangue minerals was noticed. Zones of late stage alteration, however, such as those containing quartz and calcite veins, did not appear to contain sulfide grains when observed petrographically.

6.5. Effect of particle properties

The physical properties of the particles being separated can have a great influence on DMS, as DMCs are known not only to separate based on density, but on size and to a certain extent, on particle shape (e.g. Burt, 1984; Wills, 2006; Napier-Munn, 1985b; Ferrara *et al.*, 2000).

An average of 3 400 particles was measured for each sample. This is less than is normally analysed by QEMSCAN for acquiring representative data. However, due to much larger particle sizes (up to 25 mm) than most metallurgical samples, it is not feasible to analyse more particles using this technology as it will create unreasonably long analysis times. A statistical error calculation from Jones (1987) was used to help determine if the particles analysed were sufficient for obtaining acceptable data quality. The calculation takes into account the mass % of the mineral of interest (in this case, pentlandite) and the number of particles analysed. Results for the Nkomati and Phoenix samples mostly indicated relative errors of <10%. For the 3.0 floats of the Phoenix overflow and underflow samples, where pentlandite concentrations were approximately 0.1 mass %, the number of measured particles were not always sufficient, as the Jones formula indicates a minimum of 3 600 particles for 0.1% mineral of interest. Where pentlandite makes up 0.5% of a sample, a minimum of 400 particles would be required. The smallest number of particles measured was 890 in the 3.1 floats of the Nkomati overflow. This is due to losses during sample preparation, resulting in a smaller number of polished blocks being analysed. The pentlandite content of this sample is 0.7%, indicating that the number of particles measured is adequate according to Jones (1987). In addition to the statistical error calculation, QEMSCAN data validation using major

element chemistry showed good correlation between the calculated and measured assays for all samples.

6.5.1. Particle size

The particles of both the Nkomati and Phoenix bulk samples show very similar trends in their size distribution. Particle sizes are smaller in the DMC overflow samples when compared with those of the underflow. The largest size differences occur in the denser fractions of both ores, where heavier particles that have reported to the overflow have very small particle sizes compared to the underflow (Figure 6.9). This is an indication of the misplacement of small particles to the overflow regardless of their density, because of their lower settling rate in the medium (Napier-Munn and Scott, 1990; Wills, 2006). Particle size differences are also important near the DMS cut-point where particles near the cut-point density have an equal chance of floating or sinking, and therefore tend to separate on size rather than density.

The largest size difference was noted in the Nkomati sample, where the densest fraction of the overflow, the 3.1 sinks, contained very small particles compared with all the other density classes of both the overflow and underflow. Greater than 90% of the particles in this sample are less than 2 mm, which is near the minimum size of 1 mm for the DMS. This sample also shows the highest sulfide mineral liberation because of its small particle size; however, these sulfides were rejected as the small particles were not easily recoverable.

Particle sizes measured by QEMSCAN, as well as grain sizes, are generally underestimated as the measurements are taken on two-dimensional cross sections through the particles. This can be seen particularly in the Phoenix ore, where the particles have been crushed to <25 mm in reality, however, all particle sizes measured by QEMSCAN were less than 13 mm. The measured data can still give a good representation of the distribution of sizes within a sample. Increasing the number of particles analysed decreases the error in these measurements as more random cross sections are measured (Pascoe *et al.*, 2007).

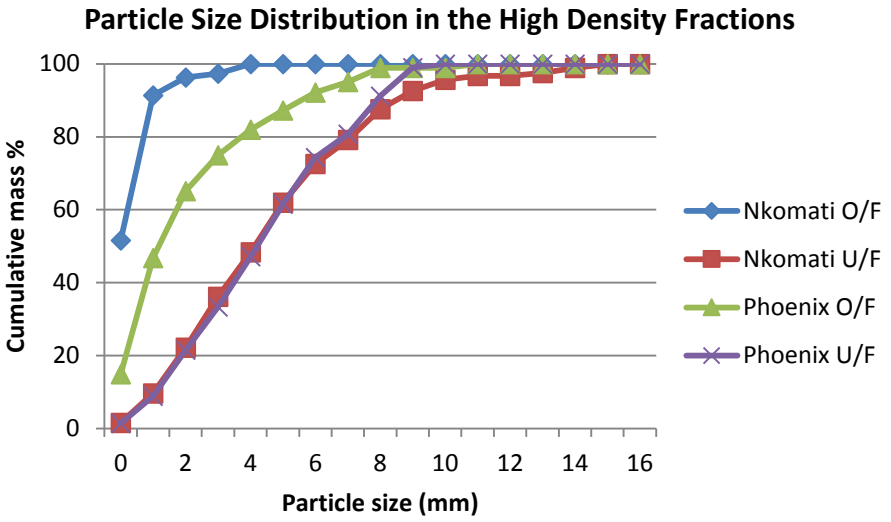

Figure 6.9 Cumulative particle size distribution in the high density fractions of the Nkomati and Phoenix DMC products

6.5.2. Particle shape

In terms of shape, both the Nkomati and Phoenix ores show preferential recovery of higher shape factor particles to the underflow (Figure 6.10). More particles with shape factors greater than 25 are found in both the underflow samples compared with the overflow samples. The overflow also shows a narrower distribution of shapes than the underflow. The shape differences are most pronounced at the DMS cut-point, particularly for the Nkomati samples. This further shows the increasing importance of particle properties affecting the separation of near-density material.

Particle elongation is also seen to be slightly higher in the underflow samples, at and lower than the DMS cut-point. This has not been observed from the higher density samples, where a similar distribution of particle elongation occurs in the overflow and underflow, particularly in the Nkomati ore where the overflow and underflow particles show an almost identical elongation distribution. In the Phoenix ore the overflow shows a more defined elongation, peaking at 0.3 – 0.4, with a wider spread observed in the underflow. Figure 6.11 shows thin sections of Nkomati ore within the 2.9 floats fraction, in which shape differences could be observed visually between particles of the DMC overflow and underflow. The underflow contains a larger proportion of elongated particles than the underflow, and these were mostly composed of alteration products such as saussurite, sericite and actinolite, which have lower hardness than primary silicates.

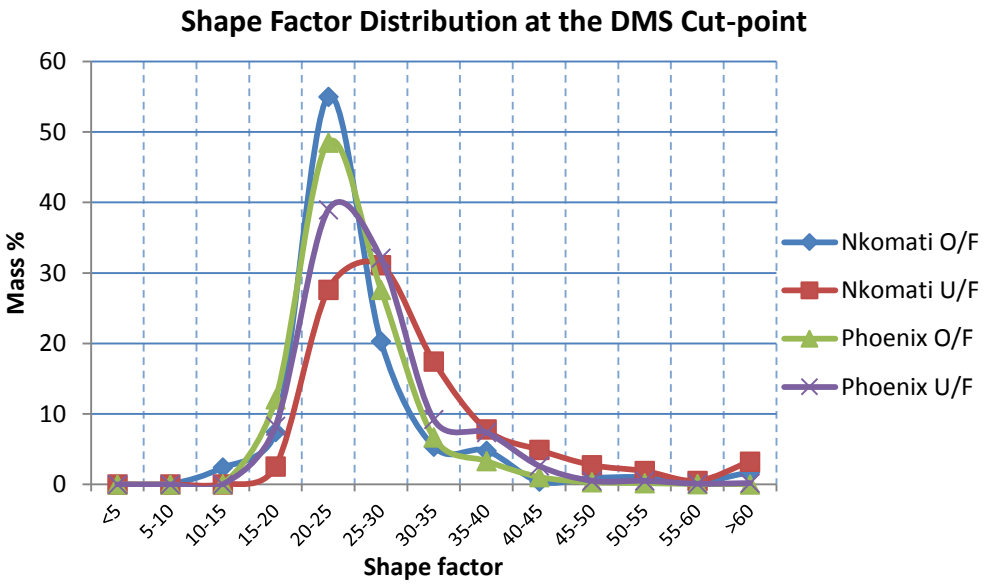

Figure 6.10 Distribution of particle shape at the DMS cut-point

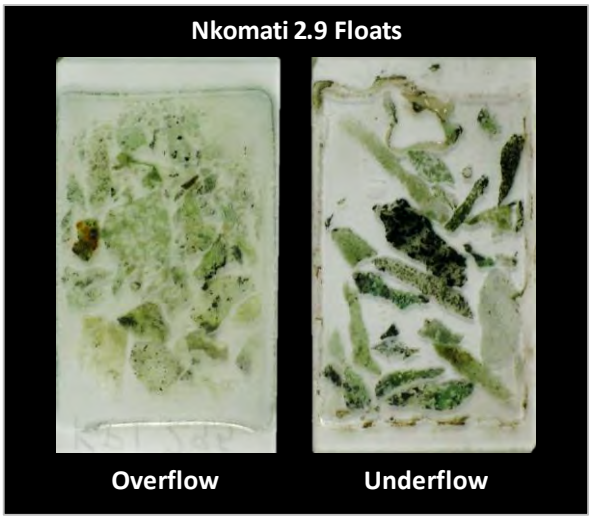

Figure 6.11 Thin sections showing Nkomati ore particles belonging to the 2.9 floats density class of the DMC overflow and underflow

It has been shown that irregular-shaped and elongate particles are more commonly rejected by density separation methods than more spherical, equidimensional or smoother particles, owing to their higher drag coefficients and lower settling rates (Napier-Munn and Scott, 1990; Furuuchi and Gotoh, 1992; Ferrara *et al.*, 2000). The present results do not conform to the general trend, with more irregular-shaped and elongated particles being preferentially recovered to the underflow. This has been described by Chaston and Napier-Munn (1974), where high shape factor and flattened or elongated particles of shells and roots have become

trapped within the dense outer flow of the cyclone. The observed trends may be also explained by turbulence and particle orientation to the flow direction, which can additionally influence which product a particle will report to (Loth, 2007).

6.5.3. Size and shape separation for the Nkomati and Phoenix ores

Figure 6.12 gives an impression of the direction of particle flow within a DMC, specifically showing the observations from the mineralogical analysis on the Nkomati and Phoenix ores. In general, particles denser than the cut-point report to the underflow and those lighter than the cut-point report to the overflow. Small dense particles tend to be rejected to the overflow. Particles with densities close to the cut-point separate more on size and shape than density, with small particles going to the overflow and larger particles, to the underflow. Higher shape factor and elongated particles are also more preferentially recovered to the underflow in this case.

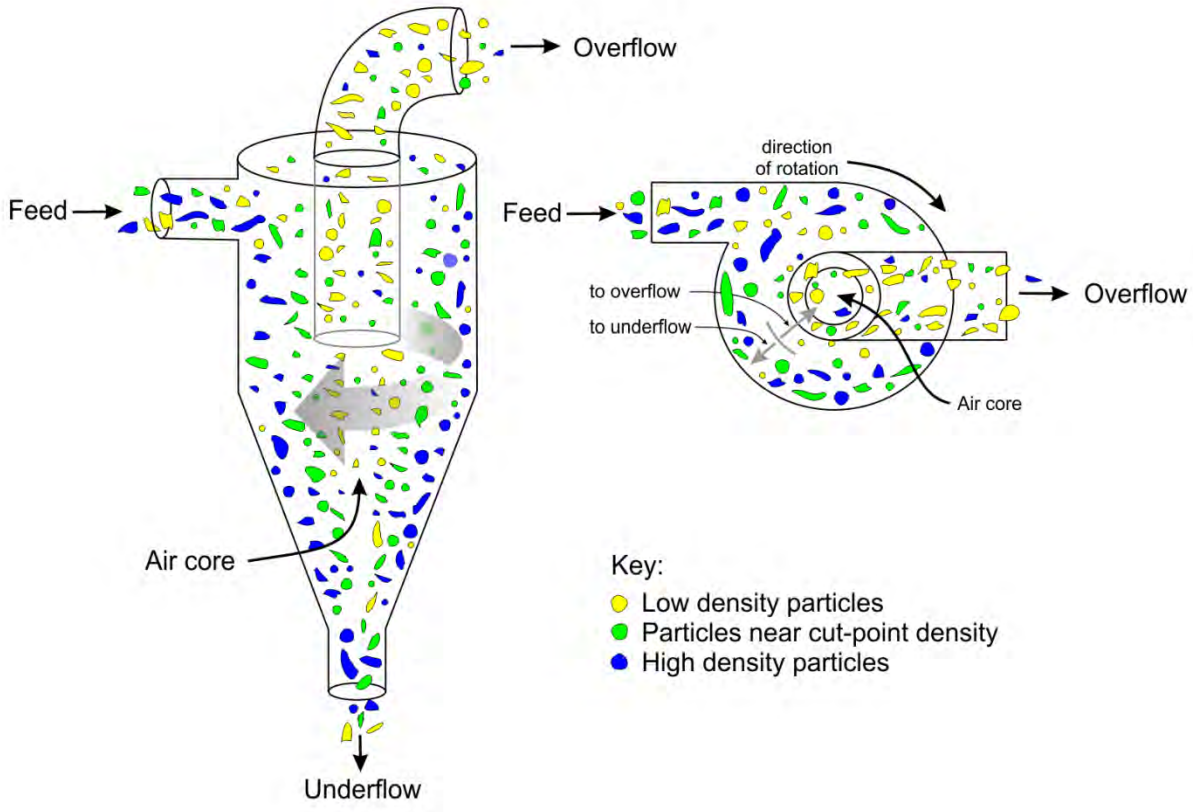

Figure 6.12 Schematic drawing of a DMC showing direction of particle movement towards the overflow and underflow

CHAPTER 7: CONCLUSIONS AND RECOMMENDATIONS

7.1. Conclusions

In addressing the aim of the research, which is to determine mineralogical properties of ores that influence the DMS process, it was found that a combination of factors contribute to the behaviour of ore particles within a DMC. These do not include other external factors and conditions responsible for the separation such as properties of the separating medium and workings of the DMC itself, which are not within the scope of this project. Although the determination of the mineralogical effects on DMS was carried out using the products of the separation rather than feed samples, the prediction of the results of a separation from analysis of the feed is an important goal of process mineralogy. The understanding of these mineralogical effects on particles of the DMC products will guide mineralogical studies used to predict DMS behaviour prior to conducting an actual separation.

The following mineralogical properties were evaluated and are presented in decreasing order of importance to DMS:

1. ***Particle density:*** Overall particle density is the main controlling factor in a density separation, and the property by which the separation can be modelled. The expected results of the separation are predicted using laboratory sink-float analysis, whereby particles are separated by density only, with negligible effects from other mineralogical or physical factors. In the dynamic environment within a DMC, other factors are shown to influence particle separation; however particle density remains the strongest control on DMS. The overall particle densities are governed by the proportion of the different minerals present in a particle and their individual SGs. The Nkomati and Phoenix ores are mineralogically complex and contain a large variety of primary and secondary gangue minerals with a wide range in SG. This means that dense particles that are recovered to the underflow do not necessarily contain the BMS that aim to be recovered, and may consist of dense gangue minerals. The gangue minerals present in an ore therefore cannot be regarded as a single component; the proportions and properties of the different mineral types have to be considered when conducting a density separation.

2. ***Sulfide texture:*** Three sulfide textures were identified in the ores: disseminated / bleb-textured, net-textured and massive. Both ores show textural variability, with the Nkomati ore displaying all three textures and the Phoenix ore mostly consisting of disseminated sulfides with minor massive sulfides. A change in sulfide texture from disseminated to net-textured to massive is linked to an increase in sulfide mineral grain size. Larger grain sizes generally show higher mineral liberation, and although liberation is poor throughout the samples because of the large particle sizes, net-textured to massive sulfides are more often recovered to the product than finely-disseminated sulfides, which dominate the overflow. The change in texture from disseminated to massive also corresponds to a change in pentlandite occurrence from flame-like lamellae in pyrrhotite to granular pentlandite. Even though flame pentlandite is the dominant occurrence throughout the ores, granular pentlandite occurs more commonly in the underflow, associated with more massive sulfides. Owing to fine grain sizes, pentlandite recovery relies on its close association with pyrrhotite.

3. ***Particle size:*** Although density differences are the basis for a density separation process, DMCs are also known to separate on particle size. Size separation is most important for particles nearing the cut-point density, which have a more-or-less equal chance of floating or sinking. These particles tend to then separate dominantly on size rather than density, with larger particles concentrated to the underflow and smaller particles rejected to the overflow. The rejection of particles less than ~2 mm to the overflow is also common even for particles of high density, as particles close to the minimum cut-off size have a low settling rate and are therefore easily dragged into the overflow.

4. ***Degree of alteration:*** Alteration of magmatic sulfide ores results in a combination of primary and secondary minerals within a rock, with a large variety of different mineral densities. An assemblage of dense primary minerals such as pyroxene and chromite may not be desirable for DMS as barren particles can be recovered together with sulfides. Most secondary minerals are much lighter than sulfides and may separate more easily; however, if the sulfides are locked within the secondary silicates they may be lost to the overflow. Epidote is the only secondary silicate denser than its precursor mineral, plagioclase, and will tend to sink during DMS. Silicate nickel content in ores might also be related to the degree of hydrothermal alteration of an ore.

5. ***Particle shape:*** Particle shape does not have a major influence on the separation of the ores studied. As in the case of size, particle shape differences are most pronounced nearer to the DMS cut-point, where factors other than density have a stronger influence on the separation. In the case of both the Nkomati and Phoenix ore separations, more irregular and elongated particles tended to sink rather than float.

7.2. Recommendations

This research has brought about questions that can be addressed in future work. The recommendations for continuation of the mineralogical research on DMS are as follows:

- The application of the methods employed in this thesis to a DMS feed sample, in order to determine theoretical washability and grade-recovery curves, which will be used to predict the outcome if DMS is applied to the ore.

- Geometallurgical mapping of the nickel ores to delineate zones dominated by disseminated, net-textured or massive sulfides. In this way, the mineralogical variability of a deposit can be understood and information used to predict which zones of a deposit are likely to be upgradeable by DMS.

- The use of stereological corrections on AutoSEM data on large particles with heterogeneous textures to assess the difference between the original and corrected data.

- Three-dimensional particle shape characterisation using X-ray computed tomography of DMS products to understand and quantify the separation of different particles based on their sphericity, flakiness, elongation, etc. This will also serve to overcome the stereological and statistical issues associated with 2D AutoSEM analysis.

- Quantification of the different ore textures in a sample, which will give an indication of the proportions of disseminated, net-textured and massive ore-dominated particles being recovered and rejected during the separation.

- Conducting flotation tests on a sample that has been preconcentrated by DMS (the sinks + fines) and a sample that has not been upgraded. A comparison of the two sets

of results will determine whether preconcentration results in higher final grades and recoveries achieved in a flotation concentrate.

- Modelling of mineralogical effects on DMS together with changes in cyclone conditions to determine their combined effect, and to identify the extent to which each type of influence controls the separation process.
- Characterisation by DMS and mineralogical analysis of different types of BMS and non-sulfide ore deposits, to understand if the mineralogical influences are the same in different deposit types.

REFERENCES

Bagai, Z., Armstrong, R. and Kampunzu, A.B. (2002) U-Pb single zircon geochronology of granitoids in the Vumba granite-greenstone terrain (NE Botswana): Implications for the evolution of the Archaean Zimbabwe craton. *Precambrian Research,* **118**, 149–168.

Baum, W. (2014) Ore characterization, process mineralogy and lab automation a roadmap for future mining. *Minerals Engineering*, **60**, 69–73.

Becker, M. (2009) *The mineralogy and crystallography of pyrrhotite from selected nickel and PGE ore deposits and its effect on flotation performance.* PhD thesis, University of Pretoria, Pretoria, 254 pp.

Becker, M., de Villiers, J. and Bradshaw, D. (2010a) The mineralogy and crystallography of pyrrhotite from selected nickel and PGE ore deposits. *Economic Geology,* **105(5)**, 1025–1037.

Becker, M., de Villiers, J. and Bradshaw, D. (2010b) The flotation of magnetic and non-magnetic pyrrhotite from selected nickel ore deposits. *Minerals Engineering*, **23**, 1045–1052.

Bergmann, C., Singh, A. and Ramlall. N. (2010) *Dense medium separation of UG2 ores.* Mintek internal presentation.

Bignell, J.D. (1978) Prediction and assessment of gravity separator performance from heavy liquid data. *Proceedings of the 11th Commonwealth Mining and Metallurgical Congress, Hong Kong*, 123–131.

Bradford, L., McInnes, C., Stange, W., de Beer, C., David, D. and Jardin, A. (1998) The development of the proposed milling circuit for the Nkomati main concentrator plant. *Minerals Engineering*, **11(12)**, 1103–1117.

Brożek, M and Surowiak, A. (2007) Effect of particle shape on jig separation efficiency. *Physicochemical Problems of Mineral Processing*, **41**, 397–413.

Burt, R.O. (1984) Developments in Mineral Processing, Volume 5: *Gravity Concentration Technology*. Elsevier Science Publishers B.V., New York, 605 pp.

Burt, R. (1999) The role of gravity concentration in modern processing plants. *Minerals Engineering*, **12(11)**, 1291–1300.

Bushell, C. (2012) The PGM flotation predictor: Predicting PGM ore flotation performance using results from automated mineralogy systems. *Minerals Engineering*, **36–38**, 75–80.

Chaston. I.R.M. and Napier-Munn, T.J. (1974) Design and operation of dense-medium cyclone plants for the recovery of diamonds in Africa. *Journal of the South African Institute of Mining and Metallurgy*, December 1974, 120–133.

Chetty, D. (2008) *A geometallurgical evaluation of the ores of the northern Kalahari manganese deposit, South Africa.* PhD thesis (unpubl.), University of Johannesburg, Johannesburg, 271 pp.

Chung, H-Y and Mungall, J.E. (2009) Physical constraints on the migration of immiscible fluids through partially molten silicates, with special reference to magmatic sulfide ores. *Earth and Planetary Science Letters*, **286**, 14–22.

Cresswell, G.M. (2001) Pre-concentration of base metal ores by dense medium separation. *SAIMM Copper, Cobalt, Nickel and Zinc Recovery Conference,* 16–18 July 2001, Victoria Falls*,* 10 pp.

Cropp, A. F., Goodall, W. R. and Bradshaw, D. J. (2013). The influence of textural variation and gangue mineralogy on recovery of copper by flotation from porphyry ore: a review. *Proceedings of the 2nd AusIMM International Geometallurgy Conference 2013,* 30 September – 2 October 2013, Brisbane, 279–291.

Davis, J.J. and Napier-Munn, T.J. (1987) The influence of medium viscosity on the performance of dense medium cyclones in coal preparation. *Proc. 3rd Int. Conf. on Hydrocyclones*, Oxford, 155–165.

de Villiers, J. and Verryn, S. (2007) Modern techniques in X-ray diffraction applied to metallurgy. *The Journal of the SAIMM*, **107**, 83–86.

Deer, W.A., Howie, R.A. and Zussman, J. (1978) *Rock-forming minerals, Volume 2A: Single- Chain Silicates (2nd edition)*. Longman Group Limited, London, 668 pp.

Deer, W.A., Howie, R.A. and Zussman, J. (1992) *An introduction to the rock-forming minerals (2nd edition).* Prentice Hall, Harlow, 696 pp.

Deer,W.A., Howie, R.A. and Zussman, J. (1997) *Rock-forming minerals, Volume 2B: Double-Chain Silicates (2nd edition).* The Geological Society, Bath, 764 pp.

Dold, B. and Fontboté, L. (2001) Element cycling and secondary mineralogy in porphyry copper tailings as a function of climate, primary mineralogy and mineral processing. *Journal of Geochemical Exploration*, **74**, 3–55.

Dunglison, M.E. (1999) *A general model of the dense medium cyclone.* PhD thesis (unpubl.), University of Queensland, Brisbane, 279 pp.

Dunglison, M., Napier-Munn, T.J. and Shi, F.N. (2000) The Rheology of Ferrosilicon Dense Medium Suspensions. *Mineral Processing and Extractive Metallurgy Review: An International Journal*, **20(1)**, 183–196.

Ecmekçi, Z., Becker, M., Tekes, E.B. and Bradshaw, D. (2010) The relationship between the electrochemical, mineralogical and flotation characteristics of pyrrhotite samples from different Ni Ores. *Journal of Electroanalytical Chemistry*, **647**, 133–143.

Evans, A.M. (1993) *Ore Geology and Industrial Minerals: An Introduction.* John Wiley and Sons (3rd edition). Wiley-Blackwell, Oxford, 400 pp.

Evans, C.L., Wightman, E.M., Manlapig, E.V. and Coulter, B.L. (2011) Application of process mineralogy as a tool in sustainable processing. *Minerals Engineering*, **24**, 1242–1248.

Fandrich, R., Gu, Y., Burrows, D. and Moeller, K. (2007) Modern SEM-based mineral liberation analysis. *Int. J. Miner. Process.,* **84**, 310–320.

Ferrara, G., Preti, U. and Meloy, T.P. (1989) Inclusion Shape, Mineral Texture and Liberation. . *Int. J. Miner. Process*., **27**, 295–308.

Ferrara, G., Bevilacqua, P., De Lorenzi, L and Zanin, M. (2000) The influence of particle shape on the dynamic dense medium separation of plastics. *International Journal of Mineral Processing*, **59**, 225–235.

FIZ-Karlsruhe (2012) *Inorganic Crystal Structure Database.* PC Version Release 2012/1, Karlsruhe, Germany.

Fuerstenau, M.C. and Han, K.N. (2003) *Principles of Mineral Processing.* Society for Mining, Metallurgy, and Exploration, Inc., Colorado, 573 pp.

Furuuchi, M. and Gotoh, K. (1992) Shape separation of particles. *Powder Technology*, **73**, 1–9.

Gauert, C. (2001) Sulphide and oxide mineralisation in the Uitkomst Complex, South Africa: origin in a magma conduit. *Journal of African Earth Sciences*, **32(2)**, 149–161.

Gauert, C., de Waal, S.A. and Wallmach, T. (1995) Geology of the ultrabasic to basic Uitkomst complex, eastern Transvaal, South Africa: an overview. *Journal of African Earth Sciences*, **21(4)**, 553–570.

Ghorbani, Y., Mainza, A.N., Petersen, J., Becker, M., Franzidis, J.-P. and Kalala, J.T. (2013) Investigation of particles with high crack density produced by HPGR and its effect on the redistribution of the particle size fraction in heaps. *Minerals Engineering*, **43–44**, 44–51.

Gilchrist, J.D. (1989) *Extraction Metallurgy (3rd edition)*. Pergamon Press, Oxford, 431 pp.

Goodall, W.R., Scales, P.J. and Butcher, A.R. (2005) The use of QEMSCAN and diagnostic leaching in the characterisation of visible gold in complex ores. *Minerals Engineering*, **18**, 877–886.

Gottlieb, P., Wilkie, G., Sutherland, D., Ho-Tun, E., Suthers, S., Perera, K., Jenkins, B., Spencer, S., Butcher, A. and Rayner, J. (2000) Using Quantitative Electron Microscopy for Process Mineralogy Applications. JOM, April, 24–25.

Grobler, J.D. and Bosman, J.B. (2009) Gravity separator performance evaluation using Qemscan® particle mineral analysis. *The 7th International Heavy Minerals Conference 'What next', SAIMM*, 91–98.

Gu, Y. (2003) Automated Scanning Electron Microscope Based Mineral Liberation Analysis: An Introduction to JKMRC/FEI Mineral Liberation Analyser. *Journal of Minerals and Materials Characterization and Engineering*, **2(1)**, 33–41.

Hagni, A.M. (2008) Phase Identification, Phase Quantification, and Phase Association Determinations Utilizing Automated Mineralogy Technology. *Journal of the Minerals, Metals and Materials Society*, April 2008, 33–37.

Haider, A. and Levenspiel, O. (1989) Drag coefficient and terminal velocity of spherical and non-spherical particles. *Powder Technology*, **58**, 63–70.

Hammerbeck, E.C.I. and Schürmann, L.W. (1998) Nickel. *In*: *The Mineral Resources of South Africa: Handbook,* Council for Geoscience, **16**, 471–482.

He, Y.B. and Laskowski, J.S. (1994) Effect of dense medium properties on the separation performance of a dense medium cyclone. *Minerals Engineering*, **7(2/3)**, 209–221.

Houseley, K., Willan, R. and Chapman, R. (1994) The effect of particle geometry on the recovery of gold grains by gravity concentration methods. Leeds University Mining Association Journal 1994, 39–53.

Hulley, V. (2005) Reactions between country rock xenoliths and the magma of the Uitkomst Complex, with implications for the origin of the sulphide mineralisation. MSc. thesis (unpubl.), University of Pretoria, Pretoria, 117 pp.

Johnson, R.S. (1986) The Phoenix and Selkirk nickel-copper sulphide ore deposits, Tati greenstone belt, eastern Botawana. In Anhaeusser, C.R. and Maske, S. (eds), *Mineral Deposits of Southern Africa*. Geological Society of South Africa, 243–248.

Jones, M.P. (1987) *Applied Mineralogy – A Quantitative Approach.* Graham and Trotman Ltd, London, 259 pp.

Kearey, P. (2001) *The New Penguin Diction of Geology (2nd edition).* Penguin Books, London.

Key, R.M. (1976) The geology of the area around Francistown and Phikwe, Northeast and Central Districts, Botswana. *Distr. Mem. Geol. Surv. Botswana*, **3**, 15–25.

King, I., Mailole, V., Duarte, K., van Zyl, S. and Bryson, M. (2007) Gravity separation and flotation testwork on the Selkirk deposit. *Mintek external report,* no. 4793.

Knorr, K. and Yang, N. (2011) Quantitative X-ray Mineralogy of Iron Ore and Scales. *Proceedings of the Iron Ore Conference, Perth, 11–13 July, 2011.*

Lastra, R. (2007) Seven practical application cases of liberation analysis. *International Journal of Mineral Processing,* **84(1–4)**, 337–347.

Lee, J., Acar, S., Doerr, D.L. and Brierly, J.A. (2011) Comparative bioleaching and mineralogy of composited sulfide ores containing enargite, covellite and chalcocite by mesophilic and thermophilic microorganisms. *Hydrometallurgy,* **105**, 213–221.

Li, C., Ripley, E.M., Maier, W.D. and Gomwe, T.E.S. (2002) Olivine and sulfur isotopic compositions of the Uitkomst Ni-Cu sulfide ore-bearing complex, South Africa: evidence for sulfur contamination and multiple magma emplacements. *Chemical Geology*, **188**, 149–159.

Loth, E. (2008) Drag of non-spherical solid particles of regular and irregular shape. *Powder Technology*, **182**, 342–353.

Lotter, N.O. (2011) Modern Process Mineralogy: An integrated multi-disciplined approach to flowsheeting. *Minerals Engineering*, **24**, 1229–1237.

Lotter, N.O., Kormos, L.J., Oliviera, J., Fragomeni, D. and Whiteman, E. (2011) Modern Process Mineralogy: Two case studies. *Minerals Engineering*, **24**, 638–650.

Louisiana State University Department of Geology and Geophysics website. www.geol.lsu.edu.

Maier, W.D., Gomwe, T., Barnes, S-J., Li, C. and Theart, H. (2004) Platinum Group Elements in the Uitkomst Complex, South Africa. *Economic Geology*, **99(3)**, 499–516.

Maier, W.D., Barnes, S-J., Chinyepi, G., Barton, J.M., Eglington, B. and Setshedi, I. (2008) The composition of magmatic Ni–Cu–(PGE) sulfide deposits in the Tati and Selebi-Phikwe belts of eastern Botswana. *Mineralium Deposita,* **43**, 37–60.

Mainza, A., Powell, M.S. and Knopjes, B. (2004) A comparison of different cyclones in addressing challenges in the classification of the dual density UG2 platinum ore. *SAIMM International Platinum Conference 2004 'Platinum Adding Value'*, 95–102.

Marape, G. and Vermaak, M.K.G. (2012) Fundamentals of pentlandite mineralogy and its effect on its electrochemical behavior. *Minerals Engineering*, **32**, 60–67.

Miller, J.D., Lin, C-L., Hupka, L. and Al-Wakeel, M.I. (2009) Liberation-limited grade/recovery curves from X-ray micro CT analysis of feed material for the evaluation of separation efficiency. *International Journal of Mineral Processing,* **93**, 48–53.

Mining Top News website. Selkirk study confirms potential 260,000-tonne nickel production for LionOre's Tati. www.miningtopnews.com.

Mishra, G. (2014) *A Geometallurgical Assessment of the Geological and Mineralogical Influences on Flotation Performance at the Nkomati Nickel Mine, Mpumalanga, South Africa.* PhD thesis (unpubl.), University of Johannesburg, Johannesburg, 283 pp.

Mishra, G., Viljoen, K.S. and Mouri, H. (2013) Influence of mineralogy and ore texture on pentlandite flotation at the Nkomati nickel mine, South Africa. *Minerals Engineering*, **54**, 63–78.

Mkhize, B. and Andrews, L. (2011) Smelter feed quality control. *Minerals Engineering*, **24**, 1365–1369.

Morgan, P. (2009) The impact of crushing plant upgrade and DMS pre-concentration on the processing capability of the Tati Nickel Concentrator. *SAIMM Base Metals Conference 2009*, Kasane, Botswana, 27-31 July 2009, 231–244.

Mphela, N. (2010) *Fundamental studies of the electrochemical and flotation behaviour of pyrrhotite.* MSc thesis, University of Pretoria, Pretoria, 242 pp.

Mudd, G.M. (2009) Nickel Sulfide Versus Laterite : The Hard Sustainability Challenge Remains. *The 48th Annual Conference of Metallurgists, Canadian Metallurgical Society, Sudbury, Ontario, Canada, August 2009*, 10 pp.

Mudd, G.M. (2010) Global trends and environmental issues in nickel mining: Sulfides versus laterites. *Ore Geology Reviews*, **38**, 9–26.

Mulaba-Bafubiandi, A.F. and Medupe, O. (2007) An assessment of pentlandite occurrence in the run of mine ore from BCL Mine (Botswana) and its impact on the flotation yield. *Proceedings of The Fourth Southern African Conference on Base Metals 2007 – 'Africa's base metals resurgence', SAIMM*, 57–75.

Mungall, J.E. and Su, S. (2005) Interfacial tension between magmatic sulfide and silicate liquids: Constraints on kinetics of sulfide liquation and sulfide migration through silicate rocks. *Earth and Planetary Science Letters*, **234**, 135–149.

Naldrett, A.J. (1973) Nickel sulphide deposits – their classification and genesis, with special emphasis on deposits of volcanic association. *Bull. Can. Inst. Min. Metall.,* **66 (648)**, 45–63.

Napier-Munn, T.J. (1985a) The Determination of the Size Distribution of Ferrosilicon Powders. *Powder Technology*, **42**, 273–276.

Napier-Munn, T.J. (1985b) Residence time of mineral particles in dense medium cyclones. *Extraction Metallurgy '8, London, 9–12 September 1985,* C98–C101.

Napier-Munn, T.J. (1991) Modelling and simulating dense medium separation processes – A progress report. *Minerals Engineering*, **4(3/4)**, 329–346.

Napier-Munn, T.J. and Scott, I.A. (1990) The effect of 131emagnetization and ore contamination on the viscosity of the medium in a dense medium cyclone plant. *Minerals Engineering,* **3(6)**, 607–613.

Napier-Munn, T.J., and Alford, R.A. (1991) The causes of heavy mineral loss from mineral sands wet concentrators. *The AusIMM Proceedings,* **No. 1,** 19–30.

Napier-Munn, T.J., Kojovic, T., Scott, I.A., Shi, F., Masinja, J.H. and Baguley, P.J. (1995) Some causes of medium loss in dense medium plants. *Minerals Engineering*, **8(6)**, 659–678.

Ntengwe, F. and Witika, L.K. Optimization of the operating density and particle size distribution of the cyclone overflow to enhance the recovery of the flotation of copper sulphide and oxide minerals. *Journal of the SAIMM*, **111**, 295–300.

Pascoe, R.D., Power, M.R. and Simpson, B. (2007) QEMSCAN analysis as a tool for improved understanding of gravity separator performance. *Minerals Engineering*, **20**, 487–495.

Pecharsky, V.K. and Zavalij, P.Y. (2005) *Fundamentals of Powder Diffraction and Structural Characterization of Materials*. Springer, New York. 713 pp.

Petruk, W. (2000) *Applied Mineralogy in the Mining Industry.* Elsevier Science B.V., Amsterdam, 268 pp.

Preti, U., Ferrara, G and Meloy, T.P. (1989) Influence of Particle Shape on Liberation. *International Journal of Mineral Processing*, **25**, 17–28.

Rietveld, H.M. (1969) A Profile Refinement Method for Nuclear and Magnetic Structures. *Journal of Applied Crystallography*, **2**, 65–71.

Robb, L.J. (2009) *Introduction to ore-forming processes*. Blackwell Science Ltd, Oxford, 373 pp.

Sarkar, A., Ripley, E.M., Li, C. and Maier, W.D. (2008) Stable isotope, fluid inclusion, and mineral chemistry constraints on contamination and hydrothermal alteration in the Uitkomst Complex, South Africa. *Chemical Geology*, **257**, 129–138.

Schena, G.D., Gochin, R.J. and Ferrara, G. (1990) Preconcentration by dense-medium separation—an economic evaluation. *Trans. Instn Min. Metall., Section C: Mineral Process. Extr. Metall.*, **99**, C21–C31.

Scott, I.A., Baguley, P.J. and Napier-Munn, T.J. (1987) The influence of medium rheology on the separation of minerals in dense medium drums and cyclones. *The AusIMM Southern Queensland Branch, Dense Medium Operators' Conference, July 1987*, 205–215.

Sibanyoni, N. (2006) Nkomati Joint Venture (MMZ Testwork). *Mintek external report, no. 4533.*

Smith, D.K. (1989) Computer analysis of diffraction data. *In:* Bish, D.L. and Post, J.E. (eds). Modern Powder Diffraction. *Reviews in Mineralogy,* **20**, Mineralogical Society of America, 369 pp.

Steenkamp, N.C. (2012) *Alteration assemblage in the lower units of the Uitkomst Complex, Mpumalanga Province, South Africa*. PhD thesis, University of Pretoria, Pretoria, 270 pp.

Stratford, K.J. and Napier-Munn, T.J. (1987) Functions for the mathematical representation of the partition curve for dense medium cyclones. *19th APCOM Symposium*, Pennsylvania, USA, 719–728.

Streckeisen, A. (1972) *Classification and Nomenclature of Plutonic Rocks.* Recommendations of the IUGS Subcommission on the Systematics of Igneous Rocks.

Suresh, P.D., Kumar, V., Sripriya, R., Chakraborty, S. and Meikap, B.C. (2010) Performance characteristics of pilot plant dense media hydrocyclone for beneficiation of coal and 3-D CFD simulation. *Chemical Engineering Science*, **65**, 4661–4671.

Tati Nickel Mining Company website. www.tatinickel.co.bw

Taylor, J.C. and Hinczak, I. (2003) *Rietveld Made Easy: A Practical Guide to the Understanding of the Method and Successful Phase Quantifications.* Sietronics Pty Limited, Canberra, 201 pp.

Theart, H.F.J. and de Nooy, C.D. (2001) The Platinum Group Minerals in two parts of the Massive Sulphide Body of the Uitkomst Complex, Mpumalanga, South Africa. *South African Journal of Geology*, **104(4)**, 287–300.

van der Wel, L., Barton, J.M and Kinny, P.D. (1998) 1.02 Ga granite magmatism in the Tati Granite-Greenstone Terrane of Botswana: Implications for mineralization and terrane evolution. *S. Afr. J. Geol.*, **101(1)**, 67–72.

van Wyk, I. (2006a) Mineralogy and flotation testwork on DMS products from Phoenix. *Mintek external report,* no. 4282.

van Wyk, I. (2006b) Gravity separation testwork on ore from the Phoenix deposit. *Mintek external report,* no. 4259.

van Zyl, S., King, I. and Bryson, M.A.W. (2009) Evaluation of the Selkirk copper-nickel deposit. *Mintek external report,* no. 5330.

Webmineral Mineralogy Database. http://webmineral.com

Wightman, E., Evans, C. and Tungpalan, K. (2014) Measurement and interpretation of textural features at meso-scale. *Proceedings of the MEI Process Mineralogy Conference,* 17–19 November 2014, Cape Town.

Wills, B.A. (2006) *Will's Mineral Processing Technology: An Introduction to the Practical Aspects of Ore Treatment and Mineral Recovery* (7th edition). Butterworth-Heinemann, Oxford, 444 pp.

Wolmarans, E., Morgan, P. and Smit, D. (2011) Commissioning of the 375ktpm fully autogenous milling circuit at Nkomati Nickel. *Proceedings of the 6th Southern African Base Metals Conference*, Phalaborwa, 18–21 July 2011, 65–86.

Woollacott, L.C. and Eric, R.H. (1994) *Mineral and Metal Extraction: An Overview*. South African Institute for Mining and Metallurgy, Johannesburg, 412 pp.

Young, R.A. (1993) The Rietveld Method. *IUCr Monographs on Crystallography* **5**. Oxford University Press, Oxford, 298 pp.

APPENDIX A: QEMSCAN DATA VALIDATION

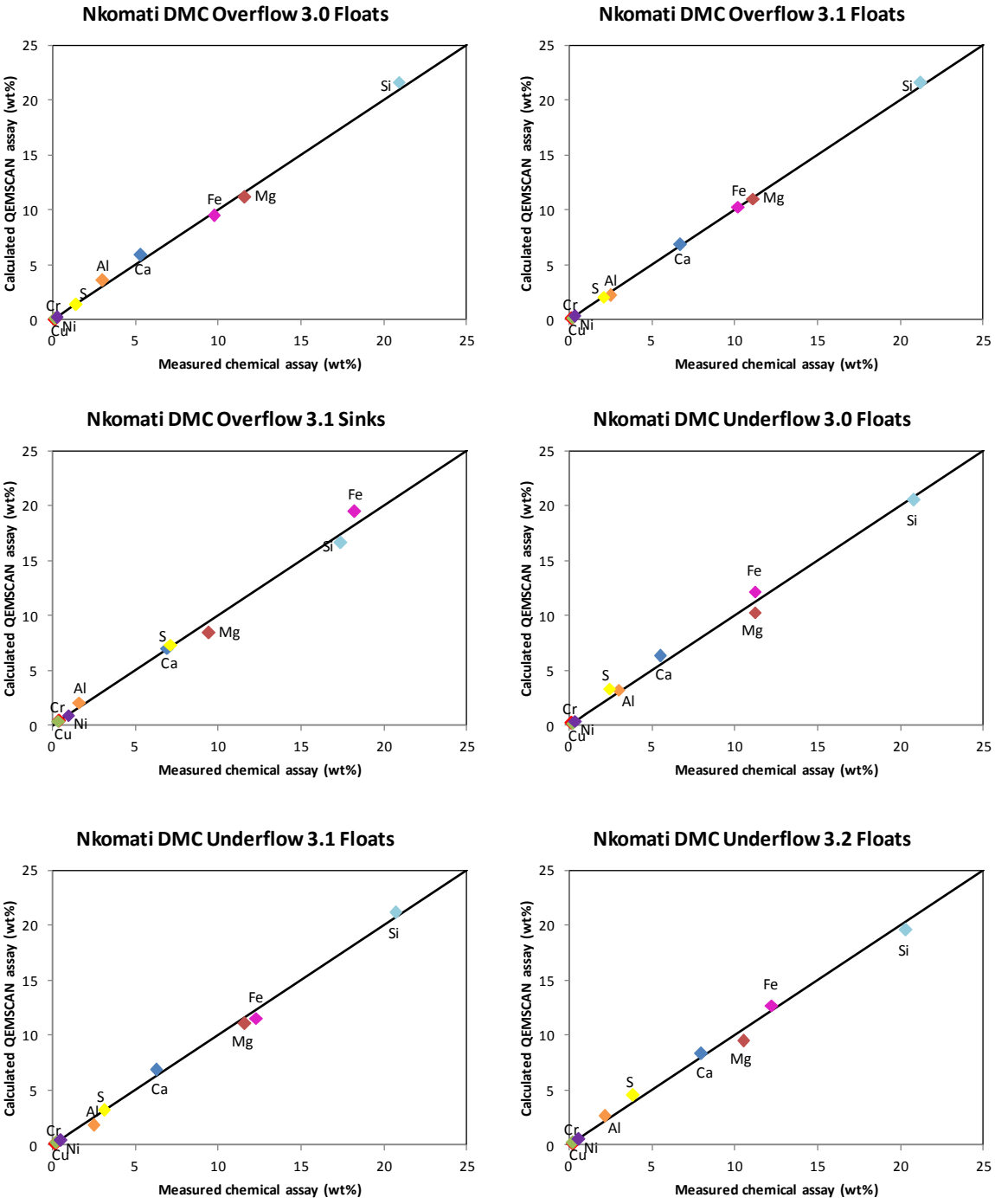

Figure A. 1 QEMSCAN data validation using measured chemistry for the Nkomati ore

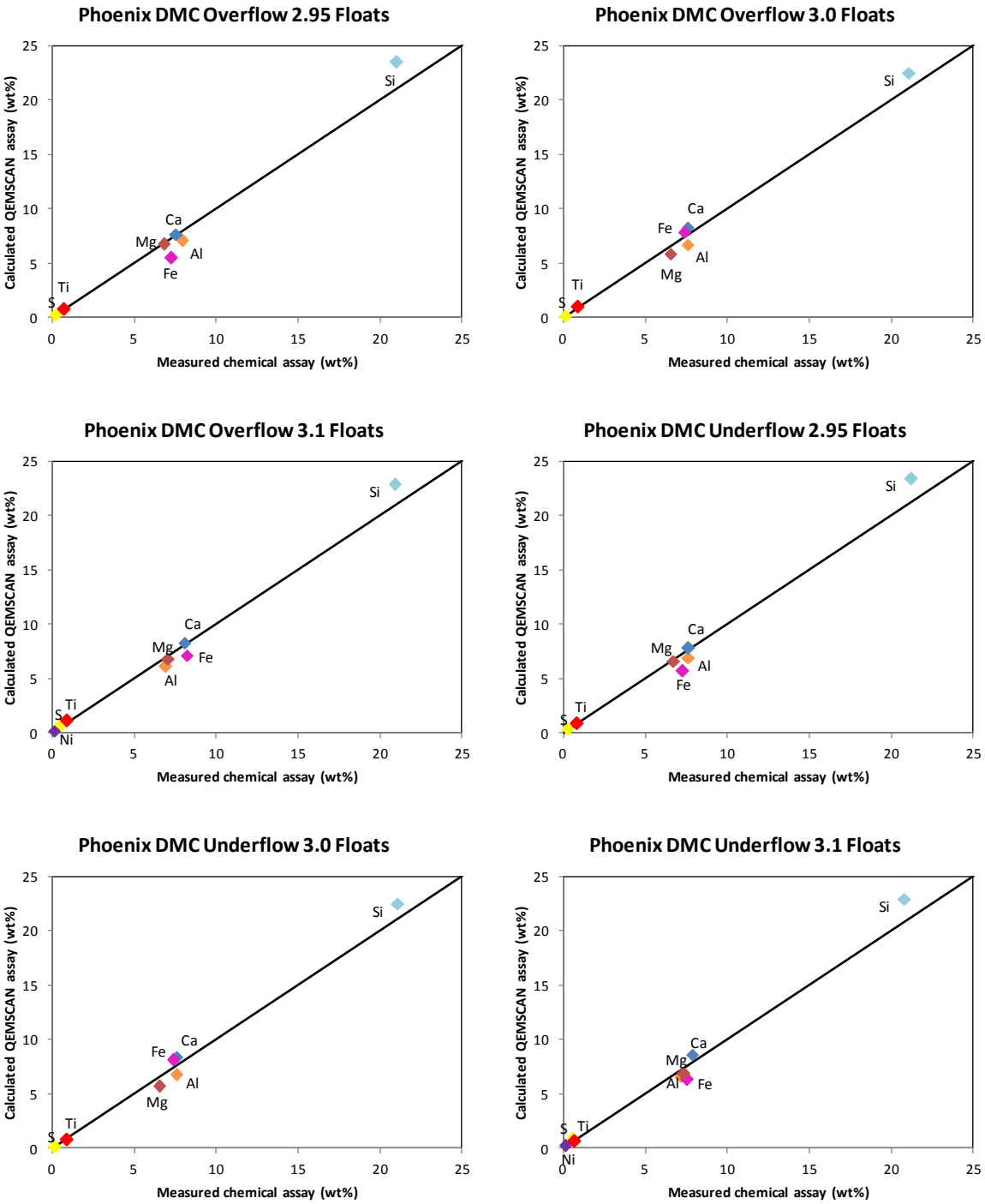

Figure A. 2 QEMSCAN data validation using measured chemistry for the Phoenix ore

APPENDIX B: DENSITY SEPARATION DATA

Table B. 1 Discrete sink-float analysis data for the Nkomati DMC feed sample

Density Fraction (SG)	Relative SG to Sinks	Mass [g]	Mass %	Grade [%]			Recovery [%]		
				S	Cu	Ni	S	Cu	Ni
+ 3.4	3.4	1872.7	3.85	19.08	0.55	2.52	24.0	13.1	22.5
- 3.4 + 3.3	3.3	1106.0	2.27	10.66	0.36	1.40	7.9	5.1	7.4
- 3.3 + 3.2	3.2	3318.2	6.82	6.40	0.27	0.87	14.3	11.2	13.7
- 3.2 + 3.1	3.1	7951.6	16.33	4.51	0.19	0.63	24.1	19.2	23.9
- 3.1 + 3.0	3.0	9297.0	19.10	2.63	0.23	0.36	16.4	27.2	16.0
- 3.0 + 2.95	2.95	7326.9	15.05	0.99	0.05	0.16	4.9	4.7	5.6
-2.95 + 2.9	2.9	5365.6	11.02	0.92	0.11	0.15	3.3	7.5	3.8
-2.9 + 2.8	2.8	8881.6	18.24	0.70	0.05	0.15	4.2	5.7	6.4
- 2.8	2.7	3562.0	7.32	0.35	0.14	0.05	0.8	6.3	0.8
Total [Calculated]	-	48681.6	100.00	3.06	0.16	0.43	100.0	100.0	100.0
Total [Measured]	-	-	-	2.98	0.15	0.41	-	-	-
Variance [%]	-	-	-	2.52	7.58	6.39			

Table B. 2 **S**ink-float analysis data for the Nkomati DMC underflow

Density Fraction (SG)	Relative SG to Sinks	Mass [g]	Mass %	Cum. Mass to Sinks [%]	Grade [%]			Recovery [%]			Cumulative Grade to Sinks [%]			Cumulative Recovery to Sinks [%]		
					S	Cu	Ni	S	Cu	Ni	S	Cu	Ni	S	Cu	Ni
+ 3.4	3.4	2003.1	6.7	6.7	15.80	0.46	2.31	21.8	13.4	21.6	15.80	0.46	2.31	21.8	13.4	21.6
- 3.4 + 3.3	3.3	1531.9	5.1	11.8	9.01	0.34	1.36	9.5	7.6	9.7	12.86	0.41	1.90	31.3	21.0	31.3
- 3.3 + 3.2	3.2	5241.6	17.5	29.3	6.23	0.29	0.84	22.5	22.1	20.6	8.90	0.34	1.27	53.7	43.1	51.9
- 3.2 + 3.1	3.1	5991.1	20.0	49.3	3.86	0.21	0.57	15.9	18.3	15.9	6.85	0.29	0.98	69.6	61.4	67.8
- 3.1 + 3.0	3	12027.8	40.2	89.5	3.11	0.18	0.49	25.7	31.5	27.5	5.17	0.24	0.76	95.4	92.8	95.4
- 3.0 + 2.95	2.95	2292.9	7.7	97.2	2.41	0.17	0.35	3.8	5.7	3.7	4.96	0.23	0.73	99.2	98.5	99.1
-2.95 + 2.9	2.9	584.6	2.0	99.1	1.19	0.12	0.21	0.5	1.0	0.6	4.88	0.23	0.72	99.7	99.5	99.7
-2.9 + 2.8	2.8	214.5	0.7	99.9	2.21	0.13	0.31	0.3	0.4	0.3	4.86	0.23	0.72	100.0	99.9	100.0
- 2.8	2.7	41.0	0.1	100.0	0.44	0.13	0.09	0.0	0.1	0.0	4.86	0.23	0.72	100.0	100.0	100.0
Total [Calculated]	-	29928.5	100.0	-	4.86	0.23	0.72	100.0	100.0	100.0	-	-	-	-	-	-
Total [Measured]	-	-	-	-	5.63	0.23	0.67	-	-	-	-	-	-	-	-	-

Table B. 3 Sink-float analysis data for the Nkomati DMC overflow

Density Fraction (SG)	Relative SG to Sinks	Mass [g]	Mass %	Cum. Mass to Sinks [%]	Grade [%]			Recovery [%]			Cumulative Grade to Sinks [%]			Cumulative Recovery to Sinks [%]		
					S	Cu	Ni	S	Cu	Ni	S	Cu	Ni	S	Cu	Ni
- 3.2 + 3.1	3.1	124.3	0.4	0.4	7.12	0.33	0.95	2.8	1.2	2.1	7.12	0.33	0.95	2.8	1.2	2.1
- 3.1 + 3.0	3.0	3952.4	13.3	13.7	2.06	0.17	0.32	25.9	19.0	22.1	2.21	0.17	0.34	28.7	20.2	24.2
- 3.0 + 2.95	2.95	5405.3	18.1	31.8	1.40	0.11	0.26	24.1	16.8	24.6	1.75	0.14	0.29	52.7	37.0	48.7
-2.95 + 2.9	2.9	9225.0	30.9	62.7	0.88	0.09	0.18	25.8	23.3	29.0	1.32	0.11	0.24	78.5	60.3	77.8
-2.9 + 2.8	2.8	6672.4	22.4	85.1	0.81	0.14	0.15	17.2	26.5	17.5	1.19	0.12	0.21	95.7	86.8	95.3
-2.8 + 2.7	2.7	1512.8	5.1	90.2	0.58	0.17	0.08	2.8	7.3	2.2	1.15	0.12	0.21	98.5	94.0	97.4
- 2.7	2.6	2923.5	9.8	100.0	0.16	0.07	0.05	1.5	6.0	2.6	1.06	0.12	0.19	100.0	100.0	100.0
Total [Calculated]	-	29815.7	100.0	-	1.06	0.12	0.19	100.0	100.0	100.0	-	-	-	-	-	-
Total [Measured]	-	-	-	-	0.95	0.10	0.13	-	-	-	-	-	-	-	-	-

Table B. 4 Discrete sink-float analysis data for the Phoenix DMC feed sample

Density Fraction (SG)	Relative SG to Sinks	Mass [g]	Mass %	Grade [%]			Recovery [%]		
				S	Cu	Ni	S	Cu	Ni
+ 3.4	3.4	531	1.3	23.10	2.45	6.92	39.6	17.1	41.4
- 3.4 + 3.3	3.3	103	0.3	13.80	2.07	0.06	4.6	2.8	0.1
- 3.3 + 3.2	3.2	97	0.2	8.18	2.40	1.71	2.6	3.1	1.9
- 3.2 + 3.1	3.1	1826	4.6	2.62	0.82	0.62	15.5	19.7	12.7
- 3.1 + 3.0	3.0	8754	22.1	0.67	0.26	0.20	19.0	29.3	19.7
- 3.0 + 2.95	2.95	5591	14.1	0.20	0.07	0.06	3.6	5.1	4.0
-2.95 + 2.9	2.9	10052	25.4	0.27	0.10	0.10	8.8	12.8	11.3
-2.9 + 2.8	2.8	6967	17.6	0.18	0.07	0.07	4.1	6.4	5.7
-2.8 + 2.7	2.7	2887	7.3	0.14	0.05	0.05	1.3	1.9	1.6
- 2.7	2.6	2791	7.0	0.12	0.05	0.05	1.0	1.8	1.6
Total [Calculated]	-	39599	100.0	0.78	0.19	0.22	100.0	100.0	100.0
Total [Measured]	-	-	-	0.92	0.17	0.28	-	-	-
Variance [%]	-	-	-	14.6	13.1	19.9			

Table B. 5 Sink-float analysis data for the Phoenix DMC underflow

Density Fraction (SG)	Relative SG to Sinks	Mass [g]	Mass %	Cum. Mass to Sinks [%]	Grade [%]			Recovery [%]			Cumulative Grade to Sinks [%]			Cumulative Recovery to Sinks [%]		
					S	Cu	Ni	S	Cu	Ni	S	Cu	Ni	S	Cu	Ni
+ 3.4	3.4	721	2.4	2.4	29.60	2.51	7.22	45.80	15.60	46.63	29.60	2.51	7.22	45.8	15.6	46.6
- 3.4 + 3.3	3.3	370	1.2	3.6	16.00	2.58	4.00	12.71	8.23	13.26	24.99	2.53	6.13	58.5	23.8	59.9
- 3.3 + 3.2	3.2	806	2.7	6.3	4.78	1.44	1.05	8.26	10.00	7.58	16.40	2.07	3.97	66.8	33.8	67.5
- 3.2 + 3.1	3.1	4246	14.1	20.4	1.61	0.68	0.39	14.67	24.88	14.83	6.18	1.11	1.50	81.4	58.7	82.3
- 3.1 + 3.0	3.0	12992	43.2	63.7	0.52	0.29	0.11	14.50	32.47	12.80	2.34	0.55	0.55	95.9	91.2	95.1
- 3.0 + 2.95	2.95	5665	18.9	82.5	0.13	0.08	0.05	1.58	4.05	2.54	1.83	0.45	0.44	97.5	95.2	97.7
-2.95 + 2.9	2.9	3635	12.1	94.6	0.24	0.11	0.05	1.87	3.45	1.63	1.63	0.40	0.39	99.4	98.7	99.3
-2.9 + 2.8	2.8	1494	5.0	99.6	0.17	0.09	0.05	0.55	1.15	0.67	1.56	0.39	0.37	99.9	99.8	99.9
- 2.8	2.7	116	0.4	100.0	0.24	0.17	0.05	0.06	0.17	0.05	1.55	0.39	0.37	100.0	100.0	100.0
Total [Calculated]	-	30045	100.0	-	1.55	0.39	0.37	100	100	100	-	-	-	-	-	-
Total [Measured]	-	-	-	-	1.29	0.33	0.35	-	-	-	-	-	-	-	-	-

Table B. 6 Sink-float analysis data for the Phoenix DMC overflow

Density Fraction (SG)	Relative SG to Sinks	Mass [g]	Mass %	Cum. Mass to Sinks [%]	Grade [%]			Recovery [%]			Cumulative Grade to Sinks [%]			Cumulative Recovery to Sinks [%]		
					S	Cu	Ni	S	Cu	Ni	S	Cu	Ni	S	Cu	Ni
+ 3.2	3.2	16	0.1	0.1	6.67	0.86	1.45	1.8	0.4	1.4	6.67	0.86	1.45	1.8	0.4	1.4
- 3.2 + 3.1	3.1	60	0.2	0.3	1.94	0.62	0.44	2.0	1.2	1.6	2.94	0.67	0.65	3.8	1.6	3.1
- 3.1 + 3.0	3.0	795	2.6	2.9	0.58	0.22	0.12	7.9	5.6	5.9	0.79	0.26	0.17	11.7	7.2	9.0
- 3.0 + 2.95	2.95	4432	14.7	17.6	0.18	0.09	0.05	13.6	12.0	13.8	0.28	0.11	0.07	25.3	19.3	22.8
-2.95 + 2.9	2.9	7148	23.8	41.4	0.17	0.09	0.05	20.8	20.8	22.3	0.22	0.10	0.06	46.1	40.0	45.1
-2.9 + 2.8	2.8	10056	33.4	74.8	0.21	0.13	0.05	36.1	41.8	31.3	0.21	0.11	0.05	82.2	81.8	76.4
-2.8 + 2.7	2.7	1719	5.7	80.5	0.28	0.16	0.05	8.2	8.8	5.4	0.22	0.12	0.05	90.5	90.6	81.7
- 2.7	2.6	5869	19.5	100.0	0.10	0.05	0.05	9.5	9.4	18.3	0.19	0.10	0.05	100.0	100.0	100.0
Total [Calculated]	-	30095	100.0		0.19	0.10	0.05	100.0	100.0	100.0	-	-	-	-	-	-
Total [Measured]	-	-	-	-	0.15	0.09	0.05	-	-	-	-	-	-	-	-	-

APPENDIX C: CHEMICAL ASSAYS

Table C. 1 Major element chemistry for the Nkomati head sample

Sample	Rep.	Weight %													
		Mg	**Al**	**Si**	**Ca**	**Ti**	**V**	**Cr**	**Mn**	**Fe**	**Co**	**Ni**	**Cu**	**Zn**	**S**
-12 mm	1	11.0	2.77	19.6	5.69	0.25	<0.05	0.18	0.14	11.8	<0.05	0.40	0.15	<0.05	2.98
-12 mm	2	11.1	2.75	19.6	5.75	0.25	<0.05	0.20	0.14	12.0	<0.05	0.41	0.13	<0.05	2.92
-12+1 mm	1	11.0	2.87	19.3	5.52	0.26	<0.05	0.19	0.14	12.0	<0.05	0.40	<0.05	<0.05	2.67
-1 mm	1	10.3	2.54	17.5	5.54	0.24	<0.05	0.30	0.14	14.1	0.05	0.63	0.25	<0.05	5.51
2.8 floats	1	6.1	3.63	26.3	4.96	0.20	0.25	0.07	0.09	4.33	<0.05	<0.05	0.14	<0.05	0.35
2.9 floats	1	12.2	3.66	20.3	4.17	0.27	<0.05	0.09	0.12	8.99	<0.05	0.13	<0.05	<0.05	0.70
2.95 floats	1	12.2	3.38	19.9	4.51	0.32	<0.05	0.08	0.13	9.66	<0.05	0.15	0.11	0.06	0.92
3.0 floats	1	12.2	3.19	19.9	5.10	0.31	<0.05	0.09	0.14	9.98	<0.05	0.16	<0.05	<0.05	0.99
3.1 floats	1	11.6	2.61	18.5	5.61	0.25	<0.05	0.13	0.14	11.6	<0.05	0.36	0.23	<0.05	2.63
3.2 floats	1	10.6	2.05	17.9	7.59	0.22	<0.05	0.22	0.17	14.2	<0.05	0.63	0.19	<0.05	4.51
3.3 floats	1	9.9	1.93	16.9	7.08	0.23	<0.05	0.25	0.17	17.1	<0.05	0.87	0.26	<0.05	6.4
3.3 floats	2	9.9	1.93	16.9	7.07	0.23	<0.05	0.25	0.17	17.0	<0.05	0.86	0.27	<0.05	-
3.4 floats	1	8.8	1.83	14.1	4.94	0.22	<0.05	0.69	0.15	22.7	0.09	1.39	0.37	<0.05	10.77
3.4 floats	2	8.9	1.82	14.4	5.04	0.22	<0.05	0.61	0.15	22.7	0.08	1.40	0.35	<0.05	10.55
3.4 sinks	1	5.9	1.41	9.8	3.66	0.17	<0.05	1.04	0.12	34.0	0.14	2.52	0.55	<0.05	19.08

'-' = not measured

Table C. 2 Major element chemistry for the Nkomati overflow

Sample	Rep.	Weight %												
		Mg	Al	Si	Ca	Ti	V	Cr	Mn	Fe	Co	Ni	Cu	S
Head	1	11.3	3.13	19.8	4.63	0.29	0.45	0.07	0.13	8.20	<0.05	0.13	0.10	0.96
Head	2	11.3	3.18	20.0	4.65	0.29	0.45	0.06	0.13	8.22	<0.05	0.12	0.10	0.93
2.7 floats	1	4.02	3.29	33.0	4.43	0.17	<0.05	0.06	0.08	2.63	<0.05	<0.05	0.07	0.16
2.7 floats	2	4.01	3.29	33.2	4.45	0.17	<0.05	0.06	0.08	2.53	<0.05	<0.05	0.07	0.16
2.8 floats	1	7.73	3.98	22.0	7.27	0.29	<0.05	0.06	0.14	5.84	<0.05	0.083	0.17	0.58
2.9 floats	1	11.3	3.76	21.9	3.99	0.29	0.06	0.07	0.13	8.06	<0.05	0.15	0.14	0.81
2.95 floats	1	12.1	3.28	22.5	4.27	0.33	0.06	0.06	0.14	9.23	<0.05	0.18	0.09	0.88
3.0 floats	1	11.6	3.00	20.9	5.33	0.39	<0.05	0.10	0.15	9.73	<0.05	0.26	0.11	1.40
3.1 floats	1	11.1	2.48	21.2	6.72	0.28	<0.05	0.13	0.17	10.2	<0.05	0.32	0.17	2.06
3.1 sinks	1	9.47	1.62	17.5	6.93	0.26	0.06	0.37	0.29	18.2	0.08	0.94	0.33	7.12
3.1 sinks	2	9.39	1.63	17.3	6.91	0.26	0.06	0.36	0.29	18.2	0.08	0.96	0.33	-

'-' = not measured

Table C. 3 Major element chemistry for the Nkomati underflow

Sample	Rep.	Weight %												
		Mg	**Al**	**Si**	**Ca**	**Ti**	**V**	**Cr**	**Mn**	**Fe**	**Co**	**Ni**	**Cu**	**S**
Head	1	10.50	2.10	17.0	6.28	0.26	0.07	0.28	0.16	13.7	<0.05	0.67	0.23	5.63
2.8 floats	1	7.96	3.71	22.9	6.24	0.22	0.09	0.05	1.57	5.22	<0.05	0.09	0.12	0.44
2.8 floats	2	8.05	3.71	22.9	6.27	0.22	0.09	<0.05	1.57	5.21	<0.05	0.08	0.13	0.43
2.9 floats	1	11.60	3.30	19.8	5.26	0.24	0.08	0.13	0.15	10.2	<0.05	0.31	0.13	2.21
2.95 floats	1	11.80	3.20	21.1	5.21	0.33	<0.05	0.07	0.15	9.51	<0.05	0.21	0.12	1.19
3.0 floats	1	11.20	2.98	20.8	5.49	0.34	0.06	0.11	0.15	11.2	<0.05	0.35	0.17	2.41
3.1 floats	1	11.60	2.48	20.7	6.24	0.24	0.06	0.14	0.18	12.3	<0.05	0.49	0.18	3.11
3.2 floats	1	10.50	2.14	20.3	7.95	0.24	0.07	0.20	0.18	12.2	<0.05	0.57	0.21	3.86
3.3 floats	1	9.80	2.05	19.1	7.35	0.24	0.05	0.34	0.18	15.5	0.06	0.84	0.29	6.23
3.4 floats	1	8.86	1.95	16.4	5.42	0.25	<0.05	0.58	0.18	20.2	0.09	1.36	0.34	9.01
3.4 sinks	1	6.10	1.51	11.7	3.89	0.20	<0.05	0.79	0.31	29.5	0.15	2.34	0.46	15.8
3.4 sinks	2	6.08	1.49	11.6	3.87	0.20	<0.05	0.79	0.31	29.6	0.15	2.28	0.46	-

'-' = not measured

Table C. 4 Major element chemistry for the Phoenix head sample

Sample	Rep.	Weight %												
		Mg	**Al**	**Si**	**Ca**	**Ti**	**V**	**Cr**	**Mn**	**Fe**	**Co**	**Ni**	**Cu**	**S**
-12 mm	1	5.86	7.66	21.4	6.42	0.59	0.08	0.06	0.11	7.41	<0.05	0.25	0.21	0.91
-12 mm	2	5.86	7.64	21.4	6.41	0.60	0.09	0.06	0.11	7.37	<0.05	0.25	0.20	0.92
-12+1 mm	1	5.79	7.38	20.7	6.22	0.69	0.09	0.05	0.11	8.17	<0.05	0.34	0.29	1.34
-1 mm	1	6.00	7.67	21.2	6.57	0.58	0.11	0.07	0.11	7.18	<0.05	0.28	0.17	0.91
2.7 floats	1	1.53	7.37	27.9	2.64	0.21	<0.05	0.10	<0.05	2.37	<0.05	<0.05	<0.05	0.12
2.7 floats	2	1.54	7.36	27.9	2.64	0.21	<0.05	0.10	<0.05	2.39	<0.05	<0.05	<0.05	0.11
2.8 floats	1	2.02	7.76	27.1	3.27	0.24	<0.05	<0.05	<0.05	2.87	<0.05	<0.05	<0.05	0.14
2.9 floats	1	5.69	8.16	19.8	6.13	0.41	<0.05	<0.05	0.10	5.83	<0.05	0.07	0.07	0.18
2.95 floats	1	6.38	7.76	20.4	6.72	0.65	<0.05	0.06	0.11	7.04	<0.05	0.10	0.10	0.27
3.0 floats	1	6.35	7.46	20.4	6.84	0.77	<0.05	0.06	0.12	7.19	<0.05	0.06	0.07	0.20
3.1 floats	1	6.99	7.21	20.1	7.16	0.69	<0.05	0.08	0.12	7.91	<0.05	0.19	0.24	0.67
3.1 floats	2	6.98	7.13	20.1	7.11	0.69	<0.05	0.08	0.12	7.94	<0.05	0.21	0.27	-
3.2 floats	1	6.95	6.52	19.1	6.98	0.54	<0.05	0.08	0.12	9.91	<0.05	0.62	0.82	2.62
3.3 floats	1	5.31	5.48	16.0	6.22	0.95	<0.05	0.08	0.12	17.1	<0.05	1.71	2.40	8.18
3.4 floats	1	0.63	7.11	26.2	0.89	0.36	<0.05	0.06	0.05	4.34	<0.05	0.06	2.07	13.8
3.4 sinks	1	1.67	1.42	4.82	1.55	0.13	<0.05	0.17	<0.05	42.5	0.12	6.92	2.45	23.1

'-' = not measured

Table C. 5 Major element chemistry for the Phoenix overflow

Sample	Rep.	Weight %											
		Mg	Al	Si	Ca	Ti	Cr	Mn	Fe	Co	Ni	Cu	S
Head	1	5.25	7.68	23.6	6.01	0.48	0.06	0.11	5.66	<0.05	<0.05	0.08	0.15
Head	2	5.27	7.75	23.7	6.09	0.48	0.05	0.10	5.55	<0.05	<0.05	0.10	0.15
2.7 floats	1	0.77	7.14	31.6	2.23	0.18	<0.05	<0.05	1.64	<0.05	<0.05	<0.05	0.08
2.7 floats	2	0.79	7.31	32.0	2.25	0.18	<0.05	<0.05	1.68	<0.05	<0.05	<0.05	0.08
2.75 floats	1	3.31	8.47	25.8	4.59	0.35	<0.05	0.07	4.38	<0.05	<0.05	0.17	0.22
2.8 floats	1	5.24	8.69	22.8	5.74	0.41	0.05	0.09	5.66	<0.05	<0.05	0.16	0.2
2.9 floats	1	6.34	8.69	21.5	7.16	0.38	0.06	0.11	6.29	<0.05	<0.05	0.13	0.18
2.95 floats	1	6.81	7.92	21.0	7.56	0.68	0.07	0.12	7.25	<0.05	<0.05	0.09	0.15
3.0 floats	1	6.68	7.46	21.2	7.59	0.97	0.07	0.13	7.99	<0.05	<0.05	0.09	0.16
3.1 floats	1	7.07	6.91	20.9	8.07	0.86	0.09	0.14	8.21	<0.05	0.12	0.22	0.38
3.2 floats	1	6.66	5.90	19.5	8.02	1.43	0.11	0.23	11.60	<0.05	0.44	0.62	1.75
3.2 sinks	1	5.10	3.63	13.4	4.97	2.17	0.58	0.91	24.70	0.09	1.43	0.86	5.59
3.2 sinks	2	5.07	3.56	13.3	4.92	2.18	0.59	0.91	24.90	0.09	1.46	0.86	-

'-' = not measured

Table C. 6 Major element chemistry for the Phoenix underflow

Sample	Rep.	Weight %													
		Mg	**Al**	**Si**	**Ca**	**Ti**	**V**	**Cr**	**Mn**	**Fe**	**Co**	**Ni**	**Cu**	**Zn**	**S**
Head	1	6.87	7.16	20.1	7.50	0.63	<0.05	0.08	0.12	8.58	<0.05	0.35	0.33	1.29	<0.05
2.7 floats	1	0.83	7.03	31.6	2.40	0.20	<0.05	<0.05	<0.05	1.71	<0.05	<0.05	0.08	<0.05	0.11
2.75 floats	1	3.54	8.45	25.3	4.57	0.35	<0.05	<0.05	0.07	4.42	<0.05	<0.05	0.35	0.15	0.18
2.8 floats	1	5.81	8.69	21.9	6.49	0.36	<0.05	0.06	0.10	6.02	<0.05	<0.05	0.15	<0.05	0.24
2.9 floats	1	6.41	8.16	21.4	7.46	0.50	<0.05	0.07	0.11	6.59	<0.05	<0.05	0.09	<0.05	0.16
2.9 floats	2	6.42	8.24	21.4	7.49	0.50	<0.05	0.06	0.11	6.60	<0.05	<0.05	0.09	<0.05	-
2.95 floats	1	6.69	7.62	21.2	7.60	0.79	<0.05	0.07	0.12	7.28	<0.05	<0.05	0.11	<0.05	0.20
3.0 floats	1	6.54	7.58	21.1	7.58	0.85	<0.05	0.07	0.12	7.36	<0.05	<0.05	0.08	<0.05	0.14
3.1 floats	1	7.32	7.19	20.8	7.85	0.64	<0.05	0.08	0.12	7.56	<0.05	0.11	0.29	<0.05	0.5
3.2 floats	1	7.46	6.58	20.0	7.79	0.51	<0.05	0.13	0.12	8.79	<0.05	0.39	0.68	<0.05	1.52
3.3 floats	1	6.71	6.26	17.9	7.31	0.45	<0.05	0.17	0.12	12.5	0.05	1.05	1.44	<0.05	4.76
3.3 floats	2	6.69	6.22	17.9	7.45	0.45	<0.05	0.17	0.12	12.4	0.05	1.05	1.44	<0.05	4.79
3.4 floats	1	4.24	3.67	11.2	3.77	0.28	<0.05	0.47	0.11	27.0	0.14	4.00	2.58	<0.05	16.00
3.4 sinks	1	1.54	1.34	4.3	1.50	0.10	<0.05	0.18	0.05	43.6	0.23	7.22	2.51	<0.05	29.60

'-' = not measured

APPENDIX D: MINERALOGICAL DATA

Table D. 1 EPMA silicate grain analyses for Nkomati ore (lld – lower than limit of detection)

Grain No.	Oxide Weight %										Total	Mineral Name
	Na_2O	MgO	Al_2O_3	SiO_2	K_2O	CaO	TiO_2	Cr_2O_3	FeO	NiO		
1	0.04	28.26	21.89	29.10	0.05	0.63	lld	0.03	5.63	0.09	85.73	chlorite
2	0.02	22.02	21.15	29.26	0.03	0.06	lld	0.14	16.17	0.19	89.04	
3	0.04	21.88	20.97	29.78	0.03	0.04	lld	0.14	15.91	0.16	88.96	
4	lld	29.53	21.85	29.91	0.03	0.94	1.04	lld	4.53	0.05	87.89	
5	lld	29.52	21.80	29.91	0.03	0.92	1.04	0.03	4.36	0.09	87.71	
6	lld	31.29	21.40	30.40	0.10	0.43	0.35	lld	3.40	0.07	87.42	
7	lld	33.14	21.84	31.06	0.07	0.04	0.05	lld	2.30	0.05	88.56	
8	lld	32.55	19.78	31.29	lld	0.10	0.03	lld	3.00	lld	86.75	
9	0.05	30.36	13.06	32.13	lld	0.26	lld	lld	6.49	lld	82.34	
10	0.03	26.96	15.83	32.46	lld	0.04	lld	lld	12.49	0.05	87.85	
11	0.12	22.95	15.82	36.85	7.39	0.17	0.05	lld	8.99	0.10	92.44	biotite
12	0.08	23.89	15.67	37.06	7.14	0.25	0.04	lld	8.68	0.08	92.89	
13	0.09	7.46	14.55	37.24	8.47	0.05	4.31	lld	24.08	lld	96.25	
14	0.37	20.00	17.22	37.67	9.20	0.06	1.85	lld	9.30	0.08	95.77	
15	0.12	26.29	14.16	38.37	5.68	0.09	0.29	0.10	7.66	0.12	92.88	
16	lld	30.77	12.85	38.51	3.33	0.28	0.02	lld	6.16	lld	91.92	
17	0.62	21.31	15.13	38.67	9.26	0.02	4.55	0.37	6.37	0.07	96.36	
18	0.45	21.66	15.11	38.68	9.31	lld	4.07	0.36	6.40	0.06	96.11	
19	0.03	17.97	11.62	40.88	8.97	0.10	0.22	lld	14.34	lld	94.13	
20	0.04	18.02	11.49	41.07	9.03	0.09	0.19	lld	14.25	lld	94.19	
21	0.30	16.70	13.26	41.85	7.77	3.68	4.90	0.40	11.01	0.09	99.96	

22	lld	36.49	2.20	40.15	lld	0.02	0.60	lld	4.49	lld	83.96	
23	0.02	37.44	1.80	42.92	0.02	1.04	0.05	lld	3.95	0.05	87.28	
24	0.03	39.67	0.04	43.14	0.05	0.13	lld	lld	5.67	0.17	88.90	
25	lld	42.99	0.03	44.21	lld	lld	lld	lld	1.80	lld	89.03	**serpentine**
26	lld	42.58	0.08	44.43	lld	0.05	lld	lld	2.43	lld	89.57	
27	lld	42.80	0.06	44.72	lld	0.02	0.03	lld	2.01	lld	89.66	
28	0.04	29.60	0.21	61.85	0.05	0.04	lld	lld	4.40	0.06	96.27	
29	0.02	26.32	0.07	61.94	0.02	lld	lld	lld	7.43	0.12	95.93	
30	0.08	28.98	0.15	61.99	0.06	0.03	lld	lld	4.45	0.13	95.88	
31	0.03	27.96	0.15	62.25	0.04	0.10	lld	lld	4.94	0.11	95.58	
32	0.05	29.72	0.03	62.41	0.03	0.02	lld	lld	4.08	0.09	96.42	
33	0.06	29.76	0.27	62.53	lld	0.05	lld	lld	3.19	lld	95.86	**talc**
34	0.03	29.59	0.08	62.60	0.02	0.09	lld	lld	3.86	0.13	96.40	
35	0.26	31.42	0.69	62.80	lld	0.83	lld	0.05	1.04	lld	97.09	
36	0.02	27.83	0.06	63.43	0.02	0.14	lld	lld	6.89	0.08	98.47	
37	0.12	30.74	0.61	63.76	0.04	lld	lld	lld	3.36	lld	98.64	
38	0.13	32.15	0.39	64.25	lld	0.06	lld	0.05	0.97	lld	98.00	
39	11.76	lld	19.35	68.37	0.07	0.08	lld	lld	0.13	lld	99.76	
40	11.91	lld	19.67	68.24	0.06	0.12	lld	lld	0.01	lld	100.02	
41	11.70	lld	19.99	68.12	0.05	0.13	lld	lld	0.04	lld	100.03	
42	11.78	lld	19.80	68.30	0.07	0.16	lld	lld	0.05	lld	100.16	
43	11.71	lld	19.75	68.05	0.07	0.13	lld	lld	0.04	lld	99.74	**albite**
44	11.92	lld	19.84	68.11	0.05	0.10	lld	lld	0.04	lld	100.06	
45	11.68	lld	19.83	68.24	0.07	0.10	lld	lld	0.09	lld	100.01	
46	11.69	lld	19.33	67.95	0.07	0.07	lld	lld	0.08	lld	99.19	
47	11.81	lld	19.86	67.85	0.07	0.24	lld	lld	0.09	lld	99.93	
48	11.85	lld	20.00	68.34	0.05	0.05	lld	lld	0.03	lld	100.33	
49	11.73	lld	19.91	67.94	0.07	0.12	lld	lld	0.19	lld	99.96	

50	11.62	lld	19.88	67.75	0.07	0.16	lld	lld	0.13	lld	99.61	
51	11.68	lld	19.52	67.59	0.07	0.11	lld	lld	0.07	lld	99.05	
52	11.54	lld	19.83	67.52	0.05	0.13	lld	lld	0.09	lld	99.15	
53	11.68	lld	19.48	67.59	0.07	0.14	lld	lld	0.16	lld	99.12	**albite**
54	11.76	lld	19.79	67.45	0.08	0.16	lld	lld	0.04	lld	99.28	
55	11.91	lld	19.49	68.24	0.07	0.12	lld	lld	0.07	lld	99.91	
56	11.94	lld	19.56	68.32	0.05	0.05	lld	lld	0.08	lld	100.00	
57	11.86	lld	20.02	68.10	0.05	0.08	lld	lld	0.15	lld	100.26	
58	11.89	lld	19.69	68.07	0.05	0.08	lld	lld	0.25	lld	100.03	
59	11.90	lld	19.77	67.78	0.06	0.11	lld	lld	0.46	lld	100.09	
60	11.91	lld	19.81	68.17	0.05	0.04	lld	lld	0.21	lld	100.18	
61	0.05	17.34	2.23	52.58	lld	25.74	0.39	lld	1.98	lld	100.31	
62	0.11	16.24	0.50	55.8	lld	25.63	0.03	lld	3.61	lld	101.92	
63	0.16	16.14	0.83	56.05	0.03	25.35	0.07	lld	4.24	lld	102.87	
64	0.30	16.61	1.14	54.21	0.10	21.33	0.15	0.05	6.17	0.08	100.13	**augite**
65	1.18	10.35	4.28	49.63	0.42	10.02	0.93	lld	21.61	lld	98.45	
66	1.01	23.69	7.18	49.80	0.18	10.52	0.35	0.48	4.34	lld	97.56	
67	0.05	15.73	4.91	49.88	0.02	25.22	0.66	0.04	3.48	lld	99.99	
68	0.27	17.13	2.15	49.91	lld	19.04	0.34	0.63	7.24	0.06	96.78	
69	1.82	21.88	7.88	49.44	0.19	11.75	1.36	0.50	4.01	lld	98.84	
70	0.31	13.3	3.85	51.98	0.82	12.38	1.93	lld	15.39	lld	99.95	
71	0.37	15.09	2.27	53.04	0.11	12.29	0.29	0.04	13.77	lld	97.27	
72	0.30	9.45	2.66	53.22	0.22	12.46	0.06	lld	21.25	lld	99.61	
73	0.45	13.97	3.79	53.73	0.43	12.49	0.23	lld	14.99	lld	100.08	
74	0.45	13.97	3.79	53.73	0.43	12.49	0.23	lld	14.99	lld	100.08	**actinolite**
75	0.44	12.27	2.57	54.71	0.19	9.76	0.20	lld	19.87	lld	100.01	
76	0.35	16.77	4.02	55.15	0.14	12.87	0.12	0.05	10.69	lld	100.16	
77	0.28	17.70	2.40	55.37	0.05	12.82	0.12	lld	10.04	lld	98.79	
78	0.18	16.21	1.60	55.57	0.04	13.08	lld	lld	12.06	lld	98.73	

79	0.15	16.31	1.61	55.65	0.04	13.04	0.16	lld	11.79	lld	98.75	**actinolite**
80	0.14	19.41	0.82	55.75	0.03	12.52	0.04	lld	7.64	lld	96.34	
81	0.26	17.57	1.08	56.59	0.06	12.46	0.15	lld	10.92	lld	99.09	
82	0.14	17.82	0.72	56.61	lld	12.82	0.04	lld	10.83	lld	98.98	
83	0.13	18.32	0.77	56.87	0.03	12.87	0.04	lld	9.72	lld	98.75	
84	0.11	19.13	1.23	57.03	0.03	12.96	0.07	lld	8.20	lld	98.76	
85	0.21	17.21	1.05	57.17	0.08	12.73	0.13	lld	11.28	lld	99.86	
86	0.15	17.97	0.45	57.54	0.03	12.22	lld	0.07	10.98	lld	99.41	
87	0.09	15.85	0.66	57.87	0.03	13.19	lld	0.03	12.81	lld	100.53	
88	0.29	21.58	0.90	57.99	0.06	12.20	0.07	lld	6.04	0.05	99.18	
89	0.05	23.37	0.12	58.00	0.02	13.00	0.03	lld	2.93	lld	97.53	
90	0.04	19.04	0.21	59.00	lld	13.04	lld	lld	9.33	lld	100.67	

Table D. 2 EPMA pyrrhotite grain analyses for Nkomati ore (wt%)

Grain No.	S	Fe	Ni	Total
1	39.42	59.59	0.59	99.59
2	38.70	60.20	0.48	99.38
3	37.96	60.72	0.42	99.10
4	38.50	60.78	0.40	99.69
5	38.76	60.05	0.63	99.45
6	39.49	59.83	0.41	99.73
7	38.69	60.90	0.38	99.97
8	38.56	60.50	0.64	99.70
9	39.47	59.89	0.39	99.75
10	39.49	60.15	0.65	100.29
11	38.82	60.30	0.46	99.58
12	39.19	59.50	0.62	99.31
13	39.21	59.88	0.57	99.66

Table D. 3 EPMA pentlandite grain analyses for Nkomati ore (wt%)

Grain No.	S	Fe	Co	Ni	Total
1	33.50	31.07	1.89	34.20	100.66
2	33.43	30.91	1.92	34.32	100.58
3	33.29	30.27	1.94	34.29	99.78
4	33.34	31.22	1.85	34.31	100.73
5	33.53	31.03	1.87	34.07	100.50
6	33.31	30.75	2.02	34.16	100.24
7	33.56	30.71	1.87	34.23	100.37
8	33.26	30.82	1.94	34.40	100.42
9	33.40	30.69	1.92	34.20	100.20
10	33.25	30.67	1.85	34.52	100.28
11	33.25	30.99	1.99	34.26	100.49
12	33.30	30.80	1.99	34.42	100.50
13	33.42	30.80	1.86	34.11	100.19
14	33.07	30.72	2.03	34.11	99.94
15	33.24	30.72	1.94	34.31	100.22
16	33.22	29.93	1.85	34.44	99.44
17	33.48	30.69	1.96	34.23	100.36
18	33.33	30.97	2.05	34.33	100.68
19	33.45	29.64	1.90	34.93	99.92
20	33.31	30.90	1.97	34.45	100.63
21	33.24	30.50	1.88	34.34	99.96
22	33.44	30.62	1.96	34.35	100.37
23	33.23	30.45	1.93	34.47	100.08
24	33.39	31.04	1.83	34.33	100.59
25	33.42	30.41	1.91	34.56	100.30

26	33.45	30.93	2.00	34.18	100.56
27	33.21	30.87	2.01	34.26	100.35
28	33.30	30.42	1.92	34.61	100.25
29	33.41	30.93	1.88	34.12	100.34
30	33.42	30.68	1.90	34.35	100.36
31	33.23	30.70	1.87	34.29	100.08
32	33.15	30.82	1.98	34.35	100.30
33	33.48	30.85	1.85	34.30	100.47
34	33.31	30.45	1.88	34.39	100.04
35	33.23	31.04	2.07	34.04	100.38
36	33.25	30.74	1.95	34.24	100.18
37	33.35	30.96	1.81	34.22	100.34
38	33.19	30.31	1.92	34.47	99.90
39	33.21	31.10	1.86	34.21	100.38
40	33.41	31.44	1.99	33.83	100.66
41	33.94	30.79	1.92	33.92	100.57
42	33.31	30.76	2.03	33.99	100.10
43	33.65	30.98	1.88	34.23	100.75
44	33.42	30.94	2.08	34.09	100.52
45	34.07	30.58	1.92	34.01	100.58
46	33.46	30.92	1.84	34.11	100.33
47	33.54	30.65	1.89	34.37	100.44
48	33.43	31.04	1.91	34.10	100.48

Table D. 4 EPMA silicate grain analyses for Phoenix ore (lld – lower than limit of detection)

Grain No.	Oxide Weight %									Total	Mineral Name
	Na_2O	MgO	Al_2O_3	SiO_2	K_2O	CaO	TiO_2	FeO	NiO		
1	0.20	20.60	8.10	49.30	lld	9.50	lld	9.40	0.06	97.16	
2	0.30	19.40	2.50	55.30	lld	12.40	lld	6.80	lld	96.70	
3	0.30	18.00	3.40	56.70	lld	13.30	0.10	7.50	0.07	99.37	
4	0.40	17.40	7.60	50.90	0.10	12.10	0.10	8.80	0.06	97.46	
5	0.40	18.10	3.90	54.10	lld	12.80	0.10	7.70	0.06	97.16	
6	0.70	16.40	7.00	51.80	0.10	12.70	0.20	10.10	0.08	99.08	
7	0.60	17.30	5.70	51.90	0.10	12.20	0.10	9.50	0.09	97.49	
8	0.60	18.60	4.70	53.10	lld	12.10	0.20	9.40	0.04	98.74	
9	0.70	19.00	5.50	52.10	lld	12.70	0.20	9.60	lld	99.80	
10	0.70	17.50	6.50	50.80	0.10	12.20	0.20	9.50	0.07	97.57	
11	0.30	19.80	3.70	55.50	lld	12.40	0.10	7.90	0.08	99.78	
12	0.20	19.40	2.90	53.90	lld	12.30	0.10	8.50	0.04	97.34	
13	0.40	21.10	2.50	56.40	lld	12.20	0.10	7.90	0.16	100.76	**hornblende**
14	0.10	21.80	0.60	57.30	lld	13.40	lld	5.90	0.13	99.23	
15	0.10	20.00	2.00	54.80	lld	12.80	lld	8.00	0.09	97.79	
16	0.20	20.30	2.70	54.20	lld	12.40	0.10	7.80	0.06	97.76	
17	0.30	18.70	3.70	52.30	lld	11.10	0.10	11.10	0.09	97.39	
18	0.50	18.60	5.40	52.80	0.10	12.20	lld	10.90	0.09	100.59	
19	0.50	18.10	5.70	52.00	0.10	12.00	0.10	11.30	lld	99.80	
20	0.40	17.40	4.10	53.30	0.10	12.60	0.10	9.80	lld	97.80	
21	0.40	19.60	3.90	53.80	lld	13.20	0.20	7.60	lld	98.70	
22	0.90	16.20	7.40	51.30	0.10	12.30	0.30	11.10	lld	99.60	
23	0.70	17.30	6.00	52.90	0.10	12.30	0.40	9.90	0.04	99.64	
24	0.40	19.00	3.30	55.80	lld	12.70	0.20	9.00	0.07	100.47	
25	0.50	17.20	5.40	51.80	0.10	12.50	0.10	10.00	lld	97.60	
26	0.40	19.00	3.40	54.00	lld	12.10	0.20	9.10	lld	98.20	

27	0.50	17.30	5.60	50.40	0.10	15.00	0.40	8.00	lld	97.30	
28	0.60	17.40	4.40	52.80	0.10	12.60	0.10	10.00	lld	98.00	
29	0.30	18.30	2.80	55.00	0.10	12.80	0.10	10.80	lld	100.20	
30	0.70	17.70	6.50	53.10	0.10	12.10	0.20	10.20	0.11	100.71	
31	0.10	18.40	0.90	51.60	lld	5.30	0.60	21.60	0.04	98.54	
32	0.10	16.40	2.20	49.90	lld	7.20	0.60	23.00	lld	99.40	
33	0.10	22.10	1.00	52.50	lld	4.80	0.40	19.20	0.06	100.16	
34	0.30	11.20	1.40	51.10	0.20	13.70	0.70	19.70	lld	98.30	**ferroactinolite**
35	0.30	10.60	2.10	48.70	0.10	12.00	0.60	25.30	lld	99.70	
36	0.10	11.70	0.80	49.30	lld	6.80	0.60	30.50	lld	99.80	
37	0.10	10.40	0.60	47.90	lld	5.40	0.50	34.00	lld	98.90	
38	1.40	14.90	12.40	48.40	0.10	12.80	0.30	9.10	0.06	99.46	
39	1.40	14.80	12.10	47.10	0.10	12.40	0.20	9.00	0.07	97.17	
40	1.20	16.50	8.50	49.90	0.10	12.10	0.30	9.80	0.04	98.44	
41	0.60	18.30	7.70	52.10	0.30	11.80	0.20	9.80	0.05	100.85	
42	1.10	16.30	7.90	49.80	0.20	12.00	0.30	9.10	0.05	96.75	
43	1.10	17.10	8.20	51.70	0.20	12.40	0.40	9.40	0.09	100.59	
44	1.30	15.00	10.70	47.90	0.30	12.20	0.40	10.70	0.05	98.55	
45	0.90	15.90	7.80	50.10	0.20	12.30	0.20	10.50	0.05	97.95	
46	1.20	15.40	9.20	48.20	0.30	12.00	0.30	10.70	0.05	97.35	
47	1.30	14.90	10.60	47.90	0.30	12.30	0.30	11.30	0.06	98.96	**actinolite**
48	1.00	16.80	8.70	49.90	0.20	12.20	0.20	10.90	0.04	99.94	
49	1.30	15.50	10.40	48.10	0.10	11.70	0.50	10.80	0.05	98.45	
50	1.50	15.60	10.10	47.50	0.10	11.40	0.50	10.40	0.12	97.22	
51	1.40	16.50	9.80	48.20	0.10	11.30	0.60	10.20	0.09	98.19	
52	1.70	15.80	10.80	48.40	0.10	12.00	0.60	10.80	lld	100.20	
53	1.50	16.20	10.40	49.30	0.10	11.90	0.50	10.60	lld	100.50	
54	1.40	15.20	10.30	47.10	0.10	11.90	0.60	10.50	lld	97.10	
55	1.30	16.70	9.80	48.50	0.10	11.90	0.50	10.00	0.11	98.91	

56	1.40	16.50	10.20	47.50	0.10	11.30	0.50	10.20	lld	97.70	
57	1.50	17.00	10.50	48.80	0.10	11.80	0.50	10.40	lld	100.60	
58	0.20	12.30	1.30	50.60	lld	14.70	0.80	19.40	lld	99.30	**augite**
59	0.30	15.60	2.50	51.60	lld	18.40	0.90	9.80	lld	99.10	
60	0.20	16.70	2.80	50.90	lld	16.00	1.00	11.90	lld	99.50	
61	0.20	14.30	1.80	50.70	lld	16.90	1.10	14.30	lld	99.30	
62	0.20	12.40	0.90	52.60	lld	20.40	0.20	13.00	lld	99.70	
63	0.20	16.60	2.30	52.10	lld	16.70	0.80	10.90	lld	99.60	
64	0.20	15.90	1.80	49.80	lld	15.80	1.00	15.10	0.04	99.64	
65	0.20	16.30	2.80	50.00	lld	15.80	1.00	13.30	0.06	99.46	
66	0.20	14.60	2.20	50.30	lld	18.00	1.10	13.10	lld	99.50	
67	0.20	12.20	1.00	49.80	lld	14.20	0.70	21.20	lld	99.30	
68	0.30	16.10	1.70	50.60	lld	17.30	0.90	12.70	0.04	99.64	
69	0.20	17.80	1.80	51.80	lld	16.60	0.80	10.70	lld	99.70	
70	0.20	17.60	2.10	51.10	lld	18.00	0.90	9.80	lld	99.70	
71	0.20	16.30	2.00	50.20	lld	15.70	1.00	13.80	lld	99.20	
72	0.52	lld	33.24	40.11	lld	23.71	lld	1.44	lld	99.02	**zoisite**
73	0.43	lld	34.60	39.34	lld	23.81	lld	0.28	lld	98.46	
74	0.26	lld	34.59	38.96	lld	24.03	lld	0.50	lld	98.33	
75	0.31	lld	34.43	39.43	lld	24.14	lld	0.48	lld	98.78	
76	0.22	lld	32.66	39.71	lld	24.23	lld	2.81	lld	99.64	
77	0.28	lld	32.61	39.54	lld	24.17	lld	2.87	lld	99.48	
78	lld	lld	34.98	39.10	lld	25.20	lld	0.29	lld	99.57	
79	lld	0.24	31.90	40.01	lld	23.40	lld	1.52	lld	97.06	
80	0.60	lld	33.80	41.35	lld	23.74	lld	0.66	lld	100.15	
81	lld	0.17	30.76	38.22	lld	24.46	0.05	3.70	lld	97.37	
82	5.27	0.07	28.28	54.82	0.29	11.16	0.11	0.59	lld	100.58	
83	5.19	0.07	28.14	53.56	0.26	11.10	0.10	0.76	lld	99.19	
84	0.76	lld	35.80	44.32	lld	19.31	lld	0.06	lld	100.25	

85	4.14	0.06	29.33	52.11	0.42	12.64	0.04	0.65	lld	99.39	
86	3.79	0.15	30.05	51.22	0.34	13.16	0.05	0.93	lld	99.69	
87	4.09	0.08	25.84	57.63	0.83	10.62	0.03	0.61	lld	99.73	
88	2.10	lld	34.26	46.63	lld	16.97	lld	0.17	lld	100.14	
89	2.72	lld	33.63	47.81	lld	16.50	lld	0.07	lld	100.72	
90	4.99	0.08	28.98	52.41	0.30	11.82	0.10	0.72	lld	99.40	
91	6.18	0.06	27.60	55.21	0.46	10.16	0.09	0.76	lld	100.52	
92	5.77	0.06	27.29	54.19	0.40	10.72	0.10	0.71	lld	99.23	
93	5.02	0.10	29.12	53.18	0.28	12.08	0.06	0.83	lld	100.66	**plagioclase**
94	8.04	lld	25.41	58.26	0.05	7.37	0.03	0.21	lld	99.36	
95	9.60	0.09	23.86	61.11	0.80	3.66	lld	0.19	0.05	99.37	
96	2.89	lld	33.30	47.89	0.21	15.64	lld	0.18	lld	100.12	
97	4.22	0.15	29.66	51.44	0.18	13.40	0.08	0.89	0.06	100.08	
98	4.98	0.12	28.81	52.93	0.26	12.38	0.11	0.83	lld	100.43	
99	5.13	0.12	28.03	54.49	0.28	11.90	0.11	0.81	lld	100.87	
100	4.06	0.15	30.64	51.34	0.17	13.59	0.10	0.79	lld	100.84	
101	4.87	0.16	28.51	52.92	0.24	12.59	0.10	0.89	lld	100.29	
102	4.55	0.07	31.01	51.28	0.54	12.25	lld	0.17	0.04	99.91	
103	2.77	0.04	32.77	47.79	0.51	14.92	lld	0.15	0.11	99.06	
104	3.99	0.07	31.39	50.49	0.44	13.17	lld	0.27	lld	99.81	
105	5.18	lld	29.57	51.88	0.05	12.11	lld	0.05	0.14	98.98	
106	6.01	lld	28.69	54.45	0.06	10.54	lld	0.25	lld	100.00	
107	lld	20.87	20.90	24.61	lld	0.07	lld	15.36	0.10	81.90	
108	lld	20.73	20.94	24.74	lld	0.05	0.03	15.30	0.07	81.85	
109	lld	21.14	20.96	24.78	lld	0.04	lld	15.38	0.08	82.37	
110	0.06	20.50	20.67	25.11	lld	0.09	lld	14.95	0.11	81.49	
111	0.04	20.89	21.21	26.04	0.04	0.09	0.03	15.16	0.07	83.57	
112	lld	23.23	21.52	27.16	lld	lld	0.05	11.95	0.16	84.07	
113	lld	27.13	18.27	27.59	lld	0.03	0.03	9.52	0.10	82.66	
114	lld	23.75	21.99	27.71	lld	lld	0.04	12.16	0.17	85.84	

115	lld	24.32	20.60	27.79	0.14	0.22	0.14	11.14	0.05	84.40	**chlorite**
116	0.08	22.05	21.85	27.89	lld	0.19	0.05	13.69	0.14	85.93	
117	lld	24.51	22.42	28.03	lld	0.06	0.05	10.31	0.30	85.69	
118	lld	24.32	22.52	28.39	lld	0.08	0.05	11.51	0.12	86.99	
119	lld	23.17	21.23	30.81	1.09	0.28	0.25	9.10	0.26	86.18	
120	0.13	20.49	13.13	37.81	0.17	1.46	0.15	13.68	0.11	87.13	
121	0.06	21.25	12.84	37.84	0.15	1.14	0.17	14.27	0.14	87.86	
122	0.13	20.48	12.91	37.98	0.20	1.54	0.15	13.58	0.15	87.13	

Table D. 5 EPMA pyrrhotite grain analyses for Phoenix ore (wt%)

Grain No.	S	Fe	Ni	Cu	Total
1	39.42	57.98	2.10	lld	99.53
2	39.34	59.00	1.21	0.08	99.64
3	39.29	58.72	1.22	0.05	99.28
4	39.33	58.06	1.92	lld	99.31
5	39.27	58.04	2.05	lld	99.37
6	39.43	58.11	2.14	lld	99.70
7	39.29	57.66	2.22	lld	99.21
8	39.45	58.95	1.21	lld	99.63
9	39.43	58.61	1.37	lld	99.41
10	39.58	58.68	1.11	lld	99.37
11	39.48	57.99	1.57	lld	99.05
12	39.59	58.61	1.37	lld	99.61
13	39.96	58.75	1.22	lld	99.93
14	39.43	57.94	2.00	lld	99.38
15	39.57	58.58	1.44	lld	99.61
16	39.51	59.01	1.25	lld	99.78
17	39.59	59.55	0.61	lld	99.76
18	39.46	59.14	0.69	lld	99.29
19	39.50	59.42	0.74	lld	99.68
20	39.44	57.44	2.68	lld	99.55
21	39.38	57.41	3.09	0.08	99.96
22	39.40	56.92	3.53	lld	99.90
23	39.20	57.72	2.75	0.19	99.85
24	39.29	57.79	2.69	lld	99.77
25	39.36	56.28	4.40	lld	100.04
26	39.34	56.63	3.79	lld	99.76
27	39.23	57.33	2.63	lld	99.21
28	39.27	56.47	3.70	lld	99.47
29	39.37	57.76	2.32	lld	99.48
30	39.29	56.76	3.44	lld	99.50
31	39.39	56.89	3.30	lld	99.58
32	39.17	57.65	2.79	0.06	99.67
33	39.27	58.02	2.10	0.08	99.47
34	39.37	57.91	2.07	lld	99.36
35	39.42	56.06	3.78	lld	99.26
36	39.77	57.42	2.72	lld	99.92
37	39.55	56.37	3.47	lld	99.39
38	39.42	56.76	3.08	lld	99.26
39	39.42	56.44	3.61	lld	99.48
40	39.37	58.62	1.24	lld	99.24
41	39.30	58.51	1.28	lld	99.09
42	39.26	58.83	1.13	lld	99.22
43	39.48	58.83	1.06	0.08	99.44
44	39.87	58.70	1.01	lld	99.61

45	39.42	59.09	0.90	lld	99.41
46	39.21	58.78	0.94	lld	98.93
47	39.19	58.95	1.06	lld	99.24
48	39.14	58.84	1.12	lld	99.11
49	39.45	58.73	1.11	lld	99.29
50	39.41	58.53	1.07	lld	99.02

Table D. 6 EPMA pentlandite grain analyses for Phoenix ore (wt%)

Grain No.	S	Fe	Co	Ni	Total
1	33.36	29.11	0.37	37.19	100.03
3	32.73	28.61	0.46	37.51	99.31
4	32.88	28.87	0.54	37.36	99.65
5	32.37	29.18	0.61	37.59	99.76
7	32.86	28.84	0.58	37.86	100.14
8	32.79	29.05	0.60	37.25	99.70
9	33.00	28.85	0.55	37.71	100.12
10	32.58	29.33	0.47	37.41	99.79
11	32.78	29.13	0.60	37.76	100.27
12	32.99	29.33	0.58	37.51	100.40
13	32.78	29.40	0.43	37.81	100.41
14	32.51	29.28	0.55	37.38	99.72
15	32.77	29.22	0.62	37.66	100.27
16	32.83	29.43	0.57	37.66	100.48
17	32.60	29.30	0.57	37.84	100.32
18	32.63	29.29	0.46	37.29	99.66
19	32.74	29.16	0.50	37.56	99.96
20	32.79	29.23	0.57	37.46	100.04
21	32.66	29.44	0.57	37.46	100.13
22	32.56	29.29	0.63	37.12	99.60

Table D. 7 Quantitative XRD results for the Nkomati DMC Feed and Overflow (mass %; F = floats, S = sinks)

Mineral	DMC Feed	2.7 F	2.8 F	2.9 F	2.95 F	3.0 F	3.1 F	3.1 S
actinolite	23.1	2.5	7.5	13.6	27.9	36.7	36.3	18.0
albite	6.3	25.1	17.8	10.0	8.8	5.9	5.4	2.6
chalcopyrite	1.0	0.0	0.0	0.0	0.1	0.2	0.3	0.8
clinochlore	15.9	17.6	22.9	32.4	25.9	17.4	14.9	7.1
pentlandite	0.6	0.0	0.0	0.0	0.2	0.2	0.2	1.5
pyrrhotite 4C	3.2	0.0	0.6	1.5	0.5	1.0	2.8	12.2
talc	8.5	3.8	6.8	12.3	11.4	8.4	6.6	4.3
calcite	7.3	15.5	20.2	9.0	3.6	4.2	5.3	3.0
quartz	2.4	29.4	8.8	4.6	1.5	0.8	0.6	0.2
chrysotile	3.9	3.6	5.1	6.1	5.3	3.6	3.8	2.4
biotite	0.0	0.0	0.0	0.0	0.0	0.0	0.0	0.0
dolomite	3.7	0.0	5.9	2.4	1.7	1.5	3.8	5.9
pyrrhotite 3C	5.7	0.0	0.9	1.9	2.7	2.7	3.1	5.7
magnetite	4.4	2.2	0.9	1.8	4.0	2.7	2.1	6.8
lizardite	0.9	0.1	0.5	1.0	0.9	0.5	0.7	1.0
rutile	2.3	0.0	2.1	3.5	3.9	3.9	2.5	0.9
augite	10.9	0.0	0.0	0.0	1.7	10.3	11.0	27.7
R_{wp}	*5.72*	*8.47*	*6.21*	*6.58*	*5.48*	*4.62*	*4.3*	*3.22*
GOF	*3.92*	*5.07*	*4.21*	*4.90*	*4.12*	*3.44*	*3.13*	*2.67*

Table D. 8 Absolute one sigma errors on XRD values for the Nkomati DMC Feed and Overflow

Mineral	DMC Feed	2.7 F	2.8 F	2.9 F	2.95 F	3.0 F	3.1 F	3.1 S
actinolite	1.70	0.40	0.54	1.20	2.20	2.90	2.00	0.93
albite	0.87	2.10	1.10	0.94	0.80	0.62	0.57	0.56
chalcopyrite	0.15	0.00	0.00	0.00	0.10	0.10	0.09	0.81
clinochlore	1.90	1.50	1.80	2.80	2.40	1.90	1.40	1.50
pentlandite	0.16	0.00	0.00	0.00	0.09	0.09	0.08	0.15
pyrrhotite 4C	0.61	0.00	0.21	0.71	0.28	0.25	0.38	0.82
talc	0.85	0.50	0.58	1.10	0.10	0.82	0.58	0.43
calcite	0.67	1.30	1.20	0.78	0.44	0.45	0.42	0.31
quartz	1.60	4.50	1.60	1.40	1.60	2.00	1.30	1.70
chrysotile	0.58	0.55	0.48	0.69	0.50	0.54	0.41	0.38
dolomite	0.42	0.00	0.43	0.33	0.26	0.21	0.31	0.37
pyrrhotite 3C	0.73	0.00	0.30	0.77	0.47	0.37	0.42	0.69
magnetite	0.52	0.34	0.20	0.34	0.44	0.33	0.24	0.43
lizardite	0.26	0.47	0.29	0.31	0.24	0.33	0.22	0.17
rutile	0.33	0.00	0.36	0.53	0.48	0.48	0.35	0.32
augite	1.00	0.00	0.00	0.00	0.67	1.80	0.85	1.40

Table D. 9 Quantitative XRD results for the Nkomati DMC Underflow (mass %; F = floats, S = sinks)

Mineral	2.8 F	2.9 F	2.95 F	3.0 F	3.1 F	3.2 F	3.3 F	3.4 F	3.4 S
actinolite	10.5	19.9	28.8	35.4	32.1	22.5	18.5	20.6	17.6
albite	17.7	4.7	6.0	7.2	5.1	4.9	4.9	3.7	2.7
chalcopyrite	0.0	0.0	0.0	0.0	0.0	0.0	0.6	0.8	1.1
clinochlore	30.0	29.3	25.2	19.0	16.9	9.8	7.5	6.9	3.4
pentlandite	0.0	0.0	0.0	0.0	0.0	0.0	0.0	0.0	0.0
pyrrhotite 4C	0.9	6.7	3.5	6.6	7.9	8.0	11.2	16.7	24.9
talc	6.8	13.0	11.7	8.2	9.2	6.6	5.8	4.5	3.0
calcite	2.9	1.9	2.6	1.7	1.8	6.0	4.7	4.3	5.5
quartz	14.0	3.0	2.0	1.0	0.0	0.4	0.2	0.4	0.0
chrysotile	3.7	2.9	1.3	1.1	1.1	0.7	0.4	0.3	3.2
biotite	0.0	0.0	0.0	0.0	0.0	0.0	0.0	0.0	0.0
dolomite	4.2	2.5	3.1	2.6	4.4	3.8	4.2	4.6	2.7
pyrrhotite 3C	0.0	0.0	0.0	0.0	0.0	1.8	4.2	7.0	11.5
magnetite	1.4	2.1	3.5	4.1	6.6	4.3	5.1	4.6	2.9
lizardite	1.6	3.1	2.3	1.4	1.4	1.2	1.1	0.9	0.8
rutile	0.2	0.5	1.5	1.4	1.2	0.2	0.2	0.3	1.0
augite	5.1	8.1	8.8	10.4	12.2	26.3	26.1	15.2	10.4
siderite	1.2	1.9	0.0	0.0	0.0	0.0	0.0	0.0	0.0
sphalerite	0.0	0.0	0.0	0.0	0.0	0.0	0.4	0.7	0.9
olivine	0.0	0.0	0.0	0.0	0.0	0.0	0.0	5.1	4.7
clinozoisite	0.0	0.0	0.0	0.0	0.0	3.5	0.0	0.0	2.0
chromite	0.0	0.0	0.0	0.0	0.0	0.0	0.0	0.0	1.3
R_{wp}	*5.22*	*5.06*	*4.68*	*4.36*	*4.5*	*4.08*	*3.61*	*3.04*	*2.89*
GOF	*3.66*	*3.76*	*3.44*	*3.26*	*3.36*	*2.98*	*2.75*	*2.43*	*2.52*

Table D. 10 Absolute one sigma errors on XRD values for the Nkomati DMC Underflow

Mineral	2.8 F	2.9 F	2.95 F	3.0 F	3.1 F	3.2 F	3.3 F	3.4 F	3.4 S
actinolite	4.00	4.90	6.70	8.70	6.60	2.20	2.00	1.90	2.90
albite	5.90	1.40	6.00	1.90	1.20	4.89	0.59	0.53	0.61
chalcopyrite	0.00	0.00	0.00	0.00	0.00	0.08	0.11	0.12	0.20
clinochlore	10.00	7.20	6.10	5.10	4.00	2.70	2.50	2.30	3.00
pentlandite	0.00	0.00	0.00	0.00	0.00	0.00	0.00	0.00	0.00
pyrrhotite 4C	0.46	1.60	0.87	1.60	1.60	0.73	0.92	1.20	3.60
talc	2.40	3.10	2.80	2.10	1.90	0.58	0.50	0.42	0.53
calcite	1.00	0.62	0.77	0.60	0.48	0.42	0.42	0.42	0.54
quartz	27.00	20.00	20.00	22.00	0.00	0.33	0.56	0.11	0.00
chrysotile	1.40	1.00	0.80	0.75	0.70	0.65	0.68	0.68	0.55
biotite	0.00	0.00	0.00	0.00	0.00	0.00	0.00	0.00	0.00
dolomite	1.40	0.66	0.75	0.69	0.93	0.42	0.44	0.47	0.54
pyrrhotite 3C	0.00	0.00	0.00	0.00	0.00	0.46	0.65	0.79	1.80
magnetite	0.58	0.57	0.86	1.10	1.40	0.49	0.49	0.46	0.60
lizardite	0.60	0.80	0.59	0.43	0.36	0.21	0.17	0.16	0.20
rutile	3.80	2.80	3.50	3.40	1.70	0.79	0.71	0.33	13.00
augite	1.90	2.10	2.10	2.60	0.00	1.90	1.80	1.20	1.70
siderite	0.41	0.47	0.00	0.00	0.00	0.00	0.00	0.00	0.00
sphalerite	0.00	0.00	0.00	0.00	0.00	0.00	0.07	0.08	0.15
olivine	0.00	0.00	0.00	0.00	0.00	0.00	0.00	0.64	0.80
clinozoisite	0.00	0.00	0.00	0.00	0.00	0.00	0.00	0.00	0.70
chromite	0.00	0.00	0.00	0.00	0.00	0.00	0.00	0.00	0.26

Table D. 11 Quantitative XRD results for the Phoenix DMC Feed and Overflow (mass %; F = floats, S = sinks)

Mineral	DMC Feed	2.7 F	2.75 F	2.8 F	2.9 F	2.95 F	3.0 F	3.1 F	3.2 F	3.2 S
clinochlore	7.3	3.8	9.4	10.5	8.3	11.1	10.2	7.9	3.8	8.8
pyrrhotite 4C	1.4	0.0	0.0	0.0	0.0	0.0	0.0	1.4	3.2	11.5
quartz	7.5	37.2	22.2	12.1	3.7	3.8	5.7	3.7	3.7	2.1
albite	30.7	44.7	42.6	40.0	26.3	25.4	26.0	17.2	16.6	13.2
clinozoisite	11.2	7.9	8.4	9.2	5.6	4.9	4.9	8.8	9.1	9.0
chalcopyrite	0.0	0.0	0.0	0.0	0.0	0.0	0.0	1.0	1.8	1.8
actinolite	21.2	1.3	5.2	10.1	26.2	28.7	26.7	30.1	22.8	11.3
calcite	2.3	1.2	2.0	1.9	0.6	0.6	0.8	1.1	1.6	3.5
dolomite	0.9	0.4	2.5	3.7	3.1	3.7	4.0	5.1	5.8	4.5
biotite	4.1	0.0	0.0	0.0	2.8	2.4	1.8	2.8	2.0	1.2
magnetite	3.2	1.3	2.1	2.4	2.6	3.5	3.4	3.9	6.6	11.6
orthoclase	0.0	0.0	0.0	0.0	0.0	0.0	0.0	0.0	0.0	0.3
augite	9.1	2.1	5.1	9.4	19.3	14.7	15.3	14.4	19.3	13.0
ilmenite	0.4	0.0	0.0	0.1	1.2	1.0	0.8	1.3	1.8	3.3
lizardite	0.3	0.0	0.0	0.0	0.0	0.0	0.0	0.6	0.7	1.9
zeolite	0.3	0.1	0.4	0.6	0.3	0.2	0.3	0.2	0.2	0.1
talc	0.0	0.0	0.0	0.0	0.0	0.0	0.0	0.5	1.0	2.9
R_{wp}	*4.44*	*7.26*	*5.27*	*5.12*	*4.42*	*4.35*	*5.22*	*4.01*	*3.65*	*2.47*
GOF	*2.99*	*4.13*	*3.28*	*3.28*	*2.95*	*2.87*	*3.34*	*2.69*	*2.58*	*2.04*

Table D. 12 Absolute one sigma errors on XRD values for the Phoenix DMC Feed and Overflow

Mineral	DMC feed	2.7 F	2.75 F	2.8 F	2.9 F	2.95 F	3.0 F	3.1 F	3.2 F	3.2 S
clinochlore	0.38	0.46	0.80	1.10	0.78	0.53	0.66	0.49	0.57	0.81
pyrrhotite 4C	0.16	0.00	0.00	0.00	0.00	0.00	0.00	0.19	0.22	0.32
quartz	0.12	1.10	1.60	1.20	0.37	0.24	0.33	0.15	0.13	0.10
albite	0.55	1.30	3.10	3.90	2.10	0.89	1.10	0.77	0.75	0.72
clinozoisite	0.62	0.65	0.93	1.10	0.75	0.55	0.65	0.66	0.68	0.82
chalcopyrite	0.00	0.00	0.00	0.00	0.00	0.00	0.00	0.18	0.13	0.14
actinolite	0.42	0.36	0.42	1.00	2.10	0.88	0.93	0.98	0.66	0.37
calcite	0.26	0.19	0.25	0.28	0.19	0.20	0.24	0.31	0.32	0.43
dolomite	0.26	0.13	0.32	0.50	0.39	0.35	0.43	0.31	0.31	0.29
biotite	0.28	0.00	0.00	0.00	0.28	0.19	0.24	0.19	0.17	0.16
magnetite	0.20	0.19	0.26	0.34	0.32	0.31	0.39	0.30	0.35	0.36
orthoclase	0.00	0.00	0.00	0.00	0.00	0.00	0.00	0.00	0.00	1.30
augite	0.24	0.21	0.45	0.95	1.50	0.52	0.62	0.55	0.61	0.45
ilmenite	0.53	0.00	0.04	0.06	0.12	0.08	0.10	0.16	0.16	0.21
lizardite	0.07	0.00	0.00	0.00	0.00	0.00	0.00	0.20	0.22	0.30
zeolite	0.03	0.03	0.05	0.07	0.04	0.03	0.04	0.03	0.03	0.02
talc	0.00	0.00	0.00	0.00	0.00	0.00	0.00	0.18	0.22	0.25

Table D. 13 Quantitative XRD results for the Phoenix DMC Underflow (mass %; F = floats, S = sinks)

Mineral	2.7 F	2.75 F	2.8 F	2.9 F	2.95 F	3.0 F	3.1 F	3.2 F	3.3 F	3.4 F	3.4 S
clinochlore	2.9	7.8	11.5	9.6	9.0	9.0	9.4	6.3	9.3	15.3	10.7
pyrrhotite 4C	0.0	0.0	1.0	0.8	0.9	0.8	1.2	1.4	7.0	21.9	35.6
quartz	36.4	19.2	6.1	3.9	3.2	3.3	3.0	0.1	2.9	1.4	0.7
albite	46.8	43.9	36.5	30.4	26.9	26.8	16.9	29.3	11.5	12.8	12.0
clinozoisite	2.8	3.5	5.6	6.9	9.2	8.5	12.3	15.3	14.7	7.2	6.1
chalcopyrite	0.0	0.0	0.0	0.0	0.0	0.0	0.0	0.2	4.5	6.7	6.0
pentlandite	0.0	0.0	0.0	0.0	0.0	0.0	0.0	0.0	1.0	4.8	8.7
actinolite	0.3	4.4	13.0	22.2	24.7	24.4	32.0	24.1	27.0	15.5	4.0
calcite	1.2	1.7	1.9	1.7	2.1	1.8	2.8	0.0	0.0	0.0	0.0
dolomite	0.3	1.3	3.4	2.1	1.9	2.4	2.1	0.0	4.4	2.6	0.4
biotite	6.6	10.1	6.2	3.3	2.8	3.2	4.8	0.0	3.8	0.8	0.0
magnetite	1.1	2.4	3.5	3.1	2.8	3.1	2.8	0.0	3.6	3.2	0.6
orthoclase	0.0	0.0	1.5	2.2	1.7	1.8	1.3	0.0	1.1	0.8	1.5
augite	1.5	4.9	9.0	12.5	13.6	13.6	10.3	20.9	8.0	2.8	1.5
ilmenite	0.0	0.0	0.1	0.4	0.7	0.7	0.5	0.0	0.2	0.2	0.1
lizardite	0.0	0.1	0.4	0.5	0.4	0.4	0.3	0.0	0.8	1.0	0.6
zeolite	0.1	0.2	0.4	0.4	0.3	0.3	0.3	2.4	0.3	0.3	0.2
hexahydrite	0.0	0.0	0.0	0.0	0.0	0.0	0.0	0.0	0.0	1.6	9.0
hydroniumjarosite	0.0	0.0	0.0	0.0	0.0	0.0	0.0	0.0	0.0	1.2	2.4
R_{wp}	*5.87*	*4.32*	*4.52*	*4.5*	*4.08*	*4.07*	*4.56*	*8.38*	*4.04*	*2.43*	*2.57*
GOF	*3.38*	*2.73*	*2.96*	*2.95*	*2.73*	*2.73*	*3.22*	*1.93*	*3.07*	*2.02*	*2.29*

Table D. 14 Absolute one sigma errors on XRD values for the Phoenix DMC Underflow

Mineral	2.7 F	2.75 F	2.8 F	2.9 F	2.95 F	3.0 F	3.1 F	3.2 F	3.3 F	3.4 F	3.4 S
clinochlore	0.43	0.43	0.05	0.42	0.37	0.39	0.40	1.20	0.50	0.62	0.70
pyrrhotite 4C	0.00	0.00	0.17	0.18	0.92	0.17	0.18	0.39	0.24	0.38	0.58
quartz	0.35	0.22	0.11	0.09	0.08	0.08	0.08	0.65	0.10	0.07	0.08
albite	0.46	0.52	0.58	0.56	0.51	0.52	0.55	2.20	0.77	0.81	0.76
clinozoisite	0.29	0.41	0.54	0.76	0.70	0.72	0.73	2.30	0.86	0.77	0.74
chalcopyrite	0.00	0.00	0.00	0.00	0.00	0.00	0.00	0.01	0.13	0.14	0.14
pentlandite	0.00	0.00	0.00	0.00	0.00	0.00	0.00	0.00	14.00	0.14	0.20
actinolite	0.13	4.36	0.28	0.36	0.36	0.36	0.46	3.60	0.50	0.31	0.23
calcite	0.15	0.20	0.23	0.27	0.27	0.26	0.29	0.00	0.00	0.00	0.00
dolomite	0.08	0.16	0.34	0.27	0.21	0.27	0.20	0.00	0.00	0.21	0.18
biotite	0.35	0.38	0.41	0.29	0.23	0.24	0.26	0.01	0.34	0.29	0.00
magnetite	0.15	0.19	0.25	0.27	0.24	0.25	0.27	0.00	0.32	0.27	0.15
orthoclase	0.00	0.00	0.12	0.15	0.13	0.14	0.15	0.00	0.16	0.16	0.23
augite	0.16	0.22	0.26	0.31	0.31	0.34	0.31	3.30	0.35	0.25	0.26
ilmenite	0.00	0.03	0.05	0.06	0.06	0.06	0.07	0.00	0.07	0.05	0.06
lizardite	0.00	0.05	0.07	0.08	0.08	0.09	0.10	0.00	0.11	0.08	0.08
zeolite	0.02	0.03	0.03	0.03	0.03	0.03	0.03	0.38	0.03	0.03	0.03
hexahydrite	0.00	0.00	0.00	0.00	0.00	0.00	0.00	0.00	0.00	0.03	0.43
hydroniumjarosite	0.00	0.00	0.00	0.00	0.00	0.00	0.00	0.00	0.00	0.10	0.11

Table D. 15 Nickel deportment in the Nkomati ore showing nickel concentration in mass %

Mineral	Overflow			Underflow		
	3.0 floats	**3.1 floats**	**3.1 sinks**	**3.0 floats**	**3.1 floats**	**3.2 floats**
pyrrhotite	6.5	7.01	8.4	8.3	7.51	8.5
pentlandite	76.0	80.92	88.6	83.2	84.41	85.6
mica	1.2	0.24	0.1	0.5	0.14	0.2
alteration minerals	10.5	6.99	1.3	4.4	4.69	2.2
pyroxene	1.0	1.12	0.9	1.3	1.08	2.1
amphibole	4.9	3.72	0.6	2.3	2.17	1.4

Table D. 16 Nickel deportment in the Phoenix ore showing nickel concentration in mass %

Mineral	Overflow			Underflow		
	2.95 floats	**3.0 floats**	**3.1 floats**	**2.95 floats**	**3.0 floats**	**3.1 floats**
pyrrhotite	4.7	3.4	7.7	5.4	2.7	7.9
pentlandite	57.2	54.4	75.7	56.2	44.1	77.7
alteration minerals	20.5	17.3	7.3	19.9	23.4	7.0
pyroxene	3.1	1.9	1.5	3.8	1.8	1.3
amphibole	14.5	23.1	7.7	14.7	28.0	6.1

Table D. 17 Cumulative sulfide grain size distribution in the Nkomati ore (mass %)

Size (µm)	Overflow			Underflow		
	3.0 floats	**3.1 floats**	**3.1 sinks**	**3.0 floats**	**3.1 floats**	**3.2 floats**
<50	1.32	0.33	0.84	0.82	0.08	0.63
<100	14.35	10.29	15.69	8.46	3.77	9.29
<150	42.80	33.07	37.95	27.70	14.82	28.80
<200	71.83	54.62	57.67	46.74	38.03	55.77
<250	83.09	66.82	71.00	58.18	60.93	75.06
<300	89.04	80.63	79.47	62.62	72.62	84.26
<350	95.01	85.37	86.58	69.14	80.38	88.80
<400	97.74	89.40	91.93	73.96	83.40	91.38
<450	98.11	94.77	94.86	82.18	87.93	92.09
<500	98.42	95.74	96.67	87.95	91.54	94.97
<550	98.78	96.92	97.66	90.80	96.09	95.83
<600	98.78	98.01	98.15	95.45	96.17	96.31
<650	99.25	98.43	98.91	96.69	98.33	98.73
<700	99.38	98.43	99.28	98.05	98.33	98.84
<750	99.38	99.67	99.59	98.07	98.33	98.84
<800	99.89	99.84	99.59	98.71	98.39	98.84
<850	99.89	99.84	99.71	98.71	98.69	98.84
<900	100.00	100.00	99.71	98.96	99.32	99.09
<1000	100.00	100.00	99.71	98.96	100.00	99.31
>1000	100.00	100.00	100.00	100.00	100.00	100.00

Table D. 18 Cumulative sulfide grain size distribution in the Phoenix ore (mass %)

Size (µm)	Overflow			Underflow		
	2.95 floats	3.0 floats	3.1 floats	2.95 floats	3.0 floats	3.1 floats
<50	18	15	12	30	20	5
<100	76	77	72	94	80	62
<150	94	94	88	98	85	80
<200	95	94	93	100	93	87
<250	95	100	99	100	93	93
<300	95	100	100	100	93	93
<350	95	100	100	100	93	95
<400	95	100	100	100	100	95
<450	99	100	100	100	100	95
<500	99	100	100	100	100	95
<550	99	100	100	100	100	95
<600	100	100	100	100	100	95
<650	100	100	100	100	100	97
<700	100	100	100	100	100	97
<750	100	100	100	100	100	97
<800	100	100	100	100	100	97
<850	100	100	100	100	100	97
<900	100	100	100	100	100	100
<1000	100	100	100	100	100	100

Table D. 19 Sulfide liberation in the Nkomati ore (mass %)

Product	SG Class	Locked	Middlings	Liberated
Overflow	3.0 floats	97.7	2.1	0.1
	3.1 floats	99.3	0.7	0.0
	3.1 sinks	51.3	43.5	5.2
Underflow	3.0 floats	87.1	12.3	0.6
	3.1 floats	99.2	0.8	0.0
	3.2 floats	91.4	7.7	0.9

Table D. 20 Sulfide liberation in the Phoenix ore (mass %)

Product	SG Class	Locked	Middlings	Liberated
Overflow	2.95 floats	96.7	3.3	0.0
	3.0 floats	100.0	0.0	0.0
	3.1 floats	93.1	6.6	0.3
Underflow	2.95 floats	99.6	0.4	0.0
	3.0 floats	100.0	0.0	0.0
	3.1 floats	88.7	11.3	0.0

Table D. 21 Cumulative particle size distribution in the Nkomati ore (mass %)

Size (mm)	Overflow			Underflow		
	3.0 floats	**3.1 floats**	**3.1 sinks**	**3.0 floats**	**3.1 floats**	**3.2 floats**
<1	4	10	52	2	2	2
<2	14	26	91	10	9	10
<3	24	37	96	19	20	22
<4	37	45	97	32	31	36
<5	49	53	100	45	43	48
<6	59	61	100	59	53	62
<7	68	72	100	75	63	73
<8	77	82	100	81	73	79
<9	87	92	100	85	80	88
<10	93	94	100	90	87	93
<11	95	97	100	94	93	96
<12	100	98	100	96	96	97
<13	100	98	100	99	97	97
<14	100	98	100	100	97	98
<15	100	99	100	100	97	99
<16	100	100	100	100	99	100
<17	100	100	100	100	100	100

Table D. 22 Cumulative particle size distribution in the Phoenix ore (mass %)

Size (mm)	Overflow			Underflow		
	2.95 floats	3.0 floats	3.1 floats	2.95 floats	3.0 floats	3.1 floats
<1	3	7	15	1	2	1
<2	13	23	47	8	12	9
<3	24	36	65	20	26	22
<4	36	45	75	33	39	33
<5	48	54	82	50	50	47
<6	62	65	87	65	61	61
<7	70	74	92	80	70	74
<8	79	82	95	91	78	81
<9	88	91	99	95	86	91
<10	94	96	99	97	93	99
<11	97	99	99	99	97	100
<12	99	99	100	99	99	100
<13	99	100	100	100	100	100
<14	100	100	100	100	100	100

Table D. 23 Shape factor distribution in the Nkomati ore

Shape Factor	Overflow			Underflow		
	3.0 floats	3.1 floats	3.1 sinks	3.0 floats	3.1 floats	3.2 floats
<20	6.7	4.7	18.8	2.6	2.6	4.6
<30	64.5	69.5	65.9	60.8	58.8	63.3
<40	21.9	20.2	12.2	26.7	25.3	26.4
<50	3.8	4.5	2.4	5.7	7.7	4.0
<60	2.4	0.6	0.3	2.6	2.5	1.2
>60	0.5	0.4	0.2	1.5	3.3	0.5

Table D. 24 Shape factor distribution in the Phoenix ore

Shape Factor	Overflow			Underflow		
	2.95 floats	3.0 floats	3.1 floats	2.95 floats	3.0 floats	3.1 floats
<10	0.1	0.0	0.0	0.0	0.0	0.0
<20	6.1	12.1	16.3	2.7	8.3	3.7
<30	77.1	76.1	66.9	69.1	71.1	75.3
<40	12.8	10.1	12.7	20.7	16.6	16.6
<50	3.3	1.4	3.1	6.3	3.2	3.8
<60	0.4	0.3	0.7	1.1	0.6	0.5
>60	0.2	0.0	0.3	0.1	0.2	0.1

Table D. 25 Elongation distribution in the Nkomati ore

Elongation	Overflow			Underflow		
	3.0 floats	**3.1 floats**	**3.1 sinks**	**3.0 floats**	**3.1 floats**	**3.2 floats**
<0.2	15.7	21.3	14.7	14.5	15.0	15.0
<0.4	39.7	38.5	36.8	29.6	35.3	35.3
<0.6	31.8	29.8	35.4	35.0	36.3	36.4
<0.8	12.7	10.4	12.8	19.9	13.3	12.8
<1	0.1	0.1	0.3	1.1	0.1	0.4

Table D. 26 Elongation distribution in the Phoenix ore

Elongation	Overflow			Underflow		
	2.95 floats	**3.0 floats**	**3.1 floats**	**2.95 floats**	**3.0 floats**	**3.1 floats**
<0.2	20.1	19.4	17.9	14.6	15.4	18.0
<0.4	39.3	40.1	38.2	37.1	33.3	44.0
<0.6	33.0	35.6	33.5	35.0	37.9	28.5
<0.8	7.5	4.9	10.3	13.2	13.0	9.3
<1	0.2	0.0	0.1	0.1	0.3	0.3